Experimental and stimulation analyses of fluorescent solvent relaxation process in biomembranes : Inflence of ions and molecular interpretation of the dye dynamics

Justyna Barucha-Kraszewska

Justyna Barucha-Kraszewska. Experimental and stimulation analyses of fluorescent solvent relaxation process in biomembranes : Inflence of ions and molecular interpretation of the dye dynamics. Biological Physics [physics.bio-ph]. Université de Franche-Comté, 2012. English. NNT : 2012BESA3010 . tel-01562046

HAL Id: tel-01562046
https://theses.hal.science/tel-01562046

Université de Franche-Comté
Laboratoire de Nanomédecine, Imagerie et Thérapeutique

L'Ecole Doctorale Homme – Environnement – Santé

Thèse de Doctorat

Spécialité Physique

présentée par

Justyna Barucha-Kraszewska

Experimental and Simulation Analyses of Fluorescent Solvent Relaxation Process in Biomembranes. Influence of Ions and Molecular Interpretation of the Dye Dynamics.

Thèse dirigée par Martin Hof et Christophe Ramseyer

soutenue le 31 octobre 2012

Jury :

Yves MELY	Professeur – Université de Strasbourg, Illkirch	Rapporteur
Semen YESYLEVSKYY	Senior Researcher – Institute of Physics of the National Academy of Sciences of Ukraine, Kiev, Ukraine	Rapporteur
Mironel ENESCU	Professeur – Université de Franche-Comté, Besançon	Examinateur
Mounir TAREK	DR CNRS – Université de Lorraine, Nancy	Examinateur
Christophe RAMSEYER	Professeur – Université de Franche-Comté, Besançon	Examinateur
Martin HOF	Professeur – J. Heyrovský Institute of Physical Chemistry of the Czech Academy of Sciences, Prague, Czech Republic	Examinateur

For my daughter:
Irmina

- Everything… Everything…
-…?
- Everything…
- What everything?
- Everything…
- What everything my dear?
- Everything… RIDES!
Irmina, 2 years old, 08/2011

"'The female mind is certainly a devious one, my lord.'
Vetinari looked at his secretary in surprise.
'Well, of course it is. It has to deal with the male one.'"
Terry Pratchett, *Unseen Academicals*

ACKNOWLEDGEMENTS

First of all, I would like to thank my supervisor, Martin Hof, whose encouragement, guidance, patience, understanding and support allowed me to grow as a scientist.

I owe my deepest gratitude to Christophe Ramseyer. Without your willingness, suggestions and helps this PhD thesis would have never been written.

I would like to express my thanks to Marek Langner from the Biophysical Student Society "Micella" for the possibility of learning how to plan scientific experiments.

It is an honour for me to thank Agnieszce Olżyńskiej and Piotrowi Jurkiewiczowi. Agnieszko and Piotrze, I am grateful for introducing me into the solvent relaxation technique, discussions, patience for all my questions and doubts. And for Carcassonne, of course :). Piotrze, thank you for all your advices, discussions, and help with corrections of my manuscript.

I am deeply indebted to Jan Sýkora for his help with SR measurements and SR equipments.

I would like to express my thanks to Sebastian Kraszewski for showing me the secrets of QM, MD, VMD and numerical simulation details.

I am extremely grateful to Semen Yesylevskyy for the help with improving my manuscript and for useful advice.

I would like to thank all collegues who worked in our group: Aleš Benda, Lenka Beranová, Barbara Gasińska (Lewandowska) – thank you for our common living in Prague, Jana Humpoličkova – for introducing me into the flavours of Czech vines, Radek Machaň, Adam Miszta, Robert Vacha – for nice collaboration with writing articles and simulation advices and Anna Kulakowska – for all time at BBC, shared evenings with ebooks and needlework. I would like to thank the 'simulation group' people for very nice atmosphere and patient for my french: Claude Girardet, Fabien Picaud and Delphine Vardanega.

I would like to show my gratitude to the administrative staff of the J. Heyrovský Institute and I would like to special thank Mrs. Vladimíra Bergerová for her help.

*Lastly, it is a pleasure to thank my family and friends. My parents for their help and support. Mateuszowi and Karolowi for great sense of humour. Malwince for everything. My husband, Sebastianowi – I thank you for your love and support. And my daughter, Irminie – you are the greatest I have :**

I express my gratitude for financial support to: J. Heyrovský Institut of Physical Chemistry and Grant Agency of the Academy of Science of the Czech Republic (via Grant No. A400400503) and Czech Ministry of education (LC512 and LC06063) and the Czech Science Foundation (Grant 203/08/0114).

List of Abbreviations

C-Hex	cyclohexane: C_6H_{12}
C-Laurdan	6-dodecanoyl-2-[*N*-methyl-*N*-(carboxymethyl)amino]naphthalene
DMF	dimethyloformamide: $(CH_3)_2NC(O)H$
DOPC	1,2-dioleoyl-*sn*-glycero-3-phosphocholine
DPPC	1,2-dipalmitoyl-*sn*-glycero-3-phosphocholine
DTMAC	4-[(*n*-dodecylthio)methyl]-7-(*N*,*N*-dimethylamino)-coumarin
EtOH	ethanol: C_2H_5OH
FRET	fluorescence resonance energy transfer
FWHM	full width at half maximum
GP	generalized polarization
GUV	giant unilamellar vesicle
HEPES	4-(2-hydroxyethyl)-1-piperazineethanesulfonic acid
HF	Hartree-Fock
L_α	liquid crystalline phase
$L_{\beta'}$	gel phase
L_c	crystalline phase
Laurdan	6-dodecanoyl-2-dime-thylaminonaphthalene
LUV	large unilamellar vesicle
MD	molecular dynamics
MLV	multilamellar vesicle
MO	molecular orbital
NAMD	Not (just) Another Molecular Dynamics - NAno scale Molecular Dynamics
Patman	6-hexadecanoyl-2-(((2-(trimethylammonium)ethyl)methyl)amino) naphthalene
PC	phosphatidylcholine lipid
PE	phosphatidylethanolamine lipid
PI	Phosphatidylinositol lipid
PS	Phosphatidylserine lipid
PME	particle mesh Ewald
POPC	1,2-palmitoyloleoyl-*sn*-glycero-3-phosphocholine
Prodan	6-propionyl-2-dimethylaminonaphthalene
QM	quantum mechanics
REES	red-edge excitation shift
SR	solvent relaxation (technique or process)
SUV	small unilamellar vesicle
TRES	time-resolved emission spectra

Aim of the Study

Many biologically important processes and phenomena in lipid membranes, such as the role of the membrane domains (rafts), asymmetry of lipid composition, membrane protein folding, the role of water in membrane functioning, are still not fully understood. In order to understand how a biological membrane functions, the role of the lipid bilayer hydration should be established and the role of water in the mobility of different segments of lipid molecules should be studied. Furthermore, the presence of ions, which are presented in the aqueous solutions around the membrane, has a significant influence on the structure and dynamical properties of lipid bilayer and other membrane component, like membrane proteins.

Fluorescent techniques are very effective tools for studying the properties of the natural or artificial lipid assemblies, because the fluorescence emission of the probe's chromophore is strongly sensitive to the polarity (hydration) and viscosity (mobility) of their environment. Therefore the choice of the fluorescent solvent relaxation method is natural for the exploration of the hydration and mobility properties in lipid membranes. Fluorescent Solvent Relaxation (SR) method is also well adapted to the observation of the strong influence of the ions on the structure and biological properties of lipid bilayer (hydration level and mobility of water molecules) in the nearest surrounding of fluorescence probe. Water concentration decreases dramatically when we approach the hydrocarbon chains of the hydrophobic region of lipid bilayer and this steep decrease at the headgroup level of lipid bilayer enforces finding of the exact location of the probe in the membrane. Quenching method, which is commonly used to localize the probe position is unfortunately not very accurate. Moreover, the behaviour of the fluorescent probe and water response after excitation (solvent relaxation process) cannot be investigated at the atomic level, using available experimental techniques.

Therefore, the involvement of the Quantum Mechanical (QM) calculations and Molecular Dynamics (MD) simulations should be very fruitful for supporting of the experimental solvent relaxation technique by determining the probe position and dynamics and for understanding of the mechanism of solvent relaxation process.

Though, the general aims of this study are the following:

- ✓ Study of the mechanisms of the influence of ions on the properties of lipid membranes by means of fluorescent solvent relaxation method.

- ✓ Analysis of spectral response of the fluorescent markers, located at different depths in the lipid bilayer hydrophobic hydrocarbon tails region.
- ✓ Building the models of the fluorescent dyes for numerical simulations in the membranes.
- ✓ Study of the location and behaviour of the fluorescent probes in their ground and excited electronic states in the hydrated model membrane.
- ✓ Molecular dynamics study of the relaxation of water molecules around the dye's chromophores after photoexcitation.

Table of Contents

Table of publications

The thesis is based on following publications, which are enclosed at the end of each chapter. They contain more detailed information and the results, which were published in collaboration with the “molecular dynamics simulation” group.

I Introduction

To understand how a biological membrane functions, one has to discover the role of water at different regions of the lipid bilayer and understand how hydration level influences the mobility of those regions. Over a long period of time the information on the lipid hydration and mobility has been gained mostly by NMR [1], neutron and X-ray diffraction [2-3] and EPR [4] experiments on the membrane systems.

The fluorescence emission of various fluorophores is strongly sensitive to the polarity and dynamics of its microenvironment, thus fluorescent experiments are expected to be useful in exploring hydration and mobility of the lipid bilayer. Particularly, time-dependent fluorescence shift experiments performed by so-called fluorescent solvent relaxation (SR) method can provide information on hydration and mobility at different regions of the lipid membranes.

Fluorescent solvent relaxation experiments are based on an ultrafast change in the dipole moment of the fluorophore after electronic excitation, to which the fluorophore microenvironment must adapt. The water relaxation, upon the dipole moment change, shifts the wavenumber of fluorescence $\nu(t)$ to lower energies. The total magnitude of that shift is proportional to the polarity of the solvation shell [5]. The kinetics of that relaxation process describes the rearrangement of the closest vicinity of the probe. It is important to know, that water shows the fastest response to the charge distribution changes upon electronic excitation in comparison to other liquids. The collective reorganization of the water hydrogen bonds occurs within few picoseconds [5]. The time scale of this rearrangement changes dramatically when the fluorophore is embedded into the biomolecular environment. Particularly, the water relaxation occurs in the nanosecond time scale when fluorescent probe is embedded into the biomembrane within the headgroup region of the lipid bilayer. The response of water molecules in the lipid bilayer is 1000 times slower than in the bulk water, which could be explained as a consequence of the phospholipid headgroup dynamics [6]. In particular, the gradient of water concentration along the z-axis of the lipid bilayer is steep [7], thus the main requirement for the application of SR method is well-defined position of the chromophore along z-axis of the membrane.

Although the locations of the dyes are usually determined by parallax fluorescence quenching experiments with spin-labelled lipids [8] a few open questions remains. Especially the width of the fluorophore position distribution is uncertain and its relocation upon excitation is possible. In this work the quantum mechanical (QM) calculations and molecular dynamics (MD) simulations were conducted for the first time to answer these questions.

In this work, QM calculations were used for determination of the force field constants for ground and excited states of the dyes. Fluorescent probes are not usual molecules for computational analysis, while the commonly used force fields, which are databases of intra- and interatomic interactions, include only parameters for “popular” molecules, such as proteins, nucleic acids and lipids [9-12]. Thus, bond lengths, interatomic angles and partial charges of fluorescent probe molecules should be obtained in a form consistent with the rest of the force field for MD simulation [13]. This pioneering work of MD simulations of the fluorescent dyes in the ground and excited states in the fully hydrated lipid membrane showed the dye position and behaviour in the microsecond time scale (up to 0.5µs). In addition, the analysis of the water rearrangement after excitation allows observing the impact of the dipole moment changes of water molecules and kinetics of solvent relaxation process on atomic level. MD simulations have considerably advanced our understanding of the measured time-dependent fluorescence shifts in the lipid bilayers. Moreover, MD simulations show the parameters which have a direct impact on hydration and mobility and thus can be linked to the measured solvent relaxation parameters such as total emission shift $v(t)$ and mean relaxation time τ.

Specific salt effects play a significant role in the membrane dynamics and structure. Ionic effects have been observed since the discovery of the Hofmeister series [14]. The influence of different monovalent anions and cations on hydration, mobility and other parameters of zwitterionic lipid membrane were studied by SR method and MD simulations [15-16]. The difference in the absorption properties of anions and cations were observed. In particular, sodium ions strongly adhere to the DOPC bilayer. They slow down mobility at the carbonyl level of lipid membrane, which is accompanied by reduction area per lipid what reduces lateral mobility. The present study allowed observing ion-membrane interactions directly (i.e. ion pairing within the membrane, counterions effects, presence of the water/hydrophobic interface).

1 Biomembranes

Biological membranes are probably the most fundamental structures of the cell [17]. Lipid molecules, different kind of proteins (integral or peripheral), polysaccharides, water and electrolytes form a membrane described by a fluid mosaic model (see Figure I.1). Cell membrane separates the interior of the cell from the extracellular media and is part of the barrier that facilitates communications between the cell interior and extracellular medium. It controls homeostasis, osmotic pressure, spontaneous diffusion and active or passive transport through the membrane [18].

Cellular membranes control many reactions that occur in the cells, such as energy production and the synthesis of cellular components. The membrane also forms intracellular spaces of cell organelles (compartments). Important functional properties of lipid bilayers are still not fully understood. The composition of the biological membranes depends on the type of the cells.

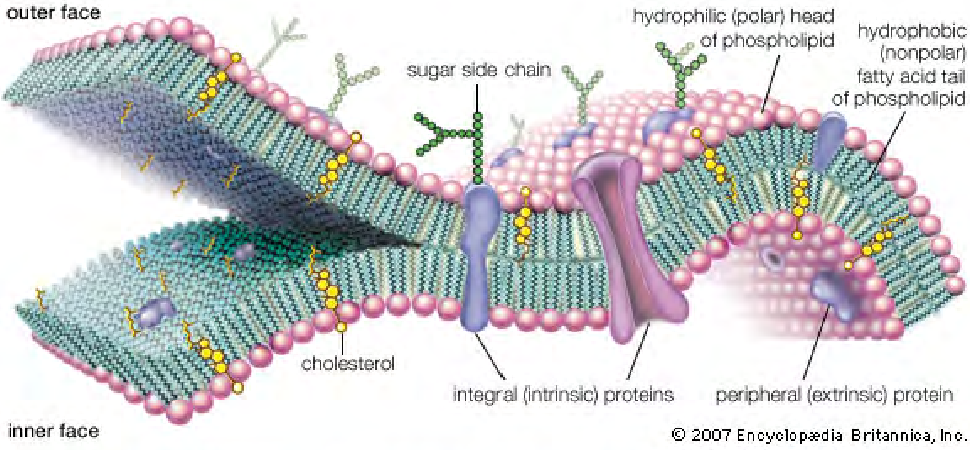

Figure I.1 Schematic representation of a biological membrane model. (From www.britannica.com/EBchecked/media/45550/A-molecular-view-of-the-cell-membrane-Intrinsic-proteins-penetrate)

2 Structure and Functions of Membrane Lipids

The lipids are main components of biological membranes. The complexity of the composition of the lipid membranes shows that the lipids are not limited to being only structural components of them. They play an important role as receptors, messengers and regulators.

Lipodomics is the science which studies the properties of lipids and lipid aggregates for the cell biology, physiology and medicine. Lipids, for instance, are used as a material for the target drug carriers [19-20] and target therapy [21].

Lipids are molecules which have hydrophobic or amphiphilic properties. A lipid molecule usually consists of a hydrophobic fatty acid tails and a hydrophilic polar head group (see Figure I.2). They are poorly soluble in aqueous solutions and are easily soluble in nonpolar solvents.

Lipids, which are present in real biological membranes, belong to three major classes:

1. **phospholipids**, which head group consist of:
    a) glycerol, e.g. glycerophospholipids (see Figure I.3),
    b) sphingosine (amino alcohol), e.g. sphingophospholipids (see Figure I.4),
2. **glycolipids** - lipid-sugar conjugates (see Figure I.5),
3. **sterols** (e.g. cholesterol or phytosterols).

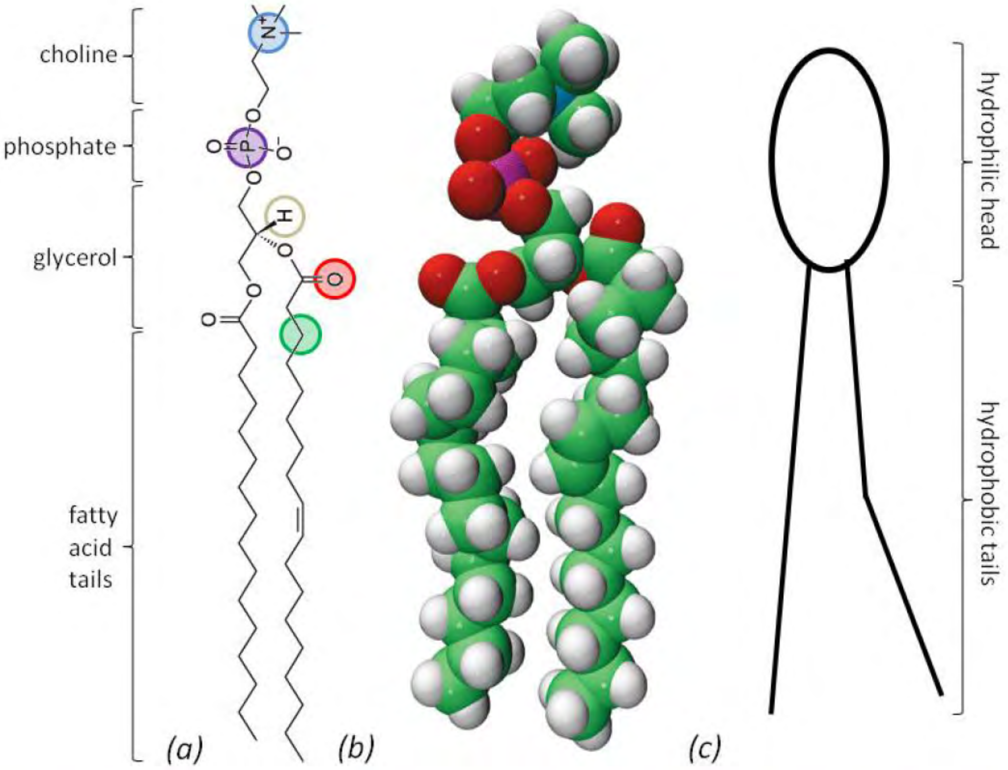

Figure I.2 Typical phospholipid - phosphatidylcholine; molecular structure (a), atomic sphere model (b), simple schematic representation (c).

Phospholipids act as a building blocks of the biological cell membranes and generally constitute 40-70% of the membrane composition, depending on the cell type. They play multiple roles in cells, such as controlling of the membrane transport and fusion or being second messengers in signal transduction.

The structure of glycerophospholipid is built on the basis of glycerol molecule. Two hydroxyl groups (numeration: 1 and 2 in Figure I.3 (a)) of this molecule are esterified to produce the carboxyl groups of the fatty acids which build the hydrophobic part of the lipid. The third glycerol hydroxyl group (numeration: 3 in Figure I.3 (a)) is esterified to phosphoric acid of lipid head group (e.g. choline for phosphatidylcholine) which creates the polar part of the lipid (see Figure I.3).

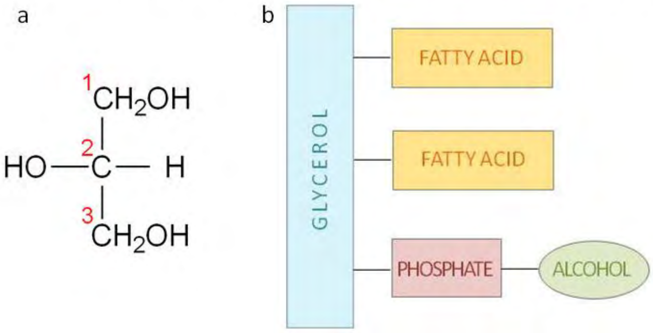

Figure I.3 Chemical formula of glycerol (a) and block diagram of the glycerophospholipid's structure (b).

Sphingolipids are the second major lipid component of the plasma membrane of eucariotic cells. They play an important role in signal transduction processes. Sphingolipids structure is built on the basis of sphingoid base, such as sphingosine (see Figure I.4). Fatty acid tail is connected with sphingosine's core by an amide bond. Sphingomyelin is the most popular sphingolipid in animal tissues but it is not present in plants or procariotes. Sphingomyelin is an important building block of the outer leaflet of membrane. Moreover, sphingomyelin with other sphingolipids and cholesterol is located in the specific sub-domains, the so-called rafts. Rafts are small (diameter 10–200 nm), heterogeneous, highly dynamic, sterol- and sphingolipid-enriched domains that compartmentalize cellular processes ("liquid-ordered" phase) surrounded by glycerophospholipids domains ("liquid-disordered" phase). This segregated region is packed more tightly than glycerophospholipid region of membrane, as a result of the interactions between long, saturated acyl chains of sphingolipids. Raft domains contain a variety of different proteins and receptors, what provides stability and important functions of the cells [22-23].

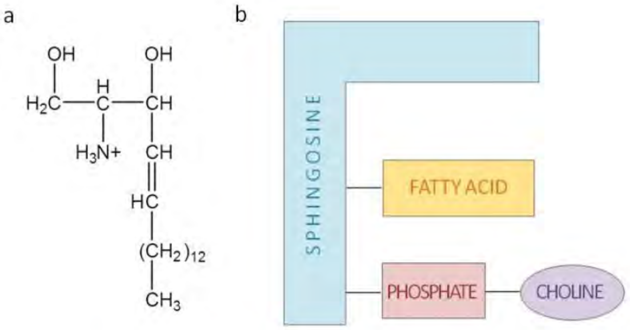

Figure I.4 Chemical formula of sphingosine (a) and block diagram of the sphingophospholipid's structure

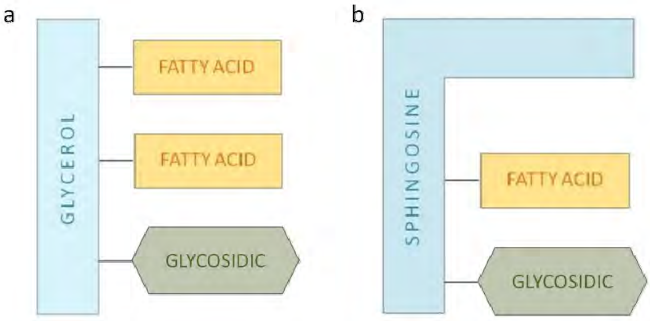

Figure I.5 Block diagrams of the glyceroglycolipids (a) and sphingoglycolipids (b) structures.

Glycolipids (lipid-sugar conjugates) are lipid molecules with mono- or poli-saccharides attached at the headgroup region. Block diagrams of glycolipids: glyceroglycolipids and sphingoglycolipids are shown in Figure I.5. They are involved in the blood type antigens (determine the blood groups) and act as receptors at the surface of the blood cells. Glycolipids are also the markers for cellular recognition.

Cholesterol (see Figure I.6) play a structural role in the membranes and in lipid metabolism.

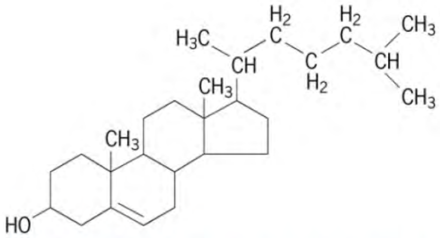

Figure I.6 Chemical formula of cholesterol.

Cholesterol is a biosynthetic precursor of vitamin D, bile acids and steroid hormones, like glucocorticoides, progesterones, oestrogens, androgens and aldosterone. Cholesterol contributes to the development and functioning of the central nervous system, therefore, brain contains more cholesterol than any other organ. Cholesterol regulates activities of many membrane proteins. The main function of cholesterol in the membrane is to modulate its fluidity by interacting with phospholipids (phosphatidylcholine and sphingomyelin). The presence of cholesterol increases the ordering (cohesion and packing) in the membranes, leading to formation of a “liquid-ordered” phase.

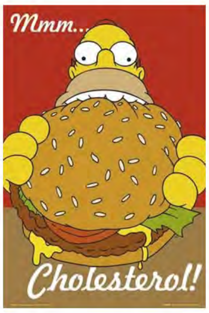

2.1 Diversity of Phospholipids

2.1.1 Phospholipids in Cells and Tissues

All cell membranes in different tissues have distinctive compositions of lipids. For example, cardiolipins and sphongomyelins are usually present in mitochondria and are rarely found in any other membranes. Differentiation of lipid composition in various cells and tissues of rat is summarised in the Table I-1 [24].

Lipid class	Heart	Liver	Erythrocytes	Plasma
Cholesterol	4.1	5.4	30.2	5.7
Phosphatidylethanolamine	33.4	19.9	20.8	
Phosphatidylinositol	3.7	4.4	3.4	
Phosphatidylserine			3.1	
Phosphatidylcholine	38.6	55.2	32.0	24.1
Sphingomyelin	1.8	2.1	8.2	2.0

Table I-1 Approximate percentage values of lipid composition of major lipid classes in rat heart, liver, erythrocytes and plasma based on [24].

The differences between lipid composition in the different cell types are huge. For example, the highest content of cholesterol is observed in the membrane of erythrocytes. Phosphatidylethanolamine and phosphatidylcholine dominate in the heart cell membranes. More than half of liver lipid composition is phosphatidylcholine.

2.1.2 Polar Heads

The lipids are also heterogeneous in terms of their polar heads, which include: choline, ethanolamine, serine, inositol, glycerol or phosphatidylglycerol (cardiolipin which is an important component of inner mitochondrial membrane) see Table I-2.

Glycerophospholipid	Name of substituent	Formula of substituent
Phosphatidic acid		$-H$
Phosphatidylethanolamine	Ethanolamine	$-(CH_2)_2 - N^+H_3$
Phosphatidylcholine	Choline	$-(CH_2)_2 - N^+(CH_3)_3$
Phosphatidylserine	Serine	$-CH_2 - CHCOO^- - N^+H_3$
Phosphatidylglycerol	Glycerol	$-CH_2 - CHOH - CH_2OH$
Cardiolipin	Phosphatidylglycerol	$-CH_2 - CHOH - CH_2 - PO_4^- - CH_2 - CHOCOR^1 - CHOCOR^2$

Table I-2 Types of the lipid polar head substituents

Phosphatidylcholine (PC) is the most abundant lipid in the membranes of animal tissues or plant membranes, but is rare in bacteria. This zwitterionic lipid is constituting a high proportion in the outer leaflet of the plasma membrane.

Phosphatidylethanolamine (PE or cephalin) is the second most abundant phospholipid in the animal and plant membranes and the major component of bacterial membranes. PE creates a more viscous membrane than phosphatidylcholine.

Phosphatidylinositol (PI) is a common negatively charged component of animal and plant membranes. PI play a major role in intracellular signalling.

Phosphatidylserine (PS) is an acidic lipid which is located mostly in the inner leaflet of animal and plant membranes. PS is a cofactor for the activation of many enzymes (e.g. protein kinase C). Phosphatidylserine is involved in the processes of blood coagulation and plays an important role in the cell apoptosis.

Cardiolipin or diphosphatidylglycerol is a phospholipid with a dimeric structure, which has four acyl chains. Cardiolipins are present mostly in mitochondria. Heart muscle is a tissue which is a reach source of cardiolipin. It plays an important role in the activation of enzymes.

Phosphatidic acid is a minor constituent of the cell membranes. It is used for biosynthesis of all other phospholipids.

2.1.3 Fatty Acids

Fatty acid tails of phospholipids are very diverse. They usually contain an even number of carbon atoms (between 14-24). The most common saturated fatty acid chains in nature contain 16 carbon atoms (palmitic or hexadecanoic acid), 18 carbons (stearic or octadecanoic acid) or 20 carbon atoms (arachidic or eicosanoic acid).

Linoleic and linolenic acids are essential fatty acids. They cannot be synthesised in animal tissues, thus they should almost always be present in the food. They are precursors of arachidonic, eicosapentaenoic (EPA) and docosahexaenoic (DHA) acids, which are vital components of all membrane lipids.

The presence of two different lengths of fatty acid tails in a single lipid molecule is common. Moreover, they can differ in their saturation (double bonded carbon atoms with *cis* or *trans* configurations); for example: 18 carbon fatty acid ($CH_3(CH_2)_7CH=CH(CH_2)_7COOH$) with *cis* isomerisation is the oleic acid, and with *trans* isomerisation is the elaidic acid. The equilibrium between saturated and unsaturated fatty acids is important since, for instance, it ensures the optimum degree of fluidity of the cell membranes. The presence of polyunsaturated fatty acids ensures a correct balance between rigidity and flexibility of membrane.

The common fatty acids of animal and plant tissues are presented in the Table I-3.

systematic name	trivial name	shorthand designation
	SATURATED FATTY ACIDS	
Tetradecanoic	Myristic	14:0
Hexadecanoic	Palmitic	16:0
Octadecanoic	Stearic	18:0
Eicosanoic	Arachidic	20:0
	MONOUNSATURATED FATTY ACIDS	
cis-9-hexadecenoic	Palmitoleic	16:1
cis-6-octadecenoic	Petroselinic	18:1
cis-9- octadecenoic	Oleic	18:1
	POLYUNSATURATED FATTY ACIDS	
9,12-octadecadienoic	Linoleic	18:2
6,9,12-octadecatrienoic	γ-linolenic	18:3
9,12,15- octadecatrienoic	α-linolenic	18:3
5,8,11,14-eicosatetraenoic	Arachidonic	20:4
5,8,11,14,17-eicosapentaenoic	EPA	20:5
4,7,10,13,16,19-docosahexaenoic	DHA	22:6

Table I-3 The common fatty acids of animal or plant origin. Based on [18]. Shorthand designation – the number before the colon specifying the number of carbon atoms, ant that after the colon, the number of double bonds.

Within the cells, fatty acids can modify activities of such enzymes as protein linases. They are also involved in regulating gene expression or are the messengers in many cellular processes.

2.2 Self-Assembly of the Lipids

The lipid molecules naturally self-assemble into complex structures when embedded in polar solvents. It is the result of the amphiphilic character of the phospholipids and the hydrophobic effects [25]. The lipid molecules tend to expose the polar groups toward the aqueous phase and minimize interaction of their hydrocarbon chains with water.

Different geometries between the hydrophilic and hydrophobic parts of the phospholipid molecule cause a differentiation of aggregated structures (see Figure I.7). The packing parameter P is a useful to characterize such structures [26]. It is expressed as:

$$P = \frac{v}{a \cdot l} \tag{1}$$

where v is the volume of the hydrophobic part, a is area occupied by the headgroup and l is the maximum hydrocarbon chain length. The values of P are connected with particular aggregate structures, e.g. when $P < 1/3$ (conical shape of the molecule) spherical micelles are created, when $1/2 < P < 1$ (cylindrical shape) vesicles and bilayers are formed and if $P > 1$ inverted hexagonal phases are formed (see Figure I.7). The cylindrical shape of phosphatidylcholine, which is the most abundant lipid in the membrane, does not induce curvature. Moreover, an increased concentration of coneshaped lipids or/and inverted cones in the lipid bilayer will increase intrinsic curvature of membrane, which may be required for membrane transport and fusion processes. Non-lamellar phases e.g. hexagonal phase is known to be important for the functioning of membrane proteins or for the membrane fusion process [27-28]. The magnitude of P is not constant for a given lipid molecule and could be also changed by pH, temperature, the presence of unsaturated fatty acid chains or electrolytes [29]. The most important phase from the biological point of view is the lamellar phase (where P = 1 and a planar bilayer is created) [30].

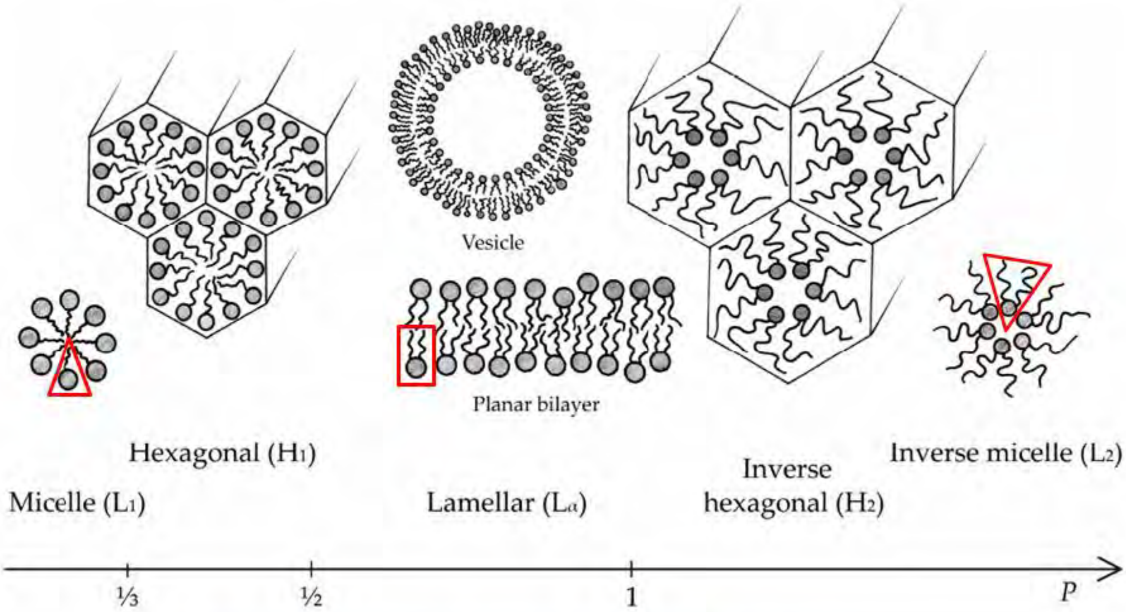

Figure I.7 The common structures of the amphiphilic aggregates.

2.3 Aggregated Structure of Lipid - Vesicle

Liposomes, which are biocompatible, noimmunogenic and easy to produce, are the most common models for cell membranes for experimental studies. Liposomes are widely used in pharmacy, cosmethology and medicine for drug delivery, building biosensors or medical nanodevices.

The liposomes are spherical vesicles build of mono- or multilamellar lipid bilayers. These Multilamellar Vesicles - MLVs - can be used for obtaining the Small Unilamellar Vesicles - SUVs – (diameter 30-70nm) by sonification process. The Large Unilamellar Vesicles - LUVs – (diameter 100-1000nm) are prepared by extrusion thought polycarbonate filters with small pores [31]. They are the most often used liposomes for experimental techniques. They were used for experimental part of this study. Special type of lipid vesicles are Giant Unilamellar Vesicles - GUVs – (diameter 5-200μm) which are prepared by electroformation method. GUVs are generally used for study of lateral lipid organisation [32-33].

2.4 Aggregated Structure of Lipid - Bilayer

Lipid bilayer is thin membrane made of two layers of lipid molecules. It could be separated to two regions: hydrocarbon tails and the head groups. However, a finer description was proposed by Marrink and Berendsen [34]. In that model, the bilayer is divided into "four – regions" (see Figure I.8). The first region is called "perturbed water". It starts at the place where bulk water molecules interact with the surface of lipid bilayer and ends where the densities of water and lipid are comparable. The second region – "headgroup" is formed at the phospholipid heads level: carbonyls, glycerols, phosphates and cholines. The third region – "soft polymer" starts at the carbonyl groups and ends where the density of the chains is comparable to liquid hexadecane. The fourth region – "decane", include the hydrocarbon tails of lipid molecules and is almost completely hydrophobic. Its low density is comparable to decane. The first two regions are part of the membrane headgroup region. The regions 3 and 4 are part of the hydrophobic interior.

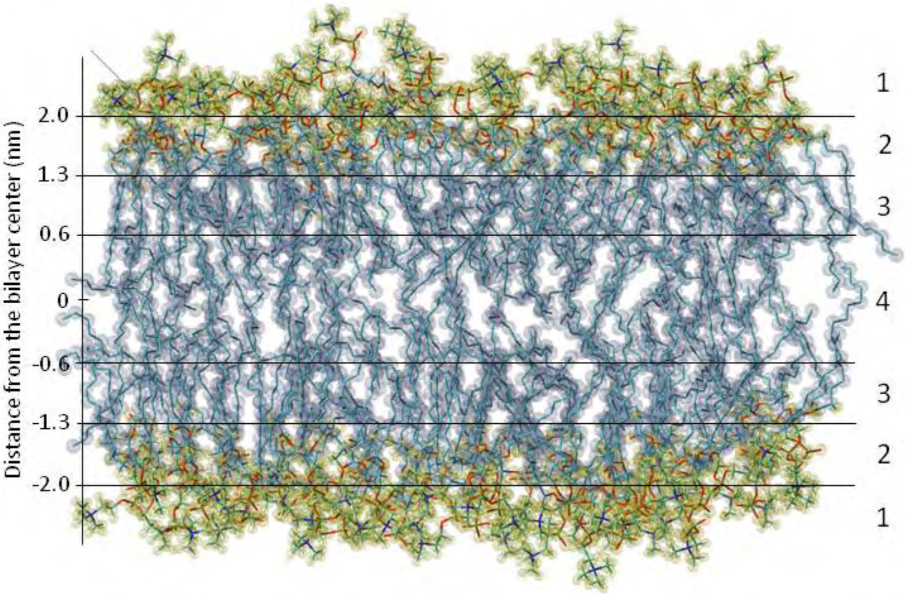

Figure I.8 Snapshot of DOPC bilayer. Vertical lines indicate the boundaries between the different regions (see text for definitions).

2.5 Dynamics of the Lipid Membrane

2.5.1 Diffusion of the Lipids

The lipid bilayer is a dynamic structure. Dynamics of the lipid molecules in bilayer includes:

- the bond stretching or angle torsions (up to few picoseconds time scale)
- wobbling and tilt motions of headgroups (nanoseconds time scale)
- rotation of lipids around their principal axis (tens of nanoseconds time scale)
- lateral diffusion (tens of nanoseconds to second time scale); see Figure I.9

- flip-flops (hours time scale); see Figure I.10.

Lateral diffusion of membrane lipids is considered to be spontaneous and quite fast in comparison with flip-flop. The velocity of the lipid is approximately 0.2mm/s. Transverse diffusion (flip-flop) involves movement of lipid molecule from one bilayer leaflet to the other. Flip-flop process is slow because relatively large amount of energy is needed for a polar head to cross the hydrophobic part of the bilayer.

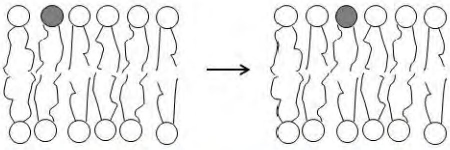

Figure I.9 Schematic representation of lipid lateral diffusion process.

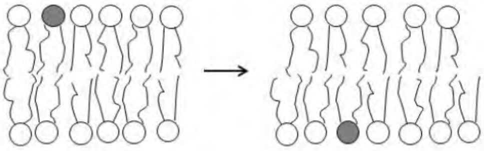

Figure I.10 Schematic representation of transverse diffusion process (flip-flop).

2.5.2 Fluidity of Bilayer

Fluidity of lipid membrane determines many bilayer properties, e.g. signal transmission, permeability. Fatty acids lengths, compositions and saturation of the tails affect the fluidity of lipid bilayer. Fatty acid chains can be ordered and rigid (crystalline phase, L_c) or disordered (liquid crystalline phase, L_α). Between these two phases is the gel phase($L_{\beta'}$), in which the chains tilt is reduced, see Figure I.11. The most common phase in living cells is liquid crystalline phase. Moreover, cholesterol is a regulator of membrane fluidity in animal cell membranes. Cholesterol increases membrane fluidity and decreases mobility of hydrocarbon tails of phospholipids.

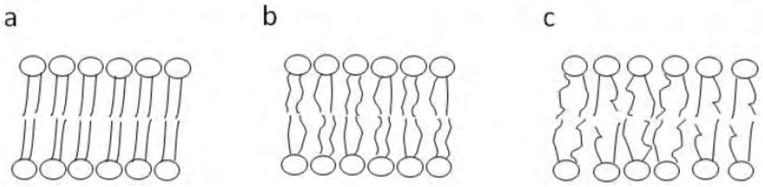

Figure I.11 Schematic representation of the structures of lamellar lipid phases: crystalline phase (a), gel (b) and liquid crystalline phase (c).

2.5.3 Permeability of Bilayer

Cell membranes are selectively permeable to different molecules through various processes (Figure I.12). Small and hydrophobic molecules (e.g.: CO_2, O_2, N_2, benzene) and small, uncharged and polar molecules (like: glycerol, ethanol, water) can diffuse passively through a lipid bilayer. Large, unchanged and polar molecules (like aminoacids, glucose, nucleotides) and the ions are not able to pass through the cell membrane spontaneously. Such substances, which have low permeability through bilayers, require proteins to carry them across cell membranes, by either passive or active transport.

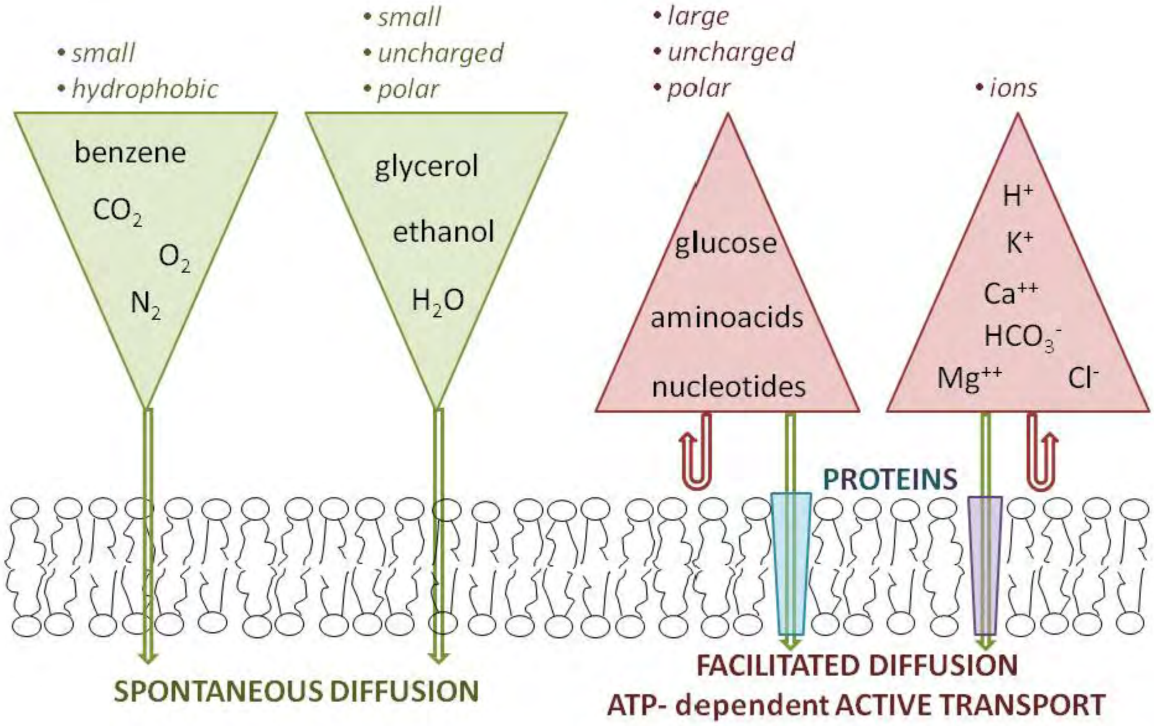

Figure I.12 Diagram of membrane permeability.

2.5.4 Asymmetry of the Membrane

Distribution of lipids in inner and outer leaflets of the eukaryotic membrane is asymmetric. Phosphatidylcholine (PC) and sphingolipids are usually located in the outer leaflet of cell membranes. Cholesterol is present in roughly equal proportions in both leaflets. Phosphatidylethanolamine (PE) and anionic phospholipids (phosphatidylinositol (PI) and phosphatidylserine (PS)) occur mostly in the inner leaflet. The differences in lipid composition in the leaflets are used by the cell to transport through the membrane, different enzymatic activities in the outer and inner membrane surfaces and position and stability of the proteins in the membrane.

2.5.5 Membrane Electrostatics

The membranes are mostly composed of zwitterionic lipids and are surrounded by ionic solutions. This causes that all electrostatic interactions between charges which are presented near and at lipid bilayer surface play a crucial role in many biomembrane processes like stability, flexibility, fusion, permeability and energy production and utilization. The transmembrane potential difference arises from a charge imbalance of salt ions across the plasma membrane. Three major components of membrane potential are distinguished: the dipole potential Ψ_d, the surface potential Ψ_s, and transmembrane potential Ψ_t (see Figure I.13).

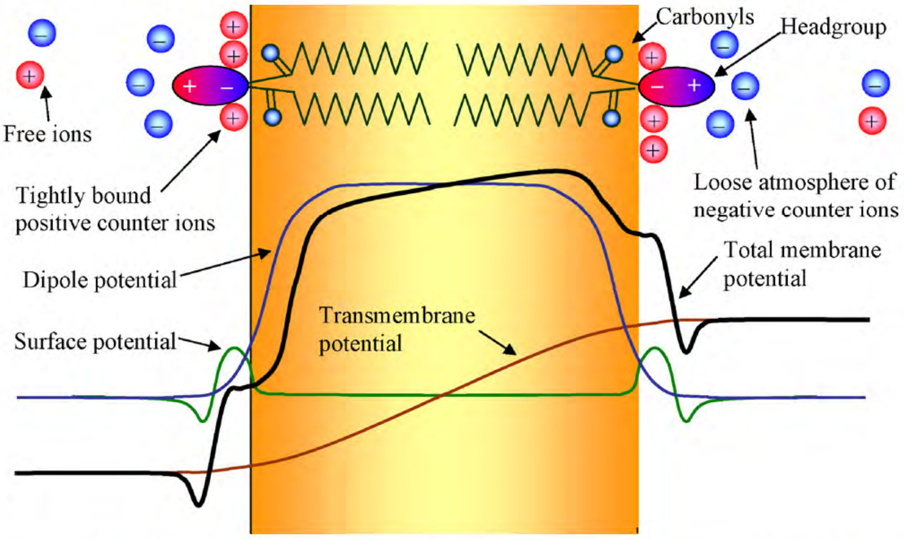

Figure I.13. The scheme of the lipid bilayer (orange region corresponds to hydrophobic core of the bilayer) with marked total membrane potential profile (black curve) with three components: the dipole potential (blue curve), the surface potential (green curve) and transmembrane potential (red curve). From [35].

2.5.5.a Dipole Potential

The dipole potential Ψ_d is formed between the hydrated lipid heads at the membrane surface and the low-polar hydrophobic core of the lipid bilayer. The dipole potential arises from the aligned dipoles ($P^- \rightarrow N^+$), which are created between phosphate (P) and choline (N) groups of phospholipid molecules, with the water dipole moments participations (see Figure I.14).

The membrane dipole potential weakly depends on the ionic composition of the surrounding medium. Therefore the origin of the Ψ_d is due to the orientation and magnitude of the dipoles in the bilayer structure. The dipole potentials at the two monolayers of bilayer create a strong virtual positive charge in the bilayer center. Such a distribution of interaction creates a strong energy barrier for the penetration of ions.

It was determined by MD simulations [36] that the dipole potential increases from ~600mV in neutral lipids bilayer to ~1000mV in the mixed (neutral and charged) bilayer. This values are much higher than experimentally obtained (200-350mV). The dipole potential obtained by experiments with hydrophobic (lipophilic) ions (the class of charged molecules, which readily permeate lipid bilayer, for example: tetraphenylborate) is probably underestimated [37] and the dipole moments obtained by MD simulation is overestimated by inaccuracies arising from conventional non-polarizable force fileds.

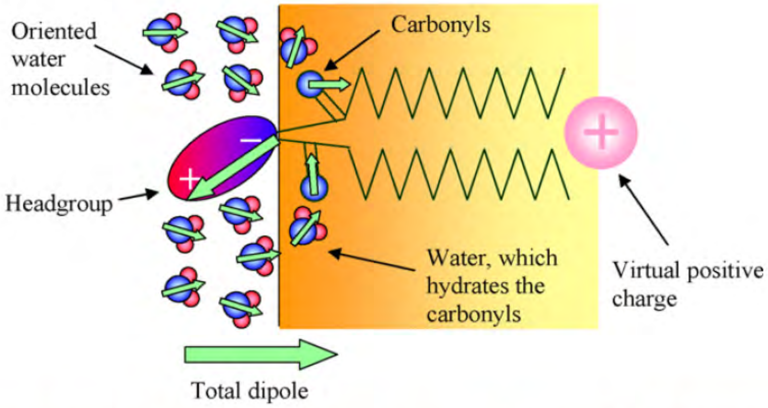

Figure I.14 The schematic illustration of the origin of dipole potential. The magnitude and orientation of the dipoles are marked by green arrows. From [35].

2.5.5.b Surface Potential

The membrane surface potential Ψ_S is created by the charges located at the water-lipid interface of lipid bilayer. It includes the charges of the lipid head groups and absorbed ions and counter ions, which reside in the vicinity of the head groups on both sides of the membrane (see Figure I.15). The surface potential depends on the type and amount of the charged lipids in the bilayer and the proton concentration (pH) and of ions.

The surface potential plays important role in the bilayers that contain charged lipids. The uncompensated charge at the membrane surface alters significantly the counter ion distribution and changes the electrostatic potential across the membrane. The different lipid composition of the leaflets of bilayer causes the difference of the surface potentials between two monolayers. It creates a significant force for the permeation of charged molecules . The interacellular leaflet of cell membrane is commonly composed of anionic lipids and this fact suggests that surface potential may play an important role in the transmembrane transport in living cells.

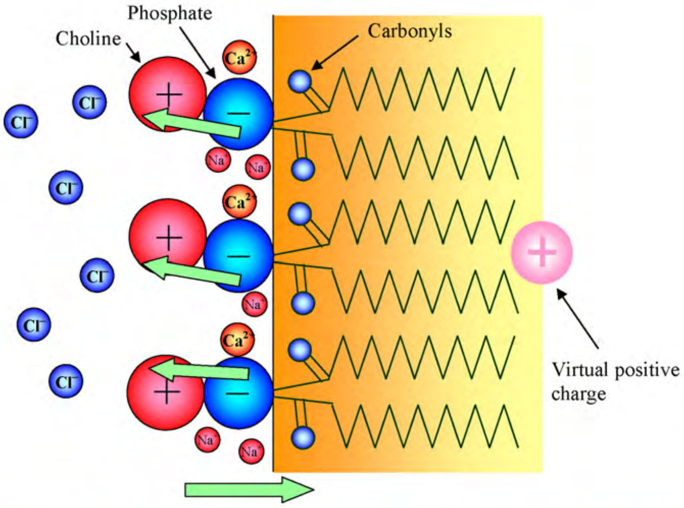

Figure I.15 Schematic distribution of ions at the surface of lipid membrane. The magnitude and orientation of the dipoles of the head groups and total dipole are marked by green arrows. From [35].

2.5.5.b(i) *Transmembrane Potential*

The transmembrane potential Ψ_t is the voltage (the difference of electrostatic potentials) between two liquid phases separated by the membrane. It electric field gradient is estimated to be of $2.5x10^7$V/m.

The interior of the cell has a negative voltage of almost a tenth of a volt lower with respect to the outside (typically about -70mV). It is formed mainly by a gradient of potassium, sodium and chloride ions, which is the result of their active transport process. The changes of the transmembrane potential (hyperpolarisation and depolarisation) play a main role in many physiological processes like action potential, ion channel gating and muscle contraction.

2.5.6 *Hydration of Lipid Membrane*

Water present into and near the membrane has different properties than the bulk water. Amphiphilic character of lipid molecule induces a gradient of the water concentration in the bilayer. Water concentration decreases drastically when approaching the hydrophobic center of membrane. Figure I.16, shows typical water density profile [3].

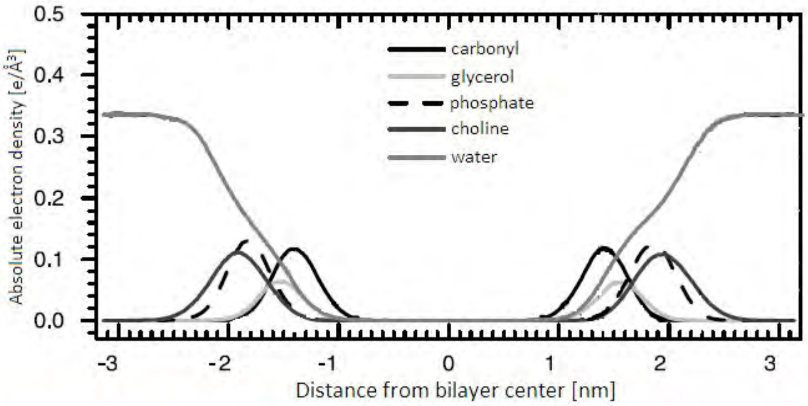

Figure I.16 Water density profile in DOPC bilayer, calculated by Scott Feller and published by [3].

We will see in the following (section I3.1) that a steep decrease of water concentration at the headgroup region of the lipid bilayer is very important for solvent relaxation response of headgroup-located fluorescent probes, which are sensitive to water concentration.

Water dynamics is also different near lipids with respect to the bulk. Generally, water molecules motions, like translational and orientational, are considerably slowed down comparing to the bulk water. Otherwise, the strength and lifetime of H-bonds are changed [34, 38] and the density of water increases [39] in the vicinity of lipid bilayer. Part of water-water H-bonds are broken and replaced by water-lipids bonds. The presence of water creates additional network interactions that affect the stability of the membrane.

2.6 Ions Effect on the Lipid Membranes

The most abundant ions present in the aqueous medium, which surrounds lipid bilayer, are Na^+, K^+, Ca^{2+}, Mg^{2+} and Cl^-. These ions play a significant role in the living cells by modulating the balance of lipid membrane surface [40], the dipole potential [41], the structure and dynamics of the lipid molecules [42-43], or intermembrane forces [44], the transition from micelles to vesicles [45] and the swelling of vesicles [46].

Franz Hofmeister proposed to classify salts according to their consistent effects on the solubility of proteins [14]. Anions were divided into two groups: those that salt-in (increase solubility) and those that salt-out (decrease solubility) proteins. The Hofmeister series order anions with increasing salting-in potency from left to right, as follows:

$$\underleftarrow{SO_4^{2-} > HPO_4^{2-} > OH^- > F^- > HCOO^- > CH_3COO^-} > \underrightarrow{Cl^- > Br^- > NO_3^- > I^- > SCN^- > ClO_4^-}$$

salt-out = kosmotropic anions   salt-in = chaotropic anions

Ions on the left of Cl^- reduce solubility of the proteins by inducing their crystallization and they are called salting-out, water-structure-makers or kosmotropic ions. Ions on the right of Cl^- are known as a salting-in, water-structure-breakers or chaotropic ions like I^-, SCN^- and ClO_4^-. These anions induce protein denaturation which usually leads to the increased solubility. The order of cations is usually given as:

$$\underleftarrow{Cs^+ > NH_4^+ > K^+ > Na^+} > \underrightarrow{Li^+ > Mg^{2+} > Ca^{2+} > La^{2+}}$$

salt-in = chaotropic cations   salt-out = kosmotropic cations

La^{2+}, Ca^{2+} and Mg^{2+} are extremely kosmotropic cations. Anions are generally known to give stronger 'Hofmeister' effect than cations.

The Hofmeister effect strongly depends on the ions kosmotropic/chaotropic properties, salt concentrations and the lipid headgroup charge [47]. The chaotropic anions experience a stronger attractive potential at the lipid membrane interface than kosmotropic anions. For cations, a more attractive potential for kosmotropic than for chaotropic cations was observed. The salt concentration effect was clearly visible and moreover, the saturation behavior was observed. Cations generate stronger effects at a negative surface, while anions at a positive one. The zwitterionic membrane represents an intermediate case.

The asymmetric distribution of lipids across a membrane is important for a variety of cellular functions. In the outer leaflet the most abundant class of lipids are phosphatidylcholines (PCs), while the inner leaflet is mostly composed of phosphatidylethanolamines (PEs) in eukaryotes. NaCl and $CaCl_2$ salts interact with zwitterionic PCs, which correspond to the outer leaflet of the plasma membrane. The PEs lipids are abundant in the inner leaflet of the membrane and face a major molar concentration of K^+ ions.

The effects of monovalent salts on lipid membrane are determined by the binding of ions to the lipid-water interface. Cations penetrate deeper into the water/lipid interface and form stable complexes with lipids. Whereas chloride anions mostly stay in the bulk water nearby the headgroups of lipids, sodium and calcium cations are able to penetrate into a membrane up to the carbonyl region. Characteristic time for binding is ~30 ns for Na^+ [48] and ~100 ns for Ca^{2+} [49]. The strongest interactions were observed for PC membranes with sodium cations. The strong Na^+/lipid binding leads to a decrease of the area per lipid. It causes also a more vertical orientation of the lipid heads and slows down the lateral mobility of lipids. The Na^+ binding increases the potential difference across a monolayer. K^+ ions bind weakly to the carbonyl region of PC membrane because of larger size of K^+ ion, which implies a smaller ionic surface charge. Therefore, the overall salt effect is much weaker in comparison with Na^+. The effect of NaCl and KCl salts on the PE membranes is much weaker than in the case of PC membranes. A primary amine in the headgroup of PE forms intra- and intermolecular hydrogen bonds which lead to a more densely packed lipids and inevitably restrict the binding of ions. Therefore, monovalent salts affecting lipid domains are able to decrease the difference in packing properties of lipids on the two sides of cell membranes [50].

3 Fluorescence Techniques

The fluorescence techniques are widely used in the studies of Biomembranes and are a very sensitive tool. The low (10^{-12}-10^{-11}M) concentration of non-toxic dyes makes the fluorescence methods almost non-invasive. Fluorescent markers are usually used to visualise or localise various biomolecules or biological structures. Fluorescence methods are also capable of investigating many important parameters of the membranes like, for example, local pH, environment polarity, concentrations of adsorbed molecules or ions, pressure or temperature [29, 51-54]. Among other things, dynamical and chemical quenching [55-59], energy transfer [59], dye adsorption [60-61], fluorescent lifetime distribution [55, 62], excimer formation [63] or the fluorescence anisotropy of hydrophobic bilayer interior [55] are used to study various properties of the lipid bilayer. The most common and simple fluorescent equipment, which allows registering the excitation and emission spectra, is the steady-state spectrofluorimeter. The analysis of excitation and emission spectra gives information about the fluorescent marker surrounding. For instance, the width of the spectrum often correlates with the heterogeneity of the probe's environment. Stokes shift measures the interaction between the probe and its surrounding. Time resolved fluorescence is used to measure fluorescence lifetime and gives opportunity to reconstruct the time resolved emission spectra (TRES).

3.1 Fluorescent Solvent Relaxation

Among other methods, fluorescent solvent relaxation (SR) technique is unique because of its ability to provide a direct information on mobility and hydration of lipid bilayer. The SR principle is simple and depicted in Figure I.17 (Jablonski diagram).

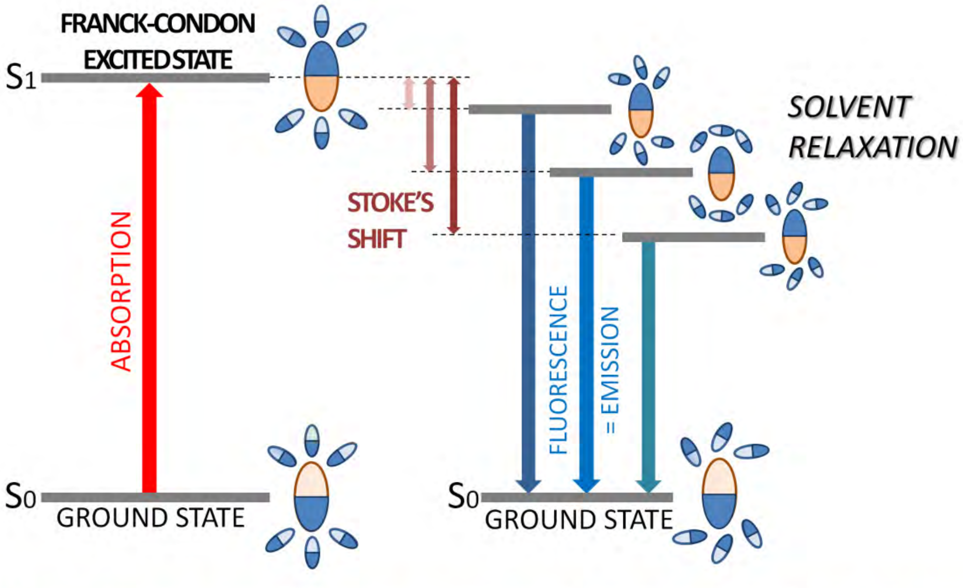

Figure I.17 Schematic diagrams presenting solvent relaxation around a probe. The reorientation motion of the solvent molecules leads to the lowering of the energy of the system resulting in the red shift of monitored TRES. For simplicity S_2 energy level is not shown in this diagram.

When fluorophore absorbs the photon (at femtoseconds time scale), its electron distribution is disturbed very fast. It drastically changes the direction and the value of the dipole moment of a dye. Fluorescent molecule goes from the ground state (S_0) to the singlet excited states (S_1 or S_2), usually to an excited vibrational level within S_1, which is called Franck-Condon excited state. The excess of the vibrational energy is rapidly lost to the solvent. If the fluorescent probe is excited to the second singlet state S_2, it rapidly relaxes to the S_1 state due to the internal conversion. The rotation or translation of the solvent molecules around the dye do not occur at the same time scale as excitation and take picoseconds or nanosecond. An equilibrium between the dye and the solvent molecules in the ground state was perturbed by excitation, therefore, solvent molecules are forced to adapt to the new orientation of the probe dipole moment and start to reorient in order to reach the free energy minimum. The solvent/dye interaction changes the Franck-Condon energy of emission and produces the shift of the energy level: so-called red-shift or Stokes shift in the emission spectra. The electronic excitation is energetically unfavourable and fluorophore relaxes to the ground state with spontaneous light emission from the singlet excited state S_1. The dynamic process starting from the non-equilibrium Franck-Condon state to the fully relaxed state is called Solvent Relaxation (SR). The increasing of the solvent polarity decreases the energy of relaxed state and increases the red-shift of emission spectra (also named Stokes shift). Energy losses between excitation and emission are observed for fluorescent molecules in solutions. One common cause of the Stokes shift is a rapid decay to the lowest vibrational level of S_1. Moreover, fluorescent dyes generally relax to higher vibrational level of the ground state. In addition to these effects, fluorescent markers can demonstrate further Stokes shift due to solvent effects, excited state reactions, complex formation, and energy transfer. The effect of solvent environment on fluorescence spectra are complex. Spectral shifts result from the solvent polarity whereby the energy of the excited state decreases with increasing solvent polarity.

The most common method for extracting the solvent relaxation information from the fluorescence signal is the analysis of the time-resolved emission spectra (TRES) of suitable fluorescence probes.

The analysis of the TRES permits extracting the solvent relaxation information from the fluorescent decay signal. TRES are received from the spectral reconstruction method [5]. Fitting by a log-normal function can give the position of the maxima of spectra $v(t)$ and their full widths at half maxima (FWHM). The total spectral shift (i.e. how far the emission spectrum is shifted during the process) and its kinetics (i.e. how fast the spectrum is shifted) can also be extracted from TRES.

3.1.1 Total Spectral Shift

The first information usually extracted from TRES is the overall shift $\Delta\nu$ which describes the difference between the energies of the Franck-Condon excited state and the fully relaxed state, which are proportional to $\nu(t=0)$ and $\nu(t=\infty)$ respectively [5] and is defined as:

$$\Delta\nu = \nu(0) - \nu(\infty) \tag{2}$$

The total spectral shift is proportional to the polarity of the dye surrounding [5] and reflects the extent of the lipid bilayer hydration. Overall shift $\Delta\nu$ usually reflects the degree of hydration of the membrane at the position where the chromophore is located.

3.1.2 Spectral Shift Kinetics

The kinetics of the spectral shift strongly depends on the mobility of the system (i.e. rotational motions of the molecules).

The correlation function is a second parameter obtained from the TRES, and is calculated as:

$$C(t) = \frac{\nu(t) - \nu(\infty)}{\nu(0) - \nu(\infty)} = \frac{\nu(t) - \nu(\infty)}{\Delta\nu} \tag{3}$$

The correlation function $C(t)$ can be analysed and compared in various ways in order to obtain a numerical parameter characterising the speed of relaxation of the solvent molecules. The relaxation time describes the mobility of the solvent molecules and reflects the viscosity of neat solvents [5]. Water in the phospholipid bilayer is fully bound to the phospholipid molecules at the headgroup level. Therefore, the relaxation kinetics observed in the lipid membrane reflects motion of water molecules and also the membrane dynamics [13]. An integrated mean solvent relaxation time τ_r can be calculated as:

$$\tau_r \equiv \int_0^\infty C(t)dt \tag{4}$$

The measured solvent relaxation process is not monoexponential and often require 3 or more exponential components. The mean relaxation time for 3-exponential process can be calculated as:

$$\tau_{3exp} = \frac{A_1\tau_1^2 + A_2\tau_2^2 + A_3\tau_3^2}{A_1\tau_1 + A_2\tau_2 + A_3\tau_3} \tag{5}$$

where A_n is the *n*-th amplitude and τ_n the *n*-th time constant of the 3-exponential function.

3.1.3 Full Width at Half Maximum of Time Resolved Emission Spectra

The temporal behaviour of the full width at half maximum (FWHM) of the TRES gives an information about the time of observed solvent relaxation. Into phospholipid bilayer [64-65] and supercooled liquids [66] FWHM passes a maximum during solvent relaxation process. In homogeneous systems the FWHM decays monotonically. In systems, where the microenvironment of the dye is inhomogeneous, FWHM of TRES passes a pronounced maximum (see Figure I.18 blue line). This effect gives the origin for the method of checking how much of the fluorescent response was captured within the time-window of experiment. For example, if only a decrease of FWHM is visible (see Figure I.18 green line), than the early part of the relaxation process is beyond the time resolution of the equipment. It is also possible that the increase of observed FWHM is only detected (see Figure I.18 orange line). It means that lifetime of used marker is not enough to monitor the entire relaxation process.

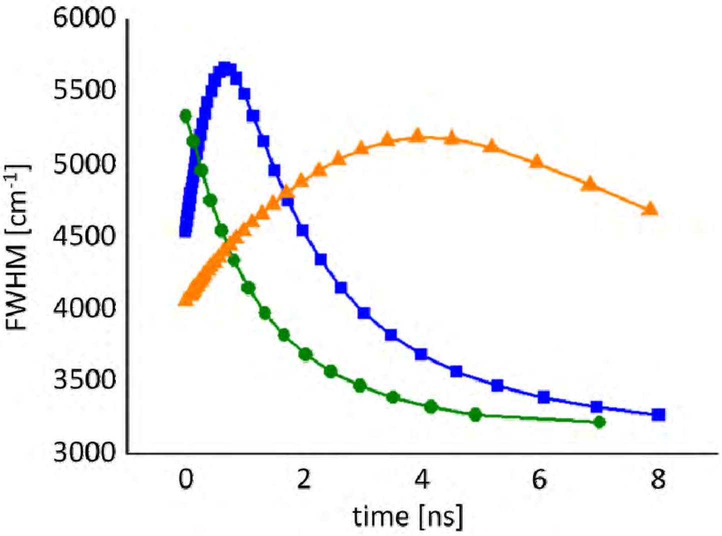

Figure I.18 The schematic representations of FWHM of TRES. See text for more details.

The examination of the time course of the FWHM is also an excellent tool to study whether a fluorescent marker has unimodal distribution in the bilayer and how wide this distribution is (i.e. bimodal distribution of dyes [54], probe relocalization upon addition of ethanol [67], or change of the hydrostatic pressure [68]). All of the above gives a reason why FWHM profiles should be studied in SR measurements very carefully.

3.1.4 Time-Zero Spectrum Estimation

For the spectral shift $\Delta\nu$ and the spectral response function $C(t)$ calculation, the position of the spectrum at time zero just after excitation has to be known.

The time-zero spectrum $\nu(0)$ is the hypothetical fluorescence emission spectrum of a fluorophore which is vibrationally relaxed and emits before any nuclear solvent motions occur. This spectrum cannot be measured directly due to the finite temporal resolutions of any equipment. It can be, however, estimated by measurements in a non-polar solvent by using absorption and the steady-state emission spectra [69]. The spectra measured in a non-polar solvent (for example in hexane) are used to simulate spectral properties of the Franck-Condon state.

The adsorption $A_{ref}(\nu)$ and emission $F_{ref}(\nu)$ spectra in non-polar solvent are measured and used to calculate the two lineshape functions:

- excitation lineshape function $g(\nu) \propto \frac{\mathrm{A_{ref}}(\nu)}{\nu}$
- emission lineshape function $f(\nu) \propto \frac{\mathrm{F_{ref}}(\nu)}{\nu}$

The absorption spectrum $A_p(\nu)$ of the dye located in the polar examined system has to be measured. When the $A_p(\nu)$ is known, it can be used to fit the shift distribution $p(\delta)$ between $A_p(\nu)$ and $g(\nu)$. Once the shift distribution parameters are known, desired time-zero spectrum F_p can be calculated using $f(\nu)$, $g(\nu)$ and $p(\delta)$. When excitation is restricted to near the peak of the absorption and the underlying $g(\nu)$ is not too much structured, the estimation process can by simplified:

$$\nu_p(t = 0) \approx \nu_p(abs) - (\nu_{ref}(abs) - \nu_{ref}(em)) \quad (6)$$

where $\nu(abs)$ denotes wavelength for maximum of absorption and $\nu(em)$ for maximum of emission, subscript (p) stands for polar system of interest, and subscript (ref) for nonpolar reference. See Figure I.19 for the illustration of the method.

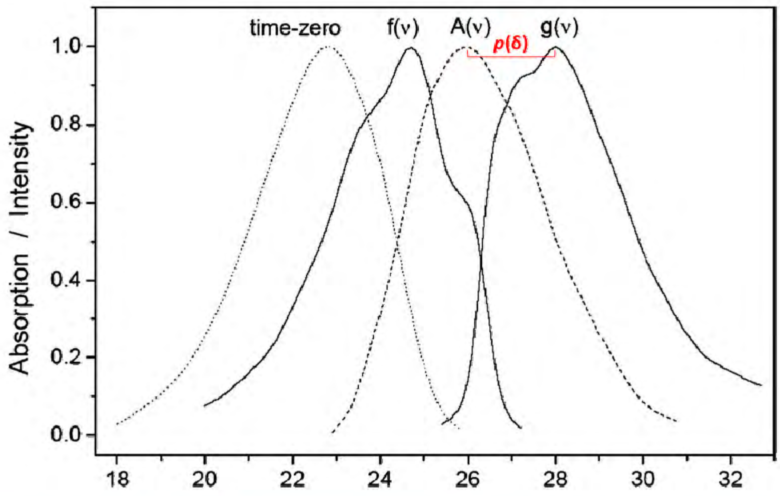

Figure I.19 The estimated time-zero fluorescence emission spectrum of 4-[(n-dodecylthio)methyl]-7-(N,N-dimethylamino)-coumarin (DTMAC) (dotted line) and the spectra used for its calculation: Absorption $g(\nu)$ and emission $f(\nu)$ lineshape functions (solid lines) obtained from data measured in cyclohexane and absorption spectrum $A_p(\nu)$ of the dye in DOPC LUVs (dashed line). All the spectra were measured at room temperature.

Knowing the proper position of TRES at time $t = 0$ not only allows calculating main SR parameters ($\Delta\nu$ and τ) correctly but also gives the percentage of the observed solvation kinetics. Time-zero estimation shows that the part of the process occurs faster than the time resolution of the apparatus and is therefore missed in the recorded data.

3.2 Solvent Relaxation Probes

The fluorescent probes are generally large organic molecules. However, only a part of the molecule is able to absorb the light by a small group of atoms which is called chromophore or fluorophore.

The solvent relaxation dyes, which are used for the lipid bilayer investigation, first of all should have a dipole moment that drastically change, during the excitation process. In addition, the chromophore must be incorporated into the lipid bilayer. It is necessary to know the exact location of the fluorophore in the membrane for characterising the relaxation properties. It is important to know where the fluorescence signal comes from (i.c. where the probe is located). Even small change in the depth of the fluorophore position can alter SR parameters drastically. A large polarity gradient exists along the normal axis of the membrane (see section I2.5.6). Therefore, SR kinetics usually changes from the value of hundreds of femtoseconds in the bulk water to few nanoseconds at the glycerol level [53, 70]. The solvent relaxation in the lipid membranes takes about 2 ns [70] and is four orders of magnitude slower than in bulk water, where the mean time is about 0.3 ps [71]. Furthermore, the structure and size of the marker should not have or have a low influence on the bilayer structure and cohesiveness. Finally, the quantum efficiency (or quantum yield, ϕ) a ratio of emitted to absorbed photons, should be high enough to keep low dye/lipid ratio. Using a series of probes with the same chromophore but with different tail lengths, located at different depths in the lipid bilayer, is generally very beneficial in terms of the spectral response from different points of the membrane. In the present work, we have used mainly naphthalene and anthroyloxy derivatives.

3.2.1 Naphthalene Derivatives

The naphthalene derivatives are commonly used in lipid membranes since they are polarity-sensitive fluorescent dyes. Following naphthalene derivatives: Prodan (*6-propionyl-2-dimethylaminonaphthalene*), Laurdan (*6-dodecanoyl-2-dime-thylaminonaphthalene*), Patman (*6-hexadecanoyl-2-(((2-(trimethylammonium)ethyl)methyl)amino) naphthalene*) and C-Laurdan (*6-dodecanoyl-2-*[N-*methyl*-N-*(carboxymethyl)*amino]naphthalene) were used in the present study (see Figure I.20). They have both an electron-donating dimethylamino group and an electron-accepting carbonyl group of a different fatty acid residue, separated by a naphthalene ring.

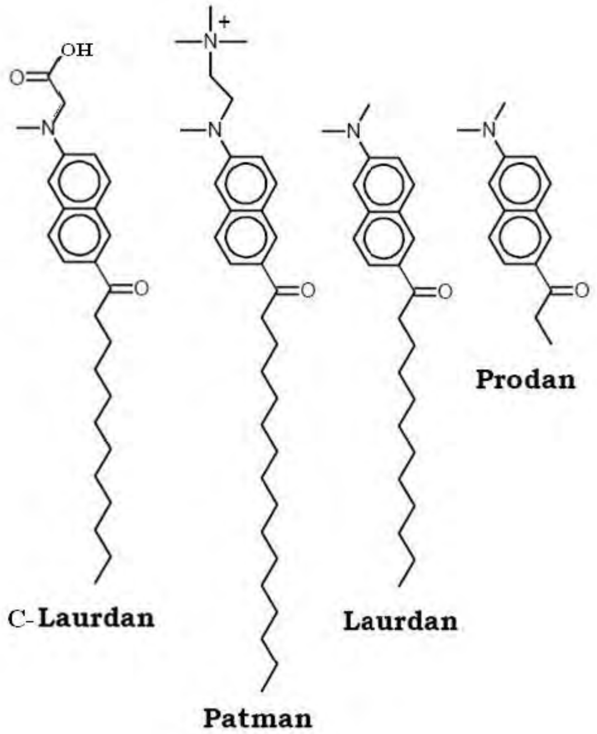

Figure I.20 Structures of the fluorescent probes: C-Laurdan, Patman, Laurdan and Prodan.

Prodan has a very short hydrophobic propionyl tail (3 carbons) therefore, the molecule is very mobile within the lipid membrane. Prodan is usually assumed to be located in the outermost region of the interface [72]. The location is however, poorly defined and locates in two distinct regions: one polar, at the interface and one less polar, at the glycerol level [7, 72-73]. Nevertheless, Prodan is successfully used for monitoring the solvent relaxation experiments.

Laurdan has a longer hydrocarbon tail (11 carbons)than Prodan, which anchors more the molecule in the hydrophobic part of the bilayer. Therefore, its location within the membrane is more stable in comparison to Prodan position. It was shown, that its chromophore stays at glycerol level of membrane, at the distance of 11.4 Å from the bilayer center [7].

Patman has a palmitoyl tail (15 carbons) and a positively charged ammonium group. Its location is stable and its movements are restricted [6] as it was shown by quenching method. Calculations show that it is located at 10.4 Å from the center of bilayer [7].

Carboxy-Laurdan (C-Laurdan) was recently synthesized by H.M.Kim [74]. C-Laurdan is a derivative of Laurdan, containing carboxyl group. C-Laurdan seems to have greater sensitivity to the membrane polarity, better water solubility, and more stable position in bilayer in comparison with Laurdan. C-Laurdan location in the lipid bilayer is still not determined experimentally.

3.2.2 Anthroyloxy Derivatives

The series of dyes, known as *n*-AS dyes (where *n* specifies the sequence number of the carbon atom to which the chromophore is fixed), with the anthroyloxy ring attached to the fatty acid chain at various positions (see Figure I.21), are useful for monitoring the solvation dynamics of the core region of lipid bilayer. These probes were reported to be located at well-defined depths along the normal axis of the bilayer [75-76]. They are able to investigate the water concentration profile of lipid bilayer.

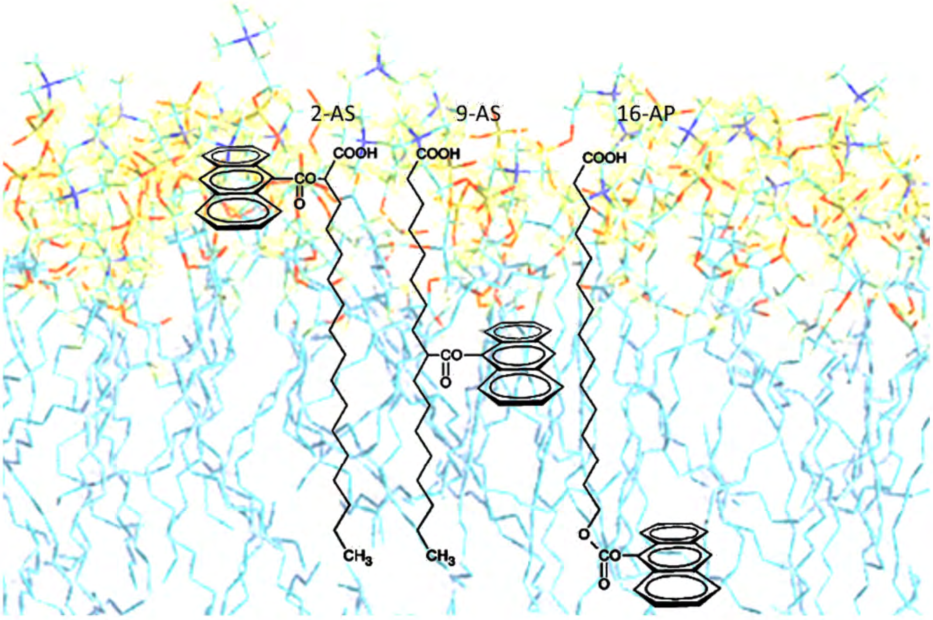

Figure I.21 Chemical structures of the fluorescent probes containing an anthroyloxy chromophore.

2-AS dye, which has anthroyloxy ring attached to the second carbon of stearic acid, has the fluorophore located at the distance 10.7 Å from lipid bilayer center. 9-AS is located at 8.8 Å from the center of bilayer. 16-AP, which has anthroyloxy ring attached to 16th carbon of the palmitic acid, is observed at 5.1 Å from the bilayer center.

3.2.3 Two-Colour Flavones-Based Fluorescence Probes

A very interesting group of fluorescent probes, that should be pointed here, are derivatives of the flavone. 3-hydroxychromone (3HC) and 3-hydroxyflavone (3HF) (see Figure I.22) are the examples of such probes, which exhibit excited-state intramolecular proton transfer (ESIPT) reaction (see Figure I.23) that generates two well-separated bands at different wavelengths in fluorescent spectra [77-80]. These probes can exist in two excited-state forms, normal (N^*), which is photo-excited initially and tautomer (T^*), which is the product of ESIPT reaction. Relative intensity of two bands depend strongly on the probe surrounding. Wavelength separation between N^* and T^* bands in emission is significant and in some cases exceeds 100nm.

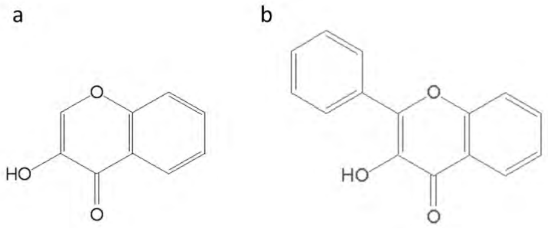

Figure I.22 Chemical structures of 3-hydroxychromon (a) and 3-hydroxyflavone (b).

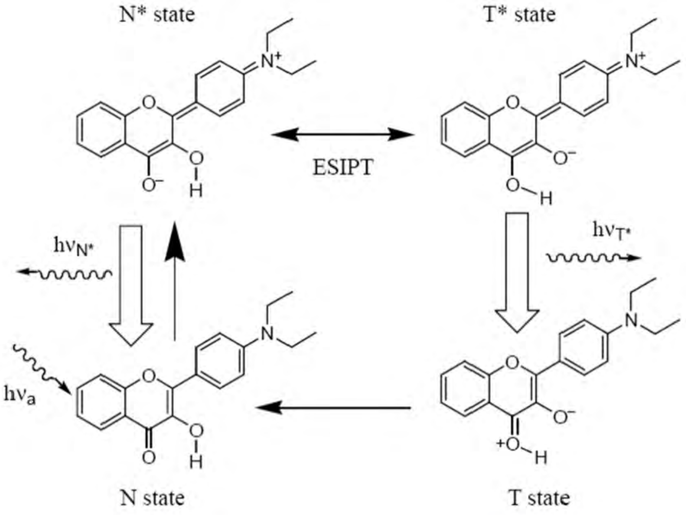

Figure I.23 The scheme of ESIPT reaction for 3HCs (the formula of 3HC derivative is presented as an example). From [81].

These probes are applicable to the probing of proteins, biomembranes and whole cells. The 3HC, 3HF and their derivatives were successfully used for incorporation into biomembranes [82-83]. They are sensitive to polarity, structural rearrangements [84], surface charge and hydration (formation of hydrogen bonds with water) [85-86] in phospholipid membrane vesicles. The 3HC and 3HF dyes have two types of localization in the bilayer. Those that form hydrogen bonds are located close to bilayer surface and those located deeper in the membrane without hydrogen bond formation. 3-hydroxychromone derivatives are able to detect many different compounds which changes the structure and dynamics of lipid bilayer like anesthetics, cholesterol [87] or ions [88].

3HC dyes are modified by adding the functional group for covalent labeling of proteins to using them as protein and peptide biosensors [89]. Derivatives of 3HC could be used as a protein ligands [90]. 3HC dyes are also successfully used for a single-cell imaging such as: cholesterol distribution [91] or changes in the surface potential [82, 86]. It is also possible to observe the cell apoptosis (programmed cell death) by using 3HC dyes. They are sensitive to the polarity and hydration of the membrane, which are changed during the early phases of apoptosis, when the anionic lipids are translocated from inner surface to the outer leaflet of cell membrane what causes the increase in the amount of negative charge at the surface of the membrane. Since changes in the distribution of anionic lipids were also observed on the surface of cancer cells, what providing the ability to monitor the effectiveness of anti-cancer drugs.

4 Numerical Tools

4.1 Goals of Numerical Simulations

Numerical simulations using HPC (high performance computing) facilities are frequently called *in silico* experiments. They allow understanding the properties of molecular assemblies based on their structure and microscopic interactions. They provide complementary information to classic *in vitro* and *in vivo* experiments and often uncover crucial information inaccessible otherwise. Numerical simulations at the molecular level are often considered as a bridge between what is happening at the atomic scale and the macroscopic world of the laboratory. To perform numerical simulations in biophysics, it is generally necessary to perform two major steps. The first is to validate the model of interaction which governs dynamics of the system. It could be achieved by using an available empirical force fields or by doing quantum mechanical (QM) calculations in order to build an appropriate one (see chapter I4.2). The second step is to solve coupled equations of the macromolecules motion in appropriate conditions like temperature and pressure (reduced to their nuclear coordinates) at times up to hundreds of nanoseconds. This is achieved by using molecular dynamics (MD) simulations either at quantum or classical levels of theory (see chapter I4.3).

4.2 Quantum Mechanics Calculation

Quantum Mechanics calculations are widely used to predict the structure (positions of atoms) and properties of studied molecule, for example absolute or relative energies, partial charges distribution and dipoles, vibrational frequencies. QM calculations can predict the molecular structure of the molecules, help in the efficient synthesis of compounds or design molecule that can interact specifically with other compound or system (catalysis or development of a new drug).

In the quantum calculations the Schrödinger equation is solved in order to determine the electronic wave function of the system or, more precisely, its electron density. Different approaches to solve the Schrödinger equation exist depending on the system under consideration and the degree of precision needed. In the simplest *ab initio* Hartree-Fock (HF) method (see I4.2.1 section), the repulsion energy between two electrons is calculated between an electron and the average electron density for the other electron. The Hartree-Fock method only evaluates the repulsion energy as an average over the whole molecular orbital. Therefore, the energies obtained by the HF method are usually larger than exact one and tend to an overestimated limit, called the Hartree-Fock limit. HF often gives satisfactory results but fails to describe delocalized electrons. In that case, the density functional theory (DFT) is much more appropriate. In DFT, the electrons are treated in terms of the density rather than independent particles. In this thesis, HF and DFT were mainly used depending on the system under investigation. The *ab initio* calculations were performed with Gaussian 03 software

[92]. The solution of the Schrödinger equation gives the electron wave functions together with the positions of the atomic nuclei. This defines unambiguously energy minimum structure of the system.

4.2.1 Hartree - Fock Method

Solving the Schrödinger equation of a quantum system requires a wave functions basis set. The Schrödinger equation is linear and thus any linear combination of solutions is also a solution. Unfortunately, it is impossible to obtain analytical solutions of the equations for systems of more than 2 or 3 electrons. A number of approximations need to be made in molecular Hamiltonian in order to solve the Schrödinger equation.

In 1927, Hartree proposed to factorize the wave function of the many-body system into a product of one-electron orthogonal and normalized wave functions and to solve the Schrödinger equation for each electron moving in the potential created by the other electrons and the nuclei. In 1930, Slater and Fock proposed an alternative to the Hartree method by approximating the wave function of a complex system of electrons by a Slater determinant of one-electron spin-orbitals. A broad basis set of functions is usually necessary to obtain reliable results, without unreasonably increasing the computation time. The basis set functions are mathematical expressions for atomic orbitals, which describe the portion of space where an electron can be found (generally centred on an atom). Initially, the atomic orbitals were described as strictly Slater orbitals, functions decreasing exponentially with the distance from the nucleus. But, from a mathematical point of view, an exponential function causes a number of problems, especially for the calculation of integrals in a system of more than two atoms. Now, the orbitals are usually approximated by linear combinations of Gaussians functions, typically three of them. This approach is easier to implement and faster to calculate, and not shows a significant loss of accuracy when the basis set functions are sufficiently large.

Note that there are many possible basis sets. The more complete they are, the results are more realistic. The simplest basis sets have the minimum number of basic functions needed to represent all the electrons of an atom. Hydrogen, for example can be described by a single Gaussian, for its single electron, which corresponds to the *1s* orbital. When the number of electrons increases, we need to attribute at least one basic function for each additional atomic orbital: *1s, 2s,* $2p_x$, $2p_y$, $2p_z$, *3s*...

For nonbonding orbitals energy is very sensitive to their position. Therefore, it is more rigorous to use a larger number of Gaussian functions to represent them. For valence orbitals, where electrons are involved in interatomic bonds, the electron density is delocalized among several atoms and thus loses its spherical symmetry. Their description can be improved in two ways:

a) by multiplication of the valence shell, where, for example two valence orbitals *s* instead of one and six orbitals *p* instead of three;
b) a polarization function can also be added to allow the deformation of the valence orbitals. That is to add additional functions to the valence orbitals of the higher secondary quantum number (*p* or *d* to the hydrogen atom, *d*, *f* and *g* for larger atoms).

Finally, the furthest electrons from the nucleus can be described by adding the diffusion function, which gives more space than the simple Gaussian. Diffuse orbitals are particularly important when the treated systems involve anions, where the probability of the presence of extra electron is much broader.

4.2.2 Density Functional Theory

The functional theory of the electron density (Density Functional Theory - DFT) is used in physics and chemistry to study the electronic structure of many-electron systems, including condensed phase. The DFT began to be popular in the 1970s. The cost of the calculations is relatively low compared to traditional methods, which are based on the wave function. Despite many code improvements over the last 40 years, there are still difficulties to adequately describe the intermolecular interactions, particularly the Van der Waals forces (dispersion of atoms), and the charge transfer during excitation (which is currently handled by time-dependent density functional theory - TD-DFT) or transition states of molecules.

4.2.3 Calculation of the Partial Charges

Apart from the energy and wave functions that are directly calculated, some other values, which are very important for the correct description of the electronic distribution, can be extracted from quantum calculations and implemented subsequently in MD force fields. One of the key parameter in the force fields is the intramolecular charge distribution, which is rather well determined and should represent the electronic partitioning between the two nuclei.

Although atomic charges are commonly used in physics and chemistry, their experimental availability is limited to the scanning tunnelling microscopy and the atomic force microscopy [93]. The method of the calculation depends mainly on the properties of the studied system. Thus, it is possible to determine the point charges by molecular dynamics simulation or Monte-Carlo simulations, aiming to reproduce the thermodynamic properties of a system. This simple method of iterative manner calculation, which gives a correct results, can only be applicable to the reduced size systems (few amino acids for example). Such a value can be estimated throughout the iterative calculation in order to converge the results of simulation with experience. The electrostatic properties are directly related to the electrons distribution and the position of the nuclei in a molecule, and it is also reasonable to consider point partial charges calculated by quantum mechanics. Many methods based on this principle have been proposed and their merits are still debated. However, some of them are more common because of their simplicity or effectiveness.

There are many methods for estimating the partial charges. All methods can be classified into one of four classes [94]:

1. *Class I charges* are those that are not determined from quantum mechanics, but from some intuitive or arbitrary approach. These approaches can be based on experimental data such as dipole moment of the molecules.
2. *Class II charges* are derived from partitioning the molecular wave function using some arbitrary, orbital based scheme.
3. *Class III charges* are based on a partitioning of a physical observable derived from the wave function, such as electron density.
4. *Class IV charges* are derived from a semiempirical mapping of a precursor charge of type II or III to reproduce experimentally determined observables such as dipole moments.

4.2.3.a Analyse of the Mulliken Charges

Mulliken charges arise from the principle of population analysis, which was originally proposed by Mulliken in 1955 [95]. Each molecular orbital (MO) φ_i can be considered as a linear combination of basis functions χ_r (atomic orbitals):

$$\varphi_i = \sum_r c_{r,i}\chi_r \tag{7}$$

and the electron density is written as:

$$|\varphi_i|^2 = c_{1,i}^2 + c_{2,i}^2 + \cdots + 2c_{1,i}c_{2,i}S_{12} + 2c_{2,i}c_{3,i}S_{23} + \cdots \tag{8}$$

where the terms S_{rs} are calculated by an integrals type $S_{rs} = \iint \chi_r\chi_s dv_1 dv_2$.

Mulliken suggested the following distribution: an electron MO φ_i contributes $c_{1,i}^2$ in the net population of χ_1, $c_{2,i}^2$ for the net population of χ_2, and $2c_{1,i}c_{2,i}S_{12}$ for the population overlap between χ_1 and χ_2 ... So, if there are n_i electrons in the φ_i MO, the net population will be $n_{r,i} = n_i c_{r,i}^2$ and the population recovery $n_{r-s,i} = n_i(2c_{r,i}c_{s,i}S_{rs})$. In the Mulliken population analysis, the charges are calculated by dividing the orbital overlap of two atoms involved equally.

This method is commonly used, but is strongly dependent on the basis set functions and molecule geometry. The Mulliken distribution of population can be justified for simple atomic orbitals, but becomes much more questionable in other cases, especially when the orbitals are delocalized.

It should be noted that the charges obtained by analysis of the populations often do not reproduce the electrostatic properties of molecule, and it is necessary to use more efficient methods, such as the derivation of charges from the electrostatic potential.

4.3 All-Atoms Molecular Dynamics Simulations

Molecular dynamics is in principle able to compute, from the laws of classical mechanics, the trajectories of atoms in crystalline phase, in solution or gas phase [96-98]. It therefore describes the evolution of a system over time. The system is considered as a set of atoms whose interactions can be described by a potential energy function, the so-called "force field".

4.3.1 The Force Field – Potential Energy Function

All MD calculations presented here where performed using CHARMM 27 force fields [99] implemented in NAMD 2.6 and 2.7 software [9]. In this force field the following empirical representation of the potential energy is described as follows:

$$U = \sum_{bonds} k_b(b-b_0)^2 + \sum_{angles} k_\theta(\theta-\theta_0)^2 + \sum_{dihedrals}\sum_{n} V_n[1+cos(n\varphi-\gamma)] + \sum_{i<j}\left[\frac{q_iq_j}{r_{ij}} - 2\varepsilon_{ij}\left(\frac{r_{ij}^*}{r_{ij}}\right)^6 + \varepsilon_{ij}\left(\frac{r_{ij}^*}{r_{ij}}\right)^{12}\right] \qquad (9)$$

This energy is composed of intra-and intermolecular contributions, described below.

4.3.1.a Intermolecular «Bonded» Interactions

The deformations of bonds and angles are modelled by harmonic oscillators. The potential energy of **deformation of the bonds** is expressed as :

$$U_b = \sum_{bonds} k_b(b-b_0)^2 \qquad (10)$$

where b is the instantaneous bond length (in Å), b_0 is the bond length (in Å) at equilibrium and k_b is the force constant (in kcal.mol^{-1}.Å^{-1}).

The **stretching of the angles** is expressed as :

$$U_a = \sum_{angles} k_\theta(\theta-\theta_0)^2 \qquad (11)$$

where θ is the instantaneous angle (in °), $\theta_0$is the equilibrium angle value (in °), and k_θ is the associated force constant (in kcal.mol^{-1}).

The **deformation of the dihedral angles** implies the geometry change of three bonds and four atoms A, B, C and D. The dihedral angle φ is the angle between the bonds AB and CD, and therefore allows the rotation around the bond BC. This energetic term of dihedral deformation contributes to the energy barrier encountered during the rotation around a bond. It is defined as follows :

$$U_d = \sum_{dihedrals}\sum_{n} V_n[1+cos(n\varphi-\gamma)] \qquad (12)$$

where V_n is the value of the rotation energy barrier (in kcal.mol^{-1}), γ the phase (in °) and φ is the instantaneous value of the dihedral angle (in °).

4.3.1.b Intramolecular «Non-Bonded» Interactions

All non-bonded interactions involve atoms belonging to the same molecule, but separated by more than three covalent bonds or to two different molecules. These interactions are described by two terms: a Lennard-Jones term, also known as terms of Van der Waals and electrostatic term, also known as Coulomb term.

4.3.1.b(i) Van der Waals Interactions

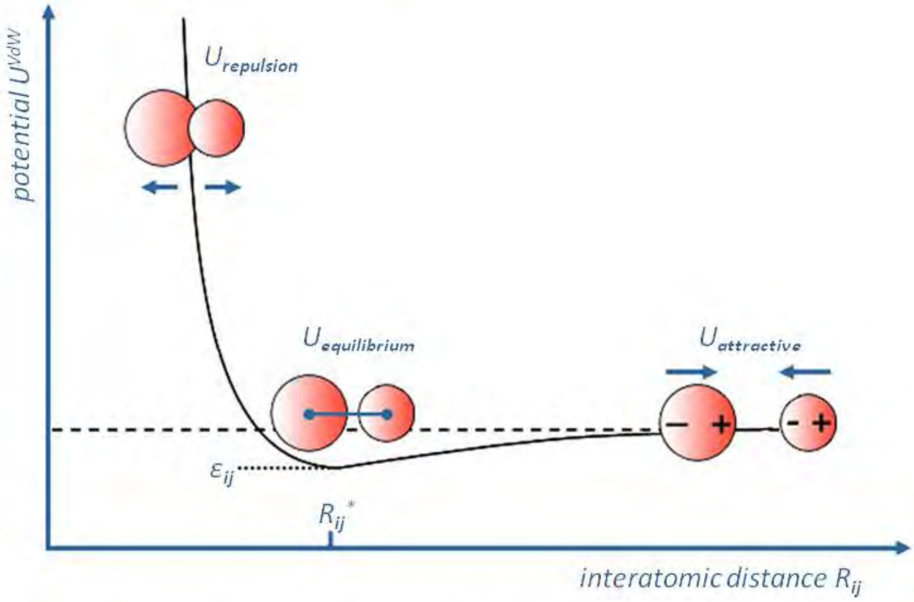

Figure I.24 The potential energy of the VAN DER WAALS interactions.

The Van der Waals interactions are represented by a potential energy U^{VdW}:

$$U^{VdW} = \sum_{i<j} \sum_{j} 2\varepsilon_{ij} \left[\frac{1}{2} \left(\frac{r_{ij}^*}{r_{ij}} \right)^{12} - \left(\frac{r_{ij}^*}{r_{ij}} \right)^{6} \right] \tag{13}$$

where ε_{ij} and r_{ij}^* are the Lennard-Jones parameters for the interaction between atoms i end j. ε_{ij} represents the minimum energy of the Van der Waals interaction at the equilibrium distance r_{ij}^* (see Figure I.24). The r_{ij}^{-6} represents the attractive interactions between two atoms and r_{ij}^{-12} is the repulsion part due to Pauli exclusion [100].

For the interaction of heteroatomic pairs (for two different atoms i end j), the effective values of Lennard-Jones parameters are calculated from the Lorentz-Berthelot mixing rules :

$$\varepsilon_{ij} = \sqrt{\varepsilon_{ii} \times \varepsilon_{jj}} \tag{14}$$

$$r_{ij}^* = \frac{r_{ii}^* + r_{jj}^*}{2} \tag{15}$$

This firstly allows for a maximum flexibility in the non-bonded interactions, and secondly, serves also to implement the excluded neighbours (atoms that are already interacting by some bonded potential) by simply setting these parameters to zero.

4.3.1.b(ii) Electrostatic Interactions

The Coulomb interactions are limited to interactions between partial point charges and written as:

$$U_{ij} = \sum_{i<j}\sum_{j}\frac{q_i\, q_j}{r_{ij}} \tag{16}$$

where q_i end q_j are the partial charges of the atoms i and j and r_{ij} is a distance between charges. As already explained above, these charges should sometimes be recalculated by *ab-initio* calculations (see chapter I4.2.3).

4.3.2 Evaluation of the «Non-Bonded» Interactions

4.3.2.a Cutoff Distance

The summation of non-bonded interactions is very costly in term of calculation time. For this reason, a cutoff distance is introduced. Cutoff distance represents the fixed, defined interaction distance, or distance within which non-bonded interaction will be directly calculated every time step. Beyond this distance, non-bonded interactions are ignored (see Figure I.25 and Figure I.28 for comparison).

4.3.2.b Double cutoff

The double cutoff method was introduced by Berendsen in 1985 [101], for reducing the calculation time of non-bonded interactions. Two radii: cutoff R_{C1} and R_{C2} are used (see Figure I.25).

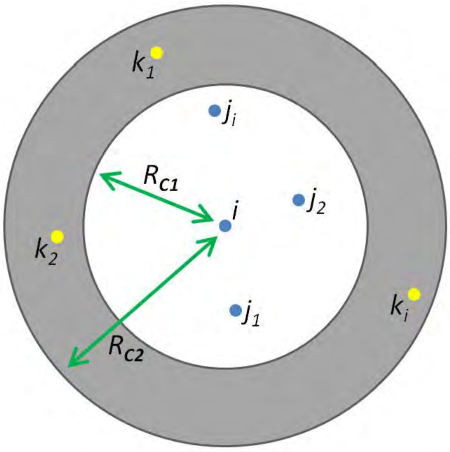

Figure I.25 The method of double cutoff.

For the atom i, the atoms j_n, which are present at the shorter distance than R_{C1}, are stored in the pair-list PL_i table and understood as a set of atoms j_n which have the non-bonded interaction with atom i. The energy of interaction of atoms k_n, for which $R_{C1} < r_{ik} < R_{C2}$ (gray zone, see Figure I.25), are stored in variable E_k^{ILD} called Long Distance Interaction.

At every step Δt of the dynamics, the energies of the non-bonded interactions are the sum of two contributions: the short distance interactions between i and PL_i calculated using the positions of the atoms in the time t, and the energy E_k^{ILD}, which is maintained constant for a defined number of steps Δt. PL_i and E_k^{ILD} are generally renewed every 10 to 50 steps of the dynamics.

4.3.2.c Long Distance Interactions

The sudden discontinuity of the energy at the *cutoff* distance causes artefacts in the motions, the conformations [102-104] or the calculated energies [105-109]. To correct such artefacts, it is possible to estimate the interactions beyond the *cutoff* (for example using EWALD summation), and at the same time to approach zero interaction for distances slightly below the *cutoff* (switching functions).

4.3.2.c(i) Summation of Ewald

The method of Ewald summation was described in 1921 [110] to improve the calculation of the electrostatic energy of the periodic systems and in particular the interaction energies in ionic environments. It assumes that a particle in the box (called cell) interacts with all other particles in the box and with all their images from the boxes located in an infinite matrix of periodic boxes, built by translation of the initial cell [96, 111]. At infinity, the overall shape of the system become quasi-spherical (see Figure I.26).

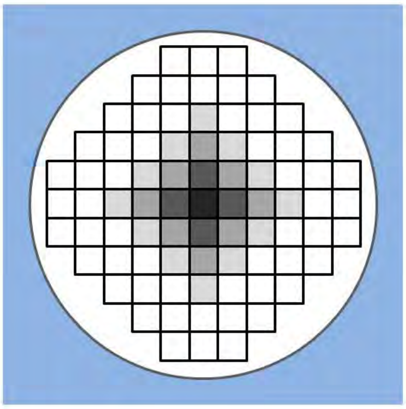

Figure I.26 The periodic cells system constructed by EWALD method.

Considering N particles in the box, at locations r_1, r_2 … r_N and possessing point charges q_1, q_2 … q_N, respectively, the expression of the Coulomb energy inside the box is as follows:

$$U = \frac{1}{2}\sum_{i=1}^{N}\sum_{\substack{j=1 \\ j\neq i}}^{N}\frac{q_i q_j}{r_{ij}} \tag{17}$$

The total Coulomb energy of interactions for this ions has to include the interactions between the periodic images:

$$U = \frac{1}{2}\sum_{|n|}^{\infty}\sum_{i=1}^{N}\sum_{\substack{j=1 \\ j\neq i}}^{N}\frac{q_i q_j}{|r_{ij} + n|} \tag{18}$$

where N is a number of charged atoms in the box, r_{ij} is a distance between the atoms i end j, q_i end q_j theirs charges, and n is a distance of the atoms from the central box; $n = n_x L_x + n_y L_y + n_z L_z$ where L_x, L_y, L_z are the dimensions of the cell.

4.3.2.c(ii) Particle Mesh Ewald (PME)

Particle-mesh Ewald is a method proposed by Tom Darden [112-113] to improve the calculation of the direct-space interactions within a finite distance using a Coulomb's Law and in reciprocal space using a Fourier transform to build a "mesh" of charges, interpolated onto a grid (see Figure I.27). It is from this charge interpolation that long-range forces can be calculated and incorporated into the non-bonded interactions in a simulated system.

The PME algorithm scales as $Nlog(N)$ is substantially faster than ordinary Ewald summation on medium to large systems.

In NAMD software the Particle Mesh Ewald (PME) method is implemented.

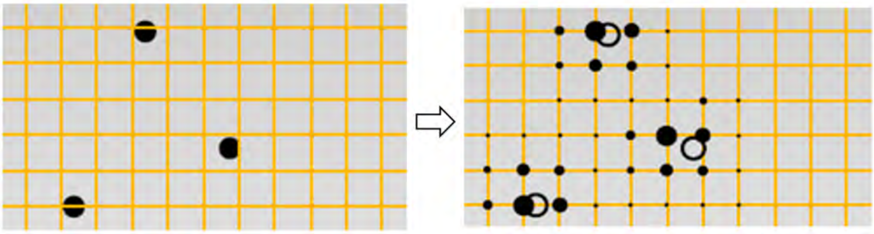

Figure I.27 Schematic representation of charges incorporation by the PMS method.

4.3.2.c(iii) Switching Functions

Two main methods exist for abridge the electrostatic terms and Van der Waals at cutoff. The first way is to vanish the forces beyond the cutoff distance. This method leads to a discontinuity in the force if the cutoff is too small or becomes very time consuming if the cutoff is very large. The second way is to use the switching functions. These functions allow a gentle smoothing of the forces and energies that are switched to zero between R_{on} and R_{off} (cutoff) to avoid discontinuity in the force. Thus, the value of switchdist must always be less than the cutoff (see Figure I.28).

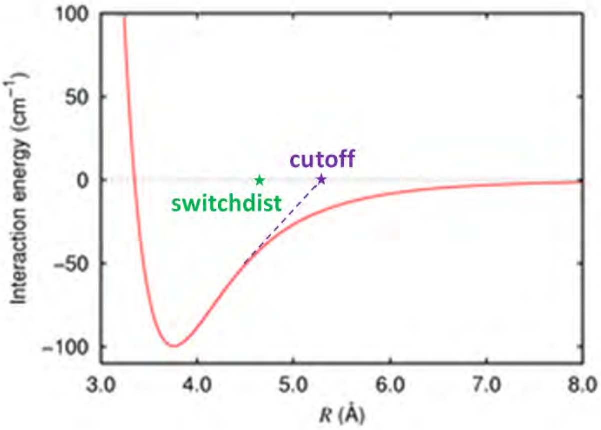

Figure I.28 Graph of Van der Waals potential with and without the application of the switching function.

4.3.3 *Energy Minimisation*

To avoid generating unphysical contacts it is necessary to minimize the potential energy of the system. For this, we used the default minimiser implemented in NAMD using either more sophisticated *conjugate gradient* method, or simpler algorithm of the *steepest descent*. Both methods are based on the derivative of the potential energy U with respect to the coordinates of each atom i:

$$\vec{F_i} = -\left(\overrightarrow{grad}U\right)_{\vec{r}_i} \tag{19}$$

Each atom is moved along the gradient exerted on it by following the slope of the energy hypersurface (see Figure I.29), which bring it to the closest local minimum from the initial configuration. However, this method does not ensure to converge all the system to the absolute energy minimum.

At each iteration k, the system of N atoms is described by a vector $\overrightarrow{X_k}$ of dimension $3N$. If we define a descent direction $\overrightarrow{S_k}$ and size of the displacement step λ_k, coordinates $\overrightarrow{X_{k+1}}$ at iteration $k+1$ are then:

$$\overrightarrow{X_{k+1}} = \overrightarrow{X_k} + \lambda_{k+1}\overrightarrow{S_{k+1}} \tag{20}$$

In the case of the method of the *steepest descent*, the direction of the slope $\overrightarrow{S_k}$ is defined by the unit vector:

$$\overrightarrow{S_k} = \frac{\overrightarrow{F_k}}{\left\|\overrightarrow{F_k}\right\|} \tag{21}$$

In the first step, λ is chosen arbitrarily, then it is increased (or decreased) according to the potential energy U decreases (or increases). This method is very effective for rapidly approaching a local minimum. It is used only at the beginning of minimization.

In the *conjugate gradient* method the gradient calculated at each step is combined with the preceding by the following:

$$\overrightarrow{S_k} = -\overrightarrow{grad}U + b_k\overrightarrow{S_{k-1}} \tag{22}$$

where b_k is the factor weighting the current and the previous gradients. The method of conjugate gradients is used to select successive search directions that eliminate repeated minimizations along the same direction.

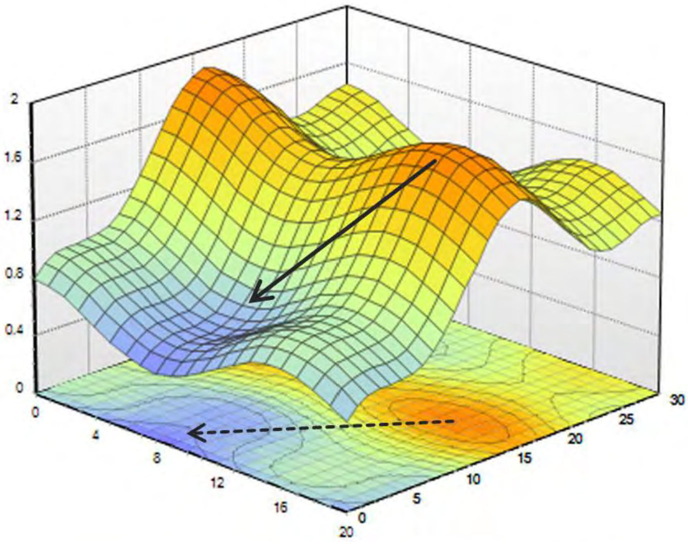

Figure I.29 Example of the energy surface. (From http://www.cyber-wit.com/images/gallery/surface1_b.png)

4.3.4 *Principles of Classical Molecular Dynamics*

Classical MD simulations provides information at the atomic level, introducing the positions (trajectory) and the velocity of the atoms over time. Simulations are calculated up to the nanosecond time scale, however simulations into the millisecond are also possible.

The MD simulation methods are based on Newton's second law :

$$\vec{F_i} = m_i \times \vec{a_i} \tag{23}$$

where $\vec{F_i}$ is the vector of the force extended on the particle, m_i is the mass of the particle and $\vec{a_i}$ is the vector of an acceleration.

The force is derived from the total potential energy U as :

$$\vec{F_i} = -\left(\overrightarrow{grad}U\right)_{\vec{r_i}} \tag{24}$$

4.3.4.a Solving Newton Equation: Verlet Algorithm

Solving a Newton equation for a large coupled system of atoms is not so simple. There are many analytical methods to cope with such kind of problems [97, 114]. All of them assume that the positions of the atoms and the dynamical properties of the system (position, velocity and acceleration) can be developed in Taylor series of the integration algorithms :

$$\vec{r}(t+\Delta t) = \vec{r}(t) + \Delta t \vec{v}(t) + \frac{1}{2}\Delta t^2 \vec{a}(t) + \frac{1}{6}\Delta t^3 \vec{b}(t) + \cdots \quad (25)$$

$$\vec{v}(t+\Delta t) = \vec{v}(t) + \Delta t \vec{a}(t) + \frac{1}{2}\Delta t^2 \vec{b}(t) + \frac{1}{6}\Delta t^3 \vec{c}(t) + \cdots \quad (26)$$

$$\vec{a}(t+\Delta t) = \vec{a}(t) + \Delta t \vec{b}(t) + \frac{1}{2}\Delta t^2 \vec{c}(t) + \cdots \quad (27)$$

where $\vec{r}$ is the vector of positions, $\vec{v}$ velocities and $\vec{a}$ accelerations.

We can also write an almost identical development to the interval $[t-\Delta t, t]$:

$$\vec{r}_i(t+\Delta t) = \vec{r}_i(t) + \Delta t \vec{v}_i(t) + \frac{1}{2}\Delta t^2 \vec{a}_i(t) + \cdots \quad (28)$$

In this case, the vector $\vec{r}_i$ at time $(t-\Delta t)$ is written as :

$$\vec{r}_i(t-\Delta t) = \vec{r}_i(t) - \Delta t \vec{v}_i(t) + \frac{1}{2}\Delta t^2 \vec{a}_i(t) - \cdots \quad (29)$$

If we add the two equations above, we obtain :

$$\vec{r}_i(t+\Delta t) = 2\vec{r}_i(t) - \vec{r}_i(t-\Delta t) + \frac{1}{2}\Delta t^2 \vec{a}_i(t) \quad (30)$$

By replacing the acceleration $\vec{a}_i(t)$ by its expression (Eq. 27) we obtain the expression of the Verlet algorithm :

$$\vec{r}_i(t+\Delta t) = 2\vec{r}_i(t) - \vec{r}_i(t-\Delta t) + \frac{\vec{F}_i}{m_i}\Delta t^2 \quad (31)$$

In this algorithm the expression of velocity does not appear explicitly and is done by the equation:

$$\vec{v}_i(t+\Delta t) = \vec{v}_i(t) + \frac{\vec{a}_i(t) + \vec{a}_i(t+\Delta t)}{2}\Delta t \quad (32)$$

The computing time is directly related to the integration step Δt. The larger it is, the shorter is computing time. The time step must remain small enough to describe the period of the fastest vibration in the system (usually the vibrations of X-H bonds). Generally a value of $\Delta t = 10^{-15}$ s (1 fs) is used.

In principle, the integration of Newton's equations preserves the total energy of the system. Thus, if the volume V of the periodic box and the number of atoms N are held constant, we generate a microcanonical ensemble (N, V, E). Due to the dynamics, it is preferable to maintain constant temperature (N, V, T), or pressure (N, P, T), rather than the total energy (N, V, E). In these two cases, the temperature or the pressure becomes independent variables which we can choose, as shown in the following two paragraphs.

4.3.4.b Control of the Temperature

We used the weak coupling method of thermal bath developed by Berendsen et al. [114]. This method is based on the modification of the equation of motion to obtain a relaxation to the reference temperature T_0:

$$\frac{dT(t)}{dt} = \frac{1}{\tau_T}[T_0 - T(t)] \quad (33)$$

where τ_T is the time of the temperature relaxation.

According to the principle of equipartition of kinetics energy by the Clausius equation (13), the temperature control in the system is performed by adjusting the velocities of the atoms using a correction factor $\lambda(t)$:

$$\lambda(t) = \sqrt{\left[1 + \frac{\Delta t}{\tau_T}\left(\frac{T_0}{T(t)} - 1\right)\right]} \quad (34)$$

The relaxation parameter τ_T may be adjusted depending on the system. It must be chosen small enough so as to maintain the average temperature near T_0, but large enough to allow for fluctuations.

In most cases, we set the reference temperature to 300 K (experimental temperature) and the relaxation time of 0.1 ps.

4.3.4.c Control of the Pressure

The pressure control is carried out similar to the temperature. In this case, the correction is applied to the box vectors and thus the position of atoms. The equations of motion are modified to obtain a first-order relaxation of the pressure P with respect to the reference pressure P_0 :

$$\frac{dP(t)}{dt} = \frac{1}{\tau_P}[P_0 - P(t)] \quad (35)$$

where τ_P is the time of the pressure relaxation.

The instantaneous pressure is depended on the volume of the simulation box $V_{xyz}(t)$ at time t, the kinetics energy of the system ($E_c(t)$) and the viral of the forces $\theta(t)$:

$$P(t) = \frac{2}{3V_{xyz}(t)}[E_c(t) - \theta(t)] \quad (36)$$

Where the virial of the forces is written as:

$$\theta(t) = \frac{1}{2}\sum_{i<j} \vec{r}_{ij}(t) \cdot \vec{F}_{ij}(t) \quad (37)$$

Here $\vec{r}_{ij}(t)$ is the distance between the atoms i and j and $\vec{F}_{ij}(t)$ is the force between atoms i on j.

For our calculations at constant pressure, we chose a reference pressure P_0 = 1 bar and a relaxation time τ_P = 100 fs.

4.3.4.d Periodic Boundary Conditions

The periodic boundary conditions are used to avoid edge effects while having a system containing a finite number of particles [97].

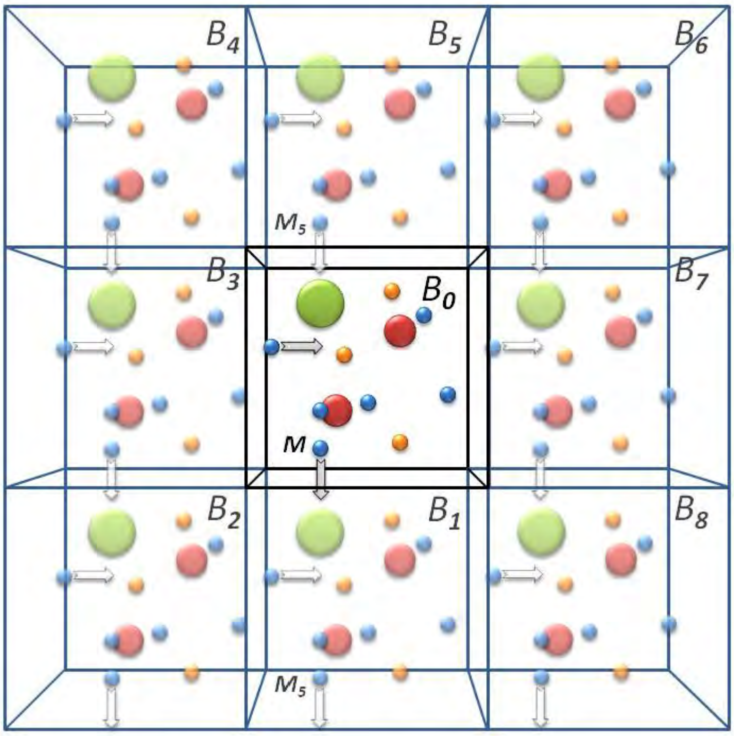

Figure I.30 Periodicity of the box following 2 dimensions.

The atoms of the simulated system are placed into a rectangular box surrounded by 26 identical boxes, images from each other by translation of the original box (B_0) in three dimensions (B_1 – B_8 see Figure I.30). Thus, the molecules in the neighbouring boxes occupy the same position that the molecules at the central box (B_0). In order to an atom A_0 does not interact with any of images A_i or simultaneously with an atom B_0 with any of images B_i, it is necessary that the dimensions R_x, R_y and R_z of the central box are larger more than twice the cutoff value.

When a molecule M is going out from the central box B_0, it passes to the adjacent box B_1. At the same time the molecule M_5, from the box B_5, is immediately replaced in the central box B_0 on the opposite side. This process applies to all boxes at the same time.

Molecular dynamics simulation will be valid when the space and time sampling is correct. The size of a simulated system (number *N* of particles), the time step of integration (*Δt*) and the total duration of the simulation must be chosen carefully in order to complete the calculations within a reasonable time. The simulation length should correspond to the time of the natural processes, which are simulated. Thus, the overall run time should correspond to the simulated kinetic study of the natural process.

The implementation of a simulation includes different stages: building the system and its immersion into a solvent, relaxation of the whole system toward an equilibrium and production runs for data analysis.

II Materials and Methods

1 Materials

Zwitterionic phospholipids: 1,2-dioleoyl-*sn*-glycero-3-phosphocholine (DOPC), 1,2-dipalmitoyl-*sn*-glycero-3-phosphocholine (DPPC) and 1-palmitoyl-2-oleoyl-*sn*-glycero-3-phosphocholine (POPC) (Avanti Polar Lipids, Inc. (Alabaster, AL, USA)) were used in this study (see Figure II.1). All lipids were stored in chloroform at -20˚C and used without further purifications.

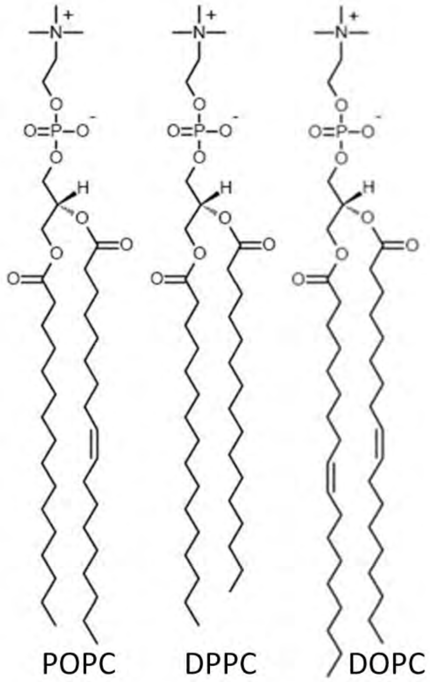

Figure II.1 Chemical structures of the lipids used in this study.

Fluorescent probes: 4-[(n-dodecylthio)methyl]-7-(N,N-dimethylamino)-coumarin (DTMAC) was synthesized and purified as described in ref [115] and naphthalene derivatives: 6-hexadecanoyl-2-(((trimethylammonium)ethyl)methyl)amino)naphthalene chloride (Patman) and 6-dodecanoyl-2-dimethylaminonaphthalene (Laurdan) were purchased from Molecular Probes (Eugene, OR,USA) (see Figure II.2)

Salts: sodium chloride (NaCl), sodium bromide (NaBr), sodium iodide (NaI), sodium thiocyanate (NaSCN) and sodium perchlorate ($NaClO_4$) were obtained from Sigma Aldrich (St.Louis, MO,USA). Salts were dissolved in Milli-Q water (Milli-Q3 system, Millipore, Etten-Leur).

All organic solvents of spectroscopic grade were supplied from Merck (Darmstadt, Germany).

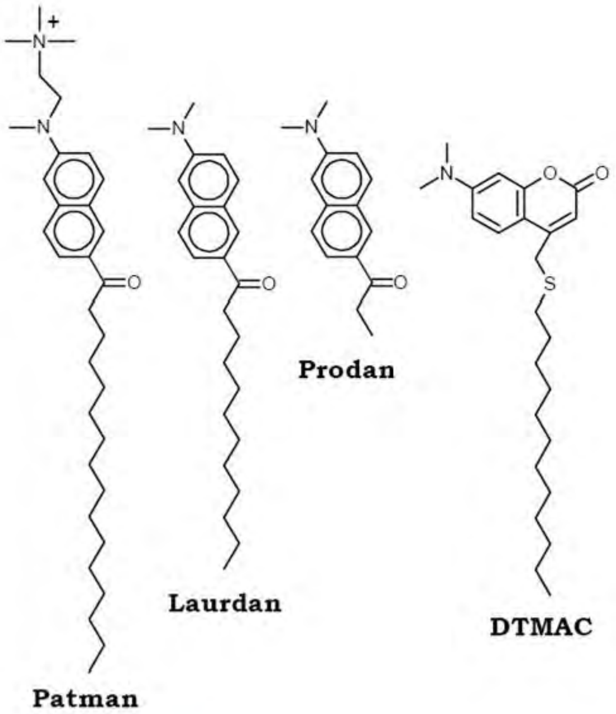

Figure II.2 Structures of the fluorescent probes used in the present study.

2 Methods

2.1 Preparation of the Vesicles

The required volumes of the chloroform solution of the lipid with the methanol solution of a selected fluorescent dye were added together to a glass tube. The final concentration of the probe in the sample was 1 mol%. Solvents were evaporated under a stream of nitrogen while being continuously heated. Samples were kept under high vacuum over night to remove residual solvent. The dry lipid/dye film was suspended in Milli-Q water or 10 mM HEPES buffer (pH=7.4, 100 mM NaCl) or with solution of the salt (150 mM or 1 M concentration) and vortexes for 4 minutes. Large Unilamellar Vesicles (LUV's) were formed by extrusion [31] through a polycarbonate membranes (Avestin, Ottava, Canada) with 100 nm pores. The prepared samples were transferred to a 1 cm quartz cuvette and equilibrated at the desired temperature for 10 minutes before measurement. Unless stated otherwise, the final concentration of the phospholipids in the sample was 1 mM.

2.2 Spectroscopic Measurements

2.2.1 Steady-State Fluorescence

All steady-state excitation and emission spectra acquisition were performed on a Fluorolog-3 spectrofluorometr (model FL3-11; Jobin Yvon Inc., Edison, NJ, USA) equipped with a Xenon-arc lamp. The spectra were collected in 1 nm steps (2 nm bandwidths were chosen for both the excitation and the emission monochromators). The temperature in the cuvette holder was maintained within ±0.1°C using a water-circulating bath.

2.2.2 Time-Resolved Fluorescence

Fluorescence decays were recorded on a 5000U Single Photon Counting setup (IBH, Glasgow, UK), using an IBH laser diode NanoLED 11 (370 nm peak wavelength, 80 ps pulse width, 1 MHz maximum repetition rate), and a cooled Hamamatsu R3809U-50 microchannel plate photomultiplier. Emission decays were recorded at a series of wavelengths spanning the steady-state emission spectrum, usually 400 – 540 nm, in 10 nm steps (emission slits: 8 nm bandwidths). To eliminate scattered light, a 399 nm cutoff filter was used. The signal was kept below 2 % of the light source repetition rate (1MHz). Data was collected in 8192 channels (0.014 ns per channel) till the peak value reached 5000 counts. The time resolution, calculated as 1/5 of the full width at half maximum (FWHM) of the instrument's response function, was about 20 ps. Fluorescence decays were fitted to multi-exponential functions (2 or 3 exponential components were used), using the iterative reconvolution procedure with IBH DAS6 software.

2.3 Calculation Methods

2.3.1 Quantum Mechanics Calculation

All quantum level calculations were performed using the Gaussian 03 software package [92]. The ground state equilibrium geometries of Prodan, Laurdan and C-Laurdan were optimized by density functional theory DFT [116-117] method with the B3LYP/6-311+G(d,p) basis set. The excited states properties of the fluorescent dyes were obtained from time dependent density functional theory TDDFT [118-120] with the same basis set as for DFT. The solvent effect was taken into consideration using the integral equation formalism of the polarizable continuum model IEFPCM [121-124]. The dipole moments (both in ground and excited states) were determined from the Mulliken charges distribution. The different levels of theory (PM3, Hartree-Fock, DFT/TDDFT, CIS) and also different methods of charge distributions analysis (Coulson, Mulliken, NBO, Merz-Kollman, RESP) were tested to obtain the best dipole moment values compared to the literature. Supplementary analysis based on construction of the Hessian matrix (the matrix of second derivatives of the energy with respect to geometry) was also performed for further use in the force field parameterization.

2.3.2 Molecular Dynamics Simulations

The commonly used force fields, that are specific databases of intra and inter-molecular interactions, include only parameters for frequently studied molecules, i.e. proteins, nucleic acids, and lipids [9-12]. Excitable molecules such as fluorescent probes are not very popular for computational analysis despite their relative importance for biological sciences. In this study, we have derived an adequate force field for the desired molecules by following a simple protocol based on our previously validated QM analyses. Models of fluorescent dye molecules, Prodan, Laurdan and C-Laurdan optimized by quantum mechanics calculations at 300 K, were prepared using parameterization tool from the molecular graphics software VMD [125] in order to use them in MD calculations at 300 K and under pressure of 1 atm. To study the behaviour of the probes in the vicinity and within lipid membrane, a DOPC lipid bilayer patch, composed of 72 lipids (36 per monolayer) and hydrated (4985 atoms of water) on each side by 35 Å water slabs, was used as a numerical model. The lipid bilayer was first generated using a pre-equilibrated lipid membrane followed by a very short energy minimization at 0 K and then we started a long equilibration run during more than 10 ns at 300 K and 1 atm. The size of the complete systems was about (50×50×100) $Å^3$.

MD simulations were performed using NAMD2.6 program [126] with the CHARMM27 [99] force field containing our own extensions for fluorescent probes. All water molecules were described by the TIP3P model [127]. A constant temperature of 300 K and a constant pressure of 1 atm were ensured by Langevin dynamics and Langevin piston Nosé-Hoover algorithm [128], respectively. Chemical bonds between hydrogen and heavy atoms were constrained to their equilibrium values, long-range electrostatic forces were evaluated using the particle mesh Ewald (PME) method [129] and the integration time step was equal to 2.0 fs.

III Results and Discussion

1 Interaction of Monovalent Ions with Phosphatidylcholine Lipid Membrane

The ionic solutions strongly influence physicochemical properties of lipid membranes. The concentration of ions influences the transmembrane potential, which, in turn, regulates the traffic of different molecules across the membrane. It is very important to understand the details of the location of ions at the water/membrane interface and the ion-membrane interactions.

In this study, different monovalent salts containing a common Cl^- anion with different cations: Na^+, NH_4^+ and Cs^+ were compared. The salts containing Na^+ cations were used, as well: NaCl, $NaClO_4$ and NaSCN.

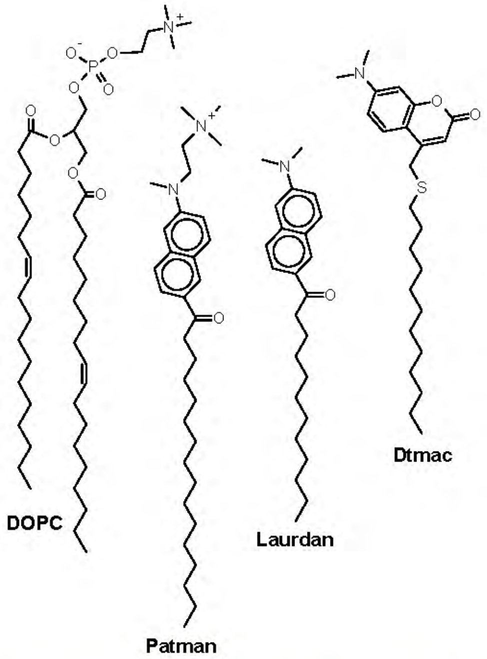

Figure III.1 Diagram of the location of Patman, Laurdan and DTMAC in DOPC membrane.

Fluorescence solvent relaxation method was used to investigate the impact of ions on the membrane properties. Mobility of water and lipid molecules and the level of polarity of the membrane head group were studied using three different fluorescent probes (Patman, Laurdan and DTMAC) located differently in the phospholipid membrane for probing three different depths in the bilayer (see Figure III.1). Two main parameters: the total emission shift $\Delta\nu$ [cm^{-1}] and the mean integrated relaxation time τ_r [ns] were obtained from TRES analysis. The total emission shift

$\Delta\nu = \nu(0) - \nu(\infty)$ gives information about the amount of emitted energy lowered due to the interaction of the dye with its surrounding. In the case of the lipid membranes, $\Delta\nu$ reports the level of membrane hydration. Relaxation kinetics is usually depicted by the mean relaxation time τ_r. This quantity in pure solvents corresponds to the macroscopical viscosity parameter, which reflects the mobility of the solvent molecules. Since water hydrating the membranes is bound to the phospholipid molecules via hydrogen bonds the observed relaxation time is very slow (10^{-9} s instead of 10^{-13} s observed in bulk water), and is believed to reveal mobility of the hydrated lipid moieties rather than the motions of free water molecules.

1.1 Acyl-Group Level of the Lipid Bilayer

Patman is known to be located at the acyl-groups level of the DOPC lipid membrane and was found by fluorescent quenching method at about 10 Å from the bilayer center [7]. Patman has the deepest location in comparison with the two other fluorescent probes, which were chosen for the present experiments (see Figure III.1).

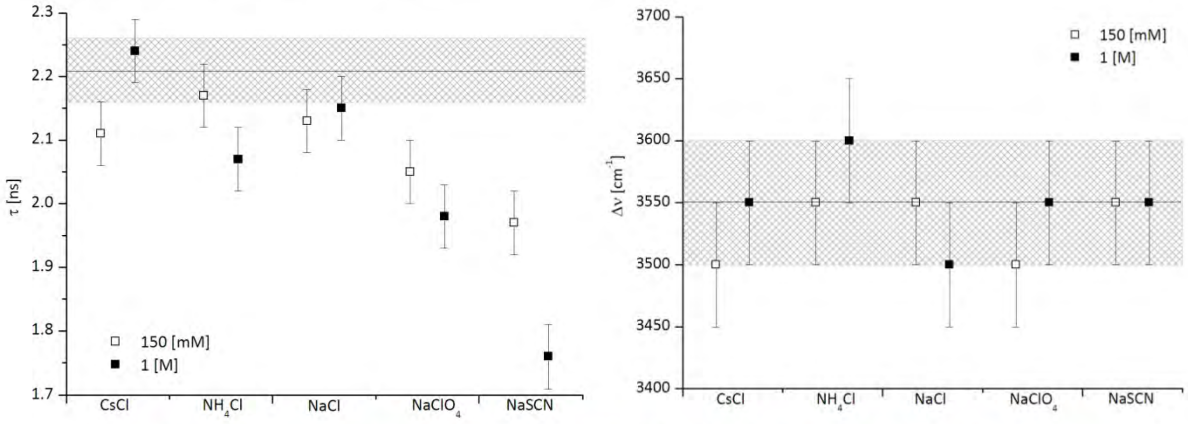

Figure III.2 Solvent Relaxation parameters for DOPC LUVs with salts, labelled with 1 mol% of Patman.

Figure III.2 shows the τ and $\Delta\nu$ dependences with various salts at different concentrations. At the acyl-group level of lipid bilayer, **sodium chloride** (sodium radius 1.02 Å) causes small increase of water molecules mobility after excitation (see Figure III.2 left inset). The values of the relaxation times obtained for two concentrations of NaCl show small decrease in comparison with sample containing DOPC vesicles in pure water. Results for LUVs suspended in pure water are depicted in Figure III.2 as the black lines with the grey areas representing the experimental error. The concentration effect is not visible for sodium chloride, which shows that an increase of osmolarity does not change bilayer properties at the acyl group level.

The **large anions** like perchlorate ClO_4^- (radius 2.5 Å) and thiocyanate SCN^- (radius 2.13 Å) cause significant increase of the relaxation kinetics, in comparison with the result obtained for LUVs suspended in pure water. It can be the result of the decrease in the rigidity of the DOPC bilayer. The presence of the large anions may broke the strong water-lipid interactions at the acyl-group level of membrane. This broken bonds could be replaced by ion-lipid interactions. The changes in the strength of interactions between molecules is observed by changes of relaxation kinetics. In the case of thiocyanate ion the effect of salt concentration is meaningful. The ClO_4^- and SCN^- anions do not significantly change the hydration at the acyl group level.

The **large cations**, ammonium NH_4^+ (radius 1.48 Å [130]) and caesium Cs^+ (radius 1.70 Å [130]), do not have such a big influence on the kinetics of movements of water molecules at the acyl level of lipid bilayer like anions. Ammonium and caesium cations increase only slightly the relaxation kinetics. Large cations do not penetrate the lipid bilayer at the depth of acyl group. Concurrently, the slight polarity perturbations are visible for both cations (see Figure III.2 right inset), which suggest that the presence of NH_4^+ and Cs^+ cations have very small impact on the bilayer hydration reaching the level of acyl group.

1.2 Carbonyl Level of the Lipid Bilayer

Laurdan is a second fluorescent marker which was used for investigation the ions impact on a different region of DOPC lipid bilayer. Laurdan is precisely located at the carbonyl level of DOPC bilayer at 11.4 Å from the bilayer center [7], more outside than Patman.

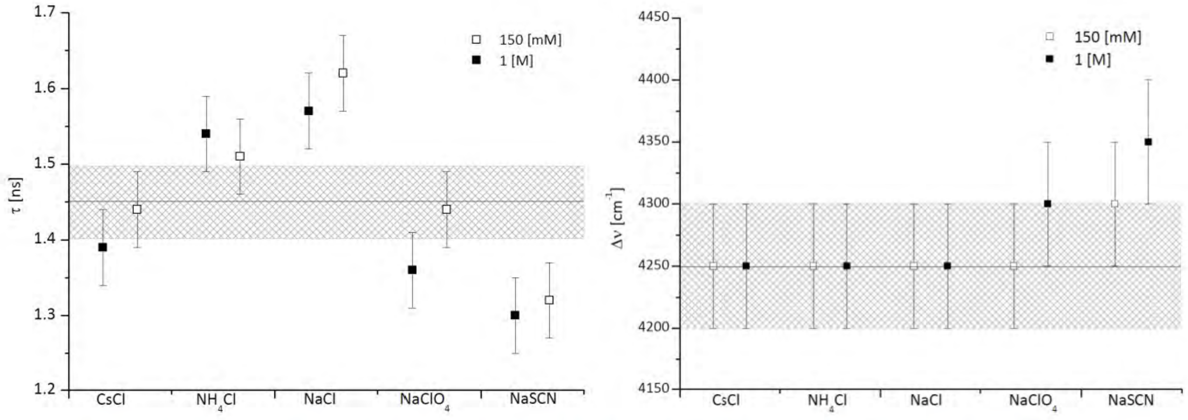

Figure III.3 Solvent Relaxation parameters for DOPC LUVs with salts, labelled with 1 mol% of Laurdan.

The presence of **sodium chloride** salt decreases the kinetics of water motions (see Figure III.3). The interactions of small Na^+ cations, with water and lipid molecules at the carbonyl level of lipid membrane, causes slowdown of the solvent response to electronic excitation of Laurdan. Slow kinetics of water reorganization is assumed here to increase bilayer rigidity. This conclusion is confirmed by simulations, which show that area per lipid decreases in the presence of NaCl from 0.72 nm^2 (in the presence of water only) to 0.69 nm^2. Sodium cations increase the bilayer rigidity. Concentration effect is only slightly stronger for 1 M NaCl than for 150 mM, which show that the increase of osmolarity does not change bilayer properties dramatically. The presence of sodium and chloride ions does not have an impact on hydration at the glycerol level of DOPC lipid bilayer. The computational simulations show that chloride anions accumulate at the water-lipid interface and does not penetrate to the head group region of the lipid bilayer.

The results presented in Figure III.3 show that anions significantly influence the relaxation time and the total spectral shift measured using Laurdan. The **large anions**: perchlorate ClO_4^- and thiocyanate SCN^- increase the kinetics of solvent relaxation. Their presence in the membrane at the carbonyl level reduces the rigidity of lipid bilayer. Small concentration effect is noted for ClO_4^- anion. The presence of both anions increases the polarity of the carbonyl region of DOPC membrane.

Ammonium NH_4^+ and caesium Cs^+, **large cations**, do not change bilayer hydration, just like the small sodium ion. In contrast, large soft anions ClO_4^- and SCN^- increase the polarity of DOPC membrane what can be the result of an increased hydration and/or the presence of the ions in the vicinity of the probe. The caesium and ammonium ions just slightly change relaxation times. Therefore we can suspect that large cations do not have a strong impact on lipid bilayer properties at the carboxyl level.

1.3 Phosphate Level of the Lipid Bilayer

DTMAC (4-[(*n*-dodecylthio)methyl]-7-(*N*,*N*-dimethylamino)-coumarin) was first time used in SR in 2005 year by Sýkora et al. [131]. The chromophore of DTMAC is found to be located at 15.3 Å from the bilayer center at the interface region, phosphate level [132], where it is in contact with bulk water.

The addition of **sodium chloride** salt causes very small increase of the relaxation kinetics (see Figure III.4 for more details). Slight concentration effect is visible. The presence of NaCl does not have any impact on the level of hydration at the phosphate groups of lipid bilayer.

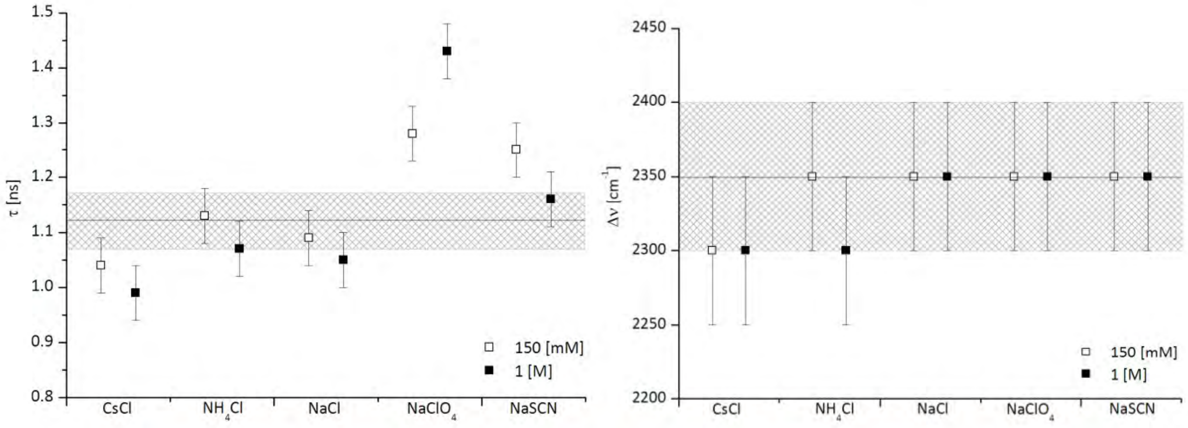

Figure III.4 Solvent Relaxation parameters for DOPC LUVs with salts, labelled with 1 mol% of DTMAC.

The **large anions** ClO_4^- and SCN^- do not have any impact on the membrane hydration. Perchlorate and thiocyanate anions significantly change the kinetics of solvent relaxation. The water molecules motions slow down in the presence of anions and the relaxation time increases. The salt concentration effect is observed for perchlorate anion.

The presence of **large cations**, caesium and ammonium, change the polarity of DTMAC surrounding and cause a small dehydration of the lipid bilayer. NH_4^+ cation does not change the kinetics of solvent relaxation. The presence of caesium ions increase the mobility of water molecules at the phosphate group of lipid bilayer.

1.4 Summary

The interactions of ions at the water/membrane interface are very important for many biological processes. Sodium ions are preferentially located in the headgroup region, whereas chloride adsorbs weaker at the outer part of the membrane (choline region). This conclusions are confirmed by experimental results obtained for NaCl in the presence of Laurdan and numerical simulation data [15-16]. Simulation show that sodium ions are preferentially located in the phosphate region of lipid bilayer and chloride ions accumulate at the membrane surface. Larger cations: NH_4^+ and Cs^+ only weakly penetrate into the headgroup region of DOPC bilayer. Larger anions: ClO_4^- and SCN^- penetrate deeper into the membrane than smaller Cl^- and significantly change the mobility and hydration of the headgroup region of the lipid bilayer [see Figure III.5].

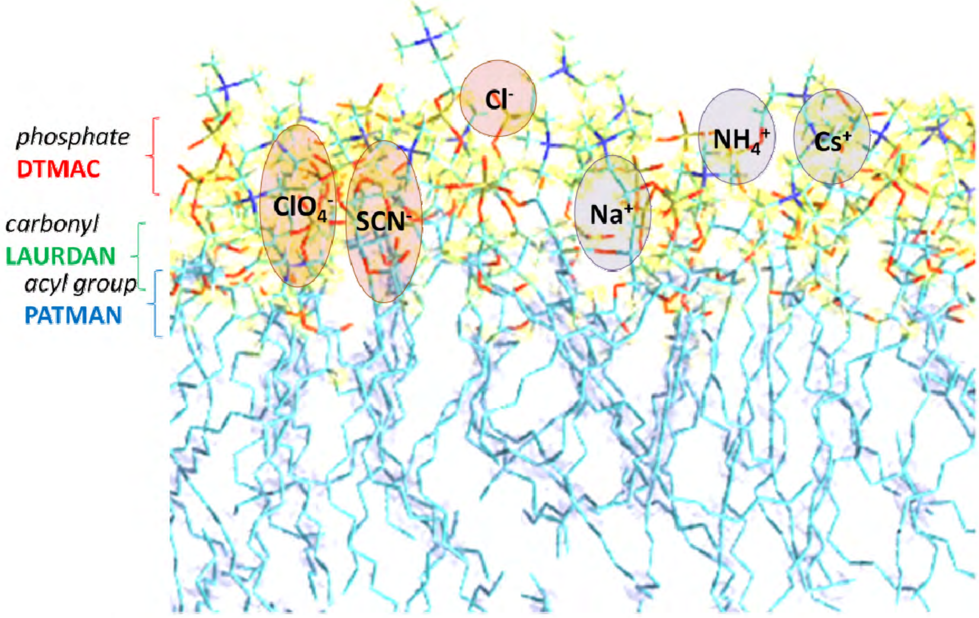

Figure III.5 Schematic representation of the ions location in lipid bilayer.

The presence of Na^+ ions at the glycerol level of DOPC membrane rigidifies the headgroup region. Similar effect is clearly visible for NH_4^+ and only slightly for Cs^+ cations. Relaxation times increase with the presence of NH_4Cl and CsCl salts, which is related to a decrease of the area per lipid.

The stronger membrane affinity is observed for anions than for cations.

Specificity of ion-membrane interactions arises from different mechanisms:

a) ion pairing – salt anions can pair with the positively charged lipid choline group, while cations can create pair with the negatively charged phosphate group and carbonyl oxygen;

b) the presence of water – hydrophobic interface implies adsorptions of large and polarisable ions;

c) counter ion attraction – ions of opposite charge tend to screen each other and therefore, adsorption of the one type of them at the membrane interface leads to the attraction of counterions.

Generally, small cations (Na^+) should be attracted to the zwitterionic membrane, while larger cations (Cs^+ and NH_4^+) should not. On the contrary, larger anions (ClO_4^-, SCN^-) adsorb to the zwitterionic membrane more easily than smaller ones (Cl^-) due to their size, polarizability and ion pairing with the choline groups of lipids.

J. Phys. Chem. A **2009,** *113,* 7235–7243

Effects of Alkali Cations and Halide Anions on the DOPC Lipid Membrane[†]

**Robert Vácha,[‡] Shirley W. I. Siu,[§] Michal Petrov,[‡] Rainer A. Böckmann,[§]
Justyna Barucha-Kraszewska,[||] Piotr Jurkiewicz,[||] Martin Hof,[||] Max L. Berkowitz,*[,⊥] and
Pavel Jungwirth*[,‡]**

Institute of Organic Chemistry and Biochemistry, Academy of Sciences of the Czech Republic and Center for Biomolecules and Complex Molecular Systems, Flemingovo nám. 2, 16610 Prague 6, Czech Republic, Theoretical & Computational Membrane Biology, Center for Bioinformatics, Saarland University, P.O. Box 15 11 50, 66041 Saarbrücken, Germany, J. Heyrovsky Institute of Physical Chemistry, Academy of Sciences of the Czech Republic, v. v. i., Dolejskova 3, 18223 Prague 8, Czech Republic, and Department of Chemistry, University of North Carolina, Chapel Hill, North Carolina 27599

Received: November 12, 2008; Revised Manuscript Received: February 10, 2009

By means of molecular dynamics simulations with an all-atom force field, we investigated the affinities of alkali cations and halide anions for the dioleoylphosphatidylcholine lipid membrane in aqueous salt solutions. In addition, changes in phospholipid lateral diffusion and in headgroup mobility upon adding NaCl were observed using fluorescence spectroscopy. The simulations revealed that sodium is attracted to the headgroup region with its concentration being maximal in the vicinity of the phosphate groups. Potassium and cesium, however, do not preferentially adsorb to the membrane. Similarly, halide anions do not exhibit a strong affinity for the lipid headgroups but merely compensate for the positive charge of the sodium countercations. Nevertheless, larger halides such as bromide and iodide penetrate deeper into the headgroup region toward the boundary with the hydrophobic alkyl chain, this effect being likely underestimated within the present nonpolarizable force field. Addition of alkali halide salts modifies physical properties of the bilayer including the electronic density profiles, the electrostatic potential, and the area per lipid headgroup.

Introduction

Electrolyte solutions strongly influence physicochemical properties of model lipid membranes. To explain this influence, much of the theoretical work often relies on classical Gouy–Chapman mean-field type theory that predicts the same type behavior for ions of the same valency.[1] The importance of the specific ionic effect for membrane biophysics was noticed by Hodgkin and Horowicz who observed that different anions produce different effects on the muscle twitch tension.[2] The increase of the ionic effect followed the series $Cl^- < Br^- < I^- < SCN^-$. Hodgkin and Horowicz observed that ordering of the anions in the above series is correlated to their lyotropic character, and therefore they proposed that it is related to the degree of adsorption of anions to the muscle membranes. Later measurement of the membrane dipole potential[3] showed that dipole potentials are reduced in the presence of salts, and the anion effectiveness follows the series $ClO_4^- > SCN^- > I^- > Br^- > Cl^- > F^- > SO_4^{2-}$. It was assumed that the reduction in the dipole potential correlates with the degree of ion adsorption to the membrane. It was also noticed that the ordering of the anions coincides with the reverse Hofmeister series.[4] More recently, the results from the osmotic stress measurements[5−7] of the interaction between lamellar membranes in different aqueous salt solutions were also interpreted as confirming the conclusion obtained from the dipole potential measurements, i.e., that the specific ionic effect follows the reverse Hofmeister series. The interpretation of the results from the osmotic stress experiments is somewhat involved, and very recent experiments, which studied nanomechanics of lipid bilayers by force spectroscopy[8] and ion binding to solid supported lipid membranes,[9] provide a more direct information on the location of ions next to lipid membranes. While the former showed an increase in lateral phospholipid−phospholipid interactions upon addition of salt,[8] results from experiments on solid-supported membranes indicated that weakly hydrated anions and strongly hydrated cations are attracted to the membrane.[9] It has been also shown by combination of various experimental techniques that cations significantly influence neutral lipid bilayers.[10,11]

Detailed information about location of ions with respect to lipid membranes can also be obtained from molecular dynamics simulations; indeed, first simulations that studied ionic aqueous solutions next to neutral zwitterionic membranes pointed out that cations and anions create a double layer at the membrane/water interface.[11,12] Specifically, it was observed that at the interface between aqueous solutions and membranes containing phosphatidylcholine (PC) headgroups, Na^+ penetrates into the headgroup region while Cl^- does not. Further simulations confirmed these observations, although detailed locations of the ions were somewhat depending on the force fields used in the simulations.[13−15] Simulations also investigated location of different cations, i.e., monovalent, divalent,[16] or even trivalent[17] ions next to membranes, while using the same counteranion (Cl^-).

Understanding the intricate details about the location of ions at the aqueous solution/membrane interface is very important

---

[†] Part of the “Robert Benny Gerber Festschrift” Special Issue.

* Corresponding authors. E-mail: pavel.jungwirth@uochb.cas.cz (P.J.); maxb@unc.edu (M.L.B.).

[‡] Institute of Organic Chemistry and Biochemistry, Academy of Sciences of the Czech Republic and Center for Biomolecules and Complex Molecular Systems.

[§] Saarland University.

[||] J. Heyrovsky Institute of Physical Chemistry, Academy of Sciences of the Czech Republic.

[⊥] University of North Carolina.

10.1021/jp809974e CCC: \$40.75

for our understanding of the mechanisms of membrane−membrane and membrane−peptide interactions that are modulated by the values of surface potentials. The location of the ions at the aqueous solution/membrane interface also sets up the value and character of the transmembrane potential, which in turn regulates the traffic across membranes. In the present paper we report on computational and experimental work we performed to study the influence of salt on a bilayer containing dioleoylphosphatidylcholine (DOPC) phospholipid molecules. Using molecular dynamics simulations technique, we systematically studied the effect of different ions, i.e., alkali cations and halide anions, on the properties of the DOPC/aqueous solution interface. In our study we first considered monovalent salts containing a common Cl^- anion with different cations such as Na^+, K^+, and Cs^+. Next, we considered salts containing a common cation (Na^+) but different anions, such as Cl^-, Br^-, and I^-. If we consider Na^+ and Cl^- as our reference ions, we can infer from our simulations how the change of the character of the ions, varying from more strongly hydrated to less strongly hydrated compared to the reference ions, influences the lipid membrane/ionic solution interface. In this respect our simulations can be compared directly with the results from the recent experiments on solid-supported membranes.[9] Additionally, we employed fluorescence spectroscopy to study how the presence of NaCl salt influences the properies of DOPC bilayers.

Methods

Computational. All molecular dynamics simulations were performed using the GROMACS 3.3.1 program package[18] We simulated five different systems, each containing 72 DOPC lipid molecules, 2627 water molecules, and 100 ions (i.e., 50 cations and 50 anions). Each system contained a specific salt: NaCl, KCl, CsCl, NaBr, or NaI. The employed numbers of water molecules and ions yield a formal 1 M concentration of salt. This higher than physiological concentration was used because Hofmeister effects are typically studied at molar ionic strengths. Moreover, higher concentrations of ions help to improve sampling.

The initial configuration of the system was taken from our previous study[19] where we equilibrated a DOPC membrane for 100 ns in pure water. Ions were inserted in the water phase and, after energy minimization and 80 ns of equilibration, 120 ns production runs were carried out with a 2 fs time-step. The system was kept within the $NP\gamma T$ ensemble with surface tension of 22 dyn/cm in the membrane plane and pressure of 1 atm in a perpendicular direction and 310 K using a Berendsen barostat and thermostat. Barostat scaling time was 1 ps with compressibility of $4.5\ 10^{-5}\ \text{bar}^{-1}$, while the thermostat time constant was set to 0.1 ps. The van der Waals and Coulomb interactions were cutoff at 1.2 nm, and the long-range Coulomb interactions were accounted for using the Particle Mesh Ewald (PME) method.[20] Lipids were described by a recently developed all-atom forcefield based on the Generalized Amber Force Field.[19] For water we employed the SPC/E model[21] and parameters for ions are presented in Table 1. The reason for using this parametrization for ions[22−25] is 2-fold. While it was originally developed with a polarizable water model, it is also consistent with the presently employed SPC/E water, as demonstrated recently.[26] Moreover, the standard AMBER ion parametrization leads to an artificially strong ion pairing (particularly for potassium);[26,27] therefore, we were avoiding it.

In order to quantify the properties of DOPC bilayer/aqueous interface we evaluated density profiles of individual species and electrostatic potentials along the normal to the bilayer. We also calculated the average number of adsorbed ions per lipid and the corresponding mean adsorption times. The former was defined as the number of ions within the distance of 0.6 nm from a phosphorus atom of any phosphate group divided by the number of lipid molecules. The choice of the phosphate center is particularly suitable for the cations. The radius of 0.6 nm was chosen to be large enough to create a continuous volume from overlapping spheres on neighboring lipid headgroups and to account also for the ion adsorption in the carbonyl region. For anions we additionally counted the number of ions within 0.6 nm from the nitrogen of choline as a center of positive charge on lipids. The choice of such distance criteria is necessarily somewhat arbitrary, nevertheless, the trends are robust within reasonable margins.

TABLE 1: Force Field Parameters Employed for Alkali Caltions and Halide Anions

	charge [e]	σ[nm]	ε[kJ/mol]
Na^+ [23]	1.000	0.235019	0.54392
K^+[24]	1.000	0.3048655	0.41840
Cs^+[25]	1.000	0.383086	0.41840
Cl^-[22]	−1.000	0.43200	0.41840
Br^-[22]	−1.000	0.47004	0.41840
I^- [22]	−1.000	0.51494	0.41840

Experimental. Fluorescence solvent relaxation (SR) and fluorescence correlation spectroscopy (FCS) measurements were performed on DOPC (Avanti Polar Lipids, Alabaster, AL) bilayer. The chloroform lipid solution was mixed with appropriate fluorescent dye. 6-Dodecanoyl-2-dimethylaminonaphthalene (Laurdan) (Invitrogen) or 4-[(*n*-dodecylthio)methyl]-7-(*N*,*N*-dimethylamino)coumarin (DTMAC) (synthesized and purified as described in ref 28) were used for SR measurements in 1:100 dye/lipid molar ratio. 2-(4,4-Difluoro-5,7-dimethyl-4-bora-3a,4a-diaza-s-indacene-3-dodecanoyl)-1-hexadecanoyl-sn-glycero-3-phosphocholine (Bodipy C12-HPC) (Invitrogen) was used for FCS in 1:100 000 dye/lipid molar ratio. The organic solvents were evaporated, and the lipid film was suspended in water (Milli-Q3 system, Millipore, Etten-Leur) or 150 mM NaCl solution. The obtained multilamellar vesicles were either extruded through polycarbonate membranes (Avestin, Ottawa, Canada) with 100 nm pores (SR) or sonicated (FCS).

Supported phospholipid bilayers (SPBs) were formed directly in the measurement cell by exposing freshly cleaved mica (Metafix, Montdidier, France) to 0.2 mM (lipid concentration) suspension of sonicated vesicles in 150 mM NaCl.[29] The suspension was stirred continuously during 4 h of incubation. Unbound vesicles were removed by flushing with 50 mL of 150 mM NaCl. For the FCS measurements in pure water, the NaCl solution was replaced after SPB creation with pure water by slow flushing. The experiments were performed at (10 ± 0.5) °C (SR) and at (23 ± 2) °C (FCS).

SR is a unique tool for measuring hydration and mobility of fully hydrated free-standing phospholipid membranes.[30] Fluorescence spectra and decays were recorded on a Fluorolog 3 (Jobin Yvon) and on an IBH 5000 U SPC equipped with an IBH laser diode NanoLED 11 and a cooled Hamamatsu R3809U-50 microchannel plate photomultiplier, respectively. The time-resolved emission spectra (TRES) were gained by the spectral reconstruction method[31] from a set of emission decays recorded at a series of wavelengths spanning the steady-state emission spectrum. The total emission shift $\Delta\nu$ and the mean integrated relaxation time τ_r, which reflect bilayer hydration and mobility, respectively, were calculated as previously described.[31]

FCS experiments were carried out on a MicroTime 200 inverted confocal microscope (Picoquant, Germany). The con-

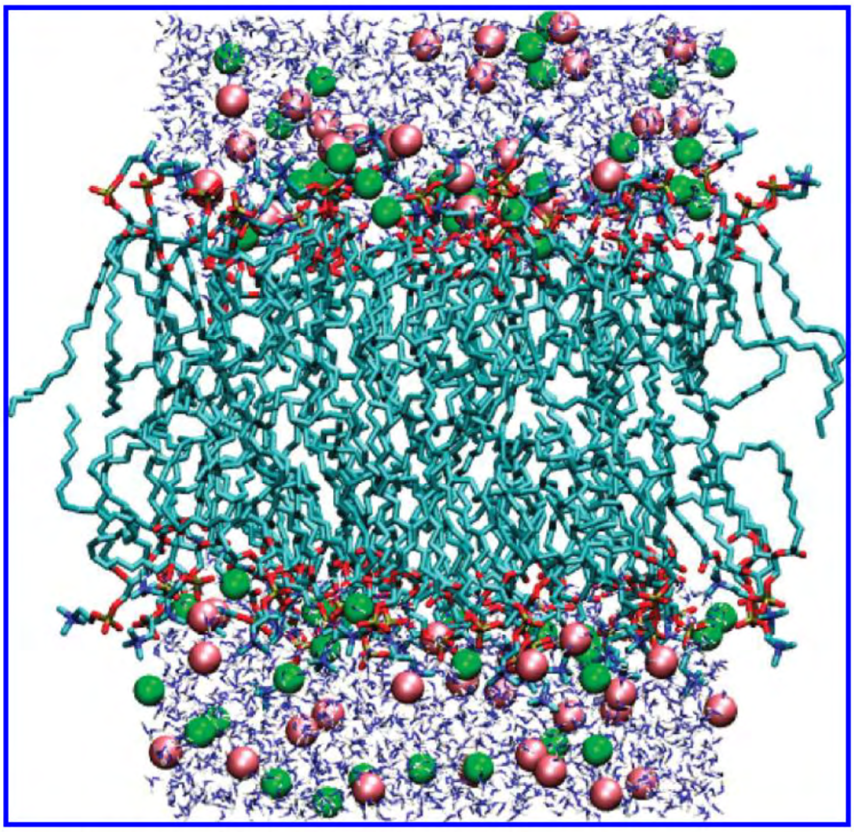

Figure 1. A representative snapshot of the DOPC bilayer in an aqueous salt solution.

figuration contained a pulsed diode laser (LDH-P-C-470, 470 nm, Picoquant, Germany), a proper filter set (clean up filter HQ470/20, dichroic mirror 490DRLP, band-pass filter HQ525/50) (Omega Optical), and a water immersion objective (1.2 NA, 60×) (Olympus). Measurements of lipid lateral diffusion were performed by the *Z*-scan method,[32] which was shown to be the only artifact-free single focus measurement of lateral diffusion coefficients.[33] A set of FCS curves was measured at various *Z* positions of the focal plane with respect to the bilayer spaced by 0.2 μm. Particular FCS curves were treated according to ref 32, and the obtained diffusion times were plotted versus normalized particle number as described in refs 34 and 35 to obtain the effective diffusion coefficient D_{eff} and the intercept with diffusion time axis characterizing the type of diffusion (i.e., free or hindered).[34,35] Fluorescence intensity scans were recorded at the plane of the bilayer and at a plane perpendicular to it to check for bilayer confluence.

Results

Computational. A representative snapshot from a MD simulation of the DOPC bilayer in the NaI solution is depicted in Figure 1. For sake of clarity and easy comparison, we present the results by first looking at salts of different cations with the same Cl^- counteranion and then at salts with different anions in the presence of the common Na^+ countercation.

Cations. *Ion Adsorption.* Total and partial electron density profiles for systems containing Cl^- anion and different countercation are shown in Figure 2. Note that the total electron density profiles are very similar; nevertheless, there are substantial differences in partial density profiles of ions. Two issues are of particular concern when discussing ion adsorption to the lipid bilayer: the amount of adsorbed ions and their preferred location. These were analyzed further by calculating the number density profiles that are shown in Figure 3. From this figure we can see that sodium ions are preferentially enhanced in the phosphate region. This is followed by a weaker adsorption of chloride at the outer part of the membrane (i.e., within the choline region). Larger sized cations such as cesium only weakly

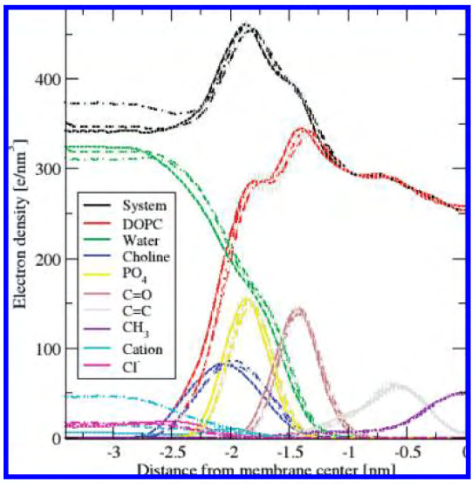

Figure 2. Total and partial electron density profiles. Full lines are for NaCl, dashed lines for KCl, and dashed-dotted lines for CsCl. Only half of the unit cell is depicted with the results being averaged over the two equivalent halves.

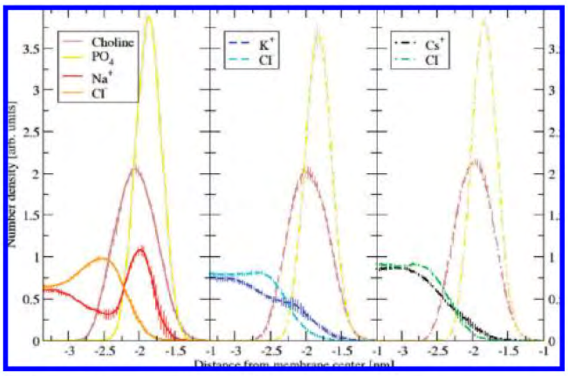

Figure 3. Number density profiles of ions at the membrane/solution interface averaged over a 40 ns trajectory segment after equilibration. Full line: NaCl; dashed line: KCl; dashed-dotted line: CsCl. Choline and phosphate densities are also depicted.

TABLE 2: Mean Values and Standard Deviations of Number of Ions Adsorbed per Lipid within a Distance of 0.6 nm from Phosphates or Cholines

	in phosphate volume	in choline volume
NaCl Na^+	0.32 ± 0.03	
NaCl Cl^-	0.09 ± 0.03	0.27 ± 0.04
KCl K^+	0.16 ± 0.03	
KCl Cl^-	0.06 ± 0.03	0.19 ± 0.04
CsCl Cs^+	0.08 ± 0.03	
CsCl Cl^-	0.04 ± 0.02	0.15 ± 0.04
NaBr Na^+	0.34 ± 0.04	
NaBr Br^-	0.09 ± 0.03	0.31 ± 0.04
NaI Na^+	0.38 ± 0.04	
NaI I^-	0.09 ± 0.03	0.34 ± 0.04

penetrate into the headgroup region and do not display a density peak, similar to the behavior of their counterions (chloride). Potassium is located somewhere between sodium and cesium, penetrating the membrane but not having a significant enhancement there. In Figure 3 we can also see that peaks of choline groups are in different locations depending on the identity of the cation, which indicates a change in the headgroup tilt in different salts.

To define the number of the adsorbed ions at the membrane, we used the adsorption criteria described in Methods. We present the number of adsorbed ions in Table 2. There are about 0.3 sodium cations per lipid molecule in the phosphate region, while there are only 0.2 potassium and 0.1 cesium ions. This means that there is one sodium per every three lipids but merely one cesium for ten lipids in the membrane. While the absolute numbers depend somewhat on the definition of the adsorption volume, the ratio between different adsorbed cations is robust. Note, that when we use for the adsorbed anions the definition of the volume around choline groups, the number of adsorbed chlorides is reaching the same value as the number of adsorbed sodium cations (compensating its charge). For the case of CsCl, using this definition the total number of adsorbed Cl^- overrides the number of adsorbed Cs^+.

Additional important parameters describing binding of ions to the membrane surfaces are the average residence time and the duration of the longest contact, which were calculated as the mean and the longest time that cations spend without interruption within the distance of 0.6 nm from phosphate atoms. The calculated values are given in Table 3. The order of magnitude difference in residence times of individual cations is in agreement with the notion of deeper penetration and stronger adsorption at the membrane surface by sodium ions compared to potassium and cesium.

TABLE 3: Residence Times of Alkali Cations and Longest Contact Times within a Distance of 0.6 nm from Phosphates[a]

	mean residence time, ps	time of the longest contact, ns
Na^+	350	120
K^+	83	30
Cs^+	44	3

[a] In all cases chloride is the counterion.

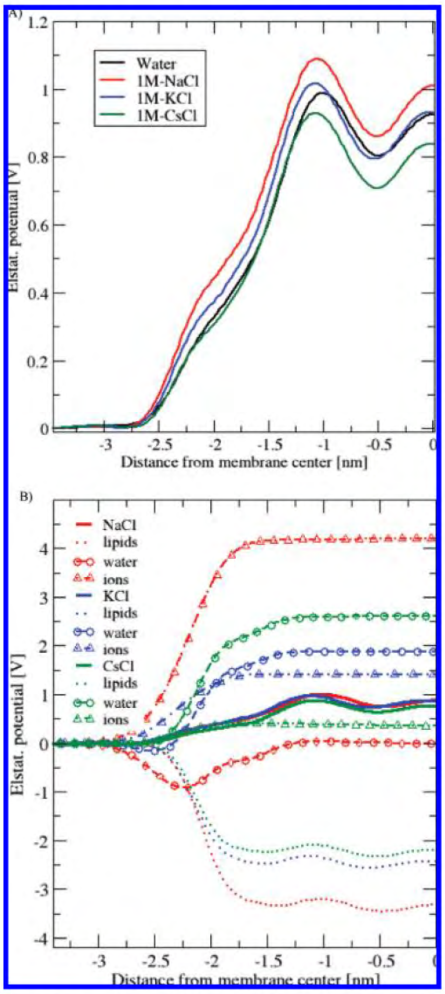

Figure 4. (A) Total and (B) partial electrostatic potentials at the membrane/solution interface for systems with varying cations. Because of symmetry only half of the unit cell is shown.

Electrostatics. The electrostatic potentials were calculated by solving the Poisson equation using the periodic boundary conditions as in ref 36. The absolute value was set to zero in the center of the solution (Figure 4). The total electrostatic profiles are similar to each other for all electrolytes as shown in Figure 4A. The residual differences occur at the headgroup region where the adsorption of ions causes a small change of the electrostatic potential compared to the system without salts. A larger increase in the surface potential compared to the case of pure water is observed for NaCl than for KCl. Moreover, the electrostatic potential in the headgroup region displays a

TABLE 4: Average Areas Per Lipid and Membrane Thickness in Different Solutions

	averaged area per lipid [nm^2]	membrane thickness [nm]
water[19]	0.72	3.6
NaCl	0.69	3.7
KCl	0.69	3.7
CsCl	0.70	3.7
NaBr	0.69	3.7
NaI	0.70	3.8

significant decrease for the case of CsCl solution when compared to the situation in pure water. Note that the potential remains practically equal to zero in the aqueous phase until it sharply rises at the edge of the membrane. The zero value close to the edge of the membrane means that the zeta potential for these systems also vanishes.

Unlike the total profiles, the partial electrostatic profiles of water, ions, and lipids differ dramatically for the studied systems (Figure 4B). The differences in profiles due to lipids are caused by change of the orientation of lipid headgroup dipoles. Electrostatic potential of ions clearly show that adsorption of NaCl at the membrane surface creates a dipolar layer (with opposite orientation to the lipid dipoles). Because of lack of appreciable adsorption, CsCl does not have a large contribution to the electrostatic profile. The effect of KCl is somewhat between NaCl and CsCl. However, the orientation of water molecules at the headgroup region compensates almost perfectly for the effect of salts. This compensation leads to the above observation that the total electrostatic profiles are very similar to each other.

Area Per Lipid, Membrane Thickness, and Lipid Diffusion. We investigated how the area per lipid changes depending on the type of cation present in the system. It was calculated as the lateral area of the simulation box in the membrane plane divided by the number of lipids in a single layer. For a given size of unit cell, we observed relatively large fluctuations in these areas, up to 0.1 nm^2 per lipid for the time scale over 100 ns. The average areas per lipid are given in Table 4. It can be seen that, compared to neat water, the area per headgroup decreases by around 5% in the presence of salts with the Cl$^-$ anion and different alkali cations, which is the same trend as observed in previous simulations of POPC lipid bilayers.[11] The observed decrease of area per lipid correlates with an increase of the membrane thickness. Note that the membrane thickness was measured as in the experiment,[37] i.e., as the distance between the two peaks in the electron density profiles of the system (Table 2). As for the area per lipid, the specific effect of different alkali cations is small.

We have also evaluated the effect of salt on lipid diffusion. Phospholipid diffusion constants were calculated similarly as in our previous work[19] and corrected for the motion of the center of mass of the corresponding leaflet. The diffusion constant in neat water of $(1.6 \pm 0.1) \times 10^{-12}$ m^2/s decreased to $(0.7 \pm 0.1) \times 10^{-12}$ m^2/s upon adding 1 M of NaCl.

Anions. *Ion Adsorption.* As shown in Figure 5, the electron density profiles are very similar for all salts with varying anions. At the same time, differences in anion adsorption can be clearly seen from the number density plots in Figure 6. This figure shows that larger anions, such as I$^-$, penetrate deeper into the membrane compared to small anions such as Cl$^-$. From the number density profiles it also follows that sodium adsorbs slightly stronger in the presence of larger counteranions; however, the differences in counterion adsorption are very small and within the statistical error. The penetration of iodide into the headgroup region is graphically demonstrated in Figures 7 and 8 which provide an overall and a zoomed-in view of the local environment around this anion at the membrane.

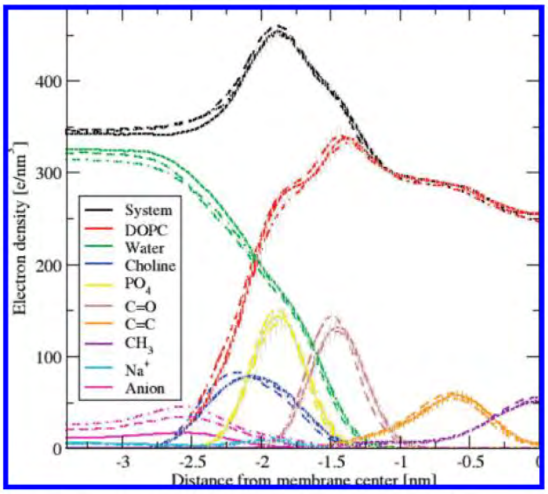

Figure 5. Total and partial electron density profiles. Full lines are for NaCl, dashed lines for NaBr, and dashed-dotted lines for NaI. Only half of the unit cell is depicted with the results being averaged over the two equivalent halves.

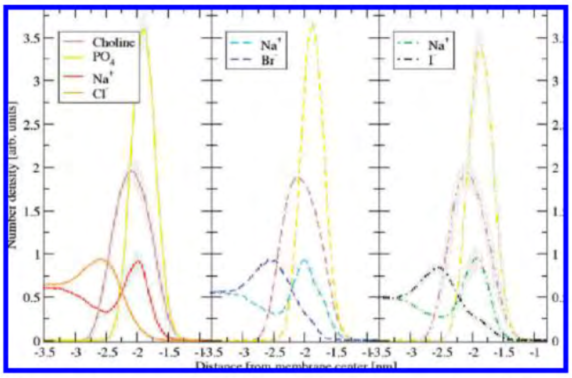

Figure 6. Number density profiles of ions at the membrane/solution interface averaged over a 40 ns trajectory segment after equilibration. Full line: NaCl, dashed line: NaBr, dashed-dotted line: NaI. Choline and phosphate densities are also depicted.

The number of adsorbed ions at the membrane is shown in Table 2. There is roughly the same number of the anions within 0.6 nm from the phosphates, while the volume around the choline group contains more larger-sized anions (such as I$^-$) than smaller ones (Cl$^-$). A similar result was obtained when the number of ions within 0.6 nm from any lipid atom was analyzed. As already mentioned above, there are about 0.3−0.4 sodium cations per lipid in the phosphate region (see Table 2), with the number of Na$^+$ in membrane slightly increasing with the size of the counteranion. Table 5 shows the residence times of sodium, depending on the type of anion, which are increasing from chloride to iodide. Interestingly, the longest time for which the Na$^+$ ion stayed adsorbed somewhat decreases as the size of counterion increases.

Electrostatics and Headgroup Orientation. For the investigated salts there is virtually no anion-specific effect of electrostatic potential across the membrane, as can be seen from Figure 9. Unlike the case of varying cations, the partial electrostatic

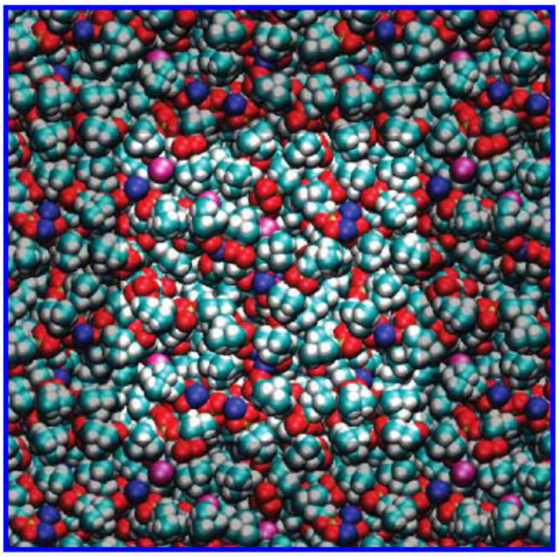

Figure 7. Top view of the NaI solution/membrane interface. Note that sodium cations (blue) and, in particular, iodide anions (pink) are able to penetrate into the headgroup region.

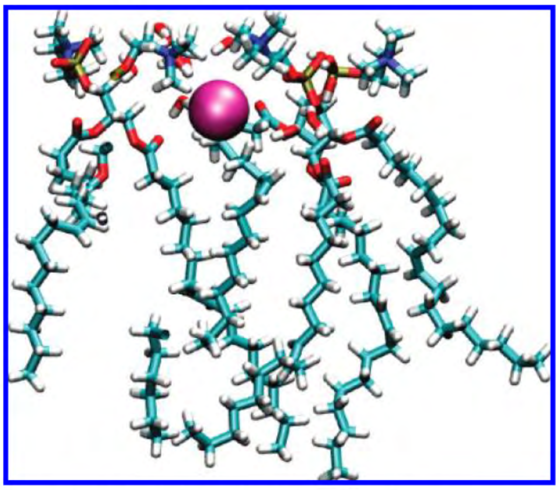

Figure 8. A detailed snapshot showing the local arrangement of phospholipids around an iodide anion which penetrated deep into the headgroup region.

TABLE 5: Residence Times and the Longest Contact Times of Sodium within a Distance of 0.6 nm around Phosphates for Aqueous Solutions with Different Halide Counteranions

	mean residence times of Na^+, ps	longest contact time of adsorbed Na^+, ns
NaCl	350	120
NaBr	400	110
NaI	530	90

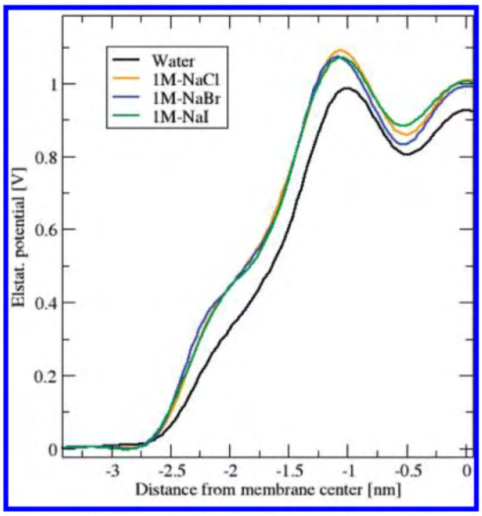

Figure 9. Total electrostatic potential at the membrane/solution interface for systems with varying anions.

TABLE 6: Peak Maximum and Half-Width at Half-Maximum of Lipid Headgroup Orientational Distributions[a]

	most probable orientation [deg]	half-width at half-maximum [deg]
water[19]	67	36/37
NaCl	61	38/61
KCl	65	40/45
CsCl	72	34/48
NaBr	57	40/57
NaI	53	43/53

[a] Note that the orientational distributions are asymmetric; therefore, we present two half-widths (left/right from the peak maximum).

profiles for different anions are also very similar to each other (data not shown here). As for the varying cations, we see that for varying anions the potential remains zero close to the membrane. It is worth mentioning that there is a significant difference in the distributions of the headgroup orientation in different solutions, as can be seen from Table 6. This orientation was computed as the angle between the vector connecting the phosphorus and the nitrogen atoms and the normal to the bilayer. Even though the distribution is quite broad it is clear that ion adsorption leads to the orientation of headgroups more outward from the membrane (heads stand more "straight"), this effect being stronger for larger anions. Note, that larger cations (Cs^+) which are not enhanced at the headgroup region have an opposite effect, with the heads being oriented more in the membrane plane (heads "lay down").

Area per Lipid. The effects of the anions on the area per lipid were analyzed in the same way as for the cations. The mean values of areas per lipid and related membrane thickness values, which are not strongly anion-dependent, are presented in Table 4. As in the case of cations, we also observed large fluctuations in the membrane area, up to 0.1 nm^2/per lipid over 100 ns time period. To be confident that we reached equilibrium, simulations for NaBr were extended up to 300 ns, and we have not observed any transition or shift in the mean area per lipid during this time period.

Experimental. The effect of NaCl on the DOPC model membrane was studied experimentally using fluorescent time-resolved solvent relaxation technique and z-scan fluorescence correlation spectroscopy, allowing determination of headgroup hydration and mobility, and lateral diffusion, respectively. For both methods, two identical bilayer systems with or without 150 mM NaCl were compared. Since already a 150 mM concentration was found to produce measurable changes, it was chosen as the physiologically relevant one. This choice also minimizes artifacts which could arise in FCS measurements if the refractive index of the sample differs appreciably from that of pure water.

TABLE 7: Solvent Relaxation Parameters Measured for 150 mM NaCl or Water Suspension of DOPC Large Unilamellar Vesicles Labeled with 1 mol% of Laurdan or DTMAC

	Laurdan			DTMAC		
	$\Delta\nu$ (cm^{-1})[a]	τ_r (ns)[b]	obsd, %[c]	$\Delta\nu$ (cm^{-1})[a]	τ_r (ns)[b]	obsd, %[c]
water	4250 ± 50	1.45 ± 0.05	76	2350 ± 50	1.12 ± 0.05	71
NaCl	4250 ± 50	1.56 ± 0.05	77	2350 ± 50	1.09 ± 0.05	74

[a] $\Delta\nu = \nu(t = 0) - \nu(t = \infty)$; $\nu(t = 0)$ − estimated;[30] $\nu(t = \infty)$ obtained from TRES reconstruction.[31] [b] Integrated relaxation time: $\tau_r = \int_0^\infty C(t)\mathrm{d}t$. [c] Percentage of observed SR process obtained by comparison of the $\Delta\nu$ values calculated using the estimated $\nu(t = 0)$ with those obtained exclusively from TRES reconstruction.[30]

Solvent Relaxation. SR experiments were performed using two fluorescent probes, Laurdan and DTMAC, which were shown to be located at two different depths of the bilayer, i.e., at the level of *sn*-1 carbonyl and at upper glycerol region.[38,39] The parameters obtained from the TRES analysis, i.e., the total emission shift ($\Delta\nu$), the mean integrated relaxation time (τ_r), and the percentage the relaxation process, which was observed, are listed in Table 7.

Analysis of the full-width at half-maximum of TRES revealed that more than 70% of the relaxation process was captured within the experimental time window (0.05−30 ns), which means that the time-dependent Stokes shift is mainly occurring on the nanosecond time scale. No polarity changes of the local environment of the dyes with salt were observed, as seen from the constant $\Delta\nu$ values. This parameter is usually attributed to the extent of membrane hydration because water is the main source of polarity in lipid membranes. However, the relaxation kinetics for Laurdan was slowed down by about 7% upon the addition of NaCl, as revealed by the τ_r values. The difference is not large but it is significant (i.e., above the resolution of the measurement). A vanishing salt effect is observed for the DTMAC probe located closer to the bulk water, i.e., at the upper glycerol level. It should be pointed out that we showed earlier that DTMAC is less sensitive than Laurdan to changes in the headgroup region.[38,39] These results indicate that the mobility of hydrated lipid headgroups is somewhat more restricted in the presence of NaCl when compared to pure water.

Z-SCAN FCS. The obtained intensity scans show confluent DOPC SPBs in both pure water and NaCl solution. No intensity loss was observed upon medium exchange. Because no buffer and no calcium was present during SPB formation, some fraction of vesicles adhered to the bilayer are present even after flushing.[29] This was observed as a short initial decrease of the fluorescent signal due to photobleaching of these immobile vesicles. Thanks to this fast bleaching no fluorescent signal from the adhered vesicles was collected during the Z-scan.

The results obtained for DOPC SPBs in NaCl and in pure water are presented in Table 8. The lateral diffusion in the NaCl solution is considerably (by more than 25%) slower than in pure water. The intercept of the diffusion time as a function of particle number with diffusion time axis is close to zero, which means that predominantly free diffusion is observed (see refs 34 and 35 for detailed explanation). All the values shown in the table are averages for at least two samples; every sample was z-scanned at two different spots before and after medium exchange. The above results show that the lateral diffusion of lipids in the DOPC-supported bilayer is somewhat restricted in the NaCl solution when compared to water.

TABLE 8: Effective Lateral Diffusion Coefficient Measured in Supported DOPC Membrane on Mica in 150 mM NaCl or in Water Using FCS Z-Scan Technique[a]

	τ_D (ms)[b]	D_{eff} ($\times10^{-12}$ m^2/s)[c]	intercept (ms)[d]
water	1.74 ± 0.31	7.9 ± 1.3	0.4 ± 0.5
NaCl	2.19 ± 0.12	6.0 ± 0.4	0.18 ± 0.14

[a] All the parameters obtained from the plot of apparent diffusion times versus the relative particle numbers as described in ref 34. [b] Mean diffusion time. [c] Effective diffusion coefficient. [d] Intercept of the linear fit to the data with diffusion time axis (i.e., relative particle number = 0).

Discussion

First, let us consider the effect of the presence of different cations, such as Na^+, K^+, or Cs^+ (with the Cl^- counterion) in the system. We observe in the simulations that sodium ions adsorb to the DOPC membrane, being preferentially located at the phosphate region. This also enables coadsorption of chloride at the choline region, which is located in the outer part of the membrane. The Na^+ and Cl^- ions thus create an electric double layer, but its potential is almost fully compensated by the orientation of waters, so that the total electrostatic profile is similar to the system without salt. In contrast, larger cations, such as cesium, do not preferentially adsorb to the membrane and only weakly penetrate the headgroup region. Potassium exhibits an intermediate behavior between sodium and cesium, penetrating the membrane but not being enhanced in the membrane region. Moreover, neither of the CsCl or KCl salts creates an ionic double layer at the membrane surface.

Our findings qualitatively agree with the results from previous simulations that smaller cations adsorb more to the membrane than larger cations.[13−15] However, our study shows a quantitative difference in the exact location where sodium ions display a peak in the density profile. Employing an all-atom forcefield, we find that sodium is primarily enhanced at the phosphate region, while in the previous studies which used a united atom force field, sodium preferred the carbonyl region or that between the carbonyls and phosphate.[11−15,40,41] Also, potassium behavior at the membrane seems to be somewhat forcefield dependent; within the present simulations, K^+ was not enhanced in the membrane as is the simulations with OPLS potassium,[14,15] while that described using the CHARMM forcefield exhibits a stronger attraction for the headgroup region.[13]

Next, we consider the effect of having different halide anions paired with a common sodium countercation. We observe a stronger affinity of anions for the membrane as we move from Cl^- to Br^- and to I^-. In other words, larger anions penetrate deeper into the membrane than smaller ones, similar to the finding in a previous computational study of a POPC membrane.[42,43] Nevertheless, we find that the differences in anion behavior are small and none of the halides is actually enhanced at the membrane, although iodide penetrates deeper into the membrane. That we observe only a small difference in anion behavior at the membrane/aqueous solution interface may, however, be due to deficiencies of the nonpolarizable force fields. It was demonstrated in the simulations of ions in water clusters[44] and ions at the water−air interface[45] that inclusion of polarization enhances the surface affinity of soft ions such as the heavier halides. Such simulations for membranes are unfortunately computationally extremely demanding; moreover, a reliable polarizable potential is not available for these systems. We are currently developing and testing a polarizable force field for phospholipid membranes, which will allow for directly addressing this issue and connecting more quantitatively to the experiment.[8,9]

Both fluorescence experiments performed in this study show trends upon adding salt which are consistent with the computational prediction of affinity and direct interaction of sodium with the bilayer. Solvent relaxation measurements do not reveal any changes of the degree of hydration of the lipid headgroups upon addition of salt, which agrees with the simulated water profiles in this region, which are practically unchanged (Figure 2). Measurements show that the presence of sodium ions rigidifies the headgroup region. The relaxation time (Table 7) increases with the presence of salt for the Laurdan dye, which is related with stiffening of the headgroups and decrease of the area per lipid (see ref 38 for comparison). This is consistent with the decrease of area per lipid upon adding salt as observed in the simulations. Also, interaction of sodium cations with hydrated oxygen atoms in the headgroup slows down the lateral and rotational diffusion of the DOPC headgroup within the bilayer. The two employed experimental approaches are based on very different concepts (i.e., while solvent relaxation is based on monitoring photophysics occurring on the nanosecond time scale, FCS analyzes fluorescence fluctuations on the millisecond time scale). Nevertheless, the effect of added salt on the behavior of the lipid bilayer (with the fluorescence label) is consistently revealed as in a similar study, where supported multilayers of POPC were studied using single point FCS measurements.[11]

It should be stressed that MD simulations, such as those presented here, are necessarily limited in their dimensional and temporal scope and can, therefore, only partially relate to the present experiments. For example, large scale fluctuations within the membrane can possibly lead to creation of pores, through which water and even ions could penetrate. Such effects, which can be present in many experiments, could not be addressed by the present simulations. Nevertheless, the same trend, i.e., slowing of the lateral lipid diffusion upon adding salt is observed both in experiment and simulation. It is also worth stressing that different experimental probes and techniques cannot be expected to be influenced to the same extent by salts since some membrane properties, such as headgroup orientation and diffusion, are more sensitive to specific ion effects than others, such as, for example, membrane thickness.

In summary, there are several physical mechanisms which determine ion-specific adsorption to aqueous DOPC membrane. Ion pairing drives small alkali cations to the negatively charged phosphate and carbonyl groups of the phospholipids. Anions are analogously, albeit more weakly attracted to the positively charged choline groups. In addition, large and soft ions can penetrate and even be enhanced at the boundary between the hydrophilic and hydrophobic regions of the membrane. Charge neutralization is another effect to consider. If one type of ions exhibits affinity to the membrane then the counterions will also be attracted to ensure interfacial neutrality. Finally, steric hindrance at the crowded headgroup region may prevent ion adsoption or at least create a kinetic barrier. This effect is likely to be particularly important for more compact phases of the bilayer.

Conclusion

Molecular dynamics simulations with an all-atom force field were performed to investigate interactions of alkali cations and halide anions with a DOPC bilayer in aqueous salt solutions. Among the investigated cations, only sodium exhibits an enhancement at the headgroup region, its concentration peaking in the vicinity of the phosphate groups. In contrast, potassium or cesium do not adsorb preferentially at the membrane. For anions the situation is different. On one hand, they tend to compensate for the positive charge of the sodium countercations by weakly accumulating at the outer headgroup region next to the choline groups. On the other hand, larger anions tend to penetrate closer to the hydrophobic region of the membrane due to a mechanism similar to their segregation at the water/vapor interface. This effect is likely to be further enhanced when polarization interactions are included into the force field.

Changes upon adding NaCl were also observed by means of fluorescence spectroscopy for phospholipid lateral diffusion and in solvent relaxation. Compared to neat water, the phospholipid lateral diffusion in 150 mM NaCl is slowed down by about 25%. Additionally, solvent relaxation in the headgroups is slowed down by ∼8%.

Specific ion effects at the phospholipid membrane influence to varying degrees physical properties of the bilayer. Compared to neat water, changes are observed in the electron density profiles and in the surface potential, as well as in the areas per lipid headgroup. While addition of alkali halide salts leads to non-negligible effects, ion specificity is weak for these properties. This can be contrasted with strongly ion specific density profiles, which indicates that different probing techniques exhibit varying sensitivity to ion specificity.

Acknowledgment. Support from the Czech Ministry of Education (grant LC512) and the Czech Science Foundation (grant 203/08/0114) is gratefully acknowledged. M.L.B. acknowledges support from the National Science Foundation grant MCB-0615469. R.A.B. and S.W.I.S. acknowledge support from the Deutsche Forschungsgemeinschaft (Graduate School Structure Formation and Transport in Complex Systems 1276/1). R.V. acknowledges support from the Czech Science Foundation (grant 203/05/H001) and from the International Max-Planck Research School. Part of the work in Prague was supported via Project Z40550506.

References and Notes

(1) McLaughlin, S. *Annu. Rev. Biophys. Biophys. Chem.* **1989**, *18*, 113–136.

(2) Hodgkin, A. L.; Horowicz, P. *J. Physiol. (Oxford, U.K.)* **1960**, *153*, 404–412.

(3) Clarke, R. J.; Lupfert, C. *Biophys. J.* **1999**, *76*, 2614–2624.

(4) Kunz, W.; Henle, J.; Ninham, B. W. *Curr. Opin. Colloid Interface Sci.* **2004**, *9*, 19–37.

(5) Petrache, H. I.; Zemb, T.; Belloni, L.; Parsegian, V. A. *Proc. Natl. Acad. Sci. U.S.A.* **2006**, *103*, 7982–7987.

(6) Aroti, A.; Leontidis, E.; Dubois, M.; Zemb, T. *Biophys. J.* **2007**, *93*, 1580–1590.

(7) Leontidis, E.; Aroti, A.; Belloni, L.; Dubois, M.; Zemb, T. *Biophys. J.* **2007**, *93*, 1591–1607.

(8) Garcia-Manyes, S.; Oncins, G.; Sanz, F. *Biophys. J.* **2005**, *89*, 4261–4274.

(9) Garcia-Celma, J. J.; Hatahet, L.; Kunz, W.; Fendler, K. *Langmuir* **2007**, *23*, 10074–10080.

(10) Pabst, G.; Hodzic, A.; Strancar, J.; Danner, S.; Rappolt, M.; Laggner, P. *Biophys. J.* **2007**, *93*, 2688–2696.

(11) Bockmann, R. A.; Hac, A.; Heimburg, T.; Grubmuller, H. *Biophys. J.* **2003**, *85*, 1647–1655.

(12) Pandit, S. A.; Bostick, D.; Berkowitz, M. L. *Biophys. J.* **2003**, *84*, 3743–3750.

(13) Gurtovenko, A. A.; Vattulainen, I. *J. Phys. Chem. B* **2008**, *112*, 1953–1962.

(14) Lee, S. J.; Song, Y.; Baker, N. A. *Biophys. J.* **2008**, *94*, 3565–3576.

(15) Cordomi, A.; Edholm, O.; Perez, J. J. *J. Phys. Chem. B* 2008.

(16) Bockmann, R. A.; Grubmuller, H. *Angew. Chem., Int. Ed.* **2004**, *43*, 1021–1024.

(17) Cordomi, A.; Edholm, O.; Perez, J. J. *J. Phys. Chem. B* **2008**, *112*, 1397–1408.

(18) Van Der Spoel, D.; Lindahl, E.; Hess, B.; Groenhof, G.; Mark, A. E.; Berendsen, H. J. *J. Comput. Chem.* **2005**, *26*, 1701–1718.

(19) Siu, S.; Vacha, R.; Jungwirth, P.; Bockmann, R. A. *J. Chem. Phys.* **2008**, *128*, 125103.

(20) Darden, T.; York, D.; Pedersen, L. *J. Chem. Phys.* **1993**, *98*, 10089–10092.

(21) Berendsen, H. J. C.; Grigera, J. R.; Straatsma, T. P. *J. Phys. Chem. A* **1987**, *91*, 6269–6271.

(22) Markovich, G.; Perera, L.; Berkowitz, M. L.; Cheshnovsky, O. *J. Chem. Phys.* **1996**, *105*, 2675–2685.

(23) Smith, D. E.; Dang, L. X. *Chem. Phys. Lett.* **1994**, *230*, 209–214.

(24) Dang, L. X.; Schenter, G. K.; Glezakou, V. A.; Fulton, J. L. *J. Phys. Chem. B* **2006**, *110*, 23644–23654.

(25) Dang, L. X. *J. Phys. Chem. B* **1999**, *103*, 8195–8200.

(26) Auffinger, P.; Cheatham, T. E.; Vaiana, A. C. *J. Chem. Theory Comput.* **2007**, *3*, 1851–1859.

(27) Chen, A. A.; Pappu, R. V. *J. Phys. Chem. B* **2007**, xxx.

(28) Epand, R. F.; Epand, R. M.; Sterk, G. J.; Thijsse, P. A.; Sang, H.; Kraayenhof, R. *Biophys. J.* **1996**, *70*, TUAM8−TUAM8.

(29) Benes, M.; Billy, D.; Benda, A.; Speijer, H.; Hof, M.; Hermens, W. T. *Langmuir* **2004**, *20*, 10129–10137.

(30) Jurkiewicz, P.; Sykora, J.; Olzynska, A.; Humplickova, J.; Hof, M. *J. Fluoresc.* **2005**, *15*, 883–894.

(31) Horng, M. L.; Gardecki, J. A.; Papazyan, A.; Maroncelli, M. *J. Phys. Chem.* **1995**, *99*, 17311–17337.

(32) Benda, A.; Benes, M.; Marecek, V.; Lhotsky, A.; Hermens, W. T.; Hof, M. *Langmuir* **2003**, *19*, 4120–4126.

(33) Dertinger, T.; Pacheco, V.; von der Hocht, I.; Hartmann, R.; Gregor, I.; Enderlein, J. *Chemphyschem* **2007**, *8*, 433–443.

(34) Humpolickova, J.; Gielen, E.; Benda, A.; Fagulova, V.; Vercammen, J.; Vandeven, M.; Hof, M.; Ameloot, M.; Engelborghs, Y. *Biophys. J.* **2006**, *91*, L23−L25.

(35) Wawrezinieck, L.; Rigneault, H.; Marguet, D.; Lenne, P. F. *Biophys. J.* **2005**, *89*, 4029–4042.

(36) Sachs, J.; Crozier, P.; Woolf, T. *J. Chem. Phys.* **2004**, *121*, 10847–51.

(37) Liu, Y.; Nagle, J. *Phys. Rev. E* **2004**, *69*, 040901.

(38) Jurkiewicz, P.; Olzynska, A.; Langner, M.; Hof, M. *Langmuir* **2006**, *22*, 8741–8749.

(39) Sykora, J.; Jurkiewicz, P.; Epand, R. M.; Kraayenhof, R.; Langner, M.; Hof, M. *Chem. Phys. Lipids* **2005**, *135*, 213–221.

(40) Biophys. J. 2008, *94*, 3565.

(41) Pandit, S.; Bostick, D.; Berkowitz, M. *Biophys. J.* **2003**, *84*, 3743–3750.

(42) Sachs, J. N.; Woolf, T. B. *J. Am. Chem. Soc.* **2003**, *125*, 8742–8743.

(43) Sachs, J. N.; Nanda, H.; Petrache, H. I.; Woolf, T. B. *Biophys. J.* **2004**, *86*, 3772–3782.

(44) Perera, L.; Berkowitz, M. *J. Chem. Phys.* **1991**, *95*, 1954–1963.

(45) Vrbka, L.; Mucha, M.; Minofar, B.; Jungwirth, P.; Brown, E. C.; Tobias, D. J. *Curr. Opin. Colloid Interface Sci.* **2004**, *9*, 67–73.

JP809974E

9504 *J. Phys. Chem. B* **2010,** *114,* 9504–9509

Mechanism of Interaction of Monovalent Ions with Phosphatidylcholine Lipid Membranes

Robert Vácha,[*,†,‡] Piotr Jurkiewicz,[*,§] Michal Petrov,[†] Max L. Berkowitz,[||]
Rainer A. Böckmann,[⊥] Justyna Barucha-Kraszewska,[§] Martin Hof,[§] and Pavel Jungwirth[†]

Institute of Organic Chemistry and Biochemistry, Academy of Sciences of the Czech Republic and Center for Biomolecules and Complex Molecular Systems, Flemingovo nám. 2, 16610 Prague 6, Czech Republic; Department of Chemistry, University of Cambridge, Lensfield Road, Cambridge, CB21EW, United Kingdom; J. Heyrovský Institute of Physical Chemistry, Academy of Sciences of the Czech Republic, v. v. i., Dolejškova 3, 18223 Prague 8, Czech Republic; Department of Chemistry, University of North Carolina, Chapel Hill, North Carolina 27599; and Computational Biology, Department of Biology, University of Erlangen-Nürnberg, 91058 Erlangen, Germany

Received: March 16, 2010; Revised Manuscript Received: June 3, 2010

Interactions of different anions with phospholipid membranes in aqueous salt solutions were investigated by molecular dynamics simulations and fluorescence solvent relaxation measurements. Both approaches indicate that the anion−membrane interaction increases with the size and softness of the anion. Calculations show that iodide exhibits a genuine affinity for the membrane, which is due to its pairing with the choline group and its propensity for the nonpolar region of the acyl chains, the latter being enhanced in polarizable calculations showing that the iodide number density profile is expanded toward the glycerol level. Solvent relaxation measurements using Laurdan confirm the influence of large soft ions on the membrane organization at the glycerol level. In contrast, chloride exhibits a peak at the membrane surface only in the presence of a surface-attracted cation, such as sodium but not potassium, suggesting that this behavior is merely a counterion effect.

Introduction

It has been observed in numerous experimental and theoretical studies that addition of salts changes the properties of lipid membranes.[1−11] Molecular dynamics simulations demonstrated salt-induced changes in lateral diffusion of phospolipids, headgroup tilt, membrane thickness, etc., which were specific for different cations.[1−3,5,11] Fewer computational studies investigated the effect of anions and either reported anionic influence on membranes[4] or similar changes for all sodium halide salt solutions (although it was observed that larger anions penetrate slightly more into the membrane than sodium).[11] In contrast, experiments primarily focused on the effects of anions that have been shown to follow the Hofmeister series.[12] For example, experiments on vesicles swelling in KCl and KBr solutions have been rationalized in terms of the enhanced presence of anions at the membrane surface.[7] Recent experiments on DPPC monolayers with sodium salt solutions showed that, while an anion adsorption explains well results for sodium salts with larger halides, those for NaF could not be fitted by such a model. A model which fits the data for all sodium salts invokes both anion adsorption and a simultaneous sodium complexation with lipids.[9,10] Such an interaction of sodium with lipid membranes was previously confirmed by fluorescence spectroscopy, which showed a slowdown in lateral diffusion of lipids and different mobility at the headgroup region.[11,13]

An important step toward understanding the interactions of biomolecules with ions in salt solution has been made by introducing the so-called “law of matching water affinities”.[14,15] This law is an empirical rule that relates the propensity of oppositely charged moieties to form contact pairs in water solution and their hydration properties. Typically, ionic species which tend to pair the most in water are those with matching hydration free energies (i.e., roughly speaking, sizes). This tendency of like-sized oppositely charged species to pair in water has been also observed in simulations[16−20] and was rationalized within a dielectric continuum model recently.[21]

In this paper, we compare different salts by varying both cations and anions: this allows us to distinguish between different mechanisms responsible for ion−membrane interaction. Moreover, we present, for the first time, results from the simulation of membrane in a salt solution performed using a polarizable force field. It has been recently shown that the inclusion of polarizability is important for the description of anions at water/hydrophobic interface, where local concentrations of large and polarizable ions can be enhanced compared to the aqueous bulk.[22−26] We paralleled our calculations with fluorescence solvent relaxation measurements using Laurdan,[27] thus providing direct information about the influence of such ions on the polarity and mobility of lipid bilayer at the glycerol level.[28]

Methods

Computation. Molecular dynamics (MD) simulations were performed using the GROMACS program package version 3.3.1.[29] Four systems were simulated: each consisted of 72 DOPC lipid molecules, 2627 water molecules, 50 cations, and 50 anions, representing a ∼1 M solution of 1:1 salt. The salt in our simulations was KI, NaI, KCl, or NaCl. The simulations were carried out for 200 ns with a 2 fs time step. The first 80

---

[*] To whom correspondence should be addressed. E-mail: rv260@cam.ac.uk (R.V.); piotr.jurkiewicz@jh-inst.cas.cz (P.J.).

[†] Institute of Organic Chemistry and Biochemistry, Academy of Sciences of the Czech Republic and Center for Biomolecules and Complex Molecular Systems.

[‡] University of Cambridge.

[§] J. Heyrovsky Institute of Physical Chemistry, Academy of Sciences of the Czech Republic.

[||] University of North Carolina.

[⊥] University of Erlangen-Nürnberg.

10.1021/jp102389k

ns were used for equilibrating the system and the following 120 ns for sampling. We employed the canonical NPγT ensemble with the surface tension of 22 mN/m in the membrane plane (*xy*-plane) and pressure of 1 atm in the perpendicular direction (*z*-axis). This particular value of the surface tension was chosen such as to match the experimental area per lipid.[30] The temperature was kept at 310 K using the Berendsen thermostat. Additional details concerning the force field and properties evaluation can be found in our previous paper,[11] where density profiles of ions of NaCl, KCl, and NaI salts solutions next to a DOPC membrane were studied.

In order to investigate the possible effect of the polarizability, we also performed a 20 ns long simulation of a DOPC membrane in a 1 M KI solution using a polarizable force field. The system setup was the same as in the nonpolarizable case, except that we employed the canonical NVT ensemble with the same value of volume as in simulations with the nonpolarizable force field. We could not perform polarizable simulations in a constant surface tension ensemble, because we do not know what value of surface tension one needs to use in order to get an experimental area per headgroup in simulations with polarizable force field. To get such information requires immense computational resources due to the use of a polarizable force field. The initial configuration in the polarizable simulation was taken from the end of a 200 ns nonpolarizable simulation. For water we employed the polarizable POL3 model[31] and polarizable ion parameters were taken from references.[23,32] The polarizable all-atom force field for the DOPC lipid was developed in a similar way as the nonpolarizable one, being based on generalized AMBER force field.[30] The partial charges of the DOPC molecule were calculated using density functional theory with the B3LYP functional and the cc-pvtz basis set.

Experiment. 1,2-Dioleoyl-*sn*-glycero-3-phosphocholine (DOPC) was purchased from Avanti Polar Lipids, Inc. (Alabaster, AL). 6-Dodecanoyl-2-dimethylaminonaphthalene (Laurdan) was obtained from Invitrogen (Eugene, OR). Salts (NaCl, NaBr, NaI, NaSCN, $NaClO_4$), supplied by Sigma-Aldrich (St. Louis, MO), were dissolved in Milli-Q water (Millipore, Etten-Leur, The Netherlands).

Large unilamellar vesicles were prepared by the extrusion method. DOPC and Laurdan were mixed in chloroform in a 1:100 dye to lipid molar ratio. Chloroform was evaporated under a stream of nitrogen and then under vacuum for at least 2 h. The resulting dry lipid film was suspended in the chosen salt solution, vortexed for 4 min, and extruded through polycarbonate membranes (Avestin, Ottawa, Canada) with a pore diameter of 100 nm. The resulting suspension was measured in 1 cm quartz cuvette thermostated by circulating water at 10 °C. For each sample, a steady-state fluorescence spectrum and a series of fluorescence decays for emission wavelengths from 400 to 540 nm (with a 10 nm step) were recorded on a Fluorolog 3 (Jobin Yvon) and on an IBH 5000 U SPC equipped with an IBH laser diode NanoLED 11 and a cooled Hamamatsu R3809U-50 microchannel plate photomultiplier, respectively. From the measured data the time-resolved emission spectra (TRES) were reconstructed and analyzed. The total emission shift $\Delta\nu$ and the mean integrated relaxation time τ_r, which reflect polarity and mobility of probe environment at the glycerol level of phospholipid bilayer, respectively, were calculated as previously described.[11]

Results

Computation. Results for DOPC in four different salt solutions, NaCl, KCl, NaI, or KI, are compared to each other in Figure 1. Here, the ion number density profiles along the axis perpendicular to the membrane are plotted. The focus is on the headgroup region, where ion profiles are strongly nonmonotonous, reflecting the complexity of the membrane/solution interface. For easier identification of the individual regions of the system, the partial density profiles of choline and phosphate groups of DOPC are also depicted. Below we provide a description of the ionic profiles for individual salts.

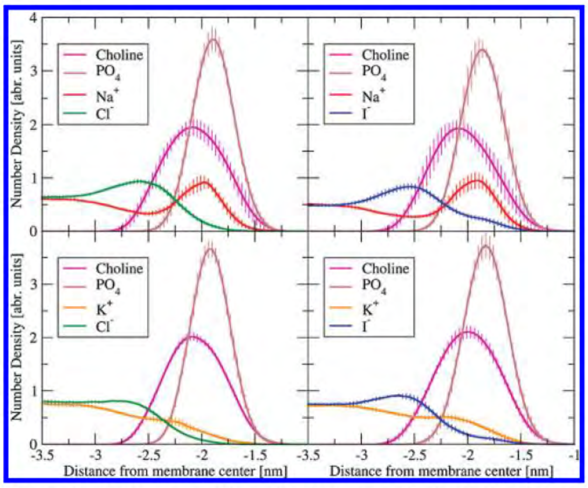

Figure 1. Ion density profiles in four different 1 M salt solutions (NaCl, NaI, KCl, and KI) next to a DOPC membrane. For easier identification of the headgroup region, partial density profiles of choline and phosphate groups are also depicted. Data were averaged over the two equivalent halves of the membrane over 120 ns.

NaCl. The densities of both ions are enhanced at the membrane (i.e., they exhibit a density peak), but the exact peak location differs. Sodium signal peaks at the phosphate region, while chloride accumulates at the membrane surface.

KCl. The density profile of the potassium cation does not exhibit an appreciable peak; nevertheless, potassium does penetrate into the headgroup region. No surface peak is observed for the chloride anion, with penetration into the headgroup region being even weaker.

NaI. Sodium cations are enhanced at the phosphate region. Iodide accumulates on the membrane surface and also penetrates deeper into the headgroup region (all the way to the region of negatively charged phosphate groups).

KI. Potassium does not exhibit a density peak but penetrates into the headgroup region. Iodide anions are weakly adsorbed on the membrane surface and penetrate deeply the headgroup region (similarly as in the case of NaI).

The ionic density profiles were analyzed in terms of the surface excess, an integral quantity appearing in the Gibbs adsorption isotherm. Evaluated values of the surface excess are as follows: $\Gamma_{NaCl} = -0.4$ mol/cm^2, $\Gamma_{KCl} = -1.4$ mol/cm^2, $\Gamma_{NaI} = +0.2$ mol/cm^2, and $\Gamma_{KI} = -0.7$ mol/cm^2. In agreement with the description of the above-given results, we observed that iodide salts are adsorbed more than chloride salts, from which those with sodium are adsorbed more than those with potassium. Note that the absolute vlaues of Na^+ and K^+ adsorption are somewhat force field dependent; however, the trend that Na^+ is adsorbed more than K^+ is conserved.[11]

Next, we analyzed the changes in the first solvation shell of anions as they approach the headgroup region. The size of the first solvation shell is determined by the location of the first minimum in the radial distribution function (RDF) between the

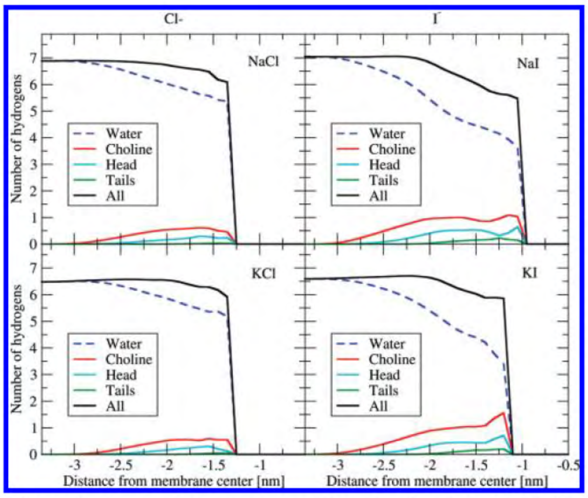

Figure 2. Averaged compositions of first solvation shells of chloride and iodide in terms of numbers of water hydrogens, shown along the *z*-axis. Partial contributions from water, choline, headgroup except choline, and lipid tails are displayed. Data were averaged over the two equivalent halves of the membrane over 120 ns.

ion and water hydrogens. For chloride the first minimum (following the first maximum) in the RDF is at 0.301 nm, while for iodide it is located at 0.340 nm. The number of hydrogens in the first solvation shell of an anion versus the distance from the membrane center is depicted in Figure 2. The total amount of hydrogens lost from the anionic solvation shell upon entering the membrane is about 1 for iodide but only 0.5 for chloride. The number of water hydrogens that are replaced by lipid atoms is about 2 for iodide and 1 for chloride. Note that iodide at the membrane interface has a significant number of acyl chain hydrogens in its first solvation shell, while chloride does not. Thus, upon entering the headgroup region, iodide is more prepared to shed off water hydrogens from its solvation shell and replace them by lipid atoms. A snapshot showing such a process is presented in Figure 3.

For completeness, we also discuss the situation in the aqueous bulk region of the investigated solutions. There is a small difference in the number of water hydrogens in the first solvation shell of an anion in the aqueous bulk when comparing solutions with different countercations. This number is about 6.9 for NaCl but 6.5 for KCl and 7.1 for NaI but 6.6 for KI (Figure 2). The decrease due to replacement of sodium by potassium is caused by an increase in ion pairing, as verified via the cation−anion radial distribution functions. The difference between sodium halide and potassium halide radial distribution functions for chloride and iodide is plotted in Figure 4. We see that both anions prefer to pair with potassium over sodium; as a result the integral values shown in the inset of Figure 4 are converging to negative values. The higher tendency of both chloride and iodide to pair with potassium over sodium is in agreement with results of ab initio calculations with a polarizable continuum solvent model, as well as with experimental activity coefficients.[16]

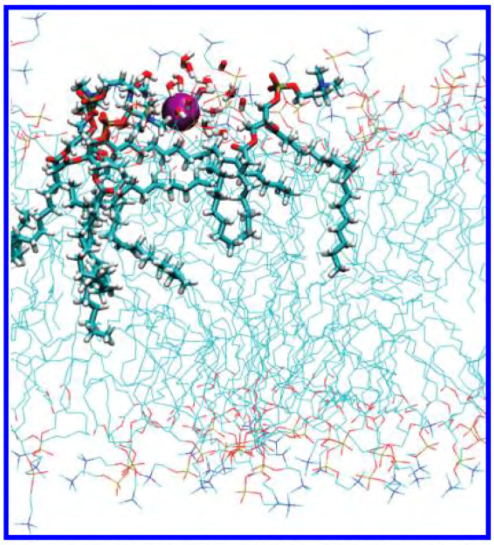

Figure 3. A simulation snapshot of iodide adsorbed at a phospholipid membrane surface. The situation illustrates iodide in contact with hydrocarbon chains of lipids surrounded by water and choline groups. Iodide is displayed in purple color and all molecules within 0.6 nm from the iodide are magnified. Remaining water molecules are not shown for clarity and lipids are depicted in lines.

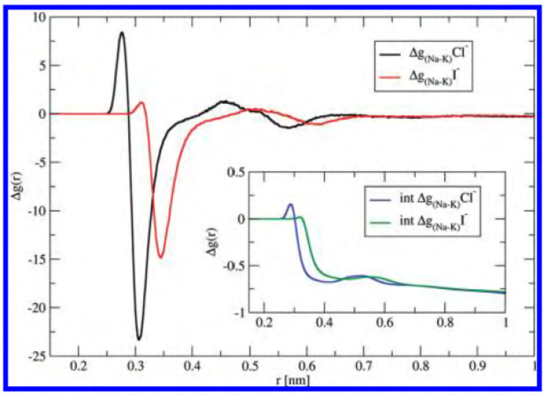

Figure 4. Difference in radial distribution functions of sodium vs potassium around chloride (black) and iodide (red) anions. The inset contains the integral values of these differences, showing a preference of potassium over sodium for both anions.

To compare the results from our simulations with experiment, we calculated the diffusion constants of lipids, as described previously.[30] The calculated diffusion coefficients for lateral diffusion of lipids are $(6 \pm 2) \times 10^{-12}$ m^2/s for NaCl solution, $(7 \pm 2) \times 10^{-12}$ m^2/s for NaI solution, $(6 \pm 2) \times 10^{-12}$ m^2/s for KCl solution, and $(11 \pm 4) \times 10^{-12}$ m^2/s for KI solution. All values lie in the range of experimental values for lipids in water or salt solution ($D = (6-7) \times 10^{-12}$ m^2/s).[11] Unfortunately, the large statistical error in calculations did not allow to perform more direct comparison. Residence times of ions at the membrane interface were evaluated in the same way as in our previous paper.[11] Both anions showed exponential distribution of residence times with a mean value of 50−80 ps. Iodide had longer residence times than chloride in both sodium and potassium salts; however, the differences are within estimated error. Both cations exhibited a power-law distribution of residence times, which were also recently observed in other simulations of membrane in salt solution.[33] The mean residence times for potassium were about 80 ps for both KCl and KI. Sodium mean residence times were roughly 300 and 500 ps in NaCl and NaI solutions.

Experiment. The influence of five different monovalent anions (Cl^-, Br^-, I^-, ClO_4^-, SCN^-) on the physical properties of model lipid bilayer was investigated using fluorescence solvent relaxation method. Large unilamellar DOPC vesicles

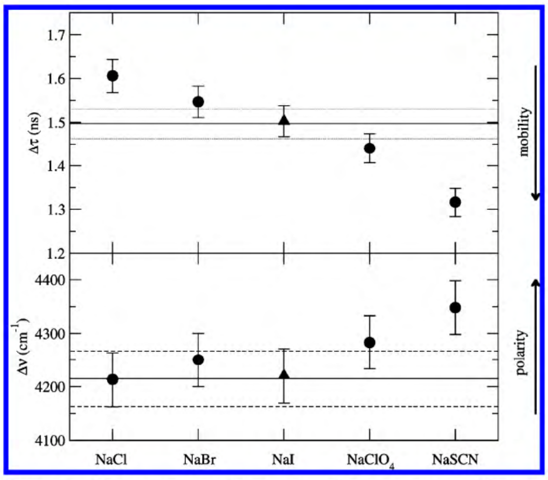

Figure 5. Fluorescence solvent relaxation parameters (integrated relaxation time, τ_r, and total spectral shift, $\Delta\nu$) obtained for Laurdan embedded in DOPC large unilamellar vesicles suspended in five different salt solutions measured at 10 °C. Salt concentration was 1 M (circles), except for sodium iodide where it was 0.15 M (triangles). Horizontal lines represent values obtained for pure water (dashed lines depict experimental uncertainty).

labeled with Laurdan were suspended in 1 M solution of sodium salts of the above-mentioned anions. Fluorescent polarity probes precisely located in phospholipid bilayer at the level of glycerol have proved to be sensitive to changes in headgroup dynamics and hydration, and hence, indirectly, to lipid packing, protein binding, headgroup tilt, or membrane curvature, to name just a few.[27,28,34]

The results presented in Figure 5 give evidence that, in contrast to small monovalent cations (data not shown), the anions significantly influence relaxation time and total spectral shift measured using Laurdan. The two parameters attributed to mobility and polarity of the lipid bilayer at its glycerol level apparently follow the Hofmeister series[12,35] in the form $Cl^- < Br^- < I^- < ClO_4^- < SCN^-$. Although the strongest changes are observed in the relaxation time, it is remarkable that the total spectral shift increase of about 150 cm^{-1} in the presence of the NaSCN in comparison to water or NaCl solution. It is worth mentioning that the latter effect is rather large when compared to solvent relaxation experiments performed on different systems and topics.

We have shown that already 0.15 M NaCl restricts headgroup mobility, when compared to the bilayer prepared in pure water.[11] Here, for 1 M concentration the effect is only slightly stronger (i.e., relaxation times are 1.56 and 1.61 ns for 0.15 and 1 M NaCl concentrations, respectively), which shows that in the case of sodium chloride, an increased osmolarity does not change bilayer properties dramatically. The polarity in the probe vicinity, $\Delta\nu$, does not change upon increasing of NaCl concentration.

From the results shown, it is evident that large soft anions (ClO_4^- and SCN^-) increase polarity and mobility at the glycerol level of DOPC bilayer. The increased polarity sensed by Laurdan can be the result of an increased hydration and/or the presence of the ions in the vicinity of the probe. Similar effects are expected for iodide. Unfortunately, at 1 M concentration, quenching of Laurdan fluorescence made solvent relaxation analysis impossible. For this ion, results obtained for 0.15 M concentration are shown. The quenching observed for higher concentrations of iodide confirms iodide penetration down to the glycerol level of phospholipid bilayer.

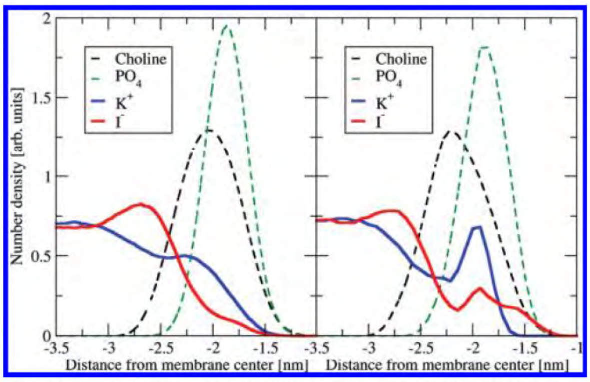

Figure 6. Effect of polarizability. Number density profiles for nonpolarizable system are shown on the left side, while the right side depicts the results of polarizable simulation, where larger ion adsorption at the membrane was observed.

Discussion

In the present simulations, we observed that chloride displays a different behavior compared to iodide at the membrane headgroup region. First of all, we observed that chloride is mostly losing its adsorption peak intensity at the membrane surface, when sodium ion is replaced by the potassium ion as the counterion. There is no such change for the iodide ion; its adsorption peak remains nearly unchanged (see Figure 1). Chloride adsorption at the headgroup region of the lipid bilayer bathed in a NaCl solution is thus caused by the electrostatic attraction to an adsorbed sodium; i.e., it is a counterion effect. In contrast, iodide affinity for the membrane is a genuine effect, independent of the presence of the countercation. The highest intensity of the iodide density peak is observed at the outermost part of the membrane where choline groups are present, which indicates appreciable iodide−choline pairing. This preferable pairing is in agreement with the empirical rule of matching hydration affinities, according to which choline as a weakly hydrated cationic group shall pair with the more weakly hydrated halide anion (i.e., iodide).[14,15]

We also analyzed the differences between chloride and iodide by studying the composition of the anionic first solvation shell. In contrast to density profiles, these results are almost the same for different countercations, Na^+ or K^+; i.e., the results to a great extent are unbiased by the nature of the countercation. This also reflects the stronger choline pairing with iodide compared to chloride. Moreover, the presence of carbon tails in the first solvation shell of iodide at the membrane demonstrates its affinity for hydrophobic interfaces. This is in agreement with previous studies of iodide at other water/hydrophobic interfaces.[22,24] Since nonpolarizable calculations underestimate anionic propensity for water/hydrophobic interfaces, we also performed a test polarizable simulation, which was computationally very demanding. The comparison between nonpolarizable and test polarizable simulations is shown in Figure 6. As anticipated, polarizability enhances iodide affinity toward the hydrophobic interior of the membrane and, consequently, it also leads to stronger membrane adsorption of potassium (counterion effect). Note that similar polarizable simulation of chloride salt solution will probably lead to increased affinity of chloride toward the membrane; nevertheless, the effect probably will be much smaller than for iodide.

The simulated different behavior at the membrane surface between a relatively small anion, chloride, and larger and softer anion, such as iodide, is supported by the present experimental results. Fluorescence relaxation spectroscopy shows that soft and large anions (perchlorate and thiocyanate) change mobility and polarity at the glycerol level of DOPC bilayer more than chloride does. Quenching of Laurdan fluorescence by iodide indicates that this anion penetrates into the membrane reaching the vicinity of the probe located at the glycerol level,[36] which is in accord with findings from simulations. On the other hand, this effect is making quantitative solvent relaxation measurements on 1 M iodide impossible. The present results are also in accord with recent experiments on DPPC monolayer with different sodium salts,[9,10] finding that the best-fitting model includes partitioning of sodium cation at the membrane headgroup region with anions adsorption proportional to their size.

On the basis of the above analysis and conclusions from our previous paper[11] that larger cations (Cs$^+$) adsorb less to the membrane than smaller ones (Na$^+$), we identify the following determining aspects of ion−lipid membrane interactions:

1. Ion Pairing. Salt anions can pair with the positively charged lipid choline group, while cations can create contacts with the negatively charged phosphate group and carbonyl oxygens. In bulk aqueous solutions the tendency for pairing is the highest for ions (charged groups) of opposite charge and matching hydration free energy (i.e., small cations prefer small anions while larger cations pair more with larger anions).[14,15]

2. Water/Hydrophobic Interface. The presence of the boundary between water and hydrocarbon chains of lipids implies adsorption of large and polarizable ions. Compared to the affinity of soft anions for the water/vapor interface,[22,24] this effect is reduced at the lipid membrane surface due to the presence of negatively charged groups of the lipid headgroups.

3. Steric Hindrance. The amount of water is rapidly decreasing upon moving from the solution to the headgroup region; moreover, water at the interface is strongly interacting with the lipid headgroups. This has consequences especially for the mobility and other dynamical properties.

4. Counterion Attraction. Salt ions of opposite charge tend to screen each other, and therefore, adsorption of one type of them at the membrane interface leads to the attraction of counterions.

The above reasoning leads to the following prediction: small cations (Na$^+$) should be attracted to the membrane, while larger cations (Cs$^+$) should not. However, even larger "hydrophobic" cations (such as tetraalkylammonium cations) are expected to be adsorbed at a membrane surface, but for a different reason: the ion hydrophobicity. Larger anions (e.g., iodide, perchlorate, and thiocyanate) adsorb to the membrane more than smaller ones (chloride) due to their size, polarizability, and ion pairing with choline group of the membrane.

Conclusions

We have investigated the properties of different salt solutions at the interface of DOPC membrane by means of molecular dynamics simulations and fluorescence spectroscopy. We have observed a difference in the adsorption properties of anions (Cl$^-$ vs I$^-$) which follows the Hofmeister series.[12,35] The existence of such a difference has been suggested based on the results from the previous experiments on vesicle swelling,[7] but the difference was less significant in the previous studies of membranes with sodium salts.[9−11] The use of potassium salts in the present study strongly underlines the differences between anions. By evaluating the composition of the first solvation shell of anions, as they adsorb at the membrane surface, we were able to identify clearly the difference between chloride and iodide, the latter being less influenced by a particular counter-cation. In addition, in our pioneering polarizable calculations we showed that the effect of polarizability leads to a stronger adsorption of iodide to the hydrophobic membrane interface. The above results are in agreement with solvent relaxation experiments.

The present study allowed us to identify mechanisms of ion−membrane interaction (i.e., ion pairing within the membrane, presence of the water/hydrophobic interface, and counterion effects). Our results are in accord with the previous measurements performed in phospholipids membranes, as well as with the measurements performed in experiments on ion pairing in salt solutions,[1−3,5,8,11] which led to an establishment of the rule of preferable ion pairing for ions with matching water affinities.[14,15] We suggest that the above-mentioned mechanisms are more general and, therefore, are also at work for other biomolecular systems containing salt solutions, thus shedding more light on the molecular foundations of ion specificity, as expressed by the Hofmeister series.[12,35]

Acknowledgment. We thank Valery Andrushchenko and Petr Bouř for valuable discussions. Support from the Czech Ministry of Education (grant LC512) and the Czech Science Foundation (grant 203/08/0114) is gratefully acknowledged. R.V. acknowledges support from the International Max-Planck Research School. Part of the work in Prague was supported via Project Z40550506. M.L.B. acknowledges the support of the Office of Naval Research.

References and Notes

(1) Pandit, S. A.; Bostick, D.; Berkowitz, M. L. *Biophys. J.* **2003**, *84*, 3743–3750.

(2) Bockmann, R. A.; Hac, A.; Heimburg, T.; Grubmuller, H. *Biophys. J.* **2003**, *85*, 1647–1655.

(3) Sachs, J. N.; Nanda, H.; Petrache, H. I.; Woolf, T. B. *Biophys. J.* **2004**, *86*, 3772–3782.

(4) Sachs, J. N.; Woolf, T. B. *J. Am. Chem. Soc.* **2003**, *125*, 8742–8743.

(5) Gurtovenko, A. A.; Vattulainen, I. *J. Phys. Chem. B* **2008**, *112*, 1953–1962.

(6) Garcia-Celma, J. J.; Hatahet, L.; Kunz, W.; Fendler, K. *Langmuir* **2007**, *23*, 10074–10080.

(7) Petrache, H. I.; Zemb, T.; Belloni, L.; Parsegian, V. A. *Proc. Natl. Acad. Sci. U.S.A.* **2006**, *103*, 7982–7987.

(8) Leontidis, E.; Aroti, A.; Belloni, L.; Dubois, M.; Zemb, T. *Biophys. J.* **2007**, *93*, 1591–1607.

(9) Leontidis, E.; Aroti, A. *J. Phys. Chem. B* **2009**, *113*, 1460–1467.

(10) Leontidis, E.; Aroti, A.; Belloni, L. *J. Phys. Chem. B* **2009**, *113*, 1447–1459.

(11) Vacha, R.; Siu, S. W. I.; Petrov, M.; Bockmann, R. A.; Jurkiewicz, P.; Barucha-Kraszewska, J.; Hof, M.; Berkowitz, M. L.; Jungwirth, P. *J. Phys. Chem. B* **2009**, *113*, 7235–7243.

(12) Kunz, W.; Henle, J.; Ninham, B. W. *Curr. Opin. Colloid Interface Sci.* **2004**, *9*, 19–37.

(13) Berkowitz, M. L.; Bostick, D. L.; Pandit, S. *Chem. Rev.* **2006**, *106*, 1527–1539.

(14) Collins, K. D. *Biophys. J.* **1997**, *72*, 65–76.

(15) Collins, K. D. *Biophys. Chem.* **2005**, *119*, 10.

(16) Jagoda-Cwiklik, B.; Vacha, R.; Lund, M.; Srebro, M.; Jungwirth, P. *J. Phys. Chem. B* **2007**, *111*, 14077–14079.

(17) Vlachy, N.; Jagoda-Cwiklik, B.; Vacha, R.; Touraud, D.; Jungwirth, P.; Kunz, W. *Adv. Colloid Interface Sci.* **2009**, *146*, 42–47.

(18) Kalcher, I.; Horinek, D.; Netz, R. R.; Dzubiella, J. *J. Phys.: Condens. Matter* **2009**, *21*, 424108–424118.

(19) Hess, B.; van der Vegt, N. F. A. *Proc. Natl. Acad. Sci. U.S.A.* **2009**, *106*, 13296–13300.

(20) Fennell, C. J.; Bizjak, A.; Vlachy, V.; Dill, K. A. *J. Phys. Chem. B* **2009**, *113*, 6782–6791.

(21) Lund, M.; Jagoda-Cwiklik, B.; Woodward, C. E.; Vacha, R.; Jungwirth, P. *J. Phys. Chem. Lett.* **2009**, *1*, 300–303.

(22) Vrbka, L.; Mucha, M.; Minofar, B.; Jungwirth, P.; Brown, E. C.; Tobias, D. J. *Curr. Opin. Colloid Interface Sci.* **2004**, *9*, 67–73.

(23) Jungwirth, P.; Tobias, D. J. *J. Phys. Chem. B* **2002**, *106*, 6361–6373.

(24) Jungwirth, P.; Tobias, D. J. *Chem. Rev.* **2006**, *106*, 1259–1281.

(25) Dang, L. X. *J. Phys. Chem. B* **2002**, *106*, 10388–10394.

(26) Dang, L. X.; Chang, T. M. *J. Phys. Chem. B* **2002**, *106*, 235–238.

(27) Sykora, J.; Jurkiewicz, P.; Epand, R. M.; Kraayenhof, R.; Langner, M.; Hof, M. *Chem. Phys. Lipids* **2005**, *135*, 213–221.

(28) Jurkiewicz, P.; Olzynska, A.; Langner, M.; Hof, M. *Langmuir* **2006**, *22*, 8741–8749.

(29) Van Der Spoel, D.; Lindahl, E.; Hess, B.; Groenhof, G.; Mark, A. E.; Berendsen, H. J. *J. Comput. Chem.* **2005**, *26*, 1701–1718.

(30) Siu, S. W. I.; Vacha, R.; Jungwirth, P.; Bockmann, R. *J. Chem. Phys.* **2008**, *128*, 125103.

(31) Caldwell, J. W.; Kollman, P. A. *J. Phys. Chem.* **1995**, *99*, 6208–6219.

(32) Dang, L. X.; Schenter, G. K.; Glezakou, V. A.; Fulton, J. L. *J. Phys. Chem. B* **2006**, *110*, 23654.

(33) Miettinen, M. S.; Gurtovenko, A. A.; Vattulainen, I.; Karttunen, M. *J. Phys. Chem. B* **2009**, *113*, 9226–9234.

(34) Sheynis, T.; Sykora, J.; Benda, A.; Kolusheva, S.; Hof, M.; Jelinek, R. *Eur. J. Biochem.* **2003**, *270*, 4478–4487.

(35) Hofmeister, F. *Arch. Exp. Pathol. Pharmakol.* **1888**, *24*, 247–260.

(36) Barucha-Kraszewska, J.; Kraszewski, S.; Jurkiewicz, P.; Ramseyer, C.; Hof, M. *Biochim. Biophys. Acta* **2010**. doi: 10.1016/j.bbamem.2010.05.020.

JP102389K

2 Fluorescent Dyes in the Hydrophobic Core Region of a Phospholipid Membrane – Solvation Dynamics

Membranes are different regarding the water presence at the different depths of the bilayer. The interface region, which includes phosphate, glycerol and carbonyl groups, represents a heterogeneous and dynamic structure. Headgroup region of bilayer is hydrated with a steep profile of water molecules (see Figure I.16 in chapter I2.5.6). These molecules, present in headgroup region of membrane, have different intermolecular structure and dynamical properties compared to the bulk solution. For example, solvation dynamics are slowed down remarkably (picoseconds timescale in a bulk water and from picoseconds to nanoseconds in the headgroup region). By contrast, the core region of the lipid bilayer is composed of hydrophobic chains of fatty acids where the water content was found to be low [133]. Probes with the anthroyloxy ring attached to the fatty acid chain at various positions, known as *n*-AS dyes (see Figure III.6) were used for monitoring the solvation dynamics in the backbone region of the lipid bilayer. n-AS, which are very sensitive to the polarity of their surroundings [75-76, 134-137], were reported to be located at well-defined graded series of depths along the normal axis of the bilayer [75-76].

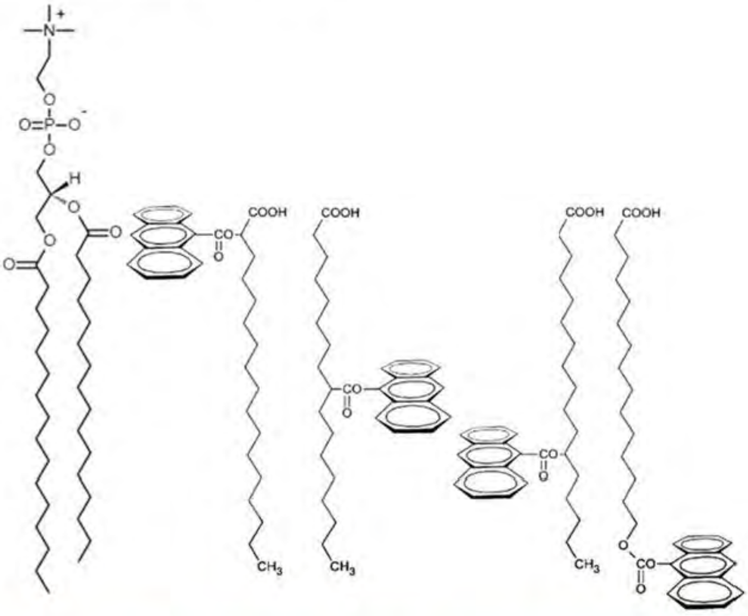

Figure III.6 Schematic structures of DPPC, 2-AS, 9-AS, 12-AS and 16-AP. Approximate localization of the *n*-AS dyes relative to the lipid molecules are depicted.

The goal of this work [138] was to examine a solvation dynamics of the hydrophobic backbone region of the POPC LUVs in varying depths, using 2-AS, 9-AS, 12-AS and 16-AP probes (Figure III.6) by recording the time-resolved emission spectra (TRES). The analysis of the TRES is able to bring new insights into the properties of the water molecules in the neighbourhood of labelled regions.

However, the TRES contain information not only about the solvation dynamics but probably also about intramolecular interactions.

2.1 Absorption and Excitation Spectra

Absorption and emission spectra were measured for *n*-AS and 16-AP dyes in POPC LUVs (*n*=2,9). All recorded absorption spectra show three well-distinguish peaks, characteristic for anthracene. They correspond to the $0 \rightarrow 2$, $0 \rightarrow 1$ and $0 \rightarrow 0$ transitions of the specie (see Figure III.7).

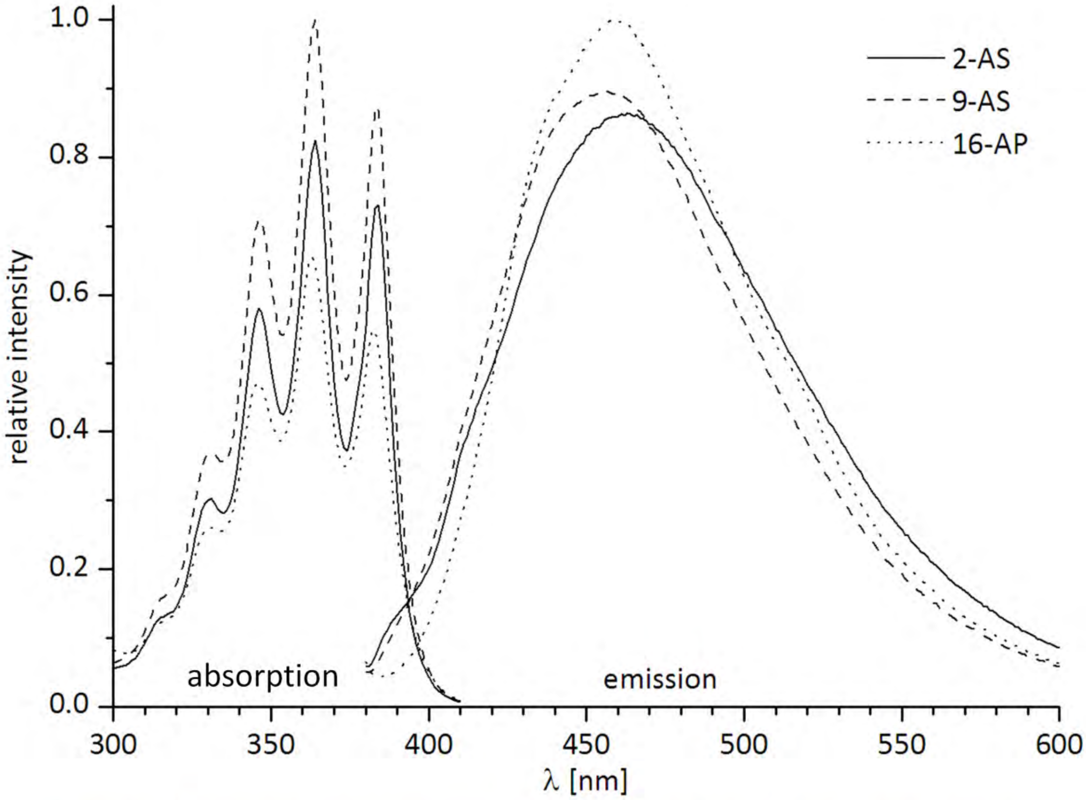

Figure III.7 Excitation and emission spectra recorded for 2-AS, 9-AS and 16-AP dyes in POPC LUVs.

The absorption spectra are identical for all measured dyes. The chromophore environment and the position of attachment to the fatty acid chain do not have any impact on the value and shape of the absorption spectra of anthracene derivative dyes.

In contrast to the invariability of the absorption spectra, the shape and position of the emission steady-state spectra show meaningful differences. Polarity and viscosity of the chromophore environment is modified by the solvent concentrations in varying depths of the backbone region of lipid bilayer. Emission spectra of 16-AP has at least two fluorescence bands, which indicate emission from at least two energetically different states. Peak, which corresponds to the most energetic state, is more pronounced. The steady-state spectra of 2-AS and 9-AS in POPC LUVs lose their fine structure and particular bands are no longer recognizable. Besides, the deeper location of the chromophore in the hydrophobic backbone leads to a slight blue shift of the emission spectra. For example 9-AS, which is located deeper in the membrane, is blue shifted in comparison to 2-AS by ~10nm (~0.59 eV).

2.2 Time-Resolved Emission Spectra

Time-Resolved Emission Spectra (TRES) were also recorded. The time evolution of the full width at half maximum (FWHM) time profiles is plotted in Figure III.8.

It has been shown that relaxation process in pure solvent is characterized by an increase at the initial times followed by a decrease of the FWHM [5, 70]. For 2-AS dye we retrieve the same behaviour since the dye is mainly located in the hydrated environment (see Figure III.8). In the case of 12-AS and 16-AP the FWHM becomes more complex, due to the increased number of processes occurring during relaxation. The steep decline observed at short times (up to 1 ns) for 12-AS and 16-AP, means that fast, additional relaxation process occurs (it will be discussed further in the text). The FWHM profile maximum depends on the kinetics of the solvation dynamics and is shifted to the shorter times when relaxation process gets faster. The maxima FWHM of the *n*-AS dyes in POPC vesicles are shifted to shorter times in the sequence: 16-AS > 12-AS > 9-AS > 2-AS (see Figure III.8). It indicates that solvent relaxation process slows down when the chromophore is located deeper in the bilayer.

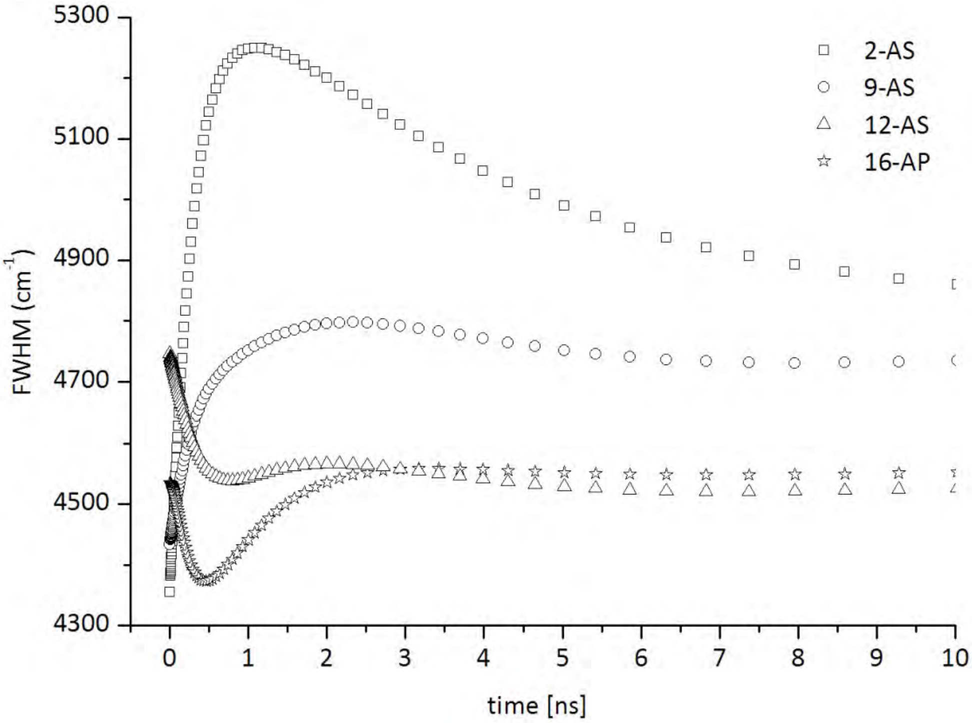

Figure III.8 Full width at half maximum time profiles of AS dyes in POPC LUVs.

The overall Stokes shift $\Delta\nu$ is the important parameter obtained from TRES analysis, which characterizes the micropolarity of the dye environment. The values of the Stokes shift for *n*-AS dyes are given in Table III-1. $\Delta\nu$ decreases with deeper location of the fluorophore in the membrane. 2-AS and 9-AS dye are reported to be located at nearly the same positions [75] although a large change of Stokes shift is observed. This values confirm the observation that water density profile along *z*-axis of the carbonyl region of the bilayer is steep [133, 139].

	$\Delta\nu$ [cm^{-1}]	τ_r [ns]	% observed
2-AS	2950	1.60	85
9-AS	2450	1.40	73
12-AS	2400	0.87	65
16-AP	2300	0.62	40

Table III-1 Characteristics obtained by analyzing correlation functions in POPC LUVs

The value of $\Delta\nu$ for 16-AP suggests that water molecules are present in the microenvironment of 16-AP chromophore. It can mean that 16-AP is not buried as deep in the backbone region of the bilayer as a results of its mobility or water molecules that can penetrate deeper in the backbone region of the bilayer through the significant dipole moment changing during excitation.

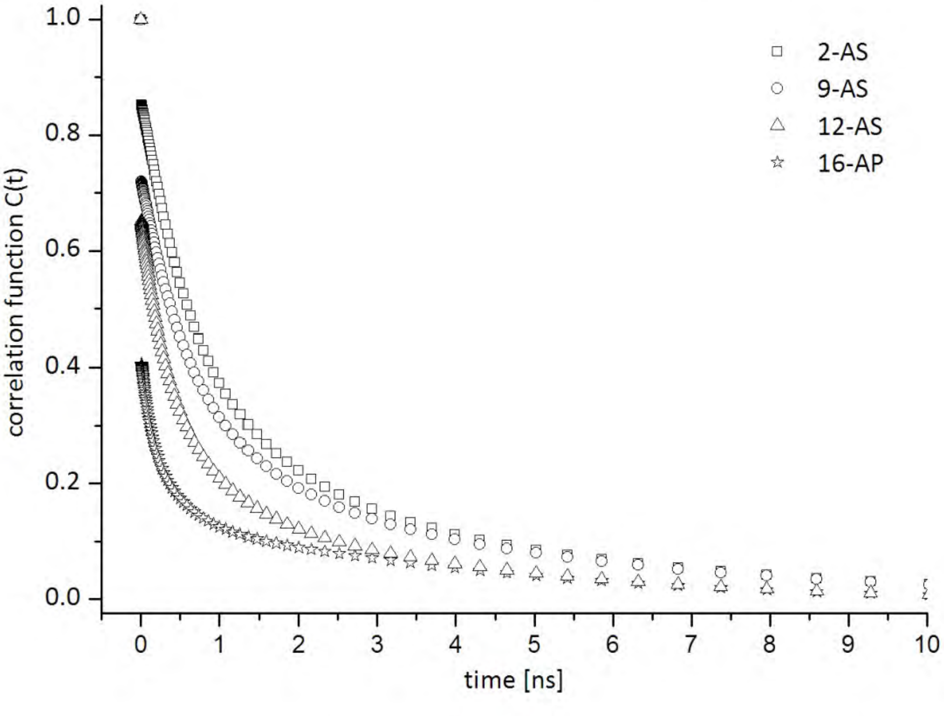

Figure III.9 Correlation functions of AS dyes in POPC LUVs

It is clearly shown that more deeper location of the *n*-AS dye chromophore in the lipid bilayer is more the whole relaxation becomes faster. This fact confirms the observation of the correlation functions (see Figure III.9), comparison of the relaxation times (see Table III-1) and amount of the relaxation process captured with the given time resolution. The solvent relaxation response of 2-AS dye, which is similar to solvation behaviour and near 2 ns relaxation time, implies that 2-AS dye occupies a similar region as a headgroup probes. 16-AP shows more complicated behaviour. The FWHM time profile becomes more complex and only 40% of the relaxation process is captured with the given time resolution. The simplest explanation is that additional, fast relaxation process dominates over the solvation response in non polar environment of the backbone region of bilayer.

2.3 Summary

The experimental data indicate that relaxation processes of *n*-AS dyes in the phospholipid bilayer are connected with the intramolecular and intermolecular (i.e.: ion-dipole interactions, dipole-dipole interactions, hydrogen bonding) dynamics of interactions. The intramolecular relaxation includes: torsional relaxation, formation of the charge-transfer states, and other rearrangement of the carboxylic moiety leading to nonpolar emitting states. At the same time, solvent relaxation occurs. These two processes are not separated from each other. The intramolecular relaxation (fastest components) occurs on a sub-nanosecond timescale. The slowest process, observed in TRES, corresponds to the diffusion part of solvent relaxation.

The solvation dynamics of lipid bilayer was measured by incorporation of the POPC membrane by using fluorescent markers which label the hydrophobic backbone region of the bilayer. The solvation contribution do not disappear completely even for the most buried 16-AP probe. Solvent relaxation kinetics becomes slower upon approaching the center of the bilayer. The Stokes shift $\Delta\nu$ is decreasing with the decrease of water concentration. The 16-AP response suggests the presence of small amount of water on its environment in the center of the hydrophobic backbone region of the lipid bilayer.

J. Phys. Chem. B **2007,** *111,* 5869−5877 **5869**

Time-Dependent Stokes Shifts of Fluorescent Dyes in the Hydrophobic Backbone Region of a Phospholipid Bilayer: Combination of Fluorescence Spectroscopy and Ab Initio Calculations

Jan Sýkora,[*,†] **Petr Slavíček,**[*,†,‡] **Pavel Jungwirth,**[§] **Justyna Barucha,**[†] **and Martin Hof**[†]

J. Heyrovský Institute of Physical Chemistry, Academy of Sciences of the Czech Republic, Dolejškova 3, 18223 Prague 8, Czech Republic, Department of Physical Chemistry, Prague Institute of Chemical Technology, Technická 5, 16628 Prague 6, Czech Republic, and Institute of Organic Chemistry and Biochemistry, Academy of Sciences of the Czech Republic, and Center for Biomolecules and Complex Molecular Systems, Flemingovo nám. 2, 16610 Prague 6, Czech Republic

Received: March 9, 2007

We explored the time-dependent Stokes shifts of fluorescent dyes containing an anthroyloxy chromophore (2-AS, 9-AS, and 16-AP) in bilayers composed of palmitoyl-oleoyl-phosphatidylcholine. The obtained data revealed a nontrivial solvation response of these dyes, which are located in the backbone region of the bilayer with a gradually increasing depth. For comparison, steady-state emission spectra in the neat solvents of various polarities and viscosities were also recorded. The results indicate that on the short picosecond time scale the AS dyes undergo complex photophysics including formation of states with a charge-transfer character. This observation is supported by ab initio calculations of the excited states of 9-methylanthroate. The slower nanosecond part of the relaxation process can be attributed to the solvation response of the dyes. A slowdown in solvent relaxation is observed upon moving toward the center of the bilayer. A mechanism similar to preferential solvation present in the mixture of a polar and nonpolar solvent is considered to explain the obtained data.

1. Introduction

Hydration of biological molecules and self-assemblies enables their proper functioning and enhances their stability. Water molecules present in the hydration layer have been proven to have completely different intermolecular structure and dynamical properties compared to the bulk solution. For instance, solvation dynamics are slowed down remarkably.[1] Phospholipid bilayers, which form a basic part of cellular membranes, belong to the most important biological systems. With respect to their structure we distinguish two main regions within the bilayer: the interface and the backbone region.[2,3] The interface region includes hydrated phosphate, glycerol, and carbonyl groups. Here, solvation dynamics take place on a rather broad time scale (with reported picosecond, subnanosecond, and up to nanosecond components).[4−6] The intrinsic thermal fluctuations in the bilayer and the spread of chromophore locations leads to a broad distribution of different microenvironments and thus to the observed "unspecific" solvent relaxation (SR) dynamics. However, as the interface is chemically highly heterogeneous, some dyes located at/close to the carbonyl groups show quite homogeneous solvation response, which occurs exclusively on the nanosecond time scale.[5,7] This part of the bilayer interface will be reffered to as the "headgroup region" further in the text. As indicated above, the interface represents a rather heterogeneous and dynamic structure comprising the hydrated and charged chemical residues, which makes the application of molecular dynamics (MD) simulation for explaining the observed nanosecond kinetics rather difficult.[8]

The backbone region is composed of the hydrophobic chains of fatty acids where the water content was found to be low.[9] The only fluorescent dyes suitable for monitoring the solvation dynamics in this region are presently the probes with the anthroyloxy ring attached to the fatty acid chain at various positions (known as *n*-AS dyes) (Figure 1). These probes were reported to be located at a well-defined graded series of depths along the normal axis of the bilayer.[10,11] It has been known for a long time that anthroyloxy-based dyes can serve as sensitive polarity probes.[10−15] It is, therefore, possible to use *n*-AS for investigating the water concentration profile and for probing the dynamics of water in the backbone region of the phospholipid bilayer.

An important insight into the nature of solvation dynamics can be provided by MD simulations. These were applied for studies of, for example, chromophores dissolved in a polar solvent[16] or at the liquid/liquid interfaces,[17] chromophores located in a mixture of polar and nonpolar solvents,[18] or in polar nanoclusters.[19] The latter two cases are specifically important for the discussion of solvation dynamics in the backbone region of the bilayer. In both cases the chromophore is incompletely solvated by the polar solvent. Molecular dynamics studies lead the to identification of different solvation time scales connected with different molecular motions, starting from a femtosecond time scale for the librational solvent response, over a picosecond time scale for solvent rearrangements around the chromophore,

---

[*] Authors to whom correspondence should be addressed. E-mail: jan.sykora@jh-inst.cas.cz; petr.slavicek@vscht.cz.

[†] J. Heyrovský Institute of Physical Chemistry, Academy of Sciences of the Czech Republic.

[‡] Prague Institute of Chemical Technology.

[§] Institute of Organic Chemistry and Biochemistry, Academy of Sciences of the Czech Republic, and Center for Biomolecules and Complex Molecular Systems.

10.1021/jp0719255 CCC: $37.00

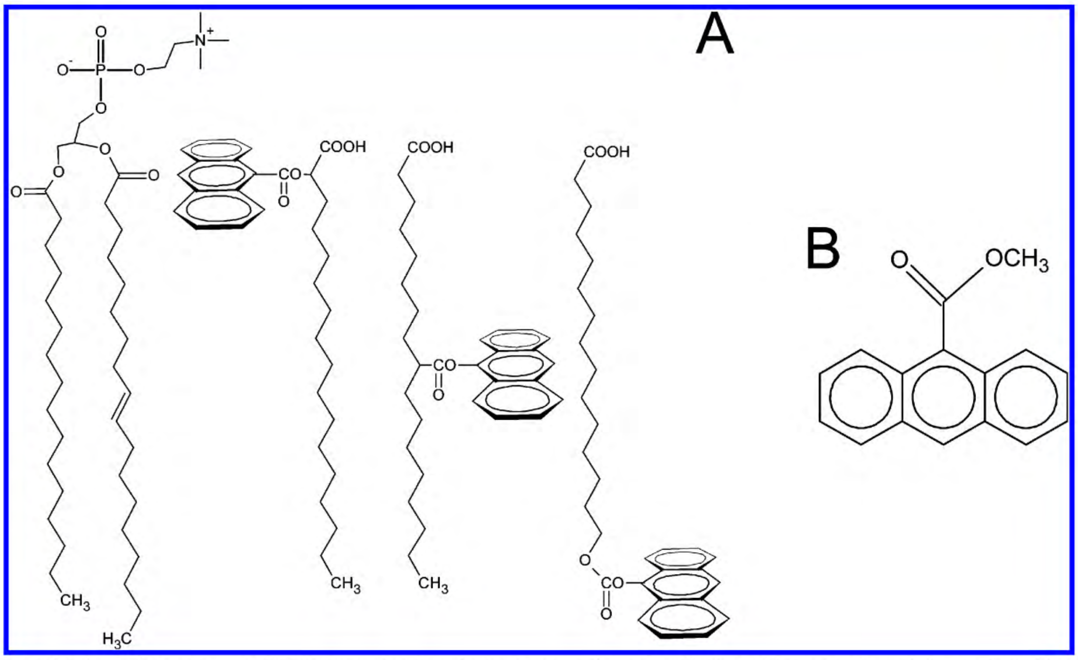

Figure 1. (A) Schematic structures of POPC, 2-AS, 9-AS, and 16-AP. Approximate localization of the *n*-AS dyes relative to the lipid molecules are depicted. (B) Structure of 9-methylanthroate (9MA).

up to the nanosecond diffusion component corresponding to the flow of the solvent molecules toward/from the excited chromophore.

The goal of this work is to probe solvation dynamics by recording the time-resolved emission spectra (TRES) in varying depths of the backbone region of the bilayer. Large unilamellar vesicles (LUVs) composed of 1-palmitoyl-2-oleoyl-phosphatidylcholine (POPC) lipid molecules are used as a model system. The inspection of the TRES is supposed to bring new insights into the properties and structure of the water molecules present in the labeled regions. However, the TRES contain information not only about the solvation dynamics but potentially also about intramolecular processes. In the case of AS dyes, the photophysics are rather complex and still not fully understood. It has, for example, never been fully satisfactorily explained why the fluorescence behavior of anthroyloxy-based dyes is strongly solvent-dependent. Detailed understanding of the intramolecular dynamics of the respective dyes is, however, vital for a correct interpretation of the TRES. To this end, the present experiments on 2-AS, 9-AS, and 16-anthroyloxy-palmitoic acid (16-AP) are also accompanied by data collected at various temperatures in different solvents of varying polarities and viscosities. The aim is to obtain a more thorough understanding of the photophysics of these dyes, which enables interpretation of the results gained from TRES.

In addition, the photophysics of the dyes are rationalized by means of quantum mechanical calculations on a smaller model system of 9-methylanthroate. Results of theoretical calculations allow us to understand the time-dependent fluorescence behavior of anthroyloxy dyes, assigning different processes to individual time scales.

The paper is organized as follows. In section 2, the employed experimental and theoretical methods are described. Results together with a discussion are presented in the third section. Section 4 concludes the paper with an outlook for future studies.

2. Materials and Methods

2.1. Experimental Methods. All probes, (2-(9-anthroyloxy)-stearic acid (2-AS), 9-(9-anthroyloxy)stearic acid (9-AS), 16-(9-anthroyloxy)palmitic acid (16-AP)), Figure 1, and 6-hexadecanoyl-2-(((2-(trimethylammonium)ethyl)methyl)amino)naphthalene chloride (Patman) were purchased from Molecular Probes and were used without any further purification. Phospholipids (1-palmitoyl-2-oleoyl-phosphatidylcholine (POPC) and dipalmitoylphosphatidylcholine (DPPC)) were supplied from Avanti Lipids. All solvents of spectroscopic grade were purchased from Merck. The preparation of DPPC and POPC LUVs was performed as described previously by extruding with 100 nm filters.[20] Absorption spectra were recorded on a Perkin-Elmer Lambda 19 spectrometer. Fluorescence spectra and decays were recorded on a Fluorolog 3 steady-state spectrometer (Jobin Yvon) and on IBH 5000 U SPC equipment. The experimental temperature was set to 27 °C, unless stated differently. Low-temperature steady-state spectra were measured on a modified Edinburgh Instruments FLFS900 spectrometer. Decay kinetics were recorded using an IBH Nanoled 11 excitation source (370 nm peak wavelength, 80 ps pulse width, 1 MHz repetition rate) and a cooled Hamamatsu R3809U-50 microchannel plate photomultiplier. The primary data consisted of a set of emission decays recorded at a series of wavelengths spanning the steady-state emission spectrum. The TRES's were obtained by the spectral reconstruction method.[21] Full width at half-maximum (fwhm(t)) and emission maxima ($\nu(t)$) profiles of the reconstructed TRES were obtained by a log-normal fitting.[21] The correlation functions $C(t)$ were calculated according to

$$C(t) = \frac{\nu(t) - \nu(\infty)}{\nu(0) - \nu(\infty)} \qquad (1)$$

where $\upsilon(0)$ and $\upsilon(\infty)$ correspond to the value obtained by "time 0 estimation" and to the value at time infinity, respectively. The kinetics of the solvation dynamics were parametrized with the so-called relaxation times τ_r

$$\tau_r = \int_0^\infty C(t)\,dt \tag{2}$$

Generally, in the studies investigating solvation dynamics the solvent relaxation time, τ_{SR}, which is defined as an integral of the correlation function, describes the kinetics of SR quantitatively. We define above the integral relaxation time τ_r, which is analogous to the SR time. However, it characterizes the time course of the overall relaxation process including both the internal intramolecular relaxation and solvent relaxation and thus gives only limited information on the individual processes leading to a time-dependent shift in the emission spectra.

2.2. Computational Methods. We have performed electronic structure calculations to investigate possible photochemical mechanisms. Several levels of description have been employed. For entry level calculations the semiempirical AM1 Hamiltonian has been utilized. To deal with excited states, the FOMO-CAS-(6/6) scheme has been used.[22] Since the semiempirical parametrization is not adequate to describe the potential energy surface far from the equilibrium geometries, we have used ab initio techniques to address this issue. The ground-state minimum of the investigated dye (9-methylanthroate) has been obtained at the MP2/6-31g* level. For exploration of the potential energy surfaces of the excited states, we have used the complete active space self-consistent field (CAS-SCF) method with an active space consisting of six electrons in six orbitals with the same basis set as above. At this level we have also performed excited-state geometry optimization. At the optimized geometries we have performed single-point CASPT2 calculations. During the CASPT2 calculations, 40 orbitals have been kept frozen to make the calculation numerically feasible. The results are, however, not particularly sensitive to the exact number of orbitals kept frozen. The calculations are essentially stable with respect to change of the active size and the number of states over which we average the energy during the orbital optimization.

All of the CAS-SCF and CASPT2 calculations have been performed with the MOLPRO electronic code package.[23] The semiempirical calculations have been performed with the modified version of the MOPAC package.[24]

3. Results and Discussion

In this section we discuss first the photophysics of the AS dyes on the basis of the absorption and steady-state fluorescence spectra. Consequently, interpretation of the spectra is then deduced from ab initio calculations. Second, we investigate the TRES's measured in the backbone region of the phospholipid bilayer. Solvation and intramolecular dynamics of the AS dyes in biomembranes are then discussed in the context of the present findings about their photophysics.

3.1. Absorption and Excitation Spectra in Different Environments. Absorption and excitation spectra were measured for the set of *n*-(9-AS) ($n = 2, 9$) and 16-(9-AP) dyes in a wide range of solvents and in POPC and DPPC LUVs. All recorded spectra show features characteristic for anthracene with three well-distinguished peaks corresponding to the 0−2, 0−1, and 0−0 transitions. (The numbers stand for the vibrational levels in the ground and excited states, respectively.[25]) The obtained values for the three main peaks of the excitation and absorption spectra are identical for all measured systems within the experimental error of 50 cm^{-1}. Maxima of excitation spectra of 2-AS are summarized in Table 1 for selected solvents and lipid systems. Only a small shift of a maximal value of 200 cm^{-1} is detected for a large range of solvents and vesicle systems. Table 2 shows the values of the middle peak maxima of the excitation spectra for the set of *n*-(9-AS) ($n = 2, 9$) and 16-(9-AP). Again, the excitation spectra and the absorption spectra (not shown here) appear to be largely invariant within the whole set of these compounds. In summary, the absorption and excitation spectra depend neither on the chromophore environment nor on the position of attachment of the fatty acid chain.

TABLE 1: Maxima of Excitation Spectra in 2-AS in Various Systems[a]

solvent	ν_1 (cm^{-1})	ν_2 (cm^{-1})	ν_3 (cm^{-1})
heptane	26 340	27 700	29 150
paraffin oil	26 150	27 550	28 900
propanol	26 200	27 600	28 970
ethanol + methanol	26 240	27 700	29 000
DPPC LUV (25 °C)	26 100	27 470	28 910
DPPC LUV (46 °C)	26 100	27 490	28 960
POPC LUV	26 080	27 500	28 990

[a] The three columns correspond to the three main peaks as described in the text.

TABLE 2: Maxima of Excitation Spectra of "AS Dyes" in Various Systems[a]

solvent	2-AS ν_2 (cm^{-1})	9-AS ν_2 (cm^{-1})	16-AP ν_2 (cm^{-1})
heptane	27 700	27 700	27 760
paraffin oil	27 550	27 550	27 550
propanol	27 600	27 620	27600
ethanol + methanol	27 700	27 700	27 680
POPC LUV	27 500	27 520	27 540

[a] The middle peak (υ_2) of the excitation spectrum is taken into account.

3.2. Fluorescence Emission Spectra. In contrast to the absorption and excitation spectra, both shape and position of the emission steady-state spectra show significant differences when modifying the polarity and viscosity of the solvent.

In nonpolar solvents, on one hand, there are at least two fluorescence bands apparent in the steady-state spectra indicating contributions from at least two energetically different fluorescent states (Figure 2A). Moreover, with the increase of viscosity the peak corresponding to the more energetic state becomes more pronounced, as is obvious for the data recorded in paraffin oil (Figure 2B). On the other hand, in polar solvents, the steady-state spectra lose their fine structure, and particular bands are no longer recognizable (Figure 3A). In addition, the spectra are broadened and red-shifted in contrast to the nonpolar solvents. In both the polar and the nonpolar environments, the recorded fluorescence spectra do not bear the mirror image relation to the absorption spectra. Apart from the dependence of the fluorescence spectra on the polarity and viscosity, an effect of the position of the anthroyloxy group can be observed.

In POPC vesicles the steady-state spectra of 2-AS and 9-AS are rather similar to those observed in polar solvents. In addition, they show the expected trend, and the deeper location of the dye leads to a slight blue shift of the emission spectrum possibly due to the polarity gradient within the bilayer (Figure 3B). In contrast, the character of the fluorescence spectrum for 16-AP is more similar to that observed in a nonpolar environment having an additional discrete band at a lower wavelength. In addition, it is red-shifted in comparison to the steady-state spectra recorded for 9-AS. This fact may be explained by inspecting TRES (section 3.5). Bearing in mind that the observed steady-state spectrum is actually a sum of the TRES and that 16-AP shows the fastest relaxation process of all three

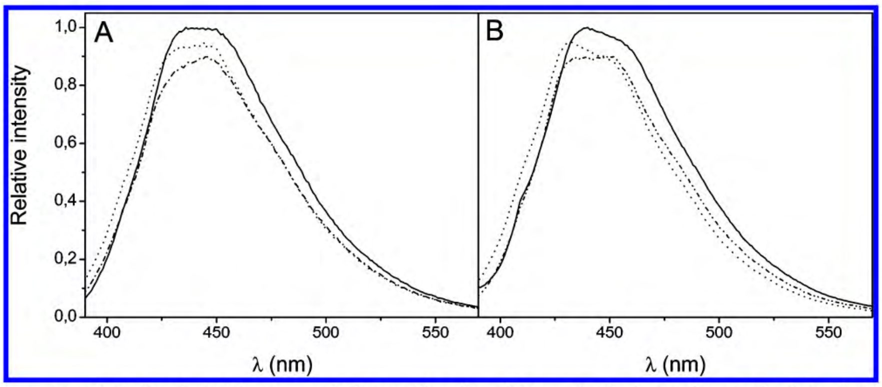

Figure 2. Emission spectra of AS dyes in (A) heptane and (B) paraffin oil: solid line, 2-AS; dotted line, 9-AS; dash−dotted line, 16-AP.

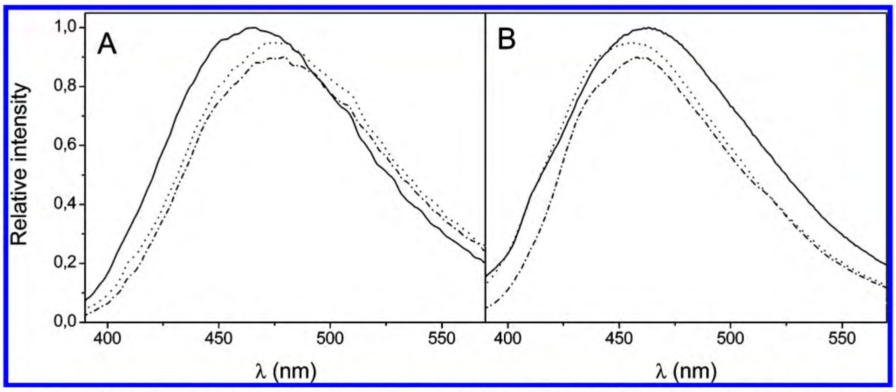

Figure 3. Emission spectra of AS dyes in (A) ethanol−methanol mixture (1:1) and (B) POPC LUVs: solid line, 2-AS; dotted line, 9-AS; dash−dotted line, 16-AP.

dyes (section 3.5), it is obvious that the more relaxed (i.e., more red-shifted) states contribute to the steady-state spectrum more markedly than in the case of 9-AS.

3.3. Quantum Chemical Calculations and the Discussion of the *n*-AS Photophysics. To gain further insight into the photophysics of the *n*-AS dyes, we have explored the excited-state potential energy surface of 9-methylanthroate (9MA) by means of quantum chemical methods. The 9MA molecule (Figure 1B) lacks the long alkyl chain and carboxylic group of the *n*-AS molecules, but it has the same anthracene-based chromophore, capped with a methyl group. It is, therefore, an excellent model system for this type of compound. The emission spectra of *n*-AS dyes and their dependence on the solvent polarity, viscosity, and temperature are qualitatively identical to those of 9MA.

Experimental information for this molecule is available both for different solvents and for an isolated molecule in the gas phase. The 9MA molecule has been studied experimentally in the condensed phase[12,26,27] and in supersonic jets.[28] Semiempirical calculations also have been performed on this molecule.[14]

The absorption spectra of this molecule exhibit anthracene-like structure with a negligible solvent shift. This is in accord with the fact that both the ground- and the excited-state dipole moments are rather low. The fluorescence spectra of 9MA are, on the other hand, strongly red-shifted and diffuse. The Stokes shift is highly solvent-dependent. The dipole moment change estimated from the Lippert−Mataga equation provides a value of 4.5 D.[12] The fluorescence spectra do not bear the mirror image relation with the absorption spectra for any solvent. The above features are also true for the 9MA molecule in the gas phase. Any suggested photochemical scheme of the 9MA dye has to explain those features as well as the polarity, temperature, and viscosity dependence of the *n*-AS fluorescence spectra.

The absence of the mirror image relation of the fluorescence and absorption spectra in the nonpolar solvents and even in the gas phase clearly indicates that a significant intramolecular relaxation takes place upon photoexcitation, which also holds true for AS dyes embedded in the membrane.[29] Two possible mechanisms can be considered: (1) conformational relaxation along the twisting coordinate or (2) formation of different structures, some of them of a charge-transfer character.

The first mechanism has been suggested by Swayanbunathan and Lim[28] for the 9MA molecule and further used by Berberan-Santos and co-workers[13] to rationalize the photophysics of the 12-AS molecule. According to this explanation, the absorption occurs mainly from the twisted configuration that is not preferential for the excited state. As a result, the excited chromophore starts to relax by intramolecular rotation. The increasing viscosity of the environment slows down the intramolecular rotation and leads to emission from initial or partially relaxed states, resulting in the growth of the blue-shifted shoulder of the steady-state spectrum. There are, however, some difficulties with this idea. By looking at the steady-state spectra in heptane and in viscous paraffin oil (Figures 2A and 2B) of all *n*-AS dyes and by inspecting the temperature scan of 2-AS in heptane from 300 to 150 K (Figure 4A) we can safely distinguish at least two emitting states. It is unclear how such a feature could be produced by an emission from a single well. The intramolecular relaxation should also be in this case much faster than that observed in the time-resolved fluorescence

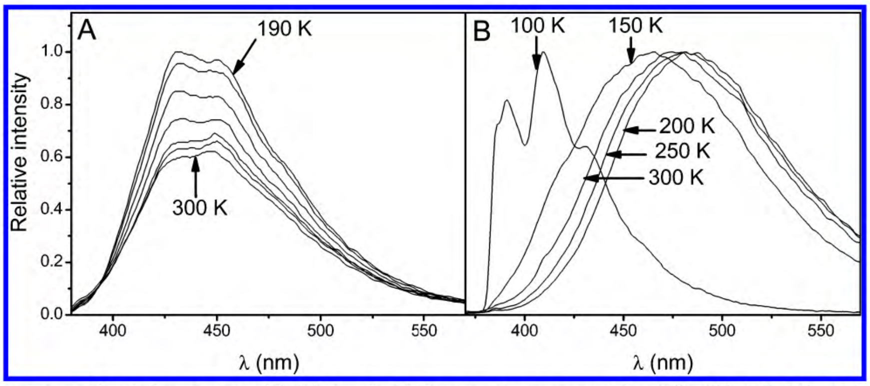

Figure 4. Temperature scan of emission spectra of 2-AS dyes in (A) heptan (spectra recorded at 300, 280, 260, 240, 220, 200, 190 K and the intensity increases with decreasing temperature monotonously) and (B) ethanol−methanol mixture (1:1).

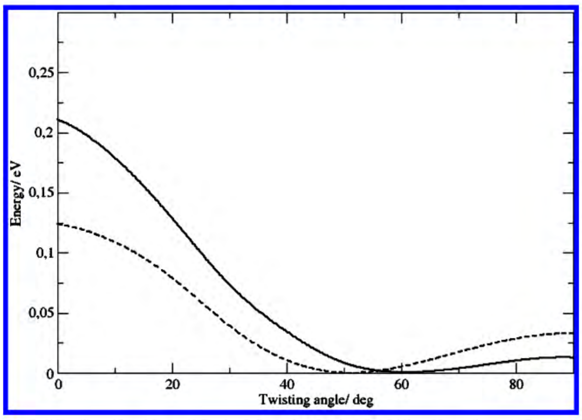

Figure 5. Relaxed torsional potentials for S_0 and S_1 states of 9-methylanthroate calculated at the AM1-FOMO-6/6 level. Full line corresponds to the S_0 state, while the dashed line corresponds to the S_1 state. The S_1 potential has been shifted by −3.2 eV.

experiments. The rotational relaxation mechanism does not explain why such a modest rearrangement could destroy the mirror image character of the fluorescence spectrum. As a matter of fact, the fluorescence spectrum of an analogous methylester of the 9-acridencarboxylic acid in tetrahydrofuran does not exhibit the broad, red-shifted spectrum of 9MA even though the torsional potential in both S_0 and S_1 states and their absorption spectra are very similar.[30]

Further evidence against the rotational relaxation mechanism comes from the present electronic structure calculations. The first excited state in the Franck−Condon region is essentially the anthracene ring $\pi\pi^*$ state. This is a nonpolar state, with a dipole moment being within 1 D from its ground-state value. The torsional curves calculated with a semiempirical AM1 Hamiltonian for the S_0 and S_1 states are depicted in Figure 5. The twisting angle in the ground state is 60°; in the S_1 relaxed state it is 50°. (CAS-SCF optimization provides similar numbers of 58° and 53.5° for the two states.) The barrier at 90° in the S_0 state is less than 0.02 eV; thus it is thermally accessible, the barrier in the S1 state being also low (0.04 eV). This is in good agreement with previous calculations of Dey[30] for a free acid, and the height of the barrier also agrees with the experimental estimate of Swayanbunathan.[28] The Stokes shift between the Franck−Condon point and the relaxed locally excited-state minimum is less than 0.3 eV. These semiempirical calculations are also in a semiquantitative agreement with CAS-SCF and CASPT2 calculations (Table 3). The dipole moment does not change significantly along the rotational coordinate. Neither the value of the Stokes shift nor the solvent dependence is, therefore, in agreement with the rotational relaxation mechanism.

TABLE 3: Characterization of Important Minima on the S_1 Potential Energy Surface of the 9MA Molecule[a]

	FC	LE	Min1	Min2	Min3
CAS/eV	0	−0.6	−0.45	−0.8	−0.7
S0/S1 gap/eV	4.7	4.25	3.3	1.9	1.8
CASPT2/eV	0	0.05	−0.2	0.4	0.85
S0/S1 gap/eV	4.2	3.91	2.6	1.9	2.5
GS dipole/D	1.9	2.0	2.1	3.3	2.1
ES dipole/D	2.3	1.9	6.5	2.1	1.1
transition dipole/D	0.38	0.65	3.4	0.12	0.27

[a] FC denotes the Franck−Condon point, LE is a locally excited state, and Min1−3 are other local minima. Energies at the CAS-SCF(6/6) and corresponding CASPT2 levels are displayed in electronvolts, relative to the FC point.

We thus addressed the question of whether there is a different geometry on the S_1 potential energy surface that would be energetically accessible, possibly lower in energy than the locally excited state. Such a structure should be of a charge-transfer character (and should, therefore, have a large dipole moment) to explain the observed polarity dependence. The search for these local minima has been performed using the CAS-SCF method with the results are summarized in Table 3 and in Figure 6. The potential energy surface of the 9MA molecule in its first excited state is rather complex. We may anticipate that for different atomic configurations the S_1 state will be dominated by configurations with a $\pi\pi^*$ transition localized in the ring, $\pi\pi^*$ transition within the COOMe moiety, nπ^* transition, or the charge-transfer $\pi\pi^*$ transition. We have localized several distinct minima on the S_1 potential energy surface with energy below or comparable with that of the locally excited (LE) state (Figure 6). These minima are denoted as Min1, Min2, and Min3. Min1 corresponds to a S_1 state minimum with a large dipole moment (6.5 D). This fits nicely with the estimate of a 9MA dipole moment change by Werner.[12] Also the estimated emission wavelength from this structure, 470 nm at the CASPT2 level, and large transition dipole moment for the emission from this state support the idea that we observe this structure in the fluorescence emission spectra. Note also that the charge-transfer (CT) state found here is further stabilized in polar solvents. Geometrically, this structure has a bent anthracene ring with a ring carbon atom connected to the out-of-plane carbonyl group. The anthracene ring in this structure is bent by 25°. There is a single bond between the carboxylic carbon and the anthracene group while the C=O bond remains

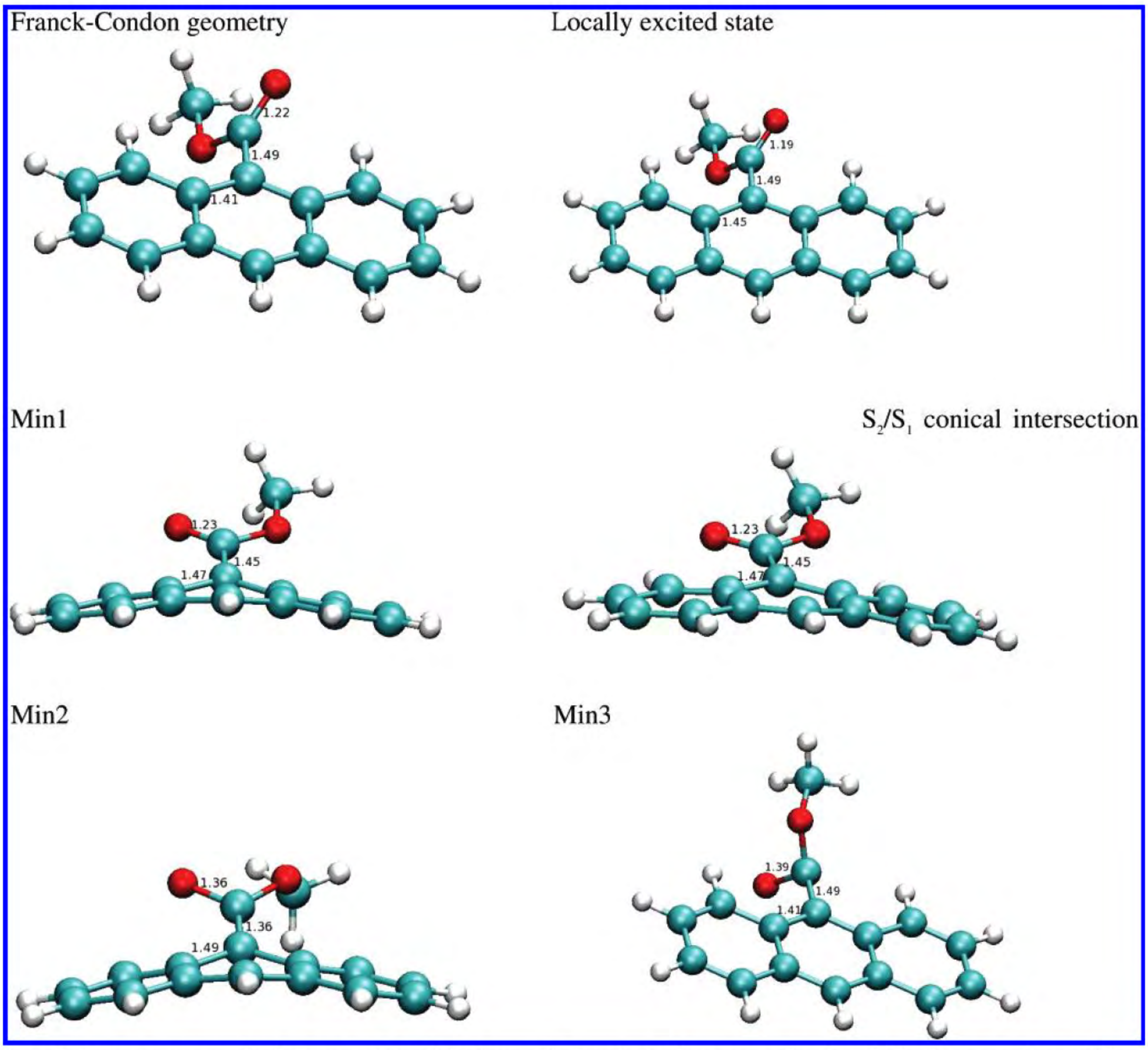

Figure 6. Important structures in the S_1 state of 9-methylanthroate. The Franck−Condon geometry has been obtained as a ground-state minimum using the MP2/6-31g* method; all of the excited-state minima and the S_2/S_1 conical intersection have been obtained by the CAS-SCF 6/6 method using the same basis.

a double one. The O═C−C_{anthr}−C dihedral angle is close to zero; however the carboxyl group is not coplanar with the anthracene ring because of its distortion. We have also found a structure originally suggested by Werner with a double bond between the anthracene ring and the carboxyl part (Min2). This state is, however, dominated by an excitation within the carboxylic group. The anthracene ring is bent in a similar way as found for a Min1 structure. We have also localized a third minimum on the S_1 potential with a planar ring geometry, elongated C═O bond, and pyramidilized carboxylic carbon (Figure 6). The two latter structures are energetically close to the LE state. However, the transition dipole moment is much smaller than that of Min1. Also the dipole moments of these structures are rather similar in the S_0 and S_1 states. This does not exclude the possibility that they contribute to the fluorescence spectra; structures of this type can be the source of the second peak observed in the experiment. Note that these states are energetically close to higher states with much larger transition dipole moments. The fact that the emission spectrum does not possess the mirror relation with the absorption spectrum even in nonpolar solvents suggests that the above states or at least some of them (presumably the state of C═O $\pi\pi^*$ character) might be responsible for the second, more energetic peak in nonpolar solvents.

We can, therefore, conclude that the following mechanism is likely to take place

$$S_0 \rightarrow S_1(\mathrm{FC}) \rightarrow \mathrm{LE} \rightarrow \mathrm{CT\ state}$$

$$\mathrm{LE} \rightarrow \mathrm{other\ distorted\ emitting\ states}$$

While the motion toward the locally excited minimum is essentially barrierless, the opposite is true for the second process. The intramolecular relaxation can thus take much longer times than was originally expected. We discuss this issue in section 3.5. Note that the conical intersection between the S_2 and the S_1 states (found from the locally excited minimum) has a geometry somewhere between the locally excited minimum and structure Min1. This intersection is energetically close to the locally excited state, suggesting that there will be only a small barrier for the escape from the locally excited state.

3.4. Temperature Scans. To validate the conclusions drawn from the theoretical simulations, we have performed temperature scans in heptane (Figure 4A) and in an ethanol−methanol mixture (Figure 4B). With decreasing temperature both polarity and viscosity are increasing. This interplay leads to a non-monotonous dependence of the solvent shift on the temperature. With the ethanol−methanol mixture we can reach a glassy state that completely freezes most of the short time conformational dynamics.

In the case of the ethanol−methanol mixture the temperature decrease from 300 to 200 K leads to a gradual red shift of the fluorescence, probably due to the increase of solvent polarity and consequent higher stabilization of the states possessing a charge-transfer character. In addition, solvent relaxation is likely to contribute to the red shift since at these temperatures SR still occurs on faster time scales than the intrinsic fluorescence. Moreover, no changes in the shape of the spectra are observed. At 150 K, the viscosity increase makes the formation of the states with a CT character difficult, and the fluorescence from the LE state prevails. Thus, a blue-shifted steady-state emission spectrum is observed. At 100 K, a polar glass is formed, which makes the solvent molecules immobile, preventing any change in the dye conformation as well as solvent relaxation. Therefore, an emission spectrum, which is supposed to be in shape and energy comparable to that of a Franck−Condon type, is observed (Figure 4B). This spectrum is blue-shifted, and the vibrational structure is visible. To find out to what extent solvent polarity influences the emission spectra in a glass system, we performed a temperature scan in a solvent with a significantly lower polarity (2-methyltetrahydrofurane). No significant difference in comparison to the spectra recorded in the ethanol−methanol mixture was observed (data not shown here).

A different picture is observed for a nonpolar solvent such as heptane. The decrease in temperature does not lead to any important spectral shift. With decreasing temperature the contribution from the more energetic excited states starts to dominate over the lower-energy charge-transfer state.

3.5. Time-Resolved Emission Spectra. The crucial point for quantitative SR studies presents the determination of "time 0 spectrum", i.e., the spectrum emitted prior to any change of the position and orientation of the solvent molecules ("Franck−Condon state"). The approximate procedure consists of subtracting the maximum of the absorption spectrum measured in the investigated system from the difference between the maxima of absorption and the emission spectra measured in a reference nonpolar solvent. For a precise description of this procedure, see a previous publication by Fee et.al.[31] Unfortunately, this approach fails in the case of the AS dyes. The above-mentioned intramolecular process introduces an additional photophysical effect in the reference nonpolar solvent. A wide range of molecules at various states contributes to the emission, which disables a simple determination of the steady-state maximum of the non-relaxed state. Thus, an alternative method must be used to obtain a reasonable "time 0 estimate". As shown above (Table 1), the absorption and excitation spectra are rather independent of both the position of attachment of the anthroyloxy group and the solvent used. Consequently, also the "time 0 spectrum" can be considered as to be almost invariant of those parameters.

It has been shown that the emission spectrum at the glassy state serves as a good approximation for "time 0 estimate" in a given solvent.[31] Moreover, the average frequency of those low-temperature spectra appears to be rather independent of the choice of solvent and position of attachment of the anthroyloxy group (e.g., $v_{\mathrm{av}} = 23\,840$ cm^{-1} and $v_{\mathrm{av}} = 23\,800$ for 16-AP in EtOH + MetOH glass and 2-AS in 2-MTHF glass, respectively). Considering those arguments, we believe that the determined v_{av} value of 23 800 cm^{-1} for 2-AS in 2-MTHF glass can be taken as a good estimate of the emission maximum of the Franck−Condon state of these AS dyes in POPC LUVs. Taking into consideration that the maximum of the excitation and absorption spectra of those dyes in LUVs differs at the most by 200 cm^{-1} from the spectrum in heptane (Table 1) and that the absolute value of the determined Stokes shifts in LUVs is about 2300 cm^{-1}, the maximal systematic error caused by the present "time 0 estimation" is lower than 10%. Thus, a "time 0 value" of 23 800 cm^{-1} is considered as a valuable estimate and serves further as an input value for constructing the correlation functions $C(t)$.

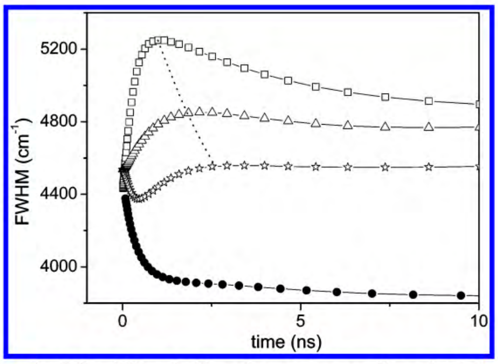

Figure 7. Full width at half-maximum time profiles of AS dyes in POPC LUVs (empty symbols) and paraffin oil (solid symbols): squares, 2-AS; triangles, 9-AS; stars, 16-AP; circles, 2-AS in paraffin oil. The dashed line illustrates the shift of the maxima toward longer times in the sequence 2-AS < 9-AS < 16-AP.

As concluded above from the steady-state emission data, a number of different states contribute to the photophysical behavior of *n*-AS dyes. Emission from different states takes place in nonpolar environments; however, the emission from the state with a CT character seems to dominate in polar systems. Naturally, solvent relaxation is present as well. These conclusions are also supported by the recorded TRES. A valuable parameter obtained by TRES is the time evolution of the fwhm. The pure solvent relaxation process is characterized by an increase at initial times followed by a decrease of the fwhm.[5,21,32] Such a behavior is clearly observed for 2-AS (Figure 7). When more processes take place the time course of the fwhm naturally becomes more complex, which is the case for 16-AP (Figure 7). The steep decline at the very early times (up to 1 ns) indicates that an additional process, which is not fully captured with the given time resolution, occurs. The origin of the complex behavior of 16-AP will be discussed further in the text.

The fwhm time profile can also serve as a rough estimate of the kinetics of the solvation dynamics. Logically, the maximum of the fwhm time dependence is shifted to the shorter times when the relaxation process gets faster. This behavior of fwhm(*t*) is nicely illustrated for dye Patman embedded in POPC LUVs measured at various temperatures (Figure 8). Patman is reported to show a pure solvent relaxation response in the fluid phase of a phospholipid bilayer.[5] Obviously, the faster SR kinetics, i.e., the shorter the solvent relaxation time τ_{SR}, the shorter times correspond to the maxima of fwhm(t) (Figure 8). The fwhm time profiles of AS dyes in POPC LUVs show similar trends, and the maxima of the slower processes are shifted to shorter times in the sequence 16-AP > 9-AS > 2-AS (see dashed line

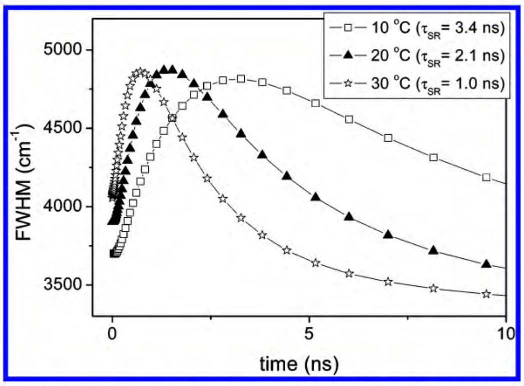

Figure 8. Full width at half-maximum time profiles of Patman in POPC LUV fors 10 °C (squares), 20 °C (triangles), and 30 °C (stars). The maxima of the fwhm's are shifted to the shorter times as the solvent relaxation becomes faster. The kinetics of solvent relaxation are described by solvent relaxation time τ_{SR}. Its values are 3.4, 2.1, and 1.0 ns for 10, 20, and 30 °C, respectively.

TABLE 4: Characteristics Obtained by Analyzing Correlation Functions in POPC LUVs and in Paraffin Oil[a]

	ν_{t0} (cm^{-1})	$\Delta\nu$ (cm^{-1})	τ_r[b] (ns)	% observed
2-AS[c]	23 800	2950	1.61	85
9-AS[c]	23 800	2450	1.40	73
16-AP[c]	23 800	2300	0.62	37
2-AS[d]	23 800	1630	0.58	44

[a] ν_{t0} corresponds to the spectral maximum of "time 0 estimate", $\Delta\nu$ is the overall Stokes shift, and % observed stands for the amount of the relaxation process that was captured with a given time resolution (30 ps). The percentage observed is obtained by comparing the values gained by the "time 0 estimation" and the first value of the TRES maximum $\nu(0)$ obtained by the "spectral reconstruction". [b] The integral relaxation time characterizes the overall relaxation process and provides only limited information on the individual processes, i.e., intramolecular relaxation and solvent relaxation. [c] In POPC LUVs. [d] In Paraffin oil.

in Figure 7). It indicates that the nanosecond relaxation process seems to accelerate when approaching the bilayer interface. In addition, the fwhm time profile obtained for the paraffin oil is almost constant on the nanosecond time scale, and only the rapid decline of the fwhm at the initial times is detected. Thus, it can be concluded that the water molecules that are absent in the paraffin oil and present in the bilayer are actually responsible for the slow nanosecond relaxation of AS dyes.

Another important parameter yielded by the TRES analysis is the overall Stokes shift that characterizes the micropolarity of the dye microenvironment. This also holds true for AS dyes featuring complex photophysics. As evident from Table 4, the Stokes shift, proportional to micropolarity, decreases with deeper location of the chromophore. Interestingly, even though the 2-AS and 9-AS dyes are reported to be located close to each other,[10] a large change in $\Delta\upsilon$ is observed. This fact supports the idea of a steep change in water density along the z-axes in the carbonyl region of the bilayer.[9,33] The comparison to the data measured in the paraffin oil, where the smallest $\Delta\upsilon$ was observed, evokes that water molecules are also present in the microenvironment of 16-AP. It means that either 16-AP is not buried as deep in the backbone region as reported previously[10] or that the chromophore itself perturbs the bilayer to the extent that water molecules can penetrate deeper. Alternatively, a significant dipole moment of the chromophore in the excited state may draw the water molecules via dipole−dipole interaction from the bilayer interface toward the backbone region of the bilayer.

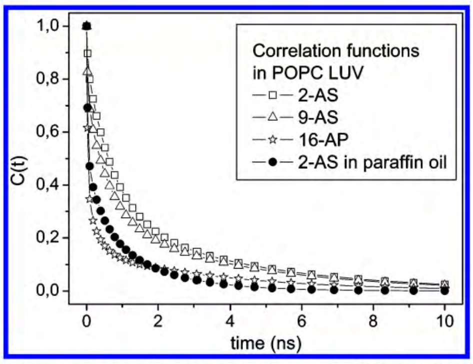

Figure 9. Correlation functions of AS dyes in POPC LUVs (empty symbols) and paraffin oil (solid symbols): squares, 2-AS; triangles, 9-AS; stars, 16-AP; circles, 2-AS in paraffin oil.

Parallel trends are found for the preferential solvation in mixtures of two liquids.[34]

By visual inspection of the correlation functions (Figure 9), by comparison of the integral relaxation times τ_r (Table 4), as well as by the amount of the relaxation process captured with the given time resolution (Table 4), it is evident that with the deeper location of the AS dyes in the bilayer the relaxation becomes faster on the whole. In the case of 2-AS, the observed behavior is similar to that of the dyes that undergo relaxation process mostly via nanosecond solvent relaxation and are located at the headgroup region.[5,35,36] Moreover, the integral relaxation time is in the range of 2 ns, implying that 2-AS occupies a similar region and features a similar solvation behavior as the already reported headgroup probes, for instance, Patman.[5] In contrast to 2-AS, 16-AP shows more complex behavior. The fwhm time profile appears to be nontrivial, and only 35% of the relaxation process is captured with the given time resolution. The reason is that a fast relaxation process dominates over the solvation response in the nonpolar environment of the backbone region. Such a conclusion is supported by the data measured in the paraffin oil, which serves as a feasible model system to the bilayer backbone. Obviously, only a minor part of the relaxation process is also captured with the given time resolution in the paraffin oil, and the relaxation times are on the same order as in the case of 16-AP embedded in POPC LUVs. The slightly slower relaxation time and the higher amount of the observed solvent relaxation can be ascribed to the larger viscosity of the paraffin oil compared to that of the backbone region of the bilayer.[37,38]

3.6. Dynamics of the *n*-AS Solvation and Intramolecular Relaxation. The experimental data indicate that the relaxation process of AS dyes in phospholipid bilayers is rather complex. The TRES reflect both intramolecular and intermolecular dynamics. The intramolecular relaxation includes torsional relaxation, formation of a charge-transfer state, and also other rearrangements of the carboxylic moiety leading to nonpolar emitting states. At the same time, solvent relaxation takes place. These two processes cannot be completely separated from each other. The rate of the LE → CT transition will most certainly depend on the polarity of the dye microenvironment. The time scale for the faster components of the solvent relaxation (libration, rearrangement, etc.) is roughly comparable with that of the intramolecular relaxation. We believe, however, that the intramolecular relaxation occurs on a subnanosecond time scale. This is supported by results of ab initio calculations. The intersection between the locally excited state and the charge-transfer state occurs only 0.2 eV above the locally excited minimum. The transition state leading to the CT state is thus energetically well accessible, and the rate of this transition is only limited by intramolecular energy transfer between modes. The same holds true for the transition to the other emitting states.

We can conclude that the slowest process observed in the time-resolved fluorescence spectra corresponds to the diffusion part of solvent relaxation. The use of n-AS dyes is, therefore, justified for solvation studies of phospholipids bilayers where the diffusion-driven solvent relaxation plays a dominant role. From the results of the time-resolved experiments the following conclusions about the solvation dynamics in the lipid bilayers can be drawn. First, as we go deeper into the bilayer the solvation contribution to the response functions becomes less significant but does not disappear completely even for the most buried 16-AP. Second, the time dependence of fwhm indicates that the solvent relaxation becomes slower upon approaching the center of the bilayer. What we observe is essentially preferential solvation in a mixture of a polar and nonpolar solvents. While the nonpolar solvent (in our case fatty acid chains) does not contribute significantly to the Stokes shift, the polar molecules (water in our case) contribute more or less proportionally to the number of surrounding solvent molecules. With decreasing water concentration we observe a decreasing Stokes shift, and the solvation process becomes longer.[39] If we considered the diffusion constant to be independent of the distance from the bilayer head, then we should in principle be able to reconstruct the water concentration profile. Unfortunately, our data at this point are too noisy for such a reconstruction. The obtained data, however, qualitatively support the results of molecular dynamical simulations. These are showing a steep decrease of water concentration from the headgroup to the backbone region of the bilayer.[40] A certain amount of water is, however, always present even in the microenvironment of the 16-AP, which is supposed to be buried in the backbone region.[10] Note also that the headgroup region of the bilayer is coarse and that the water profile reflects mostly the roughness of the surface.

4. Conclusions

We have explored the nature of light-emitting states of n-AS dyes by combining fluorescence spectroscopy with quantum chemical calculations. The recorded time-resolved emission spectra revealed a nontrivial behavior of these dyes in the backbone region of the phospholipid bilayer, showing the presence of multiple relaxation processes. Thus, steady-state fluorescence spectra were recorded in systems of varying viscosities and polarities to elucidate the n-AS photophysics. In addition, quantum chemical calculations have been performed for a model 9-methylanthroate dye. Combining these two approaches, we have shown that the mere relaxation to the locally excited state after the primary excitation cannot account for the experimentally observed behavior. Existence of an emitting state of a charge-transfer character was, therefore, suggested and confirmed by means of high-level ab initio calculations. We have also estimated the barrier between the locally excited state and the other emitting states. Time-resolved experiments have been discussed focusing on these new photophysical findings. We have concluded that time-resolved fluorescence measurements using the n-AS dye can serve as a valuable source of information on the diffusion-controlled part of solvent relaxation, while processes on femtosecond and picosecond time scales reflect in a rather complex way also intramolecular relaxation of the chromophore.

Acknowledgment. We thank the Grant Agency of the Academy of Sciences of the Czech Republic for support via Grant No. A400400503. This work also has been supported by the Czech Ministry of Education (Grant Nos. LC512 and LC06063). P.S. also thanks the Grant Agency of the Czech Republic for Postdoctoral Grant No. 203/07/P449.

References and Notes

(1) Milhaud, J. *Biochim. Biophys. Acta* **2004**, *1663*, 19.
(2) Wiener, M. C.; King, G. I.; White, S. H. *Biophys. J.* **1991**, *60*, 5610.
(3) Wiener, M. C.; White, S. H. *Biophys. J.* **1992**, *61*, 4210.
(4) Bursing, H.; Ouw, D.; Kundu, S.; Vohringer, P. *Phys. Chem. Chem. Phys.* **2001**, *3*, 23710.
(5) Sýkora, J.; Kapusta, P.; Fidler, V.; Hof, M. *Langmuir* **2002**, *110*, 571.
(6) Hutterer, R.; Schneider, F. W.; Sprinz, H.; Hof, M. *Biophys. Chem.* **1996**, *61*, 151.
(7) Jurkiewicz, P.; Olzyńska, A.; Langner, M.; Hof, M. *Langmuir* **2006**, *22*, 10741.
(8) Forrest, L. R.; Sansom, M. S. P. *Curr. Opin. Struct. Biol.* **2000**, *10*, 174.
(9) Zubrzycki, I. Z.; Xu, Y.; Madrid, M.; Tang, P. *J. Chem. Phys.* **2000**, *112*, 3437.
(10) Abrams, F. S.; Chattopadhyay, A.; London, E. *Biochemistry* **1992**, *31*, 5322.
(11) Villalain, J.; Prieto, M. *Chem. Phys. Lipids* **1991**, *59*, 9.
(12) Werner, T. C.; Hoffman, R. M. *J. Phys. Chem.* **1973**, *77*, 1611.
(13) Berberan-Santos, M. N.; Prieto, M. J. E.; Szabo, A. G. *J. Phys. Chem.* **1991**, *95*, 5471.
(14) Hutterer, R.; Schneider, F. W.; Lanig, H.; Hof, M. *Biochim. Biophys. Acta* **1997**, *1323*, 195.
(15) Chattopadhyay, A.; Mukherjee, S. *Langmuir* **1999**, *15*, 2142.
(16) Maroncelli, M. *J. Mol. Liq.* **1994**, *57*, 1.
(17) Michael, D.; Benjamin, I. *J. Chem. Phys.* **2001**, *114*, 2817.
(18) Cichos, F.; Brown, R.; Rempel, U.; von Borczyskowski, C. *J. Phys. Chem. A* **1999**, *103*, 26506.
(19) Tamashiro, A.; Rodriguez, J.; Laria, D. *J. Phys. Chem. A* **2002**, *106*, 215.
(20) Hope, M. J.; Bally, M. B.; Mayer, L. D.; Janoff, A. S.; Cullis, P. R. *Chem. Phys. Lipids* **1986**, *40*, 89.
(21) Horng, M. L.; Gardecki, J. A.; Papazyan, A.; Maroncelli, M. *J. Phys. Chem.* **1995**, *99*, 17311.
(22) Granucci, G.; Toniolo, A. *Chem. Phys. Lett.* **2000**, *325*, 79.
(23) Werner, H. J.; Knowles, P. *Molpro*, version 2002.6.
(24) Stewart, J. J. P. *Mopac 2000*; Fujitsu Limited: Tokyo, Japan, 1999.
(25) Turro, N. J. *Modern Molecular Photochemistry*; University Science Books: Sausalito, CA, 1991.
(26) Werner, T. C.; Hercules, D. M. *J. Phys. Chem.* **1969**, *73*, 2005.
(27) Werner, T. C.; Matthews, T.; Soller, B. *J. Phys. Chem.* **1976**, *80*, 533.
(28) Swayambunathan, V.; Lim, E. C. *J. Phys. Chem.* **1987**, *91*, 6359.
(29) Matayoshi, E. D.; Kleinfeld, A. M. *Biophys. J.* **1981**, *35*, 215.
(30) Dey, J.; Haynes, J. L.; Warner, I. M.; Chandra, A. K. *J. Phys. Chem.* **1997**, *101*, 2271.
(31) Fee, R. S.; Maroncelli, M. *Chem. Phys.* **1994**, *183*, 235.
(32) Richert, R. *J. Chem. Phys.* **2001**, *114*, 7471.
(33) Nagle, J. F.; Tristram-Nagle, S. *Biochim. Biophys. Acta* **2000**, *1469*, 159.
(34) Petrov, N. K. *High Energy Chem.* **2006**, *40*, 22.
(35) Dutta, P.; Sen, P.; Mukherjee, S.; Bhattacharyya, K. *Chem. Phys. Lett.* **2003**, *382*, 426.
(36) Halder, A.; Sen, S.; Das Burman, A.; Patra, A.; Bhattacharyya, K. *J. Phys. Chem. B* **2004**, *108*, 2309.
(37) Mateo, C. R.; Lillo, M. P.; Brochon, J. C.; Martlnez-Ripoll, M.; Sanz-Aparicio, J.; Acuiia, A. U. *J. Phys. Chem.* **1993**, *97*, 3486.
(38) Lopez, Cascales, J. J.; Huertas, M. L.; de la Torre, J. G. *Biophys. Chem.* **1997**, *69*, 1.
(39) Agmon, N. *J. Phys. Chem. A* **2002**, *106*, 7256.
(40) Jadlovszky, P.; Mezei, M. *J. Chem. Phys.* **1999**, *111*, 10770.

3 Numerical Studies of the Fluorescent Dyes (Prodan and Laurdan) in the Model of Fully-Hydrated Lipid Membrane

Fluorescent techniques are convenient experimental tools for investigation of lipid bilayer dynamics, properties and functions. Fluorescence study disposes of a variety of methods and a large assortment of fluorescent markers that are able to explore the membrane complexity in broad range of time scales. It is important to correctly interpret the signal coming out of the probe and some of the experimental techniques require the precise knowledge of the probe location in the membrane. We have seen before that the fluorescent response in SR technique directly depends on the probe location and report on the level of local hydration and mobility. A precise knowledge of the probe location and its stability is thus required.

In this numerical study [13]: Prodan (*6-propionyl-2-dimethylaminonaphthalene*) and Laurdan (*6-dodecanoyl-2-dime-thylaminonaphthalene*) (see Figure III.10) were investigated because of their high sensitivity to the local polarity [140-142]. The fluorescent active chromophores of the dyes contain an electro-donating amino group (blue part) and an electron-accepting carbonyl (red part). Laurdan has long hydrocarbon tail (12 carbons) and is located at the glycerol level of the bilayer at a well defined [7, 143] and more stable position than Prodan, which has short hydrocarbon tail (3 carbons). Prodan is believed to be found at two different locations in the lipid membrane: one polar, at the interface of the bilayer, and one less polar, at the glycerol level [7, 72-73].

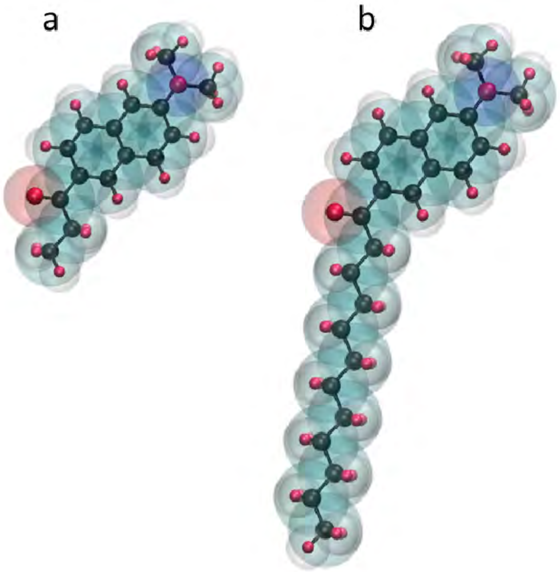

Figure III.10 Ball and sticks molecular structure of Prodan (a) and Laurdan (b). Transparent blue parts are the dimethylamino electron-donating groups and the transparent red subunits correspond to the carbonyl electron acceptors.

The experimental parallax quenching method is able to determinate the probe location in the lipid bilayer, however, it is not very precise and subject with considerable error [144]. This experimental difficulty might be resolved using computational methods. Quantum mechanical (QM) calculations and molecular dynamics (MD) simulations can be useful tools to study both the intermolecular interactions and intramolecular processes between fluorescent dye and its surrounding in the lipid bilayer.

In this work, quantum mechanical calculations were performed to obtain correct theoretical model of Prodan and Laurdan molecules in the ground and excited states. Bond lengths, interatomic angles, partial charges [145] and general dipole moments [141, 146-153], were calculated for the ground and excited states of both probes. These values were used for the construction of a force field used in MD simulations. Molecular dynamics simulations were applied for study the dyes behaviour in the system of fully-hydrated lipid bilayer at 300K.

The main goal of this study was to characterize the interactions of fluorescent probes Prodan and Laurdan in the ground and excited states with the phospholipid bilayer and water molecules. The differences in location and hydration for both dyes were compared with experimental SR data.

3.1 Quantum Mechanics Calculations

The optimized geometry of Prodan molecule in the S_0 ground state was found to be in good agreement with the available X-ray data [154]. Hessian matrix (the matrix of second derivatives of the energy with respect to geometry) was calculated for further use in the force field parameterization. The bond lengths, angles and dihedrals, which were obtained as a result of optimization calculations, were implemented to the database, structure and topology files. The electronic structures of the excited state is different from S_0 state despite their close geometries. The detailed description of the ground S_0 and excited S_1, S_2 and S_3 states are given in Table III-2 for Prodan and Table III-3 for Laurdan.

	elementary charge [e]		**μ [D]**	**E [eV]**	**osc. strength**
	nitrogen	oxygen			
S_0	0.006865	-0.39857	4.96		
S_1	0.37568	-0.3951	12.91	3.10	0.5074
S_2			16.45	3.70	0.0495
S_3			17.36	3.88	0.0000

Table III-2 Elementary charges, dipole moments (μ), absorption energies (E) and oscillatory strengths calculated for ground state S_0 and first three excited states(S_1,S_2 and S_3) of Prodan.

Calculated values of the dipole moments are in good agreement with many experimental and computational studies [141, 145-153, 155]. The partial migration of electric density from the donor (N) to the acceptor (O) increases significantly the value of the dipole moment upon electronic excitation. For further calculation, we used only the S_0 and S_1 conformations in the following MD since their oscillatory strength are large compared to S_2 and S_3 for both dye molecules.

	elementary charge [e]		μ [D]	E [eV]	osc. strength
	nitrogen	oxygen			
S_0	0.005966	-0.398741	5.74		
S_1	0.375534	-0.394224	12.93	3.30	0.4784
S_2			16.60	3.67	0.0466
S_3			17.51	3.94	0.0001

Table III-3 Elementary charges, dipole moments (μ), absorption energies (E) and oscillatory strengths calculated for ground state S_0 and first three excited states(S_1,S_2 and S_3) of Laurdan.

3.2 Molecular Dynamics Simulations

3.2.1 Location of the Dyes in the Bilayer in Both Ground and Excited States

It is well known that Prodan and Laurdan easily incorporate into the lipid membranes [72]. In this study, the fluorescent molecules in the ground state were initially placed in the bulk water, far from the DOPC bilayer. After 10 ns of simulations, they were incorporated into the membrane and remained within the lipid bilayer for the rest of the simulation time (170 ns for Prodan and 100 ns for Laurdan). The dye chromophores are found at the glycerol level of the lipid membrane and their hydrocarbon chains were inserted between hydrocarbon tails (see Figure III.11).

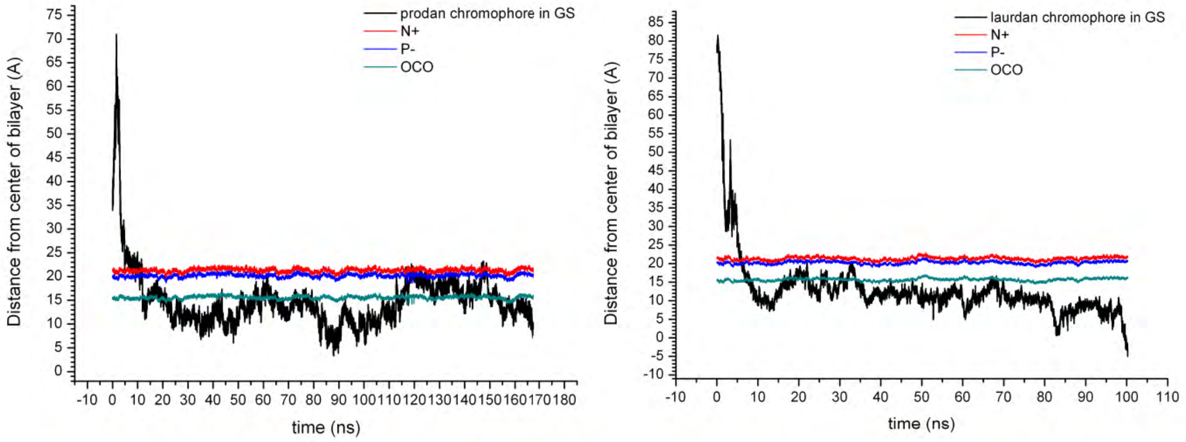

Figure III.11 Prodan (left) and Laurdan (right) chromophore positions at the ground state as a function of time of unconstrained MD simulation. The positions of ammonium (red curves), phosphorous (blue curves) and glycerol (green curves) of lipid are also plotted.

The position of Laurdan is more stable than Prodan indicating a higher Prodan mobility within the membrane. Prodan and Laurdan distributions in the bilayer are presented in the following histogram (see Figure III.12) in terms of the chromophore center distance from the bilayer center.

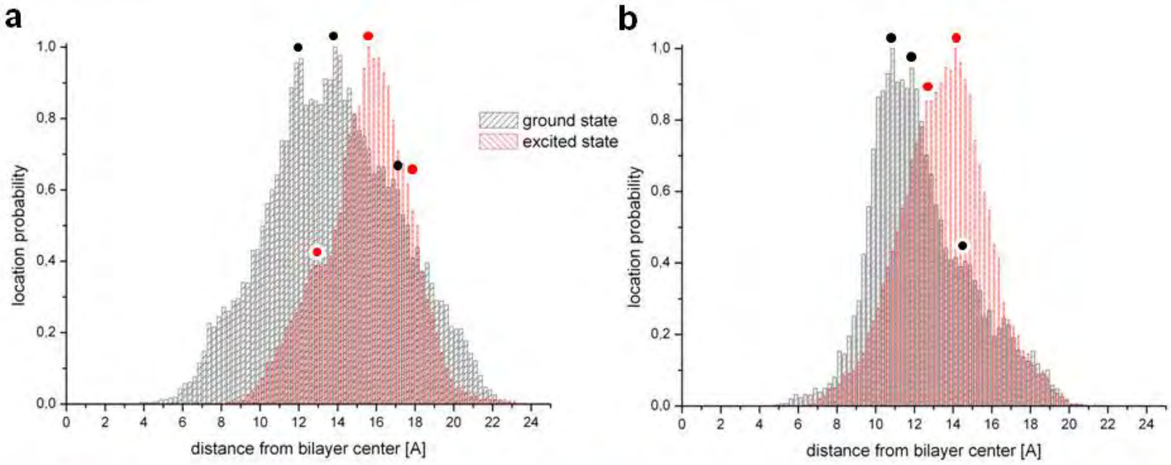

Figure III.12 Location histograms of chromophore centres of Prodan (a) and Laurdan (b) molecules in their ground (gray) and excited (red) states during performed MD simulations. Positions are show as a distance from the bilayer center.

Gaussian fits of histograms are summarized in Table III-4.

Prodan location [Å]				Laurdan location [Å]			
S_0		S_1		S_0		S_1	
12.0±2.3	<0.98>	12.9±1.7	<0.39>	10.8±1.4	<0.95>		
13.9±2.5	<1.00>	15.7±1.5	<1.00>	11.9±1.3	<1.00>	12.8±2.0	<0.85>
17.1±2.4	<0.28>	17.9±1.4	<0.28>	14.4±2.0	<0.41>	14.2±1.9	<1.00>

Table III-4 Dyes location in DOPC bilayer as a distance in [Å] from the bilayer center obtained by Gaussian fit of data shown in Figure III.12. By <> is indicated normalized amplitudes of peaks.

For Prodan in ground state, three preferable positions were found. Two of them are equally probable while the third reaches only 30% of their probability. In the excited state, the dye is shifted to membrane surface and occupy a well-defined single location. Laurdan in the ground state has also trimodal distribution. The mean value of the two dominant locations (which are spaced by about 1 Å and have similar amplitudes) of the dye in the ground state is equal to 11.4 Å and it matches exactly to the value determined experimentally [7]. Similarly to the Prodan, Laurdan in the excited state shifts toward the more polar region of the membrane and occupies a more precise location. The broader distribution of Prodan, in comparison to Laurdan, is the consequence of the short proprionyl tail which does not stabilize the position of the dye in the bilayer.

3.2.2 Impact of Dipole Moment Change on Water Molecules Organization

The fluorescence solvent relaxation technique takes full advantage of the phenomenon of the polar solvent molecule reorganization after electronic excitation of the fluorescent marker, which changes the dipole moment at the moment of the light absorption. In numerical system, it is hard to quantitatively define solvent change induced by the dye molecule since the dynamics of the dye and solvent molecules is different. They are characterized by different time scales – picoseconds for pure water rotations and nanoseconds for dye translations.

In this work, the projection of the total dipole moment vector of water molecules (μ_{water}) onto the instantaneous dipole vector of dye (μ_{dye}) were calculated. The scalar product of this two vectors has a positive or negative values corresponding to a parallel or an antiparallel organizations of both dipoles, respectively. The large value of the scalar product indicates a well organized water molecules, regardless of the dipoles relative orientation. The absolute values of the scalar product were used for interpretation purposes and are presented in Figure III.13 as a function of the distance from the chromophore center.

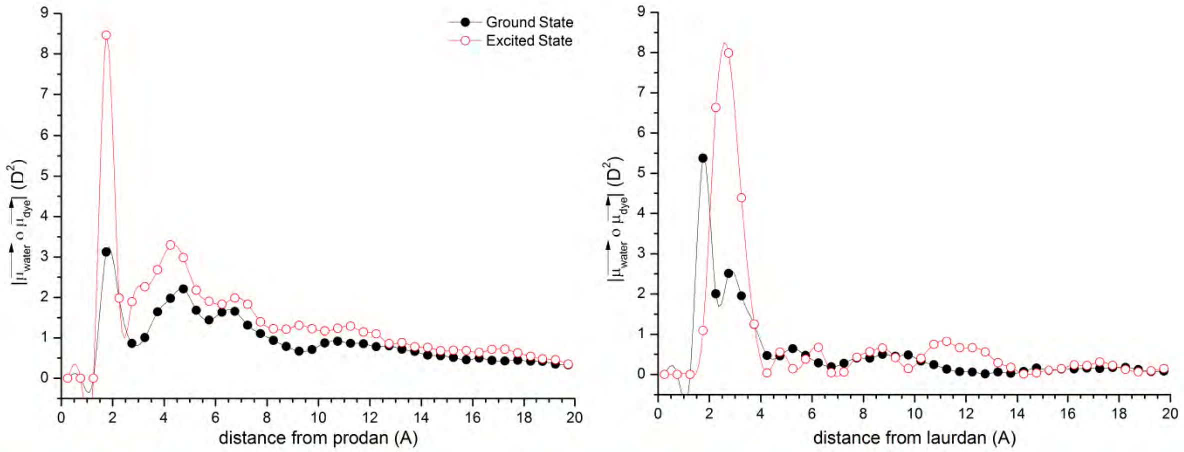

Figure III.13 Water arrangement around dye molecules Prodan (left) and Laurdan (right) in DOPC bilayer model averaged over two nanoseconds of simulations.

The effect of the dye excitation on the water molecules is observed in its closest vicinity. In the ground state Prodan directly affects its three first hydration shells at 3.0, 5.5 and 9.5 Å, whereas Laurdan have an impact on two first hydration shells at 2.5 and 4 Å from the chromophore center. The increase of dipole moments of Prodan and Laurdan generate a more organized water molecules. In case of Laurdan a weaker gain in water organization is observed.

3.2.3 Dye Dynamics in the Excited State

The changes of the dye position after excitation led us to analyze the dynamics of the dye translocation few nanoseconds after excitation. Ten initial positions of Prodan (4-19 Å) and Laurdan

(5-17 Å) in the bilayer were chosen for 4 and 6 ns of simulations, respectively. Results are presented in Figure III.14 and show maps of the dye location probability as a functions of the time after excitation for all initial configurations.

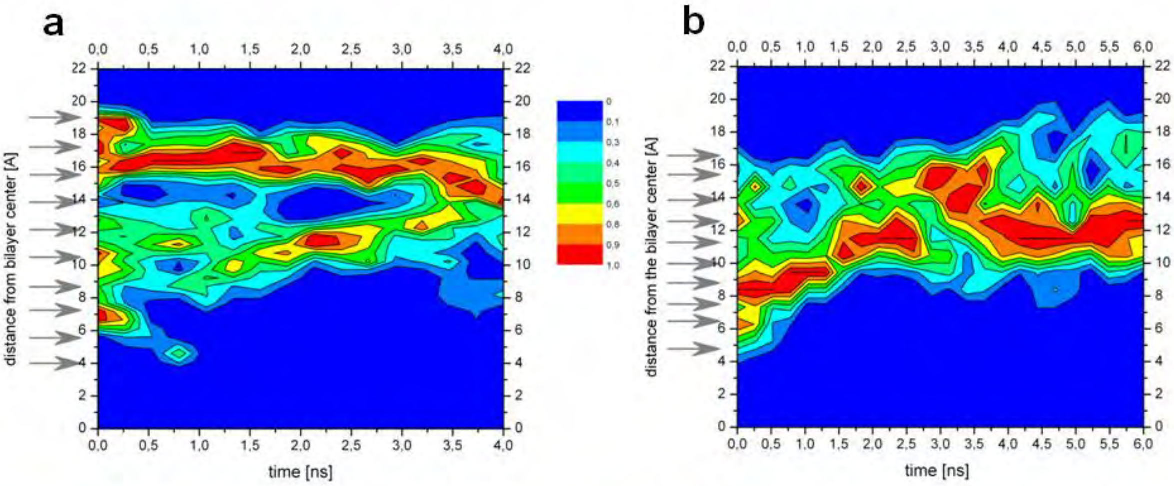

Figure III.14 Location probability of Prodan (a) and Laurdan (b) for ten molecules located at 10 different initial position, observed after excitation. The unoccupied locations are coloured blue whereas the most occupied are represented by red colour. Initial positions of both dyes are marked by arrows.

Prodan molecules show bimodal distribution (11.5 and 16 Å) 3 ns after excitation according to the previous calculations (see chapter III3.2.1). All the molecules with initial position higher than 14 Å occupy the location at 16 Å. The rest of the Prodan molecules, with initial position under 14 Å, converge to the higher position around 15 Å after 3.5 ns after excitation. Laurdan molecules 3 ns after excitation tend to occupy the most probable position found for the excited state around 15 Å (see also Table III-4). However, the location at 12 Å from the bilayer center acheved after 3.5 ns were found. It could mean that Laurdan need more than 4 ns for finding stable position. The majority of the tested dye samples change their position during first 3-4 ns after excitation, searching more energetically favorable polar environment. The time of the movement is connected with the initial location in the bilayer.

3.2.4 Water Dynamics After Dye Excitation

The solvent relaxation response is directly connected with the presence of the polar solution. For this reason, the analysis of the water behaviour obtained from simulations, was investigated in a similar way as during a solvent relaxation experiment. Experimentally, the most significant parameter obtained from SR technique is the integral relaxation time τ describing the solvent mobility in the sampled environment. The mean time constant measured in pure water is around 0.3 ps [71], whereas at the hydrated lipid bilayer is much smaller reaching 2 ns [70].

3.2.4.a Dyes in Pure Water

Prodan and Laurdan molecules were inserted in the water box mimicking the bulk water and then excited. The projection of the total water dipole vector on the instantaneous dye dipole vector as a function of the time after excitation is presented in Figure III.15, where the rearrangement of the water molecules around Prodan (a and b) and Laurdan (c and d) is demonstrated.

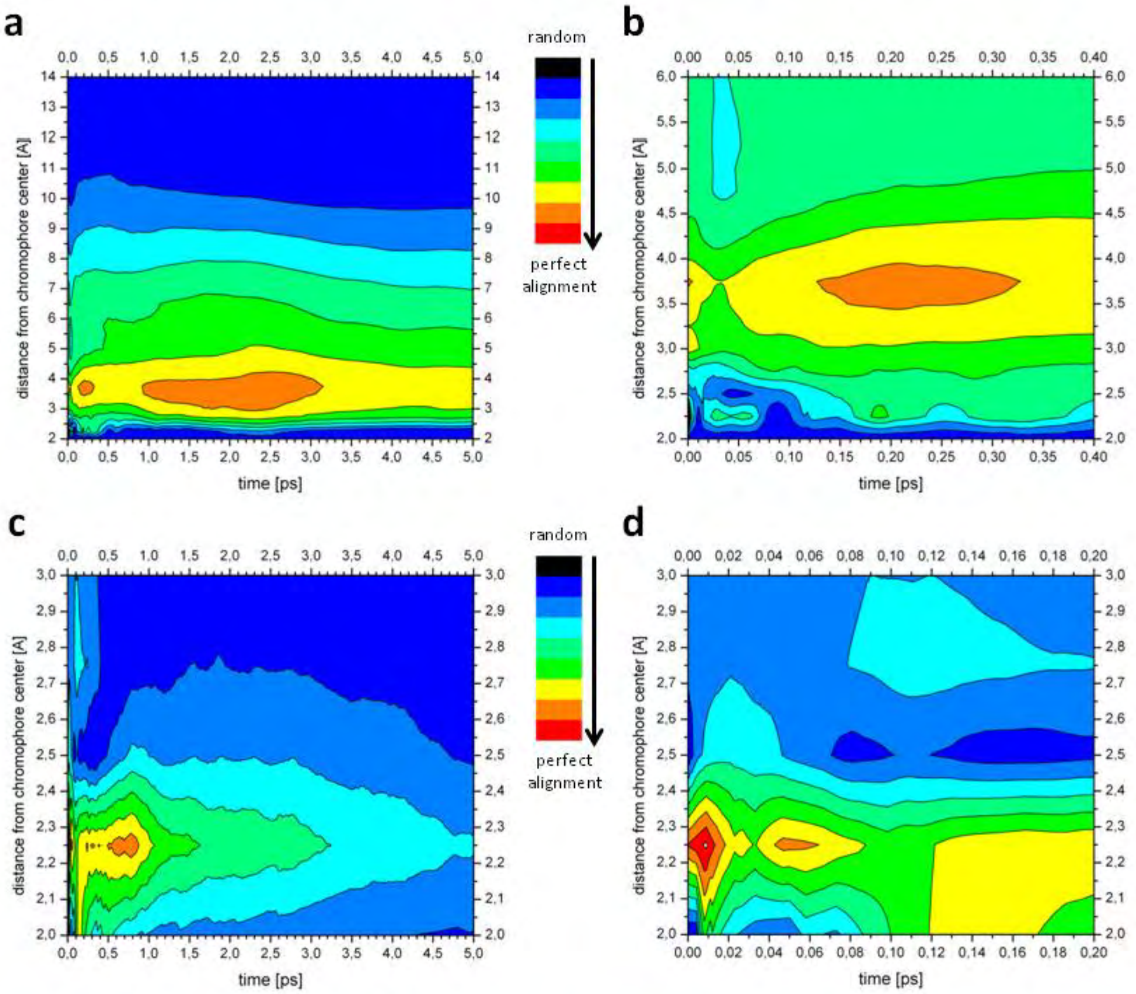

Figure III.15 Changes in dynamics of pure water behaviour around Prodan (a and b) and Laurdan (c and d) molecules induced by fluorophore excitation. Maps were plotted as a function of time (x axis) and distance from the chromophore center (y axis). Blue areas indicate the lack of the water organization and red zones correspond to the most organized water molecules vs. dye dipole vector. Maps (b) and (d) show zoomed part of the maps (a) and (c).

Results, obtained by simulations, show that water molecules react to the electronic excitation of the dye in the picoseconds time scale, what is in excellent agreement with experimental [71] and computational [156-157] data concerning relaxation times in pure water. Moreover, it is possible to define one complete cycle of the water molecules oscillation with respect to the dye dipole, followed by an immediate disarrangement, which corresponds to the local minima of calculated vector's projections. On the basis of the water oscillations, the relaxation time constants τ after excitation were found (see in Table III-5).

In case of Prodan, three reorientation cycles of water were observed in the first hydration shell ~3.5 Å from the chromophore center. The effect of the solvent rearrangement is visible at the distance 10 Å from the fluorophore center during 5 ns of simulation. Whereas Laurdan molecule has an influence only on the first hydration shell ~2.5 Å from chromophore center and water reorientation occurs faster than in case of Prodan. The solvent relaxation process is initiated within the first hydration shell and propagate on the next ones.

	τ_1[ps]	τ_2[ps]	τ_3[ps]
Prodan	0.03	0.34	3.20
Laurdan	0.03	0.10	1.00

Table III-5 Relaxation time constants (τ) calculated from the simulations of dyes in the bulk water.

3.2.4.b Dyes in the Lipid Bilayer

The next step of the "water dynamics after excitation" analysis was the study of the fully hydrated lipid bilayer. Prodan and Laurdan were initially located at ten depths like it was described previously in Chapter III3.2.3. These ten positions were chosen to reproduce the statistical average response of many dyes located at different depths in the bilayer. Data presented in this chapter are chosen for the most probable or the most repetitive positions for both dyes (12.2 Å and 11.4 Å for Prodan and Laurdan, respectively). The initial location of the probe molecules has a strong correlation with initial number of water molecules in their vicinity. In the experimental analysis two parameters, closely connected with water around dye, are determined from the TRES. First one, the total spectral shift $\Delta\nu$, which is proportional to the polarity of the dye environment (extent of membrane hydration) and second one, the integrated relaxation time τ_i, which describes mobility of water molecules.

The most representative results for Prodan and Laurdan are presented in Figure III.16. For Prodan two complete cycles of water reorganization are determined at 1.0 ns and 2.3 ns (Figure III.16a). Moreover, two overlapped cycles around 0.17 ns after excitation were found (Figure III.16b). These three times are equivalent to the experimentally determined solvent relaxation times τ_i. The total water rearrangement takes place mainly at the distances between 3 Å and 7 Å from the fluorophore center but in the case of the first relaxation cycle, the effect is observed at the distance 12 Å. Results obtained for Laurdan are presented in Figure III.16c, where three distinct cycles are also detected. Relaxation times in this case are determined to be 0.7, 2.2 and 3.4 ns. A fourth relaxation time was found around 0.05 ns, (Figure III.16d). The effect of the excitation affects hydration shell is located between 4 Å and 11 Å from chromophore center, but after 1 ns the excitation influence is limited only up to 6 Å.

From all 10 separate simulation runs at different depths in the bilayer for Prodan and Laurdan in their excited states the 20 relaxation time constants were found and are reported in Table III-6 as the intervals indicating the ranges of appeared τ_i values.

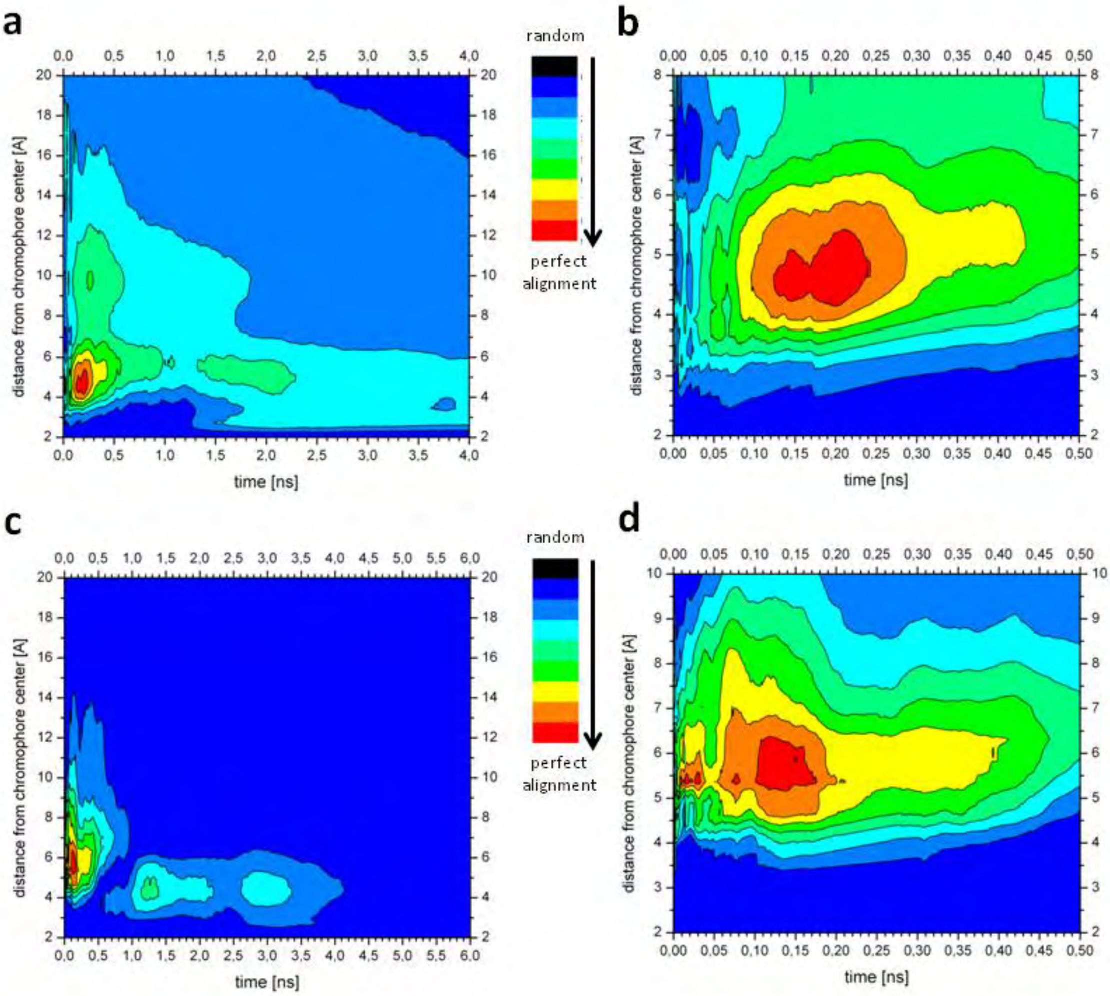

Figure III.16 Changes of water dynamics around Prodan (a and b) and Laurdan (c and d) after excitation in fully hydrated lipid bilayer environment. Maps were plotted as a function of time after excitation (x axis) and distance from the chromophore center (y axis). Maps (b) and (d) show zoomed part of the maps (a) and (c).

Between two and four relaxation times (τ_i) were found for each initial configurations. The fastest water reorganization cycle occurs within first 50 ps after excitation. Next relaxation cycle is observed during the first nanosecond. Others, much weaker, arise at later time. Relaxation times are longer for Laurdan than Prodan, which agrees with the experiment [70]. The shortest time τ_1 may be attributed to the energy dissipation by rotation of water molecules. τ_2 could be connected with water translation induced by dye dipole increasing upon excitation whereas τ_3 and τ_4 are supposed to be determined by lipid reorganization causing sub-sequent impacts on water molecules.

	τ_1[ns]	τ_2[ns]	τ_3[ns]	τ_4[ns]
Prodan	0.01 – 0.05	0.10 – 0.50	0.75 – 1.60	2.50 – more than 4.0
Laurdan	0.01 – 0.05	0.16 – 0.60	1.25 – 2.25	3.00 – more than 6.0

Table III-6 Ranges of relaxation time constants (τ_i) with dyes embedded into DOPC membrane model and gathered across multiple simulations.

The analysis of the changes in water amount around the fluorophore following excitation were performed and show small difference between Prodan and Laurdan. The number of water molecules at distance up to 5 Å from the chromophore center slightly increases by 6 ± 4 for Prodan and 9 ± 4 for Laurdan. First hydration shell around Prodan contains ~23 water molecules after dye excitation, while around Laurdan there is ~18 water molecules. The overall Stokes shift $\Delta\nu$, obtained from TRES analysis of solvent relaxation experiment, is connected to a polarity of the dye environment and is directly related to the amount of water molecules disorder by excitation. Sýkora et al. [70] have reported $\Delta\nu$ values equal to 3750 cm^{-1} for Prodan and 3450 cm^{-1} for Laurdan in egg-phosphatidylcholine at ambient temperature. The higher $\Delta\nu$ value indicate the more polar surrounding around dye like in case of Prodan, which is located closely to the water/bilayer interface. Laurdan, located deeper in the bilayer, has less polar environment and $\Delta\nu$ for it is smaller than for Prodan. This general tendency is confirmed by data from our numerical simulations.

3.2.5 Summary

The quantum calculations (QM) and molecular dynamics simulations (MD) were used to parameterize and characterize two fluorescent probes: Prodan and Laurdan in DOPC lipid bilayer.

The dipole moments, which correspond to the experimental values, were calculated for the dyes for ground and excited states by QM. Only the charges distribution in ground and excited state distinguish these two states in MD simulations.

The spontaneous diffusion of the dyes from the bulk water into the lipid bilayer was observed. The locations, calculated for Prodan, confirm the bimodal distribution observed in [72-73, 143] in lipid bilayer and the positions in the bilayer are determined. For Laurdan, locations found by quenching method [7] are well reproduced. Moreover, the specific position shift toward more polar region of the bilayer after excitation was observed for all dyes.

The solvent relaxation time scales were reproduced in MD simulations: picoseconds in pure water and nanoseconds in the lipid bilayer [13]. The four relaxation time constants were observed for the probe embedded into the lipid membrane. The two shortest (τ_1 and τ_2) can be associated to the rotation and translation of the water molecules after dye excitation. The two longest (τ_3 and τ_4) are induced by lipid reorganization caused by previous changes in the bilayer hydration. MD simulations give additional opportunities for finding the shortest relaxation time value, which is inaccessible by the experimental resolution by now.

The combinations of QM and MD methods were successful. The obtained data are in excellent agreement with experimental results coming from the solvent relaxation technique. This opens a great future (novel applications) for numerical simulations in this field of research.

Biochimica et Biophysica Acta 1798 (2010) 1724–1734

Contents lists available at ScienceDirect

Biochimica et Biophysica Acta

journal homepage: www.elsevier.com/locate/bbamem

Numerical studies of the membrane fluorescent dyes dynamics in ground and excited states

Justyna Barucha-Kraszewska [a], Sebastian Kraszewski [b], Piotr Jurkiewicz [a], Christophe Ramseyer [b],*, Martin Hof [a]

[a] Ústav fyzikální chemie J. Heyrovského AV ČR, v. v. i., Dolejškova 2155/3, 182 23 Praha 8, Czech Republic
[b] Institut UTINAM, Université de Franche-Comté, 16 Route de Gray, 25000 Besançon, France

ARTICLE INFO

Article history:
Received 7 January 2010
Received in revised form 17 May 2010
Accepted 19 May 2010
Available online 25 May 2010

Keywords:
Molecular dynamics
Fluorescent probe
Membrane
Excited state
Solvent relaxation
Prodan
Laurdan

ABSTRACT

Fluorescence methods are widely used in studies of biological and model membranes. The dynamics of membrane fluorescent markers in their ground and excited electronic states and correlations with their molecular surrounding within the fully hydrated phospholipid bilayer are still not well understood. In the present work, Quantum Mechanical (QM) calculations and Molecular Dynamics (MD) simulations are used to characterize location and interactions of two membrane polarity probes (Prodan; *6-propionyl-2-dimethylaminonaphthalene* and its derivative Laurdan; *2-dimethylamino-6-lauroylnaphthalene*) with the dioleoylphosphatidylcholine (DOPC) lipid bilayer model. MD simulations with fluorophores in ground and excited states are found to be a useful tool to analyze the fluorescent dye dynamics and their immediate vicinity. The results of QM calculations and MD simulations are in excellent agreement with available experimental data. The calculation shows that the two amphiphilic dyes initially placed in bulk water diffuse within 10 ns towards their final location in the lipid bilayer. Analysis of solvent relaxation process in the aqueous phase occurs on the picoseconds timescale whereas it takes nanoseconds at the lipid/water interface. Four different relaxation time constants, corresponding to different relaxation processes, where observed when the dyes were embedded into the membrane.

1. Introduction

Lipid bilayer is a main element of biological membranes that ensures its integrity and controls functions of membrane proteins [1–4]. In addition, the lipid bilayer is a suitable supramolecular model possessing attributes of complex systems in which a number of processes take place simultaneously at the same place but at different time scales [5]. Fluorescence techniques are convenient experimental tools to study lipid bilayers due to the existence of variety of fluorescent probes and methods able to gather data in broad range of time scales [6]. Fluorescence studies of the lipid bilayer relay on dedicated fluorescent probes interacting with the aggregate. The necessity to use a probe raises serious issues of probe effect on the studied structure. In addition, the probe reports on its immediate vicinity, which requires additional information in order to correctly interpret the experimental data. There are two major issues; the precise knowledge of the probe location and the correlation of the signal coming out of the probe with the specific lipid bilayer property. The first issue was addressed with dedicated experimental techniques [7,8] whereas the second is not yet satisfactory resolved. It is worth noting that there are number of fluorescence techniques to study various properties of the lipid bilayer, including dynamical and chemical quenching [6,9–12], energy transfer [12,13], dye adsorption [14,15], lifetime distribution [6,16], excimer formation [17,18] or anisotropy [6]. All of these techniques are usually averaged throughout the population of dyes and time and are reflecting the change of probe properties, which need to be later interpreted in term of lipid bilayer properties. However, there are also methods that probe directly selected membrane properties, e.g. fluorescent solvent relaxation (SR) [19–23], general polarization (GP) [24], and red edge excitation shift (REES) [25,26]. These ones report on the level of local hydration and mobility depending on the fluorescent probe location. They are somewhat complementary but SR technique seems to be more informative. Solvent relaxation is indeed mostly used for studying hydration and mobility of the phospholipid headgroups [22]. This method refers to dynamic processes associated with solvent reorganization (solvent relaxation) in response to a sudden change in charge distribution within the fluorophore upon an electronic excitation. Such excitation creates energetically unfavorable and unstable state in polar media, given by fast dipole moment transition, and is followed by reorientation of the solvent (water) molecules dissipating part of the absorbed energy to the environment (the lipid bilayer or the solvent). The energy loss is reflected in the total spectral shift of the emitted light toward longer wavelengths. This shift is

---

* Corresponding author. Institut UTINAM, Université de Franche-Comté, 16 Route de Gray, 25000 Besançon, France. Tel.: +33 381666482.
E-mail address: christophe.ramseyer@univ-fcomte.fr (C. Ramseyer).

0005-2736/$ – see front matter © 2010 Elsevier B.V. All rights reserved.
doi:10.1016/j.bbamem.2010.05.020

directly proportional to the polarity of the solvent. Since in lipid membranes, polarity is predominantly determined by the presence of water, the spectral shift mirrors the hydration of the membrane. Using time-resolved fluorescence instrumentation one can also follow the kinetics of the solvent rearrangement and, by this, concludes about its viscosity or local mobility in the case of lipid bilayer. Solvent relaxation in phospholipid membranes is about 10^4 times slower than in pure water, and consequently, it is very sensitive to the localization of the dye within the water–lipid interface [7,8,21,22,27]. A precise knowledge of the probe location and its stability is thus of great importance if one wants to correctly interpret solvent relaxation data. Having a set of fluorescent probes with known gradually spaced depths of locations in the bilayer allows to evaluate the amount of water and its dynamics across the membrane [7,8].

The two naphthalene derivatives presented in Fig. 1, namely Prodan (6-propionyl-2-dimethylaminonaphthalene) and Laurdan (2-dimethylamino-6-lauroylnaphthalene) are known as very useful fluorescent probes [24,28,29] due to their high sensitivity to the local polarity.

They have both an electron-donating amino group and an electron-accepting carbonyl. Prodan has a very short hydrophobic propionyl group (3 carbons). Therefore, the molecule is very mobile within the lipid membrane and can explore different locations. In fact, it was shown that, when in bilayer, Prodan locates in two distinct regions; one polar, at the interface and one less polar, at the glycerol level [30–32]. By contrast, Laurdan, with long hydrocarbon chain (12 carbons) and quaternary ammonium group attached both to its chromophore, is usually believed to be positioned at the glycerol level at a well defined location [31,33].

The experimental fluorescent SR technique gives some insights into the local membrane dynamic but again a data analysis strongly depends on the probe location. There are experimental techniques, which allow evaluation of the relative fluorophore position or its change upon membrane modification. The so-called parallax quenching method [34] relies on the determination of the distance between fluorophore and the residues that are able to alter its fluorescence. However, such approach requires also the precise knowledge of the quencher location, which in most cases, is not satisfied [35]. This intrinsic experimental difficulty may be resolved using computational methods. So far, no comprehensive works, addressing the issue of the fluorescent probe location and its alteration upon excitation have been conducted. Molecular dynamics (MD) simulations or quantum mechanical (QM) calculations can be useful tools to elucidate such question since they allow to study both the intermolecular interactions and the intra-molecular processes. Moreover, a combination of both techniques permits to observe, among other things, solvent relaxation upon electronic excitation [36]. A tremendous MD studies of lipid bilayers can be found in the literature but they do not include the fluorescent probes. In addition, only limited QM calculations were done until now for Prodan [37–45] and Laurdan [43,44]. In this work, we attempt to perform computational analysis of the two probes embedded into the lipid bilayer and to correlate our results with those recently generated with fluorescent solvent relaxation technique.

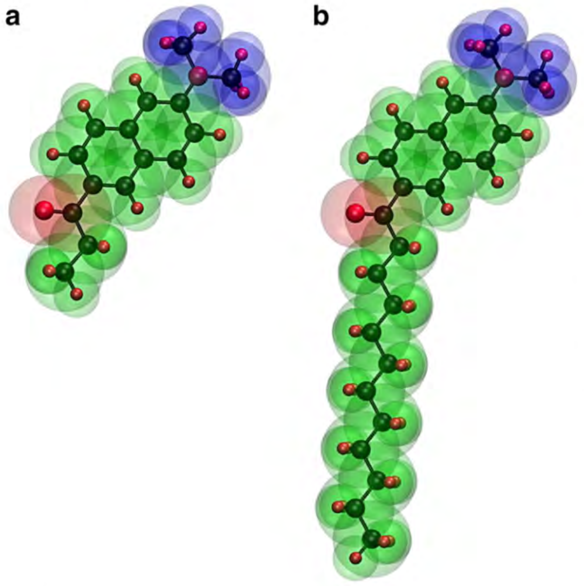

Fig. 1. Molecular structures of Prodan (a) and Laurdan (b). Transparent blue parts are the dimethylamino electron-donating groups and the transparent red subunits correspond to the carbonyl electron acceptors.

First, quantum mechanical calculations were performed to obtain correct theoretical description of Prodan and Laurdan molecules in both ground and excited states. Parameters like bond lengths, interatomic angles, partial charges [37] and general dipole moments [28,37–45] were calculated for the ground and excited states, what subsequently allows us to construct a force field for the subsequent MD simulations. Second, we have conducted MD simulations. In contrast to previous investigations on fluorescent probe molecules carried out at absolute zero temperature (0 K) and water defined as a continuum, we studied the dyes behavior at 300 K, immersed in the lipid environment. For the sake of clarity, the specific information like: absorption or emission spectra [46], the nature of the excited states, the origins of the emission process [38], detailed electronic orbital, different intramolecular charge transfer states depending on twisted or not (TICT or ICT) geometries [40,47] or multiple conformations of molecules during excitation [40] distinguished by rotational barriers [39], were not derived in the course of the present simulations.

The main objective of the present study was to characterize the interaction of fluorescence probe with the fully hydrated lipid bilayer. Our simulations were carried out for both ground and excited states. The differences in location and hydration for both dyes were compared with experimental SR data.

2. Methods

2.1. Quantum mechanics calculation

All quantum level calculations were performed using the Gaussian 03 software package [48]. The ground state equilibrium geometries of Prodan and Laurdan were optimized by density functional theory DFT [49,50] model with the 6-311+G(d,p) basis set. Only the planar conformation of Prodan molecule was investigated since it corresponds to the ground state geometry previously determined by X-ray analysis [51]. Since experimental data on Laurdan structure are very sparse, we decided to keep the same initial chromophore configuration as for Prodan for further optimizations. The excited states properties of fluorescent dyes were obtained from time dependent density functional theory TDDFT [52–54] with the same basis set as for DFT. The solvent effect was taken into consideration using the integral equation formalism of the polarizable continuum model IEFPCM [55–58]. In addition to structural data (bonds, angles…), we have also extracted, from the electronic structure of the molecules, other important values like dipole moments (both in ground and excited states) determined from the Mulliken charges distribution, excitation energy and oscillatory strength. We have tested different levels of theory (PM3, Hartree-Fock, DFT/TDDFT, CIS) and also derived different charge distributions (Coulson, Mulliken, NBO, Merz-Kollman, RESP). Surprisingly, we found that the Mulliken charges derived from DFT and TDDFT were the best compromise that led to the best dipole moment values when compared to the literature. Our method of calculation gave indeed similar planar structures with only slight deformations but importantly different charges distributions and hence the right order of dipole moment modification between ground and excited states. Note that the structural differences of the dye in its ground state and excited state can also originate from the capability of a molecule to relax its structure after Franck–Condon excitation to reach the S_1 minimum potential. Note also that a multipole analysis should be more realistic to reproduce the electric potential calculated at the quantum level, especially because our results focus mainly on the replication of total dipole moment of the dye molecules. However, the introduction of such multipole expansion in MD simulations is not largely implemented in the most exploited MD codes. Supplementary analysis based on construction of the Hessian matrix (the matrix of second derivatives of the energy with respect to geometry) was also performed for further use in the force field parameterization.

2.2. Molecular dynamics simulations

The commonly used force fields that are specific databases of intra- and inter-molecular interactions include only parameters for frequently studied molecules, i.e. proteins, nucleic acids, and lipids [59–62]. Excitable molecules such as fluorescent probes are not very popular topics for computational analysis despite their relative importance for biological sciences. In this study, we have derived a correct force field for the desired molecules by following a simple protocol based on our previously validated QM analyses. Here, models of fluorescent dye molecules, Prodan and Laurdan, already optimized by quantum mechanics calculations at 0 K, were prepared using parameterization tool from the molecular graphics software VMD [63] in order to use them in further MD calculations at 300 K and under 1 atm. Due to large differences between ground (S_0) and excited (S_1) states in their electronic structures but very close geometries, we decided to keep the same intermolecular Lennard–Jones potentials for both states and to discriminate them only by their specific partial Mulliken charges distributions. In that sense, our numerical models of Prodan and Laurdan were built in order to reproduce available experimental data. During MD simulations, dyes underwent important rotations of dimethylamino groups from 0 to about ±60° and minor deformations of aromatic rings. Nevertheless, averaged trajectories give for both dyes a planar geometry consistent with QM calculations, as it was also recently observed by Morozova et al. [43].

To study the behavior of the probes in the vicinity and within lipid membrane, a DOPC lipid bilayer, composed of 72 lipids (36 per monolayer) and hydrated on each side by 35 Å water slabs, was used as an experimental model. The lipid bilayer was first generated using a pre-equilibrated lipid membrane followed by a very short energetic optimization at 0 K and then we started a long equilibration run during more than 10 ns directly at 300 K and 1 atm to be sure to reach stability and to prevent us from classical MD artifacts before inserting a fluorescent probe into the bilayer. The size of the complete systems was about $(50\times50\times100)$ Å^3. Two main simulations were conducted separately for Prodan and Laurdan molecules both initially located in the bulk water. Each of the numerical study started with the fluorophores in their ground (GS) states. After 170 ns for Prodan or 100 ns for Laurdan, when the dyes were already spontaneously incorporated into the membrane core, the first excited (EX) state was induced by change of charges distribution on the probes. From that moment, the systems with fluorophores continuously kept in their excited states were observed for further 100 ns. This protocol was employed in order to find differences between two stationary defined states. Checking the stability of the fluorescent probes locations within phospholipid bilayer and the related dynamic water behavior, many short (up to 6 ns long) supplementary simulations for the probes in EX state initially located at different depths in the membrane were also performed. These initial configurations were directly taken from the main calculations. Short (5 ps) simulation, for free fluorescent probes surrounded only by water molecules in 50^3 Å^3 box, was also conducted.

MD simulations were performed using program NAMD2.6 [62] with the CHARMM27 [64] force field containing our own extensions for fluorescent probes. All water molecules were described by the TIP3P model [65]. A constant temperature of 300 K and a constant pressure of 1 atm were ensured by Langevin dynamics and Langevin piston Nosé-Hoover algorithm [66], respectively. Chemical bonds between hydrogen and heavy atoms were constrained to their equilibrium values, long-range electrostatic forces were evaluated using the particle mesh Ewald (PME) method [67] and the integration time step was equal to 2.0 fs.

3. Results and discussion

3.1. Quantum mechanics calculation

QM simulations are generally used for extraction of specific geometric and electronic data like bond lengths, angles, dihedrals and charges distributions. Those parameters are essential for the construction of the force field used in MD simulations. The optimized ground state S_0 geometries were found to be in good agreement with available X-ray data [51]. TDDFT calculations show that the electronic structures of the excited states are completely different from S_0 despite their close geometries. A brief description of ground (S_0) and first three excited (S_1–S_3) states is given in Table 1. Calculated values of dipole moments for each state are in good agreement with those calculated by others in many experimental and computational studies [28,37–45,68]. As it was already shown, the partial electron shift from the donor to the acceptor group increases significantly the dipole moment value upon electronic excitation. For Prodan, literature shows that the ground state dipole moment can range from 4.7 to 7 D, while in the excited state, it can vary from 8.3 to even 17.4 D. In Laurdan, S_0 was found to be characterized by a dipole moment value ranging from 4.7 to 6.3 D and in the excited state—between 8.3 and 19.8 D. Moreover, information provided by TDDFT analysis on excitation energies and oscillatory strengths was crucial to decide which excited state prevails in the experimental conditions. The excitation energies are within the experimental absorption wavelength ranging from 300 to 400 nm that corresponds to excitation energies of 3.08 to 4.12 eV. Only S_1 states are used for experimental [30,69] and computational [38–41] studies since their oscillatory strengths are large compared to S_2 and S_3 for both dye molecules. Consequently, we consider only S_0 and S_1 configurations in the following MD calculations. Throughout the rest of the paper, we will label the two states as GS and EX states in order to distinguish them from the multiple states obtained from QM simulations. Moreover, the description of molecule is subsequently different for QM and MD simulations, which naturally imply a different labeling.

3.2. Molecular dynamics simulation

3.2.1. Statistics of stationary states

Initially, large scale MD simulations were performed in order to study the partition of Prodan and Laurdan between water and lipid phases. It is well known that these amphiphilic molecules easily incorporate into lipid membranes [32]. Fluorescent molecules were thus initially placed in the bulk water, far from the DOPC membrane. After 10 ns of simulations, they were found to be subsequently incorporated into the membrane and remained within the lipid bilayer for the rest of the simulation time, as shown in Fig. 2. Detailed illustration of the insertion process into lipid bilayer can be seen in animations provided in Supplementary Information. After probes incorporation, the dyes carbonyl groups are found to be positioned at the glycerol level of the lipid bilayer with their hydrocarbon chain

Table 1
Dipole moments (μ), absorption energies (E) and oscillatory strengths calculated for ground (S_0) and first three (S_1, S_2 and S_3) excited states of Prodan and Laurdan molecules.

	S_0	S_1			S_2			S_3		
	μ [D]	μ [D]	E [eV]	osc. strength	μ [D]	E [eV]	osc. strength	μ [D]	E [eV]	osc. strength
Prodan	4.96	12.91	3.10	0.5074	16.45	3.70	0.0495	17.63	3.88	0.0000
Laurdan	5.73	12.93	3.30	0.4784	16.60	3.67	0.0466	17.51	3.94	0.0001

inserted between lipid alkyl chains. The position of Laurdan (Fig. 2b) is better defined than the Prodan one (Fig. 2a), indicating a higher Prodan mobility within the membrane. Note that similar behavior was also observed for excited states (data not shown). In order to test the effect of initial dye position on this feature, additional calculations were performed for both dyes positioned in four different starting positions, i.e. at water–lipid interface, at lipid glycerol level, deep within hydrophobic lipid tails and in the center of lipid bilayer. These simulations of 30 ns each showed that the final dye position (in the GS state) do not depend on its initial position.

Single liposomal vesicle, 100 nm in diameter, contains about 10^5 of lipid molecules and up to 10^3 fluorescent probes. The experimental sample contains, thus, a large number of fluorescent molecules, whereas in the MD simulation only a limited number can be implemented. It is, indeed, difficult to analyze more than a few dyes in one sample if one wants to keep dye to lipid ratio at reasonable level (1:100). Because of that, the specific dye locations in the membrane were statistically analyzed after 10 ns following translocation from water. Both ground (GS) and excited (EX) states were kept for about 100 ns. Although unrealistic for the EX state, this allows for averaging over long trajectory substituting for statistics of many short lifetime excited states responses as in real experiment (~4 ns, depending on wavelength and environment polarity). Resulting distributions of dyes locations are presented in Fig. 3 in terms of the chromophore center distance from the bilayer center. At first glance, the histograms are broad and it is not easy to assign the most probable values. To extract them correctly, we applied Gaussian deconvolution on the histograms. Results are listed in Table 2. Prodan in its GS state can be found in three preferred locations within the membrane (see dots in Fig. 3 and for details Table 2). Two of them are equally probable while the third has only 30% of their probability. In the EX state, the dye is shifted toward the membrane surface with only one dominant location (from 14 Å in GS to 16 Å in EX). The deeper location (12 Å in GS) does not disappear completely but its occurrence decreases by a factor of two and shifts only slightly toward 13 Å. The fact that Prodan exhibits two broader distributions in the GS state, whereas in the EX state only one occurs, clearly demonstrates that the increase of the dipole moment upon excitation results with well-defined single Prodan location. Our findings are complementary with information found in literature since it was argued by experimentalists that, due to its high mobility, Prodan has two distinct locations (and orientations) within the lipid bilayer [30,32,33]. According to our best knowledge, the exact position of Prodan has not been experimentally measured. Laurdan behaves quite differently, but its location in the GS is also trimodal, as shown in Fig. 3b. Two locations are spaced by about 1 Å and have similar amplitudes, while the third (the most outer location) has the weakest contribution (see Table 2). The mean value of the two dominant locations of the dye in the GS state is equal to 11.36 Å. It matches exactly to the value determined experimentally (11.4 Å) by the parallax fluorescence quenching method [31]. Like Prodan, Laurdan in EX state shifts toward the more polar region of the bilayer and converges in a more precise location. The narrower distributions of Laurdan, in comparison to Prodan, are likely a consequence of the stabilization of its position by its longer hydrocarbon chain and quaternary ammonium group that anchor much the molecule in phospholipid bilayer.

Fluorescence solvent relaxation technique allows measuring the dynamics of dye microenvironment polarity. In case of membranes, where water molecules are bound to lipid molecules, their rearrangement in response to the dye excitation is much slower than in pure solvents. In numerical system, it is hard to quantitatively define solvent changes induced by the dye molecule since the dynamics of the dye and solvent molecules are different. They are characterized by very distinct timescales like, for instance, picoseconds for water

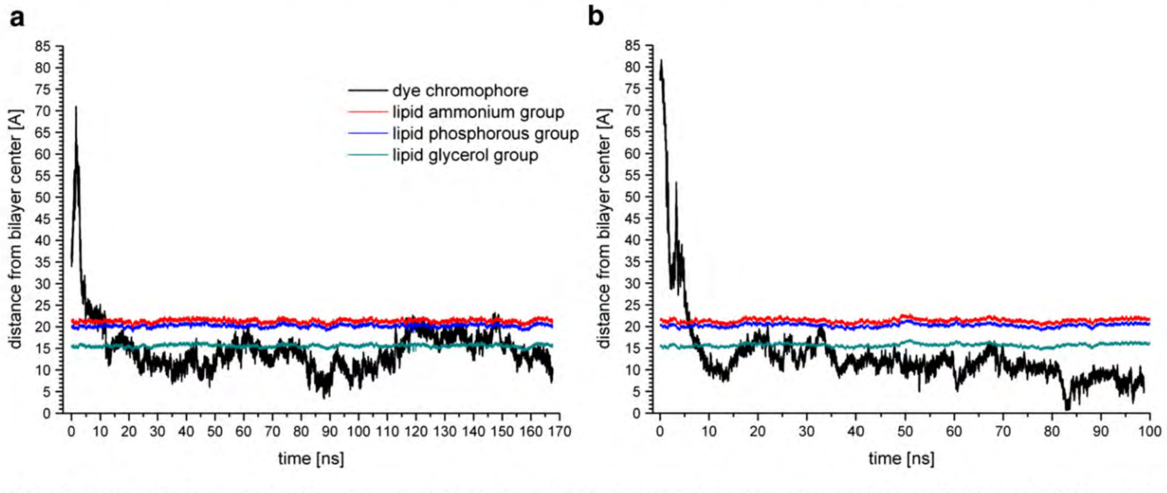

Fig. 2. The dependence of the chromophore positions at the ground state as a function of time of unconstrained MD simulation. Plot (a) shows data obtained for Prodan and plot (b) for Laurdan. Locations of the chromophore centre are depicted by black curves. The positions of ammonium (red curves), phosphorous (blue curves) and glycerol (green curves) of lipids are also plotted. Please note that simulation started with fluorescent molecule placed in the bulk water and that first 10 ns corresponds to the passive diffusion phenomenon towards the membrane surface (more details in text).

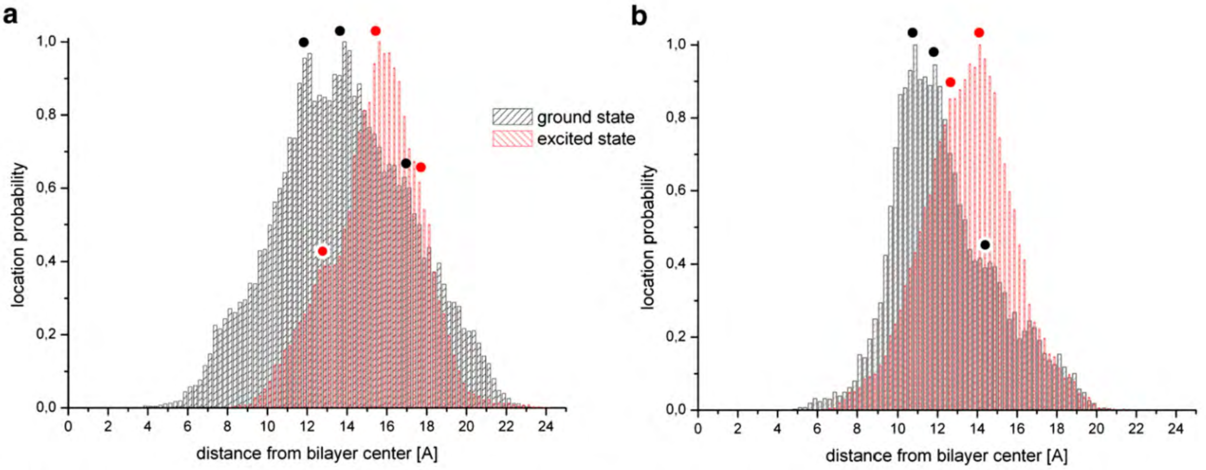

Fig. 3. Location histograms of chromophore centers of Prodan (a) and Laurdan (b) molecules in their ground (black plots) and excited (red plots) states during performed MD simulations. Positions are show as a distance from the bilayer center. Each histogram was normalized by the number of samples indicating the most probable location in given set of data. Dots correspond to the locations from Table 2.

molecule rotations and nanoseconds for dye translations. In this work, the projection of the total dipole moment vector of water molecules ($\boldsymbol{\mu}_{\mathbf{water}}$) onto the instantaneous dipole vector of dye ($\boldsymbol{\mu}_{\mathbf{dye}}$) was followed carefully. This type of treatment allows us to eliminate the effect of the dye motion in the lipid bilayer. The scalar product of these two vectors was calculated in order to quantify the water organization around the fluorescent molecule. It can have either a positive or a negative value corresponding to a parallel or an anti-parallel arrangement of both dipoles, respectively. Since the large values of the scalar product indicates a well organized water molecules, regardless of the dipoles relative orientation, the absolute value of the scalar product was used for interpretation purposes. The absolute values of the scalar averaged over 2 ns trajectories with the dyes oscillating around the most probable location within the membrane are presented in Fig. 4 as a function of the distance from the chromophore center. As expected, the effect of the dye excitation on the water arrangement is limited to its closest vicinity. For instance, Prodan in GS state directly affects its first three hydration shells occurring at 3.0, 5.5 and 9.5 Å, respectively; whereas Laurdan in GS state is able to organize only two first solvent shells at 2.5 and 4 Å from its chromophore center. For both dyes, the increase of the dipole moment upon excitation results in more organized water molecules. Additionally, the second hydration shell of Prodan in EX state is so broad that it starts to superimpose with the two adjacent water layers occurring in presence of GS state. Meanwhile, the two hydration shells of Laurdan observed in GS state merge into a single at 4 Å after dye excitation. Moreover, in contrast to Prodan, a weaker gain in water arrangement after excitation is observed. The solvent seems to be additionally altered by the substantial fluctuations of the dye, which results in less ordered configuration. This behavior may be a consequence of the long hydrocarbon tail fluctuations, which can importantly change the instantaneous dipole moment orientation of the dye at timescales even faster than the water molecules could readapt.

Table 2
Dyes locations in DOPC bilayer obtained by Gaussian deconvolution of data shown in Fig. 3. Distances (in Ångstroms) from the bilayer centre are reported with calculated normalized amplitudes of peaks (indicated by <>). GS and EX columns corresponds to ground and excited states, respectively.

Prodan location [Å]		Laurdan location [Å]	
GS	EX	GS	EX
11.97 <0.98>	12.85 <0.39>	10.84 <0.95>	
13.85 <1.00>	15.66 <1.00>	11.87 <1.00>	12.75 <0.85>
17.13 <0.28>	17.88 <0.28>	14.36 <0.41>	14.15 <1.00>

3.2.2. The dye dynamics in the excited state

The evidence of changes in dyes location upon excitation led us to analyze the dynamics of the dye translocation and the associated alterations of surrounding water molecules organization. Fluorescent probes shift toward aqueous phase is indeed a process occurring within few nanoseconds after excitation. Assuming well-converged results, independent on dye depth upon excitation, we decided to scan ten different initial positions of Prodan and Laurdan in the bilayer, selected from results of our previous simulations. The range of positions was chosen arbitrarily from 4 to 19 Å for Prodan and from 5 to 17 Å for Laurdan, which reflect ranges of locations found previously (see Fig. 3). Results presented in Fig. 5 show maps of dyes location as a function of time and for all initial configurations. Resulting dye translocations were extracted separately from each simulation as the histograms of the location probability counted on successive intervals of 0.25 ns along each collected trajectory. Then, histograms coming from each of 10 simulations of a given dye, and corresponding to the same time intervals, were summed up and normalized by the number of samples indicating the most probable location. Finally, such prepared data were gathered interval by interval in order to obtain a statistically relevant three-dimensional plot. The starting time was selected to be the instant of excitation when the dye dipole is changed. Prodan molecule shows a bimodal distribution with two main locations of 11.5 Å and 16 Å during the first 3 ns after excitation. All the molecules with the initial location higher than 14 Å occupy the position at 16 Å. The lower mode, taken by initially deeply inserted molecules, merges with the upper mode after 3.5 ns after excitation and then both converge toward the new location at around 15 Å. This may be already recognized as the preferred location found for Prodan in the EX state (Fig. 3). The Laurdan molecule, after first 3 ns of excitation, tends to reach directly the most probable position found for the EX state (around 15 Å). However, another stable location at around 12 Å remains after 3.5 ns. It could mean that Laurdan needs more than 6 ns to fully reach its statistically defined location showed in Fig. 3. Large majority of sampled dyes appear to change their position during 3–4 ns after the electronic excitation. Fluorescent molecules embedded deeply in the membrane relocate toward the

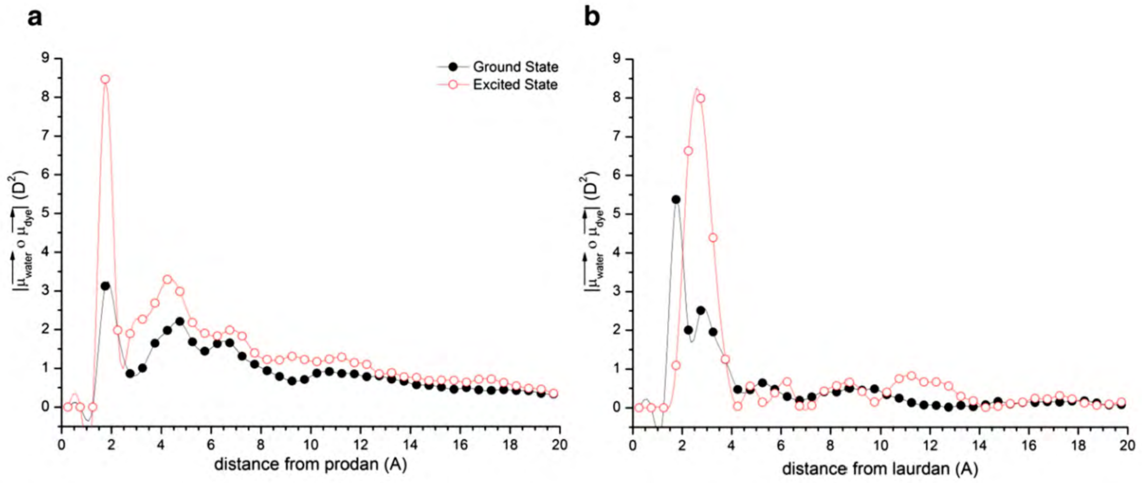

Fig. 4. Water arrangement around dye molecules, embedded into DOPC bilayer model, averaged over two consecutive nanoseconds of simulations. The absolute values of projected total water dipole vector onto Prodan (a) or Laurdan (b) dipole vector (abscissa scales), are plotted as a function of distance from the chromophore center. The bigger value means higher water organization in respect to the instantaneous probe dipole configuration.

bilayer surface driven by searching the more energetically favorable polar surrounding. The time of this movement is closely connected with the initial dye position. Nevertheless, the performed analysis is only a scan of all the range of locations with unique molecule but do not take into account an initial probability distribution as shown in Fig. 3.

3.2.3. The water dynamics after dye excitation

Because the dye response is directly linked to the presence of the polar solvent, we decided also to follow the water behavior in a similar way as during a solvent relaxation experiment. Figs. 6 and 7 present the projection of the total water dipole vector on the instantaneous dye dipole vector as a function of time, after the excitation. Trying to validate our analysis procedure, we have first simulated Prodan and Laurdan molecules inserted in the water box mimicking the bulk water. Next, the hydrated bilayer was introduced with dye molecules initially located at the same depths as indicated by arrows in Fig. 5. Experimentally, the most significant parameter obtained from SR technique is the integral relaxation time value (τ) describing the solvent mobility in the sampled environment. The mean time constant measured in pure water is around 0.3 ps [70], whereas at the lipid/water interface it is 4 orders of magnitude slower reaching 2 ns [21]. Interpretation of this experimentally observed large difference, likely induced by substantial change of polarity gradient across the bilayer normal, require precise knowledge of the fluorescent markers location. Since dye molecules start to relocate toward the bulk water after excitation, the experimental results are an average over different depths in membrane. In other words, fluorescent probes during their excited state lifetimes scan a part of the lipid bilayer. Data presented in this section are, in each case, valid for only one specific position, chosen here as the most probable or the most repetitive one.

Defining a solvent relaxation phenomenon is also not straight forward since it implies many types of processes associated to the

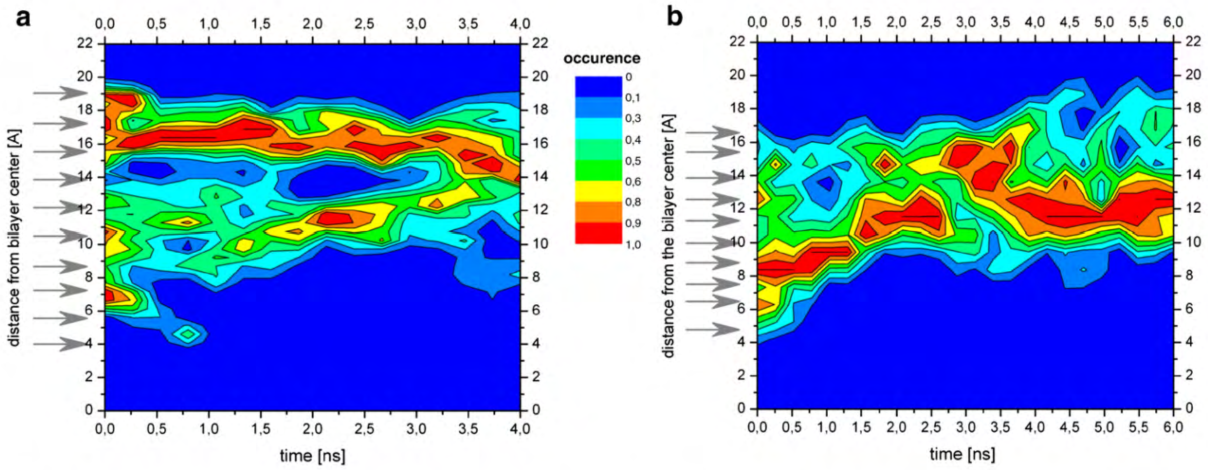

Fig. 5. Location changes of Prodan (a) and Laurdan (b) molecules after electronic excitation (starting time) merged from 10 separate MD simulations of each probe. Results are plotted as a function of time (abscissa scale) and distance from the bilayer center (ordinate scale). The unoccupied locations are colored blue whereas the most occupied are represented by red color. Arrows on the left indicate initial positions of dyes at the moment of excitation for each separately performed simulation. Please note different timescales for the two molecules.

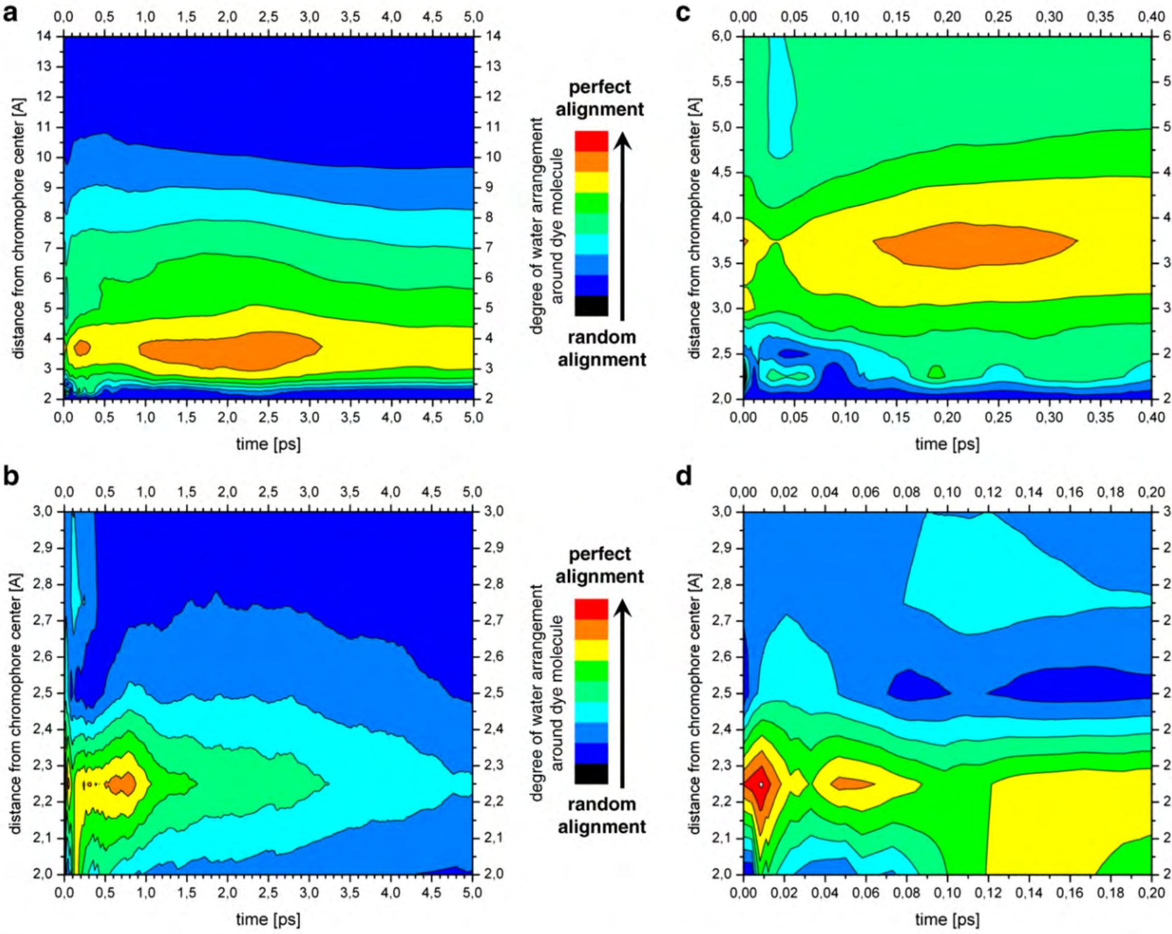

Fig. 6. Changes in dynamics of the pure water behavior around Prodan (a and c) and Laurdan (b and d) molecules, induced by fluorophore excitation. Maps were plotted as a function of time (abscissa scale) and distance from the chromophore center (ordinate scale). Blue areas indicate the lack of the water organization, green and yellow regions a progressive arrangement, while the red zones correspond to the most organized water molecules vs. dye dipole vector. Please note different scales between insets.

energy dissipation. During full atomistic simulations, we can access different levels of intramolecular energies, which are clearly distinguished by movements at separate timescales (bonds lengths oscillations, rotation or translation of the whole molecules, etc.) but in contrast to the real experiment, numerical method chosen herein give no information about interatomic energies, obviously contributing to the energy dissipation once the probe comes in the excited state. Fig. 6 presents rearrangement of bulk water around Prodan (Fig. 6a and c) and Laurdan (Fig. 6b and d) molecules after excitation. We observe that water molecules loss their induced arrangement in the picoseconds time scale, which is in excellent agreement with experimental [70] and computational [71,72] data concerning solvent relaxation in pure water. Defining one complete oscillation of water molecules (one cycle of water ordering with respect to the dye dipole, followed by an immediate disarrangement, which corresponds in Fig. 6 to the local minima of calculated vector's projections) as an important step in solvent relaxation phenomenon, we were able to link these oscillations with typical relaxation time constants (τ_i) occurring after dye excitation. All extracted times, τ_i, are listed in Table 3. In the case of Prodan, we observe three distinct cycles of water reorganization in the first hydration shell at the distance of around 3.5 Å from the chromophore center. The effect on the solvent molecules reaches up to 10 Å and is clearly visible during 5 ps of the simulation. Laurdan, in contrast, can influence only the first hydration shell at the distance of 2.0 and 2.5 Å from the chromophore center. Still three complete water-rearrangement cycles are present, but water reorganizes faster and extracted τ_i values are shorter than for Prodan. This difference is not surprising, considering that Laurdan and Prodan have the same chromophore but not the same tail, which contribute both to the dipole moment value of the dye. This first insight is in excellent agreement with earlier calculations [71,72] and experimental findings [70] justifying the applied simulation protocol. Since extracting the τ_i values depends on the definition of the limits of the whole rearrangement cycles, it was assumed that solvent relaxation process is initiated within the first water shell and then propagates on the next shells. Note that, the next relaxation cycle at a given distance (and thus for a given shell) begin before the previous one is completely propagated in the space. This can results with an overlap of cycles.

Analysis performed on numerical samples containing Prodan and Laurdan molecules, embedded into the membrane, show a strong correlation with their initial locations and initial number of water molecules in their vicinity. As mentioned before, water molecules arrangement and behavior has a preponderant role to interpret the solvent relaxation results. To quantify SR process, two parameters are determined from the time-resolved emission spectra (TRES). First,

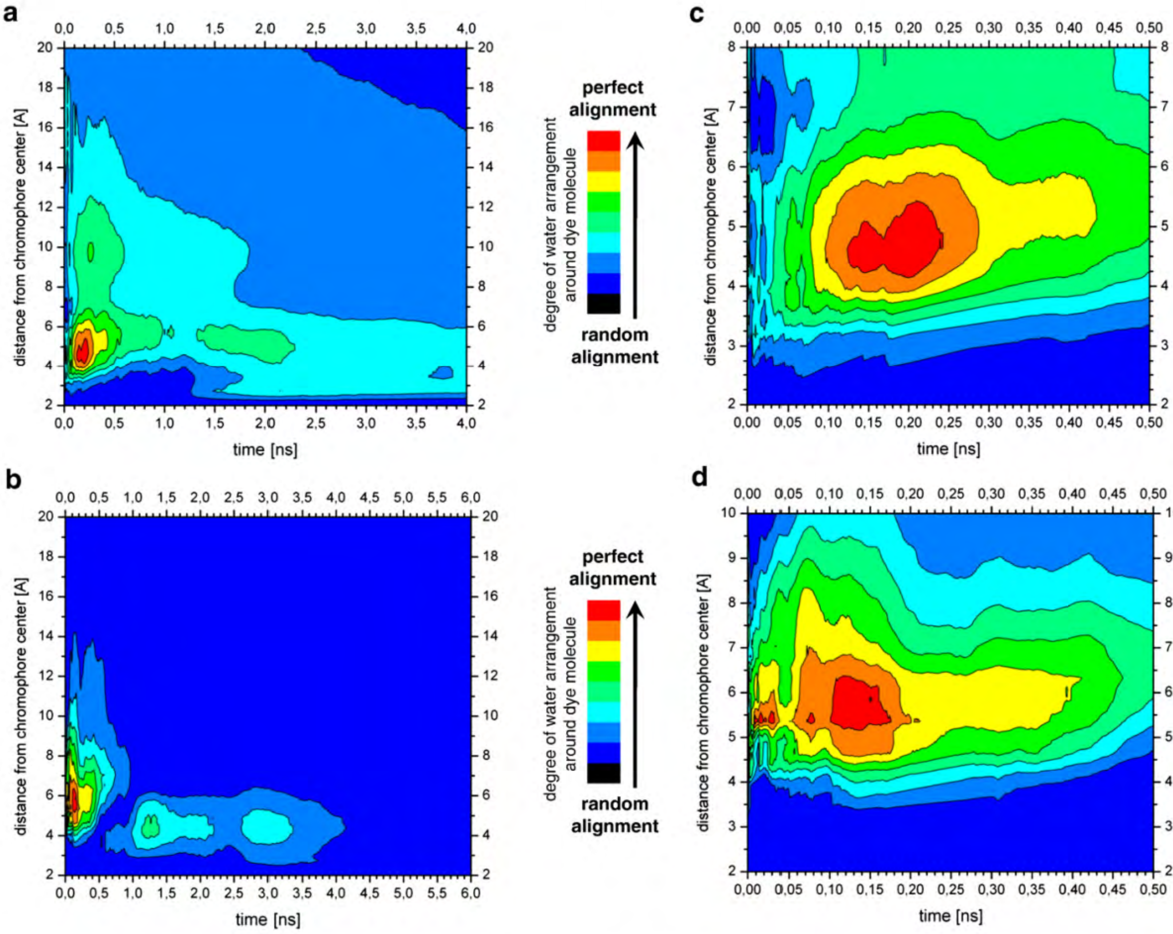

Fig. 7. Changes of water dynamics around Prodan (a and c) and Laurdan (b and d) molecules embedded into lipid membrane. Presented results correspond to the specific initial configurations of Prodan and Laurdan located at the depth of 12.2 Å and 11.4 Å, respectively. Maps were plotted as a function of time (abscissa scale) and distance from the chromophore center (ordinate scale). For color codes see Fig. 6. Please note different scales between insets.

introduced above, integrated relaxation time τ or relaxation time constants τ_i, obtained from multi-exponential fitting of the spectral response function C(t), describes mobility of water molecules. The second parameter, the total spectral shift $\Delta\nu$, is proportional to the polarity of the dye microenvironment and is believed to be correlated to the extent of membrane hydration. The most representative results, obtained for excited Prodan and Laurdan molecules when located at the distance of 12.2 Å and 11.4 Å, respectively, measured from the center of lipid bilayer are presented in Fig. 7. For Prodan only two complete cycles of water rearrangement can be clearly determined, i.e. 1.0 and 2.3 ns (Fig. 7a). However, within the first 0.5 ns after excitation (Fig. 7c) two peaks around 0.2 ns are detected. If we allow the possibility of the water rearrangement cycles to overlap, the additional local minimum could be identify at 0.17 ns after excitation, being the supplementary (third and the shortest) relaxation time in this example. The total water rearrangement take place mainly at the distance between 3 Å and 7 Å from the chromophore center but in the case of the first relaxation cycle, the effect reaches distance as far as 12 Å. Water around Laurdan presented in Fig. 7b shows three distinct cycles clearly propagating from the molecule toward the bulk water. Calculated relaxation time constants in this particular case are: 0.7, 2.2 and 3.4 ns, and again within the first half of nanosecond (Fig. 7d), there is an additional overlapping of cycles visible through a local minimum at about 0.05 ns (giving the fourth relaxation time constant in this example). The effect of excitation affects hydration shell located between 4 Å and 11 Å but after 1 ns the influence is limited only up to 6 Å.

In addition, nine short simulations for each dye molecule in their EX states were performed to obtain statistically relevant view of solvent relaxation process after probes excitation. In those simulations, the dyes were positioned at different depths in the membrane during excitation, as illustrated by arrows in Fig. 5. In contrast to the pure water, resulting relaxation times were on the nanosecond timescale. The relaxation time constants, observed over all 20 different Prodan and Laurdan excitations, are reported in Table 4 as the intervals indicating the ranges of appeared τ_i values. We were able

Table 3
Relaxation time constants (τ_i) with dyes in pure water box. Values correspond to local minima from Fig. 6.

	τ_1 [ps]	τ_2 [ps]	τ_3 [ps]
Prodan	0.03	0.34	3.20
Laurdan	0.03	0.10	1.00

Table 4
Ranges of relaxation time constants (τ_i) with dyes embedded into DOPC membrane model and gathered across multiple simulations. Please note nanosecond timescale in contrast to data shown in Table 3.

	τ_1 [ns]	τ_2 [ns]	τ_3 [ns]	τ_4 [ns]
Prodan	0.01–0.05	0.10–0.50	0.75–1.60	2.50–(more than 4.00)
Laurdan	0.01–0.05	0.16–0.60	1.25–2.50	3.00–(more than 6.00)

to find between two and four relaxation time constants τ_i for each initial configurations. The fastest rearrangement cycle occurs within the first 50 ps after excitation. Next relaxation cycle occurs during the first nanosecond. Others, much weaker, arise at later times. Relaxation times are longer for Laurdan than for Prodan, which also agrees with the experiment [21]. The results presented in this paper show that it is thus possible to retrieve kinetic parameters of solvent relaxation following excitation of fluorophore immersed in the lipid bilayer. The quantitative values calculated for two specific fluorophores, Prodan and Laurdan, match that obtained in solvent relaxation experiments, where the relaxation times constants are calculated by triple-exponential fitting fluorescent emission decays [73,74]. Moreover, a close view on the simulations reveals that the shortest time τ_1, may be attributed to the energy dissipation by rotation of water molecules. The following time τ_2 could be connected with water translation induced by dye dipole increasing upon excitation whereas the latest times (τ_3 and τ_4) are very likely determined by lipids reorganization causing subsequent impacts on water molecules. The hypothesis concerning longest times is supported by recent results of Sýkora et al. [74], showing that lipids packed in more bent vesicles, and having thus more mobile heads, exhibit faster relaxation than in large vesicles with smaller curvature.

Analysis of the changes of the amount of water around the fluorophore following excitation of dye molecules shows small difference between Prodan and Laurdan. Due to dye relocation toward surface, the number of water molecules at distance up to 5 Å from chromophore center slightly increases by 6 ± 4 for Prodan and by 9 ± 4 for Laurdan in studied cases. First hydration shell around Prodan contains thus up to 23 water molecules after dye excitation while around Laurdan there are only about 18 molecules. The overall Stokes shift $\Delta\nu$, resulting from analysis of fluorescent solvent relaxation experiment data corresponds to a polarity of a probe environment and can be directly related to the amount of water molecules involved in relaxation process. Sýkora et al. [21] have recently reported $\Delta\nu$ values equal to 3750 cm^{-1} and 3450 cm^{-1} for Prodan and Laurdan, respectively, using egg-phosphatidylcholine bilayer at ambient temperature. The higher $\Delta\nu$ value for Prodan indicates that its chromophore is in more polar surrounding, thus is surrounded by more water molecules than Laurdan, which is located deeper in the bilayer, and where less water molecules penetrate. This general tendency is also confirmed by our data.

4. Conclusions

The combination of quantum mechanical calculations (QM) and classical molecular dynamics simulations (MD) was used to characterize two fluorescent polarity sensitive probes, Prodan and Laurdan, in DOPC phospholipid membrane. A new MD protocol of dye molecules excitation was proposed for the first time. Our attempt allows extraction of important data for both ground and excited states, including impact on water and lipid molecules. Density functional theory (DFT) combined with its time dependent extension (TDDFT) enables to determine the necessary information about the chemical constitution and useful parameters for implementing MD simulations. A correct force field for the membrane fluorescent probes was thus defined for further use in MD simulations. We were able to observe passive diffusion of studied dyes from bulk water into DOPC lipid membrane. Presented statistics on dyes location along the membrane normal axis is of great importance for both experimental and theoretical studies. It reproduces the measured location of Laurdan [31] and supports the existing hypothesis of bimodal distribution of Prodan [30,32,33]. Moreover, the specific position shift toward more polar regions after excitation was observed. However, the experimental data obtained by fluorescent methods corresponds more to our results issued from the ground state than from the excited one. We suppose that marker responses during an experiment permit to uncover mostly the locations just after the excitation, still corresponding more to the ground state than for the well-established excited one. Instantaneous change of dye dipole moment, mimicking a femtosecond electronic excitation, gives also an important insight on solvent behavior. Our results show correct solvent relaxation timescales: picoseconds in pure water and nanoseconds in the headgroup region of phospholipid bilayer. We were able to observe up to four different relaxation time constants for the probes embedded into the membrane. The two shortest (τ_1 and τ_2) were associated to the rotation and translation of water molecules, respectively. The two longest time constants (τ_3 and τ_4) are very likely induced by lipids reorganization caused by previous changes in the interface hydration. The dye microenvironment mobility expressed by τ_i values could be hereby directly linked with physical phenomena occurring in measured systems. Obtained data are in excellent agreement with experimental results coming from solvent relaxation (SR) technique. In general, our computational methods allowed accessing directly typical SR parameters like relaxation time constants τ_i and shed some light on overall Stokes shift $\Delta\nu$ differences between both dyes.

Acknowledgments

Prof. Marek Langner is gratefully acknowledged for his critical reading of the manuscript. The calculations were carried out largely with the supercomputer facility at the Mésocentre a regional computational center at the University of Franche-Comté. The work was supported in part by Ministry of Education of the Czech Republic (JBK via LC06063) and Grant Agency of the Czech Republic (MH via 203/08/0114).

Appendix A. Supplementary data

Supplementary data associated with this article can be found, in the online version, at doi:10.1016/j.bbamem.2010.05.020.

References

[1] B. Baird, E.D. Sheets, D. Holowka, How does the plasma membrane participate in cellular signaling by receptors for immunoglobulin E? Biophys. Chem. 82 (1999) 109–119.
[2] D. English, Z. Welch, A.T. Kovala, K. Harvey, O.V. Volpert, D.N. Brindley, J.G.N. Garcia, Sphingosine 1-phosphate released from platelets during clotting accounts for the potent endothelial cell chemotactic activity of blood serum and provides a novel link between hemostasis and angiogenesis, FASEB J. 14 (2000) 2255–2265.
[3] F.T. Cooke, Phosphatidylinositol 3, 5-bisphosphate: metabolism and function, Arch. Biochem. Biophys. 407 (2002) 143–151.
[4] C. Luquain, V.A. Sciorra, A.J. Morris, Lysophosphatidic acid signaling: how a small lipid does big things, Trends Biochem. Sci. 28 (2003) 377–383.
[5] M. Langner, M. Przybylo, T. Borowik, A multi time-scale approach to biological systems—fluorescence studies, Pol. J. Environ. Stud. (2009).
[6] J.R. Lakowicz, Topics in Fluorescence Spectroscopy, Plenum Press, New York, 1992-2007.
[7] R. Hutterer, F.W. Schneider, H. Sprinz, M. Hof, Binding and relaxation behaviour of Prodan and Patman in phospholipid vesicles: a fluorescence and H-1 NMR study, Biophys. Chem. 61 (1996) 151–160.
[8] R. Hutterer, F.W. Schneider, W.T. Hermens, R. Wagenvoord, M. Hof, Binding of prothrombin and its fragment 1 to phospholipid membranes studied by the solvent relaxation technique, BBA-Biomembranes 1414 (1998) 155–164.
[9] A.P. Winiski, M. Eisenberg, M. Langner, S. McLaughlin, Fluorescent-probes of electrostatic potential 1-nm from the membrane-surface, Biochemistry-US 27 (1988) 386–392.

[10] M. Langner, D. Cafiso, S. Marcelja, S. McLaughlin, Electrostatics of phosphoinositide bilayer-membranes—theoretical and experimental results, Biophys. J. 57 (1990) 335–349.
[11] M. Langner, S.W. Hui, Dithionite penetration through phospholipid-bilayers as a measure of defects in lipid molecular packing, Chem. Phys. Lipids 65 (1993) 23–30.
[12] R. Hutterer, F.W. Schneider, M. Hof, Anisotropy and lifetime profiles for n-anthroyloxy fatty acids: A fluorescence method for the detection of bilayer interdigitation, Chem. Phys. Lipids 86 (1997) 51–64.
[13] B.W. Van der Meer, G. Cooker, S.Y.S. Chen, Resonance energy transfer theory and data, VCH Verlag, Weinheim, 1994.
[14] M. Langner, S.W. Hui, Merocyanine 540 as a fluorescence indicator for molecular packing stress at the onset of lamellar–hexagonal transition of phosphatidylethanolamine bilayers, BBA-Biomembranes 1415 (1999) 323–330.
[15] K. Kubica, M. Langner, J. Gabrielska, The dependence of Fluorescein-PE fluorescence intensity on lipid bilayer state. Evaluating the interaction between the probe and lipid molecules, Cell. Mol. Biol. Lett. 8 (2003) 943–954.
[16] C. Bernsdorff, A. Wolf, R. Winter, E. Gratton, Effect of hydrostatic pressure on water penetration and rotational dynamics in phospholipid-cholesterol bilayers, Biophys. J. 72 (1997) 1264–1277.
[17] G. Duportail, P. Lianos, Vesicles, Marcell Dekker, New York, 1996.
[18] R. Hutterer, A. Haefner, F.W. Schneider, M. Hof, Fluorescence microscopy and fluorescence probes, Plenum Press, New York, 1998.
[19] R. Hutterer, A.B.J. Parusel, M. Hof, Solvent relaxation of Prodan and Patman: a useful tool for the determination of polarity and rigidity changes in membranes, J. Fluoresc. 8 (1998) 389–393.
[20] R. Hutterer, M. Hof, Dynamics in diether lipid bilayers and interdigitated bilayer structures studied by time-resolved emission spectra, decay time and anisotropy profiles, J. Fluoresc. 11 (2001) 227–236.
[21] J. Sykora, P. Kapusta, V. Fidler, M. Hof, On what time scale does solvent relaxation in phospholipid bilayers happen? Langmuir 18 (2002) 571–574.
[22] P. Jurkiewicz, J. Sykora, A. Olzynska, J. Humpolickova, M. Hof, Solvent relaxation in phospholipid bilayers: principles and recent applications, J. Fluoresc. 15 (2005) 883–894.
[23] A. Sommer, F. Paltauf, A. Hermetter, Dipolar solvent relaxation on a nanosecond time scale in ether phospholipid-membranes as determined by multifrequency phase and modulation fluorometry, Biochemistry 29 (1990) 11134–11140.
[24] T. Parasassi, G. Destasio, A. Dubaldo, E. Gratton, Phase fluctuation in phospholipid-membranes revealed by Laurdan fluorescence, Biophys. J. 57 (1990) 1179–1186.
[25] S. Mukherjee, A. Chattopadhyay, Wavelength-selective fluorescence as a novel tool to study organization and dynamics in complex biological systems, J. Fluoresc. 5 (1995) 237–246.
[26] A. Chattopadhyay, Exploring membrane organization and dynamics by the wavelength-selective fluorescence approach, Chem. Phys. Lipids 122 (2003) 3–17.
[27] J. Sykora, P. Slavicek, P. Jungwirth, J. Barucha, M. Hof, Time-dependent stokes shifts of fluorescent dyes in the hydrophobic backbone region of a phospholipid bilayer: combination of fluorescence spectroscopy and ab initio calculations, J. Phys. Chem. B 111 (2007) 5869–5877.
[28] G. Weber, F.J. Farris, Synthesis and spectral properties of a hydrophobic fluorescent-probe - 6-propionyl-2-(dimethylamino)naphthalene, Biochemistry-US 18 (1979) 3075–3078.
[29] R.B. MacGregor, G. Weber, Fluorophores in polar media: spectral effects of the Langevin distribution of electrostatic interactions, Ann.N.Y.Acad.Sci. 366 (1981) 140.
[30] F. Moyano, M.A. Biasutti, J.J. Silber, N.M. Correa, New insights on the behavior of Prodan in homogeneous media and in large unilamellar vesicles, J. Phys. Chem. B 110 (2006) 11838–11846.
[31] P. Jurkiewicz, A. Olzynska, M. Langner, M. Hof, Headgroup hydration and mobility of DOTAP/DOPC bilayers: a fluorescence solvent relaxation study, Langmuir 22 (2006) 8741–8749.
[32] P.L.G. Chong, Effects of hydrostatic-pressure on the location of Prodan in lipid bilayers and cellular membranes, Biochemistry-US 27 (1988) 399–404.
[33] T. Parasassi, E.K. Krasnowska, L. Bagatolli, E. Gratton, Laurdan and Prodan as polarity-sensitive fluorescent membrane probes, J. Fluoresc. 8 (1998) 365–373.
[34] A. Chattopadhyay, E. London, Parallax method for direct measurement of membrane penetration depth utilizing fluorescence quenching by spin-labeled phospholipids, Biochemistry 26 (1987) 39–45.
[35] K.A. Kozyra, J.R. Heldt, M. Engelke, H.A. Diehl, Phase transition affects energy transfer efficiency in phospholipid vesicles, Spectrochim. Acta A 61 (2005) 1153–1161.
[36] U.F. Rohrig, I. Frank, J. Hutter, A. Laio, J. VandeVondele, U. Rothlisberger, QM/MM Car-Parrinello molecular dynamics study of the solvent effects on the ground state and on the first excited singlet state of acetone in water, Chemphyschem 4 (2003) 1177–1182.
[37] V.Y. Artukhov, O.M. Zharkova, J.P. Morozova, Features of absorption and fluorescence spectra of prodan, Spectrochim. Acta A 68 (2007) 36–42.
[38] B. Mennucci, M. Caricato, F. Ingrosso, C. Cappelli, R. Cammi, J. Tomasi, G. Scalmani, M.J. Frisch, How the environment controls absorption and fluorescence spectra of Prodan: a quantum-mechanical study in homogeneous and heterogeneous media, J. Phys. Chem. B 112 (2008) 414–423.
[39] A.B.J. Parusel, F.W. Schneider, G. Kohler, An ab initio study on excited and ground state properties of the organic fluorescence probe Prodan, J. Mol. Struc. Theochem. 398 (1997) 341–346.
[40] A. Parusel, Semiempirical studies of solvent effects on the intramolecular charge transfer of the fluorescence probe Prodan, J. Chem. Soc. Faraday T 94 (1998) 2923–2927.
[41] A.B.J. Parusel, W. Nowak, S. Grimme, G. Kohler, Comparative theoretical study on charge-transfer fluorescence probes: 6-propanoyl-2-(*N*, *N*-dimethylamino)naphthalene and derivatives, J. Phys. Chem. A 102 (1998) 7149–7156.
[42] A.B.J. Parusel, R. Schamschule, G. Kohler, Nonlinear optics. A semiempirical study of organic chromophores, J. Mol. Struc. Theochem. 544 (2001) 253–261.
[43] Y.P. Morozova, O.M. Zharkova, T.Y. Balakina, V.Y. Artyukhov, Effect of proton-donor solvent and structural flexibility of prodan and laurdan molecules on their spectral-luminescent properties, J. App. Spectrosc. 76 (2009) 312–318.
[44] N.A. Nemkovich, W. Baumann, Molecular Stark-effect spectroscopy of Prodan and Laurdan in different solvents and electric dipole moments in their equilibrated ground and Franck–Condon excited state, J. Photoch. Photobio. A 185 (2007) 26–31.
[45] A. Samanta, R.W. Fessenden, Excited state dipole moment of Prodan as determined from transient dielectric loss measurements, J. Phys. Chem. A 104 (2000) 8972–8975.
[46] B.C. Lobo, C.J. Abelt, Does Prodan possess a planar or twisted charge-transfer excited state? Photophysical properties of two Prodan derivatives, J. Phys. Chem. A 107 (2003) 10938–10943.
[47] M. Novaira, M.A. Biasutti, J.J. Silber, N.M. Correa, New insights on the photophysical behavior of Prodan in anionic and cationic reverse micelles: from which state or states does it emit? J. Phys. Chem. B 111 (2007) 748–759.
[48] M.J. Frisch, G.W. Trucks, H.B. Schlegel, G.E. Scuseria, M.A. Robb, J.R. Cheeseman, J. Montgomery, J. A., T. Vreven, K.N. Kudin, J.C. Burant, J.M. Millam, S.S. Iyengar, J. Tomasi, V. Barone, B. Mennucci, M. Cossi, G. Scalmani, N. Rega, G.A. Petersson, H. Nakatsuji, M. Hada, M. Ehara, K. Toyota, R. Fukuda, J. Hasegawa, M. Ishida, T. Nakajima, Y. Honda, O. Kitao, H. Nakai, M. Klene, X. Li, J.E. Knox, H.P. Hratchian, J.B. Cross, V. Bakken, C. Adamo, J. Jaramillo, R. Gomperts, R.E. Stratmann, O. Yazyev, A.J. Austin, R. Cammi, C. Pomelli, J.W. Ochterski, P.Y. Ayala, K. Morokuma, G.A. Voth, P. Salvador, J.J. Dannenberg, V.G. Zakrzewski, S. Dapprich, A.D. Daniels, M.C. Strain, O. Farkas, D.K. Malick, A.D. Rabuck, K. Raghavachari, J.B. Foresman, J.V. Ortiz, Q. Cui, A.G. Baboul, S. Clifford, J. Cioslowski, B.B. Stefanov, G. Liu, A. Liashenko, P. Piskorz, I. Komaromi, R.L. Martin, D.J. Fox, T. Keith, M.A. Al-Laham, C.Y. Peng, A. Nanayakkara, M. Challacombe, P.M.W. Gill, B. Johnson, W. Chen, M.W. Wong, C. Gonzalez, J.A. Pople, I. Gaussian, Gaussian 03, Revision C.02, in, Wallingford CT, 2004.
[49] P. Hohenberg, W. Kohn, Inhomogeneous electron gas, Phys. Rev. B 136 (1964) B864.
[50] W. Kohn, L.J. Sham, Self-consistent equations including exchange and correlation effects, Phys. Rev. 140 (1965) 1133.
[51] P. Ilich, F.G. Prendergast, Singlet adiabatic states of solvated Prodan—a semiempirical molecular-orbital study, J. Phys. Chem.-US 93 (1989) 4441–4447.
[52] R.E. Stratmann, G.E. Scuseria, M.J. Frisch, An efficient implementation of time-dependent density-functional theory for the calculation of excitation energies of large molecules, J. Chem. Phys. 109 (1998) 8218–8224.
[53] R. Bauernschmitt, R. Ahlrichs, Treatment of electronic excitations within the adiabatic approximation of time dependent density functional theory, Chem. Phys. Lett. 256 (1996) 454–464.
[54] M.E. Casida, C. Jamorski, K.C. Casida, D.R. Salahub, Molecular excitation energies to high-lying bound states from time-dependent density-functional response theory: characterization and correction of the time-dependent local density approximation ionization threshold, J. Chem. Phys. 108 (1998) 4439–4449.
[55] E. Cances, B. Mennucci, J. Tomasi, A new integral equation formalism for the polarizable continuum model: theoretical background and applications to isotropic and anisotropic dielectrics, J. Chem. Phys. 107 (1997) 3032–3041.
[56] B. Mennucci, E. Cances, J. Tomasi, Evaluation of solvent effects in isotropic and anisotropic dielectrics and in ionic solutions with a unified integral equation method: theoretical bases, computational implementation, and numerical applications, J. Phys. Chem. B 101 (1997) 10506–10517.
[57] J. Tomasi, B. Mennucci, E. Cances, The IEF version of the PCM solvation method: an overview of a new method addressed to study molecular solutes at the QM ab initio level, J. Mol. Struc. Theochem. 464 (1999) 211–226.
[58] B. Mennucci, J. Tomasi, Continuum solvation models: a new approach to the problem of solute's charge distribution and cavity boundaries, J. Chem. Phys. 106 (1997) 5151–5158.
[59] B.R. Brooks, R.E. Bruccoleri, B.D. Olafson, D.J. States, S. Swaminathan, M. Karplus, CHARMM: a program for macromolecular energy, minimizations, and dynamics calculations, J. Comp. Chem. 4 (1983) 187–217.
[60] E. Lindahl, B. Hess, D. van der Spoel, GROMACS 3.0: a package for molecular simulation and trajectory analysis, J. Mol. Model. 7 (2001) 306–317.
[61] D.A. Case, T.A. Darden, T.E. Cheatham III, C.L. Simmerling, J. Wang, R.E. Duke, R. Luo, K.M. Merz, B. Wang, D.A. Pearlman, M. Crowley, S. Brozell, V. Tsui, H. Gohlke, J. Mongan, V. Hornak, G. Cui, P. Beroza, C. Schafmeister, J.W. Caldwell, W.S. Ross, P.A. Kollman, AMBER 8, University of California, San Francisco, 2004.
[62] J.C. Phillips, R. Braun, W. Wang, J. Gumbart, E. Tajkhorshid, E. Villa, C. Chipot, R.D. Skeel, L. Kale, K. Schulten, Scalable molecular dynamics with NAMD, J. Comput. Chem. 26 (2005) 1781–1802.
[63] W. Humphrey, A. Dalke, K. Schulten, VMD—visual molecular dynamics, J. Molec. Graphics 14 (1996) 33–38.
[64] A.D. MacKerell, D. Bashford, M. Bellott, R.L. Dunbrack, J.D. Evanseck, M.J. Field, S. Fischer, J. Gao, H. Guo, S. Ha, D. Joseph-McCarthy, L. Kuchnir, K. Kuczera, F.T.K. Lau, C. Mattos, S. Michnick, T. Ngo, D.T. Nguyen, B. Prodhom, W.E. Reiher, B. Roux, M. Schlenkrich, J.C. Smith, R. Stote, J. Straub, M. Watanabe, J. Wiorkiewicz-Kuczera, D. Yin, M. Karplus, All-atom empirical potential for molecular modeling and dynamics studies of proteins, J. Phys. Chem. B 102 (1998) 3586–3616.
[65] W.L. Jorgensen, J. Chandrasekhar, J.D. Madura, R.W. Impey, M.L. Klein, Comparison of simple potential functions for simulating liquid water, J. Chem. Phys. 79 (1983) 926–935.
[66] S.E. Feller, Y.H. Zhang, R.W. Pastor, B.R. Brooks, Constant-pressure molecular-dynamics simulation—the Langevin piston method, J. Chem. Phys. 103 (1995) 4613–4621.
[67] T. Darden, D. York, L. Pedersen, Particle mesh Ewald: an N.log(N) method for Ewald sums in large systems, J. Chem. Phys. 98 (1993) 10089–10092.

[68] J. Catalan, P. Perez, L. J., B. G.F., Analysis of the solvent effect on the photophysics properties of 6-propionyl-2-(dimethylamino)naphthalene (PRODAN), J. Fluoresc. 1 (1991) 215–223.
[69] C.E. Bunker, T.L. Bowen, Y.P. Sun, A photophysical study of solvatochromic probe 6-propionyl-2-(n, n-dimethylamino)naphthalene (Prodan) in solution, Photochem. Photobiol. 58 (1993) 499–505.
[70] R. Jimenez, G.R. Fleming, P.V. Kumar, M. Maroncelli, Femtosecond solvation dynamics of water, Nature 369 (1994) 471–473.
[71] M. Maroncelli, G.R. Fleming, Computer-simulation of the dynamics of aqueous solvation, J. Chem. Phys. 89 (1988) 5044–5069.
[72] M. Maroncelli, Computer-simulations of solvation dynamics in acetonitrile, J. Chem. Phys. 94 (1991) 2084–2103.
[73] R. Sachl, M. Stepanek, K. Prochazka, J. Humpolickova, M. Hof, Fluorescence study of the solvation of fluorescent probes prodan and laurdan in poly(epsilon-caprolactone)-block-poly(ethylene oxide) vesicles in aqueous solutions with tetrahydrofurane, Langmuir 24 (2008) 288–295.
[74] J. Sykora, P. Jurkiewicz, R.M. Epand, R. Kraayenhof, M. Langner, M. Hof, Influence of the curvature on the water structure in the headgroup region of phospholipid bilayer studied by the solvent relaxation technique, Chem. Phys. Lipids 135 (2005) 213–221.

4 C-Laurdan – New Probe for Solvent Relaxation? – Numerical Studies in the Model of Lipid Membrane

Laurdan is a fluorescent probe widely used for various fluorescent techniques (see Figure III.17a). It was already shown that it is very sensitive to the polarity of the membrane. However, it has been shown recently that Laurdan does not accurately reflect the fluid and gel domains (rafts) in the plasma membranes by generalized polarization images (GP) of the cells [158]. Therefore, the introduction of a carboxylic group to Laurdan has been recently proposed by Kim et al. [74]. The presence of a carboxylic acid moiety in the Laurdan molecule improves the water solubility of the dye molecule. It should also cause a higher sensitivity to the membrane polarity and prevent the formation of aggregates of the dyes. There are not so many experiments with C-laurdan to date.

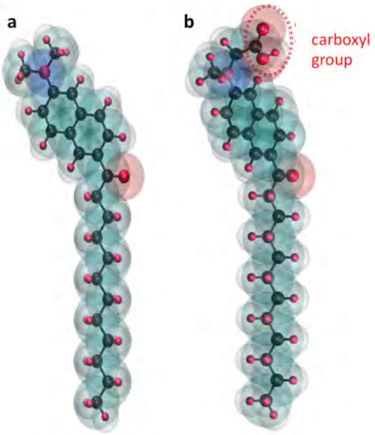

Figure III.17 Ball and sticks molecular structures of Laurdan (a) and C-laurdan (b). Transparent blue part is the dimethylamino electron-donating group and the transparent red subunit corresponds to the carbonyl electron acceptor.

C-laurdan (6-dodecanoyl-2-[*N*-methyl-*N*-(carboxymethyl)amino]naphthalene) (see Figure III.17b) has a solubility in water of 30 μM, whereas Laurdan is insoluble in water and produces aggregates at 0.1 μM [74]. The higher sensitivity to the solvent polarity of C-laurdan was confirmed in the bathochromic shifts with solvent polarity: C-Hex < DMF < EtOH < H_2O [74]. The emission spectra of C-laurdan in lipid vesicles show maximum of fluorescence at wavelength 442 nm for DPPC and 486 nm for DOPC.

C-laurdan is believed to be located at the headgroup region of lipid bilayer. In both gel and fluid phases, it is assumed to be aligned parallel to the lipid molecules. Its position is stabilized by hydrophilic interactions between its carboxylic groups and water molecules at the headgroup region of lipid bilayer.

All of the experimental properties of this new Laurdan derivative described above suggest its use in the solvent relaxation technique as a very sensitive indicator of the headgroup polarity of lipid bilayer. Solvent relaxation experiments require a precise knowledge of where the fluorescent signal comes from. Therefore, the question about the exact location of C-Laurdan probe in the membrane must be answered.

Since our previous work [13] on Prodan and Laurdan was convincing and correct, we decided to use the same protocol for C-laurdan. In this study, quantum mechanical (QM) calculations were performed to obtain the correct model of C-laurdan in the ground and excited states. Again, the parameters extracted from QM calculations were used for the construction of a force field for molecular dynamics (MD) simulations. MD simulations of C-Laurdan were performed in the fully hydrated model of DOPC lipid bilayer in the ground and excited states.

4.1 Quantum Mechanics Calculations

Based on our knowledge and corrected results of our previous simulations performed for Prodan and Laurdan [13], QM calculations were executed in the same way for C-laurdan molecule. The calculations show that the electronic structures (charge distribution) obtained for the excited state (S_1) is completely different from S_0 geometries. Table III-7 summarize the values obtained for C-laurdan.

	elementary charge [e]		**μ [D]**
	nitrogen	oxygen	
S_0	0.027741	- 0.397125	4.67
S_1	0.343232	- 0.391293	11.04

Table III-7 Partial charges and dipole moments (μ) calculated for ground (S_0) and excited (S_1) states of C-laurdan.

The dipole moments for ground and excited states were calculated from the Mulliken charges distribution. In the excited state, the dipole is more than twice the one in the ground state. They are comparable with the previous values obtained for Laurdan molecule.

4.2 Molecular Dynamics Simulations

4.2.1 Location of the Dye in the Ground and Excited States in Lipid Bilayer

From our previous calculations on Prodan and Laurdan (see III3.2.1) and from literature [72], it is well known that Laurdan easily incorporates into the lipid bilayer. To check, if a more hydrophilic Laurdan derivative also shows similar behavior, C-laurdan molecule in the ground state was initially placed in bulk water far from a fully hydrated model of DOPC membrane (see Figure III.18). As expected, the dye molecule incorporated very easily into the membrane core. It needs more time (~40 ns) than Laurdan (< 10 ns, see Figure III.19) to enter into the membrane.

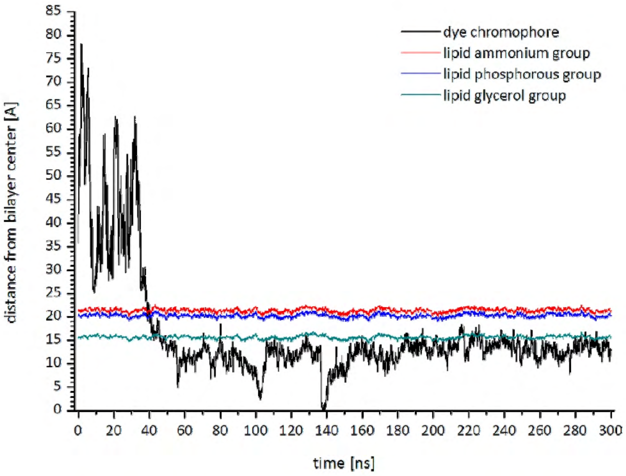

Figure III.18 C-laurdan chromophore position in the ground state (black curve) as a function of time of unconstrained MD simulation. The positions of ammonium (red curve), phosphorous (blue curve) and glycerol (green curve) of DOPC membrane are also plotted.

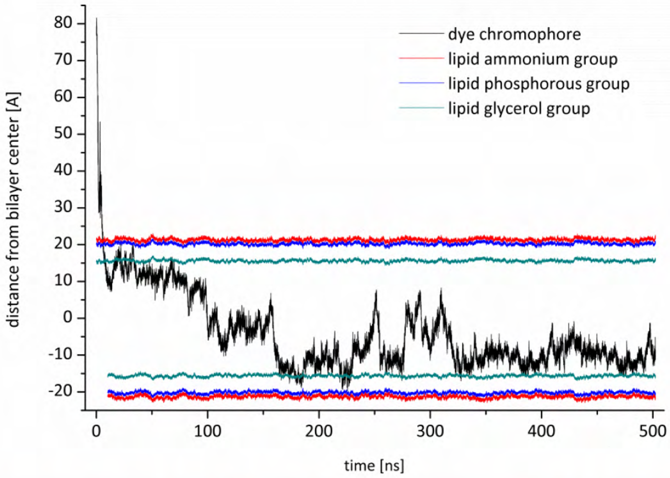

Figure III.19 Laurdan chromophore position in the ground state (black curve) as a function of time of unconstrained MD simulation. The positions of ammonium (red curve), phosphorous (blue curve) and glycerol (green curve) of DOPC membrane are also plotted.

After incorporation, C-laurdan remains within the lipid bilayer for the rest of 300 ns simulation time. The dye chromophore is found at the headgroup region of the lipid membrane and their hydrocarbon chain inserted between hydrocarbon tails of lipids.

We decided to prolong the simulations of Laurdan in the ground state to reach the time value similar to one of C-Laurdan (~300 ns). Laurdan's behavior forced us to add next 200 ns to this simulation up 500 ns. Surprisingly, we observed one particular Laurdan movement from one bilayer leaflet to another (flip-flop). Laurdan is probably able to overcome the barrier of hydrophobic tails.

Kim et al. [74] suggested that C-laurdan is aligned more parallel to the lipid molecules than Laurdan because of its hydrophilic interaction between the carboxyl group with water molecules presented at the interface region of bilayer. We have also verified this feature.

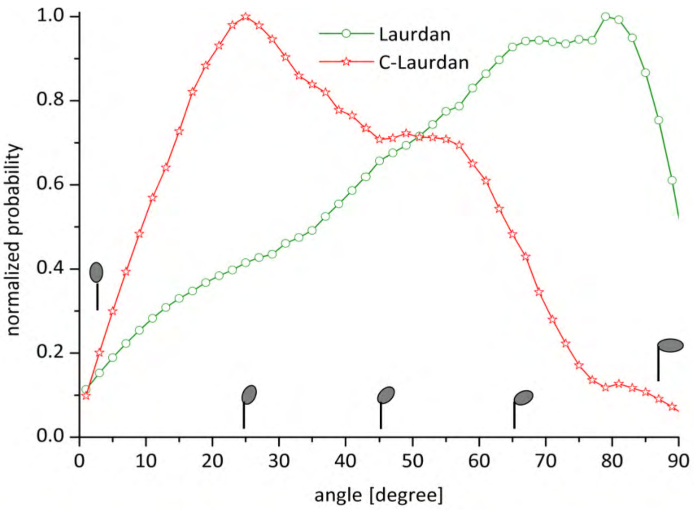

Figure III.20 The angle of Laurdan (–○–) and C-laurdan (–★–) chromophores relative to the normal axis of DOPC bilayer.

It is clearly visible in Figure III.20 that Laurdan is oriented more perpendicularly to the normal axis of the bilayer. The addition the hydrophilic group to the Laurdan molecule drastically changes the orientation of the dye chromophore. C-laurdan is found oriented more parallel to the lipids.

The positions of Laurdan and C-laurdan in the bilayer were calculated from the histograms (see Figure III.21) using a Gaussian fit. Histograms collect the data from 100 ns simulations for Laurdan in both ground and excited states and 300 and 280 ns for C-laurdan in ground and excited states, respectively.

Position calculated for excited state from such long simulations cannot be correct, since fluorescent probe has relatively short lifetime (~4 ns) and dye does not have enough time to equilibrate after excitation. Effective excited position is thus proposed as a solution of this inconsistency.

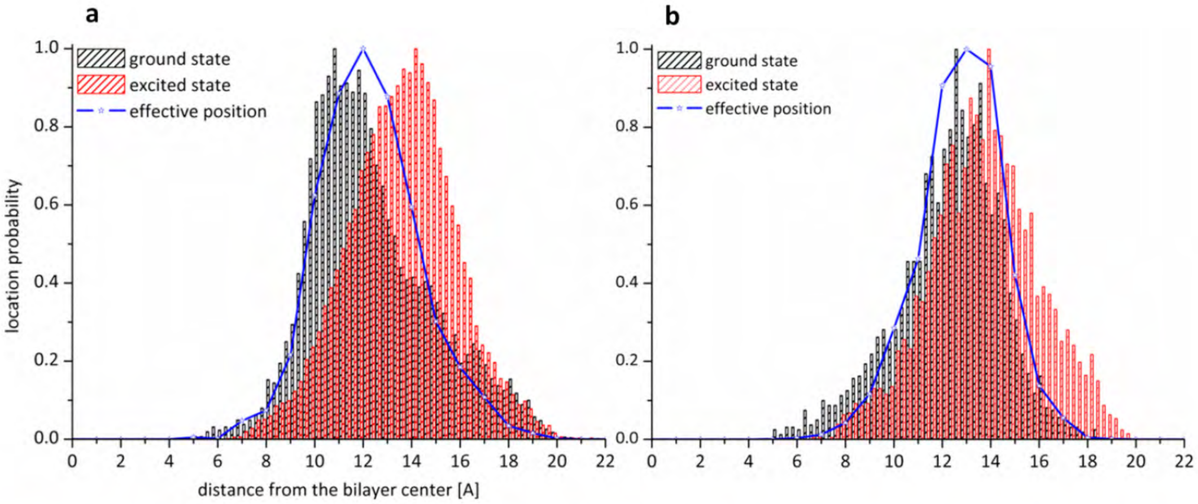

Figure III.21 Histogram of chromophore center of Laurdan (a) and C-Laurdan (b) molecules in their ground (gray plot) and excited (red plot) states during performed MD simulations. Effective excitation position is marked by blue-stars line. Positions are shown as the distance from the bilayer center.

To retrieve the location probability of the dyes in the membrane during their excited state more than one simulation for each particular position is needed. Basing on presented histograms calculated for the ground state (see Figure III.21 (grey plot)) one need to perform as many short (6 ns) simulations in the excited state as exist different initial locations. We propose here to fit the number of these excitations accordingly to the location probability shown in Figure III.21 (grey plot). We decided to perform five runs for the most probable location, which is the absolute minimum from the statistical point of view.

For less probable locations we decreased this number of MD runs gradually and accordingly to the location probability histogram (see Figure III.21) getting for instance for Laurdan only one MD run in excited state with initial location at 8 Å, 16 Å and 17 Å from bilayer center, two MD runs at 15 Å, three MD runs at 9 Å and 14 Å, five MD runs at 10 Å and 13 Å, and six MD runs at 11 Å and 12 Å, respectively. For C-Laurdan we performed one MD run in excited state for chromophore location at 9 Å and 16 Å from bilayer center, two MD runs for initial location at 10 Å, three MD runs at 11 Å and 15 Å, four MD runs at 12 Å and 14 Å, and five MD runs at 13 Å, respectively. Every single initial configuration in the ground state of studied systems was excited by the changing of the charges distribution description from ground state to excited at time "zero" (t=0). Obtained positions of the dyes behavior just after electronic excitation were next weighted by the corresponding fluorescent decay. Decreasing the calculated location probability after excitation over the time in the range of possible excitation lifetime give us more appropriate estimation of marker delocalization after excitation than we recently proposed basing on long time one-molecule MD run [13]. The results are summarized in Figure III.21 (histograms and effective positions (blue curve)) and Table III-8.

Laurdan			**C-laurdan**		
S_0	**EFF**	**S_1**	**S_0**	**EFF**	**S_1**
10.8±1.4 <0.95>		12.8±2.0 <0.85>	12.1±1.3 <0.89>		12.1±1.6 <0.84>
11.9±1.3 <1.0>	12.0±2.1 <0.99>	14.2±1.9<1.0>	14.1±1.2 <1.0>	13.0±1.8 <0.99>	14.1±1.5 <1.0>
	weighted mean			weighted mean	
11.4	12.0	13.6	13.1	13.0	13.2

Table III-8 Dyes location in DOPC bilayer. Distances (in Ångstroms) from the bilayer center, obtained by Gaussian deconvolution of data shown in Figure III.21, are reported with calculated normalized amplitudes of peaks (indicated by <>).

For both dye, two mean positions in ground and excited states were found (see Table III-8) with a significant probability. C-laurdan in ground state (S_0) is located at 13.1 Å about 1.5 Å more outside in the bilayer than Laurdan (11.4 Å). In the excited state (S_1), the positions of Laurdan and C-Laurdan, calculated from long simulations, are almost the same. The effective position for Laurdan shows small shift to the more polar region of lipid bilayer (0.6 Å). Values, obtained for C-Laurdan, in the ground and excited state (effective position) are the same, what means that C-laurdan is stable in the membrane during the excitation process. The effective position of C-Laurdan is determined 1 Å more outside in the membrane then Laurdan. C-laurdan in the ground state is located 1.7 Å more outside from the bilayer center than Laurdan.

4.2.2 Dye Dynamics in the Excited State

The changes of the dye positions after excitation can be followed with time after few nanoseconds of excitation. All simulations of Laurdan and C-Laurdan (which were used for determining the effective position) were collected for visualization of the dye position after excitation. Results are presented in Figure III.22 (map of the dye locations as a function of the time after excitation for all initial configurations). The retrieve of the location probability of the dye in the membrane cause the observation of the series of the dyes. Figure III.23 shows the location of the group of probes from which the fluorescent signal comes after excitation. Laurdan (see Fig III.23 left inset) molecules change their position in the bilayer after excitation, but this movement is not as dramatic as it was shown in previous analysis (see Chapter III3.2.1, Figure III.12) [13]. The position of C-laurdan (see Figure III.23 right inset) is thus more stable after excitation than Laurdan position.

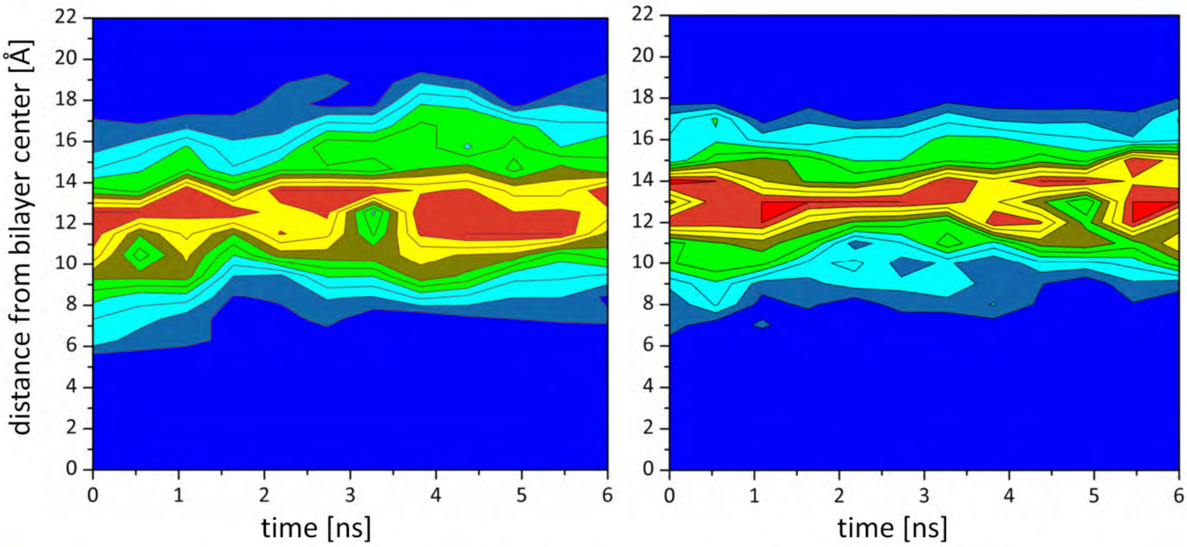

Figure III.22 Location changes of Laurdan (left plot) and C-laurdan (right plot) molecules after excitation. Result is plotted as a function of time (x-axis) and distance from the bilayer center (y-axis). The unoccupied locations are coloured blue whereas the most occupied are represented by red colour.

4.2.3 Water Dynamics after Dye Excitation

The solvent relaxation (SR) process is directly linked to the presence of polar solution around the dye molecule. For this reason, the water dipole moment reorganization after dye's dipole moment changing was investigated in a similar way as during a fluorescence SR experiment. At is was mentioned previously, the most important parameter obtained from SR technique is the integral relaxation time τ which describes the solvent mobility in the dye surrounding. Relaxation time measured in pure water is around 0.3 ps [71]. The interactions of water-lipid in the bilayer cause a slowdown of relaxation response in the membrane to few nanoseconds [70]. The study of water behavior around C-laurdan in fully-hydrated lipid bilayer were done for C-laurdan molecules which were initially located at 13 depths of bilayer as it was described in Chapter III4.2.2. Data presented in this chapter are chosen for the most representative and probable positions of C-laurdan: 9, 12, 13, 14, and 17 Å from bilayer center.

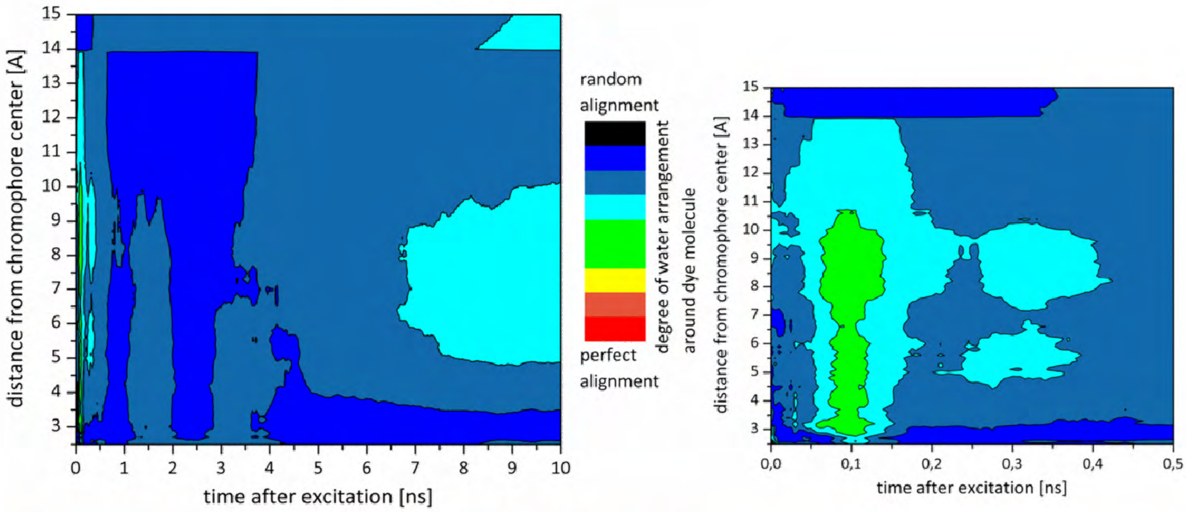

Figure III.23 Changes of water dynamics around C-laurdan molecule embedded into lipid membrane. Initial position of C-laurdan was chosen at the depth of 9Å from bilayer center. Maps were plotted as a function of time (x-axis) and distance from chromophore center (y-axis). Blue areas indicate the lack of the water organization, green and yellow regions a progressive arrangement, while red zones correspond to the most organized water molecules vs. dye dipole vector. Please note different scales between insets. Map on the right shows zoomed part of the map on the left.

Water molecules in the environment of C-laurdan, which was initially placed at position 9 Å, react on the excitation process really fast. The first water reorganization is detected 0.15 ns after excitation and takes place at the distance to 15 Å from the chromophore. Second water reaction is noted at 0.3-0.4 ns from the excitation and its range is limited to 10 Å from the chromophore (see Figure III.23 right inset). Third water rearrangement starts 7 ns after excitation and is longer than 10 ns (see Figure III.23 left inset).

For C-laurdan molecule, initially placed at the distance 12 Å from bilayer center, the first water reorganization is observed at a time shorter than 0.05 ns and has a range to 9 Å from the chromophore center (see Figure III.24 right inset). The second water rearrangement takes place at a distance from 4 Å to 10 Å from the bilayer center. It starts 1 ns after excitation and disappears after 4.5 ns (see Figure III.24 left inset). Third water perturbation is observed between 8 and 10 ns after excitation and takes place at a distance from 6-1 0Å from the center of chromophore (see Figure III.24 left inset).

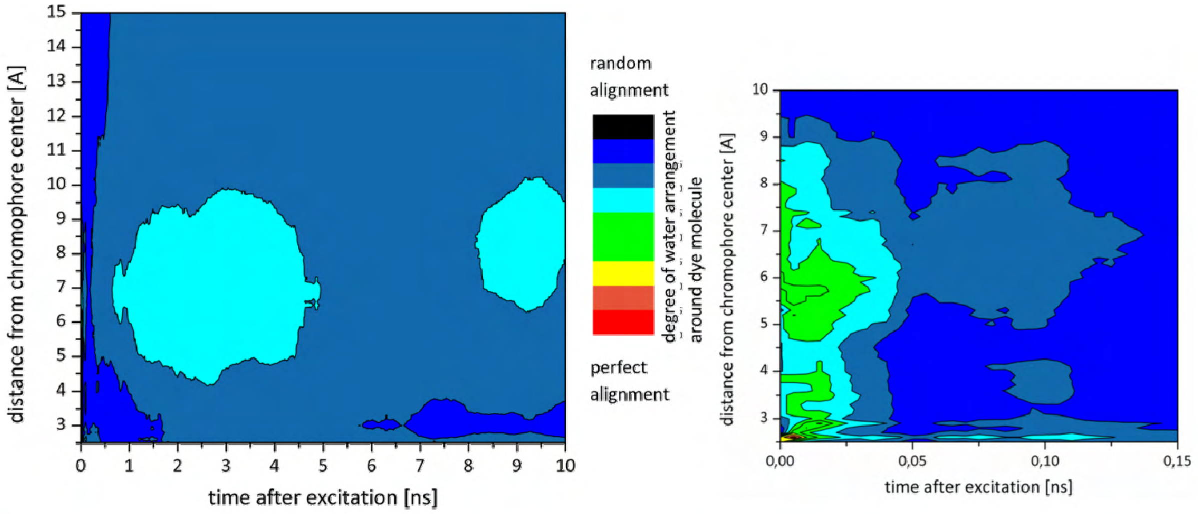

Figure III.24 Changes of water dynamics around C-laurdan molecule embedded into lipid membrane. Initial position of C-laurdan was chosen at the depth of 12Å from bilayer center. Maps were plotted as a function of time (x-axis) and distance from chromophore center (y-axis). Blue areas indicate the lack of the water organization, green and yellow regions a progressive arrangement, while red zones correspond to the most organized water molecules vs. dye dipole vector. Please note different scales between insets. Map on the right shows zoomed part of the map on the left.

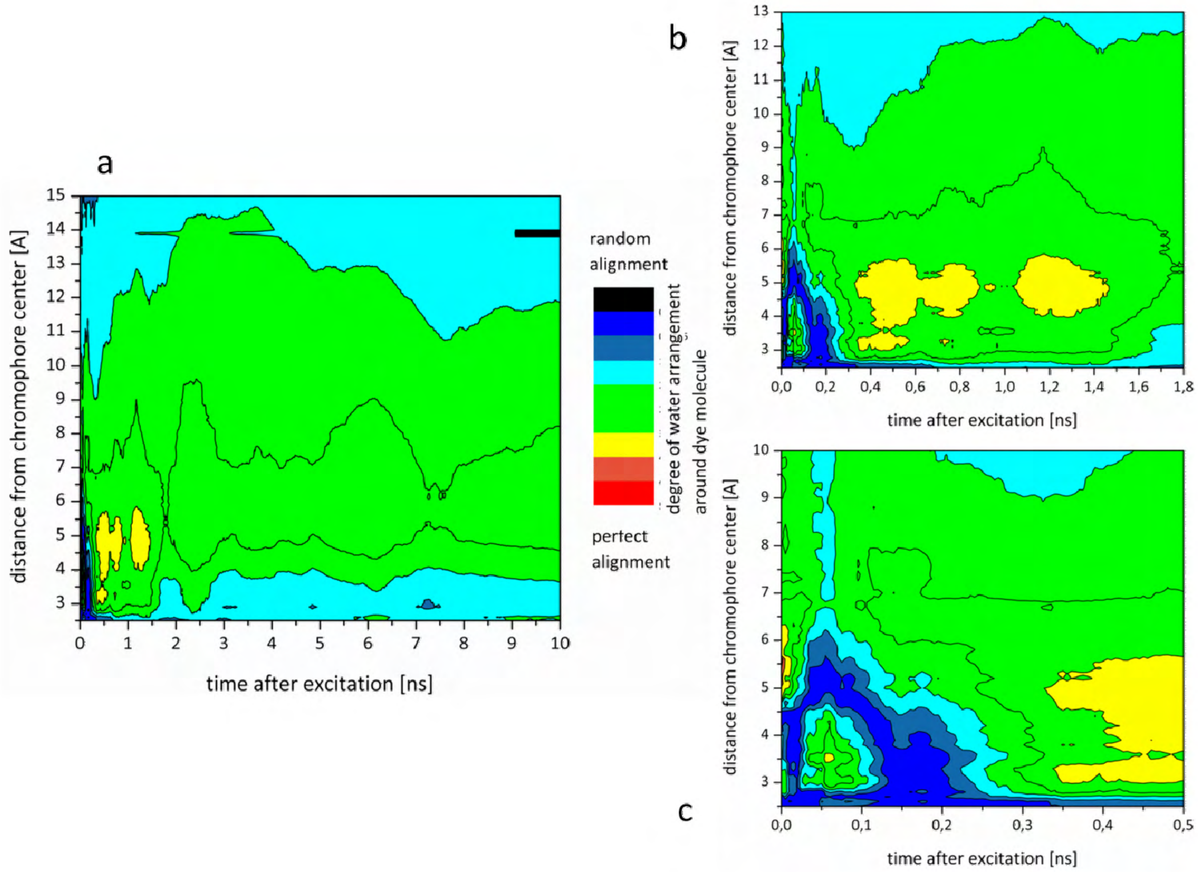

Figure III.25 Changes of water dynamics around C-laurdan molecule embedded into lipid membrane. Initial position of C-laurdan was chosen at the depth of 13Å from bilayer center. Maps were plotted as a function of time (x-axis) and distance from chromophore center (y-axis). Blue areas indicate the lack of the water organization, green and yellow regions a progressive arrangement, while red zones correspond to the most organized water molecules vs. dye dipole vector. Please note different scales between insets. Maps (b) and (c) show zoomed part of the map (a).

The most probable position of C-laurdan in bilayer was calculated near 13 Å from bilayer center. The water behavior, around the dye located at this level, after excitation is presented in Figure III.25. The impact of the dye dipole changes after the excitation perturbed water molecules very extensively, up to 10 ns after excitation, over the distance more than 15 Å from the chromophore center (see Figure III.25a). First water rearrangement was found 10 ps after excitation (see Figure III.25c). Second and third reorganization are detected around 0.35 – 0.85 ns and 1.1 – 1.5 ns after excitation (see Figure III.25b).

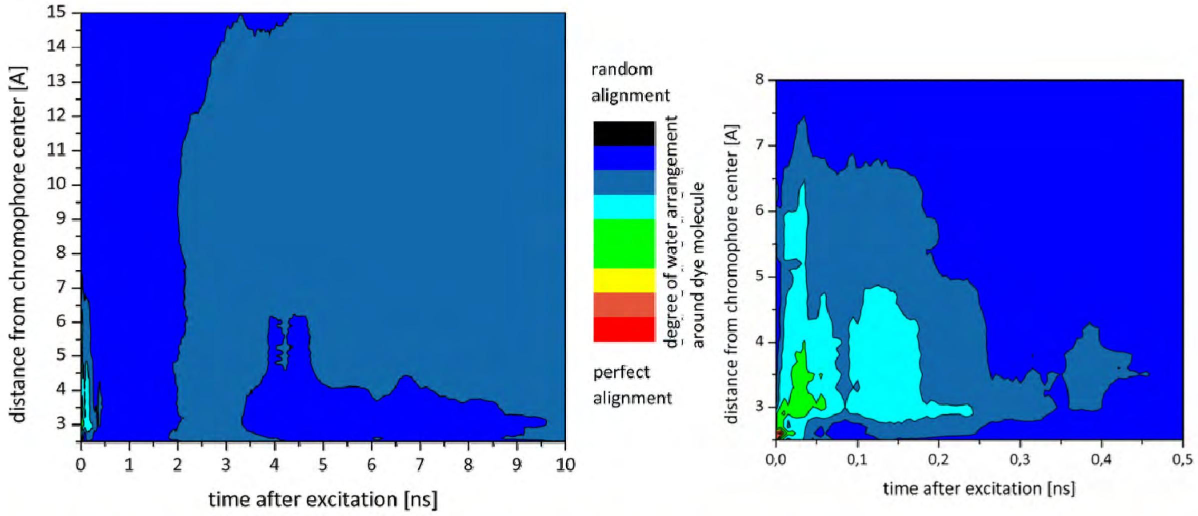

Figure III.26 Changes of water dynamics around C-laurdan molecule embedded into lipid membrane. Initial position of C-laurdan was chosen at the depth of 14Å from bilayer center. Maps were plotted as a function of time (x-axis) and distance from chromophore center (y-axis). Blue areas indicate the lack of the water organization, green and yellow regions a progressive arrangement, while red zones correspond to the most organized water molecules vs. dye dipole vector. Please note different scales between insets. Map on the right shows zoomed part of the map on the left.

Two short water relaxation changes were observed for C-laurdan initially located at 14 Å from the bilayer center (see Figure III.26). The first takes place at the distance to 6.5 Å from chromophore center and second to 5 Å. The strongest water reaction is noted 10 ps after excitation and second, weaker, 10-20 ps after excitation (see Figure III.26 right).

C-laurdan, which is initially located 17 Å from bilayer center, has contact with free water molecules, which are present at the interface region of lipid bilayer. Water perturbation is observed at distances up to 12 Å from the chromophore center and water reorganization takes time longer than 10 ns (see Figure III.27a). First water response is detected up to 3 ps after excitation and has a range greater than 7 Å from chromophore (see Figure III.27c). Two next water rearrangements are observed 0.15 – 0.25 ns and around 0.4 ns after excitation (see Figure III.27b). Fourth water reorganization is observed between 1.5 - 2 ns after excitation and is unfinished up to 10 ns (see Figure III.27a).

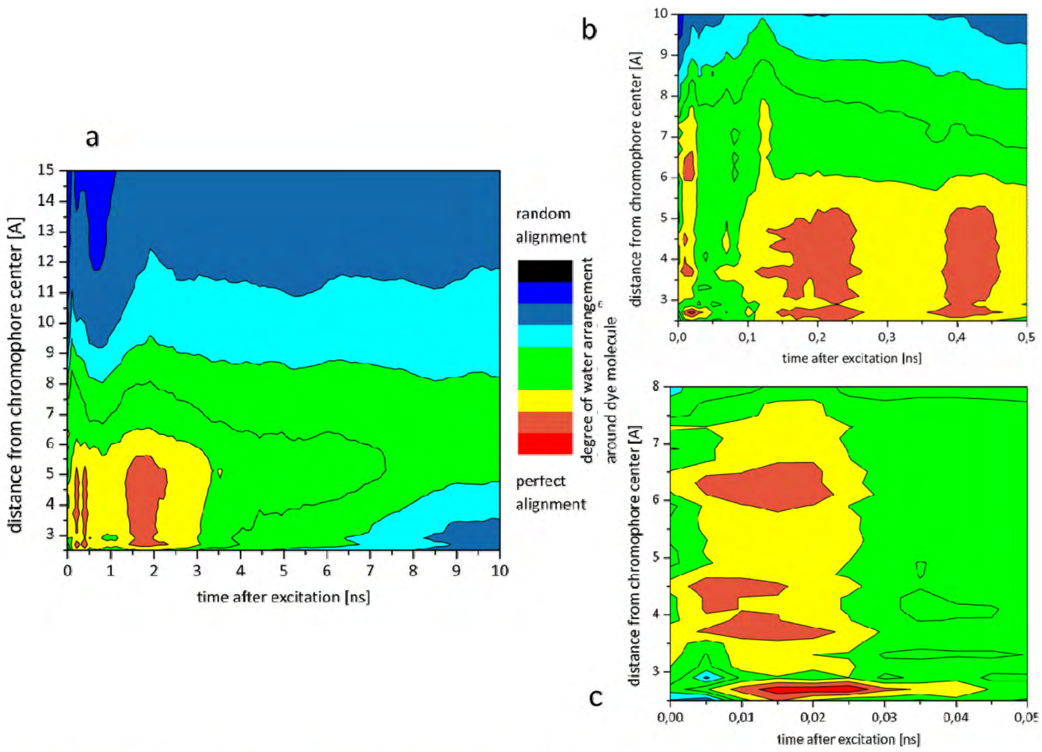

Figure III.27 Changes of water dynamics around C-laurdan molecule embedded into lipid membrane. Initial position of C-laurdan was chosen at the depth of 17Å from bilayer center. Maps were plotted as a function of time (x-axis) and distance from chromophore center (y-axis). Blue areas indicate the lack of the water organization, green and yellow regions a progressive arrangement, while red zones correspond to the most organized water molecules vs. dye dipole vector. Please note different scales between insets. Maps (b) and (c) show zoomed part of the map (a).

We have analyzed the 13 short simulations (10 ns), where C-Laurdan molecules were initially located at different depths in the lipid bilayer. From this 13 simulations, we can estimate the relaxation time constants τ_i. There are reported in Table III-9 as intervals indicating the ranges of appeared τ_i values.

	τ_1	τ_2	τ_3	τ_4
C-laurdan	0.01 - 0.03	0.15 - 0.8	2.0 – 10.0	7 - more than 10ns
Laurdan	0.01 - 0.05	0.16 - 0.6	1.25 - 2.5	3 - more than 6ns

Table III-9 Ranges of relaxation time constants (τ_i) with Laurdan and C-laurdan embedded into DOPC membrane model and gathered across multiple simulations.

Between two and four relaxation times τ_i were found for all initial configurations. The fastest water organization cycle, which corresponds to the first relaxation time τ_1, occurs within first 30 picoseconds after excitation. This time may be attributed to the rotational motions of water molecules. Next relaxation cycle was found during hundreds of picoseconds (τ_2) and could be connected with water translational movements. Third and fourth relaxation times τ_3 and τ_4

correspond most likely to lipid reorganization causing subsequent impacts on water molecules and were determined to be more than 2 ns after excitation.

4.2.4 Summary

We conducted quantum calculations and molecular dynamics simulations in order to characterize new fluorescent probe C-laurdan in DOPC bilayer.

Quantum mechanical calculations allowed us to obtain a correct description of the dye for characterizing electronic properties of the dye for MD simulations

We were also able to observe the passive diffusion of the dye from bulk water to DOPC lipid membrane. Equilibrium dye locations were analyzed.

C-laurdan is oriented more parallel to lipid molecules in comparison to Laurdan and has generally more stable position after excitation because of the presence of carboxyl group in its chromophore. Furthermore, the effective position of C-laurdan in the ground state, is ~ 1 Å closer to bilayer surface than one of Laurdan due to the presence of carboxyl group.

Four relaxation time constants were estimated from the solvent relaxation studies. Values of relaxation times are received in the correct nanoseconds time scale.

Our research confirm the assumptions of Kim et al. [74] about the usefulness of C-laurdan probe for lipid raft imaging and further supports its potential application for the studies of headgroup region of lipid bilayer by solvent relaxation technique.

Will C-Laurdan dethrone Laurdan in fluorescent solvent relaxation techniques for lipid membrane study?

Justyna Barucha-Kraszewska,* Sebastian Kraszewski, Christophe Ramseyer

Laboratoire de Nanomédecine, Imagerie et Thérapeutique, EA4662, Université de Franche-Comté, Centre Hospitalier Universitaire de Besançon, 16 Route de Gray, 25000 Besançon, France

ABSTRACT

Development of fluorescence methods involves the necessity of understanding the fluorescent probes behaviour in their ground and excited states. In the case of the advanced techniques, as for instance for fluorescent solvent relaxation (SR) method, the position of the dyes in the lipid bilayer and their response after excitation are necessary parameters to correctly analyze the experiment. In the present work, we focus on two fluorescent markers: Laurdan (6-lauroyl-2-(N,N-dimethylamino)naphthalene) and its derivative C-Laurdan (6-dodecanoyl-2-[*N*-methyl-*N*-(carboxymethyl)amino]naphthalene) recently proposed for lipid raft visualization.[H.M.Kim *et al.*, ChemBioChem, 8 (2007) 553] C-Laurdan, by the presence of the carboxyl group, has an advantages over Laurdan having the higher sensitivity to the membrane polarity and higher water solubility, thus not creating aggregates in plasma membranes. This theoretical study, employing Quantum Mechanical (QM) and Molecular Dynamics (MD) simulations in the fully hydrated lipid membrane model, compare the atomic properties and dynamic characteristics of both probes taking into account their fluorescence lifetimes. So coupled simulations are useful tool to visualize the probe behaviour in its ground and excited states, and to get a molecular view on interactions with its surrounding. This study supplements the knowledge of the novel C-Laurdan molecule suggesting that, besides the lipid raft imaging, this marker can considerably extend the capabilities of SR method.

KEYWORDS:
Molecular dynamics, Fluorescent probe, Lipid Membrane, Excited state, Solvent Relaxation, Water Dynamics, Laurdan, Carboxy-Laurdan, dye location, effective possition,

Langmuir, **DOI:** 10.1021/la304235r, Publication Date (Web): January 2, 2013

IV Conclusions & Perspectives

The application of Quantum Mechanical (QM) calculations and Molecular Dynamics (MD) simulations can extend the capabilities of the experimental fluorescent Solvent Relaxation (SR) method and allow observing the behaviour of individual molecules, which is not possible in experiment.

The SR method, using the fluorescent probes located at different well-defined locations in the membrane, allows characterizing the polarity and viscosity at the different depths in the lipid bilayer.

In this work, the influence of monovalent ions on the membrane properties was investigated by SR method for the first time. In order to investigate an impact of the ions on the membrane parameters three fluorescent dyes located differently in the lipid bilayer (Prodan, Laurdan and DTMAC) were used. The following conclusions could be drawn from this experiment :

- ✓ Sodium ions are located in the phosphate region of the DOPC bilayer whereas chloride ions are much weaker absorbed at the water/bilayer interface (choline region).
- ✓ Large cations (NH_4^+ and Cs^+) only weakly penetrate into the headgroup region of bilayer.
- ✓ Larger anions (ClO_4^- and SCN^-) penetrate deeper into the bilayer in the comparison to small chloride anions and cause significant changes in the membrane properties.

Previous molecular dynamics simulations of the location of ions confirm our experimental results and show that SR is suitable to study the influence of ions on the membrane properties [15-16].

In this study, four fluorescent dyes (*n*-AS, where *n* = 2, 9, 12 and 16-AP) with the same chromophore (anthroyloxy ring attached to the fatty acid chain at various positions *n*) were used for better understanding the phenomena, which occur at the hydrophobic region of the bilayer:

- ✓ The solvation contribution to the response function becomes less significant for the dyes located deeply in the membrane but does not disappear completely even for the most buried 16-AP dye, which suggest the presence of small amount of water in the hydrophobic region of POPC bilayer.
- ✓ Solvent relaxation kinetics becomes slower upon approaching the center of the bilayer.
- ✓ The solvent relaxation processes of *n*-AS dyes in the POPC bilayer are rather complex and reflect both intramolecular and intermolecular dynamics.

The studies of the molecular interactions between the water and the dye molecules were performed by numerical calculations :

- ✓ QM calculations were used to create adequate models of three fluorescent dyes (Prodan, Laurdan and C-laurdan) in their ground and excited states for further MD simulations for the first time.
- ✓ MD simulations allow finding position of the dye in the lipid membrane in the ground state and after excitation.
- ✓ MD simulations reproduce correctly solvent relaxation timescale – picoseconds in pure water and nanoseconds in the membrane.
- ✓ Four relaxation times were found for the probes embedded into the lipid bilayer. Two shortest are associated to the rotation and translation of the water molecules and two longest are induced by lipid reorganization.
- ✓ Thus, MD simulation give additional opportunities for finding shortest relaxation time, which is inaccessible in the experimental methods.

MD simulations of the deprotonated form of fluorescent dye C-Laurdan should be done in the future in conjunction with experimental C-Laurdan study of usage in SR techniques. Our results open the perspective for the experimental determination of the C-Laurdan position in the membrane by the fluorescent quenching method.

Solvent relaxation and molecular dynamics simulations are complementary methods that are able to explain hydration and packing effects in the lipid bilayer. SR and MD methods both benefit from this connection. SR gains a tool to illustrate the examined phenomena and to test the produced hypothesis on the molecular level. MD is the independent method for theoretical validation of obtained results at atomistic level. Combining MD simulations and SR experiments in determining location of the probe and simulating dynamics of water and lipids in the dye environment provides important insights into the phenomena in the dye microenvironment.

V References

1. Westlund, P.O., *Line shape analysis of NMR powder spectra of (H2O)-H-2 in lipid bilayer systems.* Journal of Physical Chemistry B, 2000. **104**(25): p. 6059-6064.
2. Gawrisch, K., et al., *Hydration of POPC bilayers studied by H-1-PFG-MAS-NOESY and neutron diffraction.* European Biophysics Journal with Biophysics Letters, 2007. **36**(4-5): p. 281-291.
3. Tristram-Nagle, S. and J.F. Nagle, *Lipid bilayers: thermodynamics, structure, fluctuations, and interactions.* Chemistry and Physics of Lipids, 2004. **127**(1): p. 3-14.
4. Marsh, D., *Polarity and permeation profiles in lipid membranes.* Proceedings of the National Academy of Sciences of the United States of America, 2001. **98**(14): p. 7777-7782.
5. Horng, M.L., et al., *Subpicosecond Measurements of Polar Solvation Dynamics - Coumarin-153 Revisited.* Journal of Physical Chemistry, 1995. **99**(48): p. 17311-17337.
6. Hutterer, R., et al., *Binding and relaxation behaviour of Prodan and Patman in phospholipid vesicles: A fluorescence and H-1 NMR study.* Biophysical Chemistry, 1996. **61**(2-3): p. 151-160.
7. Jurkiewicz, P., et al., *Headgroup hydration and mobility of DOTAP/DOPC bilayers: A fluorescence solvent relaxation study.* Langmuir, 2006. **22**(21): p. 8741-8749.
8. Chattopadhyay, A. and E. London, *Parallax Method for Direct Measurement of Mmembrane Penetration Depth Utilizing Fluorescence Quenching by Spin-Labeled Phospholipids.* Biochemistry, 1987. **26**(1): p. 39-45.
9. Phillips, J.C., et al., *Scalable molecular dynamics with NAMD.* J. Comput. Chem., 2005. **26**(16): p. 1781-1802.
10. Brooks, B.R., et al., *CHARMM - a Program for Macromolecular Energy, Minimization, and Dynamics Calculations.* Journal of Computational Chemistry, 1983. **4**(2): p. 187-217.
11. Lindahl, E., B. Hess, and D. van der Spoel, *GROMACS 3.0: a package for molecular simulation and trajectory analysis.* Journal of Molecular Modeling, 2001. **7**(8): p. 306-317.
12. Case, D.A., et al., *AMBER 8.* 2004, San Francisco: University of California.
13. Barucha-Kraszewska, J., et al., *Numerical studies of the membrane fluorescent dyes dynamics in ground and excited states.* Biochimica Et Biophysica Acta-Biomembranes, 2010. **1798**(9): p. 1724-1734.
14. Kunz, W., J. Henle, and B.W. Ninham, *'Zur Lehre von der Wirkung der Salze' (about the science of the effect of salts): Franz Hofmeister's historical papers.* Current Opinion in Colloid & Interface Science, 2004. **9**(1-2): p. 19-37.
15. Vacha, R., et al., *Effects of Alkali Cations and Halide Anions on the DOPC Lipid Membrane.* Journal of Physical Chemistry A, 2009. **113**(26): p. 7235-7243.
16. Vacha, R., et al., *Mechanism of Interaction of Monovalent Ions with Phosphatidylcholine Lipid Membranes.* Journal of Physical Chemistry B, 2010. **114**(29): p. 9504-9509.
17. van Meer, G., *Lipid traffic in animal cells.* Annual review of cell biology, 1989. **02**(5): p. 247-275.
18. Christie, W.W. *The lipid library.* 2006; Available from: www.lipidlibrary.co.uk.
19. Langner, M. and T.E. Kral, *Liposome-based drug delivery systems.* Polish Journal of Pharmacology, 1999. **51**(3): p. 211-222.

20. Woodle, M.C. and D.D. Lasic, *Sterically Stabilized Liposomes.* Biochimica Et Biophysica Acta, 1992. **1113**(2): p. 171-199.
21. Escriba, P.V., *Membrane-lipid therapy: a new approach in molecular medicine.* Trends in Molecular Medicine, 2006. **12**(1): p. 34-43.
22. Brown, D.A. and E. London, *Functions of lipid rafts in biological membranes.* Annual Review of Cell and Developmental Biology, 1998. **14**: p. 111-136.
23. Simons, K. and E. Ikonen, *Functional rafts in cell membranes.* Nature, 1997. **387**(6633): p. 569-572.
24. Christie, W.W., *Rapid separation and quantification of lipid classes by high performance liquid chromatography and mass (light-scattering) detection.* Journal of Lipid Research, 1985. **26**: p. 507-512.
25. Whitesides, G.M. and B. Grzybowski, *Self-assembly at all scales.* Science, 2002. **295**(5564): p. 2418-2421.
26. Israelachvili, J.N., S. Marcelja, and R.G. Horn, *Physical Principles of Membrane Organization.* Quarterly Reviews of Biophysics, 1980. **13**(2): p. 121-200.
27. Dowhan, W., *Molecular basis for membrane phospholipid diversity: Why are there so many lipids?* Annual Review of Biochemistry, 1997. **66**: p. 199-232.
28. Lindblom, G. and L. Rilfors, *Cubic Phases and Isotropic Structures Formed by Membrane-Lipids - Possible Biological Relevance.* Biochimica Et Biophysica Acta, 1989. **988**(2): p. 221-256.
29. Sein, A., et al., *Salt-Induced Transition from a Micellar to a Lamellar Liquid-Crystalline Phase in Dilute Mixtures of Anionic and Nonionic Surfqctants in Aqueous-Solution.* Langmuir, 1993. **9**(7): p. 1714-1720.
30. Albert, B., Bray, D., Lewis, J., Raff, M., Roberts, K., Watson, J. D., *Molecular Biology of the Cell.* 1989, New York: Garland.
31. Hope, M.J., et al., *Generation of Multilamellar and Unilamellar Phospholipid-Vesicles.* Chemistry and Physics of Lipids, 1986. **40**(2-4): p. 89-107.
32. Bagatolli, L.A., *Direct observation of lipid domains in free standing bilayers: from simple to complex lipid mixtures.* Chemistry and Physics of Lipids, 2003. **122**(1-2): p. 137-145.
33. Bagatolli, L.A., *To see or not to see: Lateral organization of biological membranes and fluorescence microscopy.* Biochimica Et Biophysica Acta-Biomembranes, 2006. **1758**(10): p. 1541-1556.
34. Marrink, S.J. and H.J.C. Berendsen, *Simulation of Water Transport Through a Lipid-Membrane.* Journal of Physical Chemistry, 1994. **98**(15): p. 4155-4168.
35. Demchenko, A.P. and S.O. Yesylevskyy, *Nanoscopic description of biomembrane electrostatics: results of molecular dynamics simulations and fluorescence probing.* Chemistry and Physics of Lipids, 2009. **160**(2): p. 63-84.
36. Gurtovenko, A.A., et al., *Cationic DMPC/DMTAP lipid bilayers: Molecular dynamics study.* Biophysical Journal, 2004. **86**(6): p. 3461-3472.
37. Schamberger, J. and R.J. Clarke, *Hydrophobic ion hydration and the magnitude of the dipole potential.* Biophysical Journal, 2002. **82**(6): p. 3081-3088.
38. Marrink, S.J., M. Berkowitz, and H.J.C. Berendsen, *Molecular-Dynamics Simulation of a Membrane Water Interface - The Ordering of Water and Its Relation to The Hydration Force.* Langmuir, 1993. **9**(11): p. 3122-3131.
39. Nagle, J.F. and M.C. Wiener, *Structure of Fully Hydrated Bilayer Dispersions.* Biochimica Et Biophysica Acta, 1988. **942**(1): p. 1-10.
40. Eisenberg, M., et al., *Adsorption of Mono-Valent Cations to Bilayer Membranes Containing Negative Phospholipids.* Biochemistry, 1979. **18**(23): p. 5213-5223.
41. Clarke, R.J. and C. Lupfert, *Influence of anions and cations on the dipole potential of phosphatidylcholine vesicles: A basis for the Hofmeister effect.* Biophysical Journal, 1999. **76**(5): p. 2614-2624.

42. Sachs, J.N., et al., *Changes in phosphatidylcholine headgroup tilt and water order induced by monovalent salts: Molecular dynamics simulations.* Biophysical Journal, 2004. **86**(6): p. 3772-3782.
43. Zhao, W., et al., *Atomic-scale structure and electrostatics of anionic palmitoyloleoylphosphatidylglycerol lipid bilayers with Na+ counterions.* Biophysical Journal, 2007. **92**(4): p. 1114-1124.
44. Petrache, H.I., et al., *Salt screening and specific ion adsorption determine neutral-lipid membrane interactions.* Proceedings of the National Academy of Sciences of the United States of America, 2006. **103**(21): p. 7982-7987.
45. Renoncourt, A., et al., *Specific alkali cation effects in the transition from micelles to vesicles through salt addition.* Langmuir, 2007. **23**(5): p. 2376-2381.
46. Claessens, M., et al., *Charged lipid vesicles: Effects of salts on bending rigidity, stability, and size.* Biophysical Journal, 2004. **87**(6): p. 3882-3893.
47. Garcia-Celma, J.J., et al., *Specific anion and cation binding to lipid membranes investigated on a solid supported membrane.* Langmuir, 2007. **23**(20): p. 10074-10080.
48. Bockmann, R.A., et al., *Effect of sodium chloride on a lipid bilayer.* Biophysical Journal, 2003. **85**(3): p. 1647-1655.
49. Bockmann, R.A. and H. Grubmuller, *Multistep binding of divalent cations to phospholipid bilayers: A molecular dynamics study.* Angewandte Chemie-International Edition, 2004. **43**(8): p. 1021-1024.
50. Gurtovenko, A.A. and I. Vattulainen, *Effect of NaCl and KCl on phosphatidylcholine and phosphatidylethanolamine lipid membranes: Insight from atomic-scale simulations for understanding salt-induced effects in the plasma membrane.* Journal of Physical Chemistry B, 2008. **112**(7): p. 1953-1962.
51. Epand, R.F., et al., *Fluorescent probes of membrane surface properties.* Biochimica Et Biophysica Acta-Biomembranes, 1996. **1284**(2): p. 191-195.
52. Gabrielska, J., et al., *The effect of cholesterol on the adsorption of phenyltin compounds onto phosphatidylcholine and sphingomyelin liposome membranes.* Applied Organometallic Chemistry, 2004. **18**(1): p. 9-14.
53. Hutterer, R., et al., *Binding of prothrombin and its fragment 1 to phospholipid membranes studied by the solvent relaxation technique.* Biochimica Et Biophysica Acta-Biomembranes, 1998. **1414**(1-2): p. 155-164.
54. Klymchenko, A.S., et al., *Bimodal distribution and fluorescence response of environment-sensitive probes in lipid bilayers.* Biophysical Journal, 2004. **86**(5): p. 2929-2941.
55. Lakowicz, J.R., *Topics in Fluorescence Spectroscopy.* 1992-2007, New York: Plenum Press.
56. Winiski, A.P., et al., *Fluorescent -Probes of Electrostatic Potential 1-nm from the Membrane-Surface.* Biochemistry, 1988. **27**(1): p. 386-392.
57. Langner, M., et al., *Electrostatics of Phosphoinositide Bilayer-Membranes - Theoretical and Experimental Results.* Biophysical Journal, 1990. **57**(2): p. 335-349.
58. Langner, M. and S.W. Hui, *Dithionite Penetration Through Phospholipid-Bilayers as a Measure of Defects in Lipid Molecular Packing.* Chemistry and Physics of Lipids, 1993. **65**(1): p. 23-30.
59. Hutterer, R., F.W. Schneider, and M. Hof, *Anisotropy and lifetime profiles for n-anthroyloxy fatty acids: A fluorescence method for the detection of bilayer interdigitation.* Chemistry and Physics of Lipids, 1997. **86**(1): p. 51-64.
60. Langner, M. and S.W. Hui, *Merocyanine 540 as a fluorescence indicator for molecular packing stress at the onset of lamellar-hexagonal transition of phosphatidylethanolamine bilayers.* Biochimica Et Biophysica Acta-Biomembranes, 1999. **1415**(2): p. 323-330.
61. Kubica, K., M. Langner, and J. Gabrielska, *The dependence of Fluorescein-PE fluorescence intensity on lipid bilayer state. Evaluating the interaction between the probe and lipid molecules.* Cellular & Molecular Biology Letters, 2003. **8**(4): p. 943-954.
62. Bernsdorff, C., et al., *Effect of hydrostatic pressure on water penetration and rotational dynamics in phospholipid-cholesterol bilayers.* Biophysical Journal, 1997. **72**(3): p. 1264-1277.

63. Hutterer, R., Haefner, A., Schneider, F.W., Hof, M., *Fluorescence microscopy nad fluorescence probes*. 1998, New York: Plenum Press.
64. Hof, M., *Solvent Relaxation in Biomembranes*. 1999, Berlin: Springer Verlag.
65. Sykora, J., et al., *ABA-C-15: A new dye for probing solvent relaxation in phospholipid bilayers.* Langmuir, 2002. **18**(24): p. 9276-9282.
66. Yang, M. and R. Richert, *Observation of heterogeneity in the nanosecond dynamics of a liquid.* Journal of Chemical Physics, 2001. **115**(6): p. 2676-2680.
67. Hutterer, R. and M. Hof, *Probing ethanol-induced phospholipid phase transitions by the polarity sensitive fluorescence probes Prodan and Patman.* Zeitschrift Fur Physikalische Chemie-International Journal of Research in Physical Chemistry & Chemical Physics, 2002. **216**: p. 333-346.
68. Chong, P.L., S. Capes, and P.T.T. Wong, *Effects of Hydrostatic-Pressure on the Location of Prodan in Lipid Bilayers - a FT-IR Study.* Biochemistry, 1989. **28**(21): p. 8358-8363.
69. Fee, R.S. and M. Maroncelli, *Estimating the Time-Zero Spectrum in Time-Resolved Emission Measurements of Solvation Dynamics.* Chemical Physics, 1994. **183**(2-3): p. 235-247.
70. Sykora, J., et al., *On what time scale does solvent relaxation in phospholipid bilayers happen?* Langmuir, 2002. **18**(3): p. 571-574.
71. Jimenez, R., et al., *Femtosecond Solvation Dynamics of Water.* Nature, 1994. **369**(6480): p. 471-473.
72. Chong, P.L.G., *Effects of Hydrostatic-Pressure on the Location of Prodan in Lipid Bilayers and Cellular Membranes.* Biochemistry, 1988. **27**(1): p. 399-404.
73. Moyano, F., et al., *New insights on the behavior of PRODAN in homogeneous media and in large unilamellar vesicles.* Journal of Physical Chemistry B, 2006. **110**(24): p. 11838-11846.
74. Kim, H.M., et al., *A two-photon fluorescent probe for lipid raft imaging: C-laurdan.* Chembiochem, 2007. **8**(5): p. 553-559.
75. Abrams, F.S., A. Chattopadhyay, and E. London, *Determination of the Location of Fluorescent-Probes Attached to Fatty-Acids Using Parallax Analysis of Fluorescence Quenching - Effect of Carboxyl Ionization State and Environment on Depth.* Biochemistry, 1992. **31**(23): p. 5322-5327.
76. Villalain, J. and M. Prieto, *Location and Interaction of N-(9-Anthroyloxy)-Stearic Acid Probes Incorporated in Phosphatidylcholine Vesicles.* Chemistry and Physics of Lipids, 1991. **59**(1): p. 9-16.
77. McMorrow, D. and M. Kasha, *Intramolecular Excited-State Proton-Transfer in 3-Hydroxyflavone - Hydrogen-Bonding Solvent Perturbations.* Journal of Physical Chemistry, 1984. **88**(11): p. 2235-2243.
78. Klymchenko, A.S., et al., *Modulation of the solvent-dependent dual emission in 3-hydroxychromones by substituents.* New Journal of Chemistry, 2003. **27**(9): p. 1336-1343.
79. Klymchenko, A.S. and A.P. Demchenko, *Multiparametric probing of intermolecular interactions with fluorescent dye exhibiting excited state intramolecular proton transfer.* Physical Chemistry Chemical Physics, 2003. **5**(3): p. 461-468.
80. Klymchenko, A.S. and A.P. Demchenko, *Electrochromic modulation of excited-state intramolecular proton transfer: The new principle in design of fluorescence sensors.* Journal of the American Chemical Society, 2002. **124**(41): p. 12372-12379.
81. Yesylevskyy, S.O., A.S. Klymchenko, and A.P. Demchenko, *Semi-empirical study of two-color fluorescent dyes based on 3-hydroxychromone.* Journal of Molecular Structure-Theochem, 2005. **755**(1-3): p. 229-239.
82. Klymchenko, A.S., et al., *Novel two-band ratiometric fluorescence probes with different location and orientation in phospholipid membranes.* Chemistry & Biology, 2002. **9**(11): p. 1199-1208.
83. Klymchenko, A.S., et al., *Ultrasensitive two-color fluorescence probes for dipole potential in phospholipid membranes.* Proceedings of the National Academy of Sciences of the United States of America, 2003. **100**(20): p. 11219-11224.

84. Bondar, O.P., V.G. Pivovarenko, and E.S. Rowe, *Flavonols - new fluorescent membrane probes for studying the interdigitation of lipid bilayers.* Biochimica Et Biophysica Acta-Biomembranes, 1998. **1369**(1): p. 119-130.
85. Duportail, G., et al., *On the coupling between surface charge and hydration in biomembranes: Experiments with 3-hydroxyflavone probes.* Journal of Fluorescence, 2002. **12**(2): p. 181-185.
86. Duportail, G., et al., *Neutral fluorescence probe with strong ratiometric response to surface charge of phospholipid membranes.* Febs Letters, 2001. **508**(2): p. 196-200.
87. Turkmen, Z., et al., *A triterpene oleanolic acid conjugate with 3-hydroxyflavone derivative as a new membrane probe with two-color ratiometric response.* Journal of Biochemical and Biophysical Methods, 2005. **64**(1): p. 1-18.
88. Roshal, A.D., et al., *Flavonols and crown-flavonols as metal cation chelators. The different nature of Ba2+ and Mg2+ complexes.* Journal of Physical Chemistry A, 1998. **102**(29): p. 5907-5914.
89. Klymchenko, A.S., S.V. Avilov, and A.P. Demchenko, *Resolution of Cys and Lys labeling of alpha-crystallin with site-sensitive fluorescent 3-hydroxyflavone dye.* Analytical Biochemistry, 2004. **329**(1): p. 43-57.
90. Ercelen, S., et al., *The binding of novel two-color fluorescence probe FA to serum albumins of different species.* International Journal of Biological Macromolecules, 2005. **35**(5): p. 231-242.
91. Shynkar, V.V., et al., *Two-color fluorescent probes for imaging the dipole potential of cell plasma membranes.* Biochimica Et Biophysica Acta-Biomembranes, 2005. **1712**(2): p. 128-136.
92. Frisch, M.J., et al., *Gaussian 03, Rev. C.02.* 2004, Gaussian, Inc.: Wallingford CT.
93. Gross, L., et al., *Measuring the Charge State of an Adatom with Noncontact Atomic Force Microscopy.* Science, 2009. **324**(5933): p. 1428-1431.
94. Cramer, C.J., *Essentials of Computational Chemistry: Theories and Models.* 2004.
95. Mulliken, R.S., *Electronic population analysis on CAO-MO molecular wave functions 1.* J. Chem. Phys., 1955. **23**(10): p. 1833-1840.
96. van Gunsteren, W.F., *The role of computer-simulations techniques in protein engineering.* Prot. Eng., 1988. **2**(1): p. 5-13.
97. van Gunsteren, W.F. and H.J.C. Berendsen, *Computer simulation of molecular dynamics: methodology, applications, and perpectives in chemistry.* Angew. Chem. Int. Ed. Engl., 1990. **29**: p. 992-1023.
98. van Gunsteren, W.F., et al., *Molecular mechanics in biology: from structure to function, taking account of solvation.* Annu. Rev. Biophys. Biomol. Struct., 1994. **23**: p. 847-863.
99. MacKerell, A.D., et al., *All-atom empirical potential for molecular modeling and dynamics studies of proteins.* Journal of Physical Chemistry B, 1998. **102**(18): p. 3586-3616.
100. Weiner, S.J., et al., *A new force-field for molecular mechanical simulation of nucleic-acids and proteins.* J. Am. Chem. Soc., 1984. **106**(3): p. 765-784.
101. Berendsen, H.J.C., et al., *Molecular Dynamics and Protein Structure.* 1985, Western Springs: Polycrystal Book Service
102. Brooks, C.L., B.M. Pettitt, and M. Karplus, *Structural and energetic effects of truncating long ranged interactions in ionic and polar fluids.* J. Chem. Phys., 1985. **83**(11): p. 5897-5908.
103. van Gunsteren, W.F., P.K. Weiner, and A.J. Wikinson, eds. *Computer simulation of biomolecular systems.* 1993, ESCOM Leiden: Dordrecht.
104. Schreiber, H. and O. Steinhauser, *Molecular-dynamics studies of solvated polypeptides - Why the cutoff scheme does not work.* Chem. Phys., 1992. **168**(1): p. 75-89.
105. Aqvist, J. and T. Hansson, *On the validity of electrostatic linear response in polar solvents.* J. Phys. Chem., 1996. **100**(22): p. 9512-9521.
106. Aqvist, J. and T. Hansson, *Analysis of electrostatic potential truncation schemes in simulations of polar solvents.* J. Phys. Chem. B, 1998. **102**(19): p. 3837-3840.

107. Ashbaugh, H.S., S. Sakane, and R.H. Wood, *Reply to comment on "Electrostatic potentials and free energies of solvation of polar and charged molecules".* J. Phys. Chem. B, 1998. **102**(19): p. 3844-3845.
108. Hummer, G., et al., *Reply to comment on "Electrostatic potentials and free energies of solvation of polar and charged molecules".* J. Phys. Chem. B, 1998. **102**(19): p. 3841-3843.
109. Hummer, G., et al., *Electrostatic potentials and free energies of solvation of polar and charged molecules.* J. Phys. Chem. B, 1997. **101**(16): p. 3017-3020.
110. Ewald, P.P., *The calculation of optical and electrostatic grid potential.* Ann. Phys.-Leipzig, 1921. **64**(3): p. 253-287.
111. Allen, M.P. and D.J. Tildesley, *Computer Simulation of Liquids.* 1989, Oxford: Clarendon Press.
112. Darden, T., D. York, and L. Pedersen, *Particle Mesh Ewald - An N.Log(N) Method for Ewald Sums in Large Systems.* Journal of Chemical Physics, 1993. **98**(12): p. 10089-10092.
113. Essmann, U., et al., *A Smooth Particle Mesh Ewald Method.* Journal of Chemical Physics, 1995. **103**(19): p. 8577-8593.
114. Berendsen, H.J.C., et al., *Molecular dynamics with coupling to an external bath.* J. Chem. Phys., 1984. **81**: p. 3684-3690.
115. Epand, R.F., et al., *New fluorescent probes for evaluating the polarity properties of membrane interfaces.* Biophysical Journal, 1996. **70**(2): p. TUAM8-TUAM8.
116. Hohenberg, P. and W. Kohn, *Inhomogeneous Electron Gas.* Physical Review B, 1964. **136**(3B): p. B864-&.
117. Kohn, W. and L.J. Sham, *Self-Consistent Equations Including Exchange nad Correlation Effects.* Physical Review, 1965. **140**(4A): p. 1133-&.
118. Stratmann, R.E., G.E. Scuseria, and M.J. Frisch, *An efficient implementation of time-dependent density-functional theory for the calculation of excitation energies of large molecules.* Journal of Chemical Physics, 1998. **109**(19): p. 8218-8224.
119. Bauernschmitt, R. and R. Ahlrichs, *Treatment of electronic excitations within the adiabatic approximation of time dependent density functional theory.* Chemical Physics Letters, 1996. **256**(4-5): p. 454-464.
120. Casida, M.E., et al., *Molecular excitation energies to high-lying bound states from time-dependent density-functional response theory: Characterization and correction of the time-dependent local density approximation ionization threshold.* Journal of Chemical Physics, 1998. **108**(11): p. 4439-4449.
121. Cances, E., B. Mennucci, and J. Tomasi, *A new integral equation formalism for the polarizable continuum model: Theoretical background and applications to isotropic and anisotropic dielectrics.* Journal of Chemical Physics, 1997. **107**(8): p. 3032-3041.
122. Mennucci, B., E. Cances, and J. Tomasi, *Evaluation of solvent effects in isotropic and anisotropic dielectrics and in ionic solutions with a unified integral equation method: Theoretical bases, computational implementation, and numerical applications.* Journal of Physical Chemistry B, 1997. **101**(49): p. 10506-10517.
123. Tomasi, J., B. Mennucci, and E. Cances, *The IEF version of the PCM solvation method: an overview of a new method addressed to study molecular solutes at the QM ab initio level.* Journal of Molecular Structure-Theochem, 1999. **464**(1-3): p. 211-226.
124. Mennucci, B. and J. Tomasi, *Continuum solvation models: A new approach to the problem of solute's charge distribution and cavity boundaries.* Journal of Chemical Physics, 1997. **106**(12): p. 5151-5158.
125. Humphrey, W., A. Dalke, and K. Schulten, *VMD: Visual molecular dynamics.* Journal of Molecular Graphics, 1996. **14**(1): p. 33-&.
126. Phillips, J.C., et al., *Scalable molecular dynamics with NAMD.* Journal of Computational Chemistry, 2005. **26**(16): p. 1781-1802.
127. Jorgensen, W.L., et al., *Comparison of Simple Potential Functions for Simulating Liqiud Water.* Journal of Chemical Physics, 1983. **79**(2): p. 926-935.

128. Feller, S.E., et al., *Constant-Pressure Molecular-Dynamics Simulation - The Langevin Piston Method.* Journal of Chemical Physics, 1995. **103**(11): p. 4613-4621.
129. Darden, T., D. York, and L. Pedersen, *Particle mesh Ewald: An N.log(N) method for Ewald sums in large systems.* J. Chem. Phys., 1993. **98**(12): p. 10089-10092.
130. Marcus, Y., *Thermodynamics of Solvation of Ions .5. Gibbs Free-Energy of Hydration at 298.15-K.* Journal of the Chemical Society-Faraday Transactions, 1991. **87**(18): p. 2995-2999.
131. Sykora, J., et al., *Influence of the curvature on the water structure in the headgroup region of phospholipid bilayer studied by the solvent relaxation technique.* Chemistry and Physics of Lipids, 2005. **135**(2): p. 213-221.
132. Davies, S.M.A., et al., *Regulation of CTP: Phosphocholine cytidylyltransferase activity by the physical properties of lipid membranes: An important role for stored curvature strain energy.* Biochemistry, 2001. **40**(35): p. 10522-10531.
133. Zubrzycki, I.Z., et al., *Molecular dynamics simulations of a fully hydrated dimyristoylphosphatidylcholine membrane in liquid-crystalline phase.* Journal of Chemical Physics, 2000. **112**(7): p. 3437-3441.
134. Werner, T.C. and R.M. Hoffman, *Relation Between an Excited-State Geometry Change and Solvent Dependence of 9-Methyl Anthroate Fluorescence.* Journal of Physical Chemistry, 1973. **77**(13): p. 1611-1615.
135. Berberansantos, M.N., M.J.E. Prieto, and A.G. Szabo, *Excited-State Intramolecular Relaxation of the Lipophilic Probe 12-(9-Anthroyloxy)Stearic Acid.* Journal of Physical Chemistry, 1991. **95**(14): p. 5471-5475.
136. Hutterer, R., et al., *Solvent relaxation behaviour of n-anthroyloxy fatty acids in PC-vesicles and paraffin oil: A time-resolved emission spectra study.* Biochimica Et Biophysica Acta-Biomembranes, 1997. **1323**(2): p. 195-207.
137. Chattopadhyay, A. and S. Mukherjee, *Depth-dependent solvent relaxation in membranes: Wavelength-selective fluorescence as a membrane dipstick.* Langmuir, 1999. **15**(6): p. 2142-2148.
138. Sykora, J., et al., *Time-dependent stokes shifts of fluorescent dyes in the hydrophobic backbone region of a phospholipid bilayer: Combination of fluorescence spectroscopy and ab initio calculations.* Journal of Physical Chemistry B, 2007. **111**(21): p. 5869-5877.
139. Gurtovenko, A.A., *Asymmetry of lipid bilayers induced by monovalent salt: Atomistic molecular-dynamics study.* Journal of Chemical Physics, 2005. **122**(24).
140. Parasassi, T., et al., *Phase Fluctuation in Phospholipid-Membranes Revealed by Laurdan Fluorescence.* Biophysical Journal, 1990. **57**(6): p. 1179-1186.
141. Weber, G. and F.J. Farris, *Synthesis and spectral properties of a hydrophobic fluorescent-probe - 6-propionyl-2-(dimethylamino)naphthalene.* Biochemistry-US, 1979. **18**(14): p. 3075-3078.
142. MacGregor, R.B. and G. Weber, *Fluorophores in polar media: spectral effects of the Langevin distribution of electrostatic interactions.* Ann.N.Y.Acad.Sci., 1981. **366**: p. 140.
143. Parasassi, T., et al., *Laurdan and Prodan as polarity-sensitive fluorescent membrane probes.* J. Fluoresc., 1998. **8**(4): p. 365-373.
144. Kozyra, K.A., et al., *Phase transition affects energy transfer efficiency in phospholipid vesicles.* Spectrochimica Acta Part a-Molecular and Biomolecular Spectroscopy, 2005. **61**(6): p. 1153-1161.
145. Artukhov, V.Y., O.M. Zharkova, and J.P. Morozova, *Features of absorption and fluorescence spectra of prodan.* Spectrochim. Acta A, 2007. **68**(1): p. 36-42.
146. Mennucci, B., et al., *How the environment controls absorption and fluorescence spectra of Prodan: A quantum-mechanical study in homogeneous and heterogeneous media.* J. Phys. Chem. B, 2008. **112**(2): p. 414-423.
147. Parusel, A.B.J., F.W. Schneider, and G. Kohler, *An ab initio study on excited and ground state properties of the organic fluorescence probe Prodan.* J. Mol. Struc.-Theochem, 1997. **398**: p. 341-346.

148. Parusel, A.B.J., R. Schamschule, and G. Kohler, *Nonlinear optics. A semiempirical study of organic chromophores.* J. Mol. Struc.-Theochem, 2001. **544**: p. 253-261.
149. Parusel, A.B.J., et al., *Comparative theoretical study on charge-transfer fluorescence probes: 6-propanoyl-2-(N,N-dimethylamino)naphthalene and derivatives.* J. Phys. Chem. A, 1998. **102**(36): p. 7149-7156.
150. Parusel, A., *Semiempirical studies of solvent effects on the intramolecular charge transfer of the fluorescence probe Prodan.* J. Chem. Soc. Faraday T, 1998. **94**(19): p. 2923-2927.
151. Morozova, Y.P., et al., *Effect of proton-donor solvent and structural flexibility of prodan and laurdan molecules on their spectral-luminescent properties.* Journal of Applied Spectroscopy, 2009. **76**(3): p. 312-318.
152. Nemkovich, N.A. and W. Baumann, *Molecular Stark-effect spectroscopy of Prodan and Laurdan in different solvents and electric dipole moments in their equilibrated ground and Franck-Condon excited state.* J. Photoch. Photobio. A, 2007. **185**(1): p. 26-31.
153. Samanta, A. and R.W. Fessenden, *Excited state dipole moment of Prodan as determined from transient dielectric loss measurements.* J. Phys. Chem. A, 2000. **104**(39): p. 8972-8975.
154. Ilich, P. and F.G. Prendergast, *Singlet adiabatic states of solvated Prodan - A semiempirical molecular-orbital study.* J. Phys. Chem.-US, 1989. **93**(11): p. 4441-4447.
155. Catalan, J., et al., *Analysis of the solvent effect on the photophysics properties of 6-propionyl-2-(dimethylamino)naphthalene (PRODAN).* J. Fluoresc., 1991. **1**(4): p. 215-223.
156. Maroncelli, M., *Computer-simulations of solvation dynamics in acetonitrile.* J. Chem. Phys., 1991. **94**(3): p. 2084-2103.
157. Maroncelli, M. and G.R. Fleming, *Computer-simulation of the dynamics of aqueous solvation.* J. Chem. Phys., 1988. **89**(8): p. 5044-5069.
158. Gaus, K., et al., *Visualizing lipid structure and raft domains in living cells with two-photon microscopy.* Proceedings of the National Academy of Sciences of the United States of America, 2003. **100**(26): p. 15554-15559.

RESUMÉ DE LA THÈSE EN FRANÇAIS

ANALYSE EXPERIMENTALE ET NUMERIQUE DES PROCESSUS DE RELAXATION DE SOLVENT DANS UNE MEMBRANE BIOLOGIQUE. ROLE DES IONS ET INTERPRETATION MOLECULAIRE DE LA DYNAMIQUE DES MARQUEURS FLUORESCENTS.

De nombreux processus biologiques liés aux membranes cellulaires lipidiques sont encore très mal connus. La présence d'eau et d'ions à l'interface influence les propriétés structurelles et dynamiques de la bicouche lipidique. Les techniques de fluorescence sont très utiles pour étudier les membranes en raison de la grande sensibilité des sondes à leur environnement. Nous avons utilisé la technique de relaxation de solvant (SR) pour explorer l'hydratation et la mobilité de l'eau. Nous avons également réalisé des calculs quantiques (QM) et des dynamiques moléculaires (DM) pour étayer nos expériences.
Les résultats SR montrent qu'un petit cation (Na^+) est très attiré par la membrane et augmente sa rigidité à l'opposé des cations (NH_4^+, Cs^+) plus gros. Les anions (ClO_4^-, SCN^-) s'adsorbent à l'interface plus facilement que Cl^-. Ces anions changent la mobilité et l'hydratation des têtes polaires des lipides de la bicouche. Les études SR de la zone hydrophobe de la membrane montrent que les processus de relaxation sont ici très complexes. Ils reflètent des processus rapides intramoléculaire (relaxation de torsion, transferts de charge) et des processus intermoléculaires lents. Les calculs QM ont permis de créer les champs de force de trois sondes fluorescentes (Prodan, Laurdan et C-laurdan). Les simulations DM ont permis de déterminer les positions des sondes dans une membrane DOPC. La modélisation reproduit correctement les résultats SR, en particulier les temps de relaxation : de l'ordre de la ps en solvant aqueux et de la ns dans la membrane. Les simulations MD sont complémentaires des méthodes SR et permettent de surveiller le comportement de molécules uniques.

RESUMÉ DE LA THÈSE EN ANGLAIS

EXPERIMENTAL AND SIMULATION ANALYSES OF FLUORESCENT SOLVENT RELAXATION PROCESS IN BIOMEMBRANES. INFLUENCE OF IONS AND MOLECULAR INTERPRETATION OF THE DYE DYNAMICS.

Many biologically important processes and phenomena in lipid membranes are still not fully understood. The presence of ions and water molecules has a significant influence on the structural and dynamical properties of lipid bilayers. Fluorescent techniques are versatile tools for studying the lipid membranes, because the fluorescence emission is strongly sensitive to dye environment. We have conducted fluorescent solvent relaxation (SR) experiments to explore the hydration and mobility properties in lipid membranes in the presence of different chaotropic ions. We have also carried out Quantum Mechanical (QM) calculations and Molecular Dynamics (MD) simulations for supporting the SR experiments.
SR experiments show that small cation (Na^+) is attracted to the membrane and increases rigidity of bilayer, while larger cations (NH_4^+, Cs^+) should not. Large anions (ClO_4^-, SCN^-) adsorb at the membrane interface more easily than smaller ones (Cl^-) and significantly change the mobility and hydration of the headgroup region of lipid bilayer. SR study of hydrophobic part of the membrane show that SR processes are complex there and reflect both: faster, intramolecular (torsional relaxation or formation of charge transfer state) and slower, intermolecular SR processes. QM calculations were used to create force-field for three fluorescent dyes (Prodan, Laurdan and C-laurdan). MD simulations allow determining position of the dye in the lipid membrane in the ground state and after excitation and reproduce correctly SR timescale – ps in water and ns in the membrane. MD simulations extend the capabilities of SR method and allow observing the behaviour of individual molecules.